Biochemical Analysis of Human Cancer-Associated Pseudokinases

Fiona P. Bailey

A thesis submitted to the University of Sheffield
for the degree of Doctor of Philosophy

June 2014

Department of Oncology

The University Of Sheffield.

Declaration

I declare that no portion of this work has been submitted to this, or any other University for the award of a degree. The work described below is my own, except where referenced.

Acknowledgments

I would like to thank Dr. Patrick Eyers for the fantastic opportunity of undertaking a PhD in his laboratory. Moreover, I cannot thank him enough for the constant support and guidance provided at all times throughout this PhD.

I also want to thank everybody who has collaborated with this project and has kindly contributed reagents, materials or time towards supporting this work.

I would like to acknowledge everybody at The University of Sheffield and The University of Liverpool for their support throughout the project, including Dr. Michael Trikic and Dr. Dominic Byrne for their assistance, invaluable input and thought-provoking discussions over the years.

Finally, a special note of thanks goes to my parents Pat and Richard, and brother James, who have never doubted my abilities and always provided encouragement and support.

Abstract

Mutation or aberrant expression of protein kinase domains can lead to the development of a variety of cancers, which is why these proteins have become the focus of many clinical therapies. ~10% of the human kinome have been classified as pseudokinases, because they lack at least one of the highly conserved motifs that were originally used to help define the protein kinase superfamily. Due to these deviations from the normal situation, pseudokinases were originally predicted to be catalytically inactive, often based solely upon bioinformatic sequence alignment evidence. However, the discovery of pseudokinases that can hydrolyze or bind to ATP either at, or below, the nucleotide concentrations typically found in cells, suggests that each pseudokinase requires a thorough and individual biochemical analysis using a combination of techniques in order to reveal its biological function.

Trib2 and NOK are two pseudokinases that contain a highly atypical 'DFG' metal ion binding motif, when compared to canonical kinase domains, and both are implicated in a variety of human cancers. Trib2 is predicted to be a Ser/Thr pseudokinase and is very closely related to the Trib1 and Trib3 pseudokinases in humans, and to the Tribbles pseudokinase that was originally characterized in the model fruit fly *Drosophila Melanogaster*. Along with an E3-ligase, Trib2 is required to target the tumor-suppressing transcription factor C/EBPα for degradation in cells. The results presented in this thesis include the first demonstration of a Mg^{2+} ion-independent ATP binding and autophosphorylation function for Trib2 *in vitro*.

NOK is a pseudokinase that exhibits similarity to the RPTK sub-family, however it does not have a detectable ligand-binding domain, but does contain a putative transmembrane domain that lies adjacent to the pseudokinase domain. Overexpression of NOK mRNA has been observed in a variety of cancers, but its mode of action is still unclear. I describe in this thesis that NOK localizes to the nuclear membrane of cells and contains a localization sequence that resembles the EGFR Nuclear Localization Sequence, which translocates to the nucleus via the Inner Nuclear Membrane.

Work described in this thesis also describes the development of tools to pave the way for future cellular analysis of both Trib2 and NOK, which will reveal whether these pseudokinases could be exciting, and novel drug targets in human diseases.

Contents

List of Figures and Tables

List Of Abbreviations

^{15}N	Stable ^{15}N isotope of Nitrogen (spin ½, suitable for NMR)
3’	Terminal hydroxyl end of DNA
5’	Terminal phosphate end of DNA
Å	Ångstrom
ABL	Abelson Kinase
ACC	Acetyl Co enzyme A Carboxylase
AcLDL	Acetylated low density lipoprotein
ADP	Adenosine diphosphate
ALL	Acute Lymphoblastic Leukaemia
AML	Acute Myeloid Leukaemia
Arg	Arginine
Asn	Asparagine
Asp	Aspartate
ATP	Adenosine triphosphate
BCR	Breakpoint cluster region protein
BSA	Bovine Serum Albumin
C/EBP	Ccaat-Enhancer binding protein
CAMK	Ca^{2+}/calmodulin-dependent protein kinase
CDC	Cell Devision Cycle
CDK	Cyclin dependent kinase
CML	Chronic Myeloid Leukaemia
CO_2	Carbon dioxide
COP1	Constitutive photomorphogenic protein 1
COSMIC	Catalogue of Somatic Mutations in Cancer
CRC	Colorectal cancers
CRISPR	clustered regularly interspaced short palindromic repeats

Cat-Spine	Catalytic Spine
Cy3	Cyanine Dye3
Cys	Cysteine
Da	Daltons
DAP	(N′2′-(4-aminomethyl-phenyl)-5-fluoro-N′4′-phenyl-pyrimidine-2,4-diamine, Dianilinopyrimidin
DAPI	4',6-diamidino-2-phenylindole
DDA	Data Dependent Acquisition
DMEM	Dulbecco's Moified Eagle Medium
DNA	Deoxyribonucleic Acid
DSF	Differential Scanning fluorimetry
DTT	Dithiothreitol
E. coli	Escherichia coli
ECL	Enhanced Chemiluminescence
EDTA	Ethylenediaminetetraacetic acid
EGFP	Enhanced Green Fluorescent Protein
EGFR	Epidermal Growth Facto Receptor
Ek	Enterokinase
ePK	Eukaryotic protein kinases
EPOR	Erythropoietin Receptor
ErbB	Erythroblastosis oncogene B (analogous to HER proteins)
ERK	Extracellular signal regulated kinase
ESI-MS	Electrospray Ioninsation Mass Spectrometry
FGFR	Fibroblast growth factor receptor
FITC	Fluorescence isothiocyanate
FPLC	Fast protein liquid chromatography
GF	Growth factor
Glu	Glutamate

Gly	Glycine
GSK3β	Glycogen synthase kinase beta
GST	Glutathione S-Transferase
GTP	Guanosine Triphosphate
HCCs	Hepatocarcinoma cells
HER	Human Epidermal growth factor Receptor
His	Histidine
HOXA9	Homeobox potein A9
HQSC	Heteronuclear single quantum coherence spectroscopy
IBD	Inflammatory Bowel Disease
IL8	Interleukin-8
IMAC	Immobilized metal affinity chromatography
INM	Inner Nuclear Membrane
IP	Immunoprecipitation
IPTG	Isopropyl-1-thio-β-D-galactosidase
JAK	Janus Kinase
JH	JAK homology
JM	Juxtamembrane
JNK	c-JUN N-terminal Kinases
KSR	Kinase Suppressor of RAS
LAP	Liver Enriched activator Protein
LB	Luria Bertani media
LC-MS/MS	Liquid chromatography-tandem mass spectrometry
LIC	Ligation Independent Cloning
LIP	Liver Enriched inhibitor Protein
LKB1	Liver kinase B1
Lys	Lysine

MAPK	Mitogen activated protein kinase
MBP	Myelin Basic Protein
MEK/MKK	Mitogen activated protein kinase kinase
mg	milligram
$MgCl_2$	Magnesium Chloride
min	minute
miRNA	micro RNA
ml	millilitre
MLKL	Mixed Lineage Kinase Domain Like
$MnCl_2$	Manganese Chloride
MO25α	Mouse protein 25α/Calcium binding protein 39
MR	Mutation Rate
MW	Molecular Weight (equivalent to Relative Molecular Mass)
NFκB	Nuclear factor kappa B
NH_4Cl	Ammonium Chloride
Ni-Sepharose	Nickel-Sepharose
nl	nanolitre
N-lobe	Amino terminal lobe
NLS	Nuclear Localisation Sequence
NMR	Nuclear Magnetic Resonance
NOC	Nocodazole
NOD/SCID	Non-obese/Severe combined immunodeficiency
NOK	Novel Oncogene with Kinase domain
NPC	Nuclear Pore Complexes
NSCLC	Non-Small Cell Lung Cancer
OD	Optical Density
p70S6k	p70 ribosomal S6 kinase

PAGE	Polyacrylamide Gel Electrophoresis
PBS	Phosphate Buffered Saline
PCR	Polymerase Chain Reaction
PDB	Protein Data Bank
PDGFR	Platelet-derived growth factor receptor
PFA	Paraformaldehyde
Phe	Phenylalanine
PI3K	Phosphoinositide 3-kinase
PKA	cAMP-dependent protein kinase/Protein Kinase A
P-loop	Phosphate binding loop
Pro	Proline
RAF	Rapidly Accelerated Fibrosarcoma Kinase
RNA	Ribonucleic Acid
RNF13	Ring finger protein 13
RO	Reverse Osmosis
RPTK	Receptor Protein Tyrosine Kinase
Reg-Spine	Regulatory Spine
SAC	Spindle Assembly Checkpoint
SDS	Sodium Dodecyl Sulphate
Ser	Serine
Sf9	Clonal isolate of Spodoptera frugiperda Sf21 cells
SgK	Sugen Kinase
SH	Src homology
shRNA	small hairpin RNA
siRNA	small interfering RNA
Slbo	Slow border cells
STRAD	STE20 Related kinase Adapter
STYK1	Serine Threonine Tyrosine Kinase

SuRTK106	Sugen Receptor Tyrosine Kinase 106
Tagg	Onset of aggregation temperature
TBS-T	TRIS buffered Saline and Tween-20
Tet	Tetracycline
Thr	Threonine
TLR	Toll-like Receptor
Tm	Melting Temperature
TM	Transmembrane domain
Trib	Tribbles Homologue
Trbl	Tribbles
TrCP	Transducin Repeat containing protein
TRIM	Tripartite motif protein
Tyr	Tyrosine
U	Units of activity for enzymes
Val	Valine
Ve	Elution Volume
Vo	Void Volume
VRK	Vaccinia Related Kinase
WNK	With no Lysine Kinase
YAP	Yes associated protein
Δ	Polypeptide deletion mutant
ΔTm	Melting temperature difference
$\gamma^{32}P$	The phosphate in the gamma position of ATP labelled with 32-phosphorous
μCi	microCurie

CHAPTER 1. Introduction

1.1 **Protein Kinases**

Kinase domains transfer the terminal phosphate group from a donor (usually ATP, rarely GTP) to a protein-based substrate and this can transduce an extracellular signal towards the nucleus by the propagation of a kinase cascade, e.g. the MAPK pathway (Figure 1.1A). There are a variety of substrates that can be phosphorylated, and protein kinases, of which there are 518 in the human protein kinome (Manning *et al.*, 2002), are by far the best studied class of kinase. To elicit a cellular response, protein kinases usually hydrolyse the gamma phosphate from ATP and transfer it to a substrate residue, which changes its charge and structure (Vulpetti and Bosotti, 2004). To perform this function, a set of motifs that are conserved throughout the human kinome have evolved and the presence of these motifs in polypeptides classifies them as kinase domains. On the other hand, protein phosphatases act to hydrolyse the phosphorylated amino acid, reverting the protein substrate to an alcohol (OH) group and releasing a phosphate group (PO_4^{3-}, Figure 1.1B). In addition to modification of alcoholic side chains on proteins, lipids are also phosphorylated by related kinases termed lipid kinases, e.g. PI3 kinase (Foster *et al.*, 2003, Cheek *et al.*, 2005) or sphingosine kinase (Plano *et al.*, 2014). Modification of sugars by phosphorylation is also common, e.g. glucokinase phosphorylates glucose (Peter *et al.*, 2011). The structure of human protein kinase domains has been analysed using a variety of approaches, including X-ray crystallography and NMR spectroscopy (Shin *et al.*, 2011, Toms *et al.*, 2013).

Protein kinase domains are bilobal in structure, with a small 'N-lobe', which comprises a β-sheet that consists of 5 anti-parallel strands and an important helix termed the α-C helix, which together form the ATP-binding surface, whilst the predominantly α helical C-lobe consists of the residues directly involved in catalysis. The active site, where ATP and the protein substrate binds, is located in a cleft between the two domains, with the motifs that are critical for stabilizing ATP and hydrolyzing the phosphate group lining the surface of the cleft (Figure 1.2A) (Hantschel and Superti-Furga, 2004, Hanks and Hunter, 1995, Manning *et al.*, 2002).

The best understood motifs that are conserved throughout the human kinome, which together define the protein kinase domain are, from N- to C-terminus, a glycine-rich loop, a conserved lysine in the β3 sheet, a conserved glutamate within the αC helix, a catalytic loop, a magnesium ion binding loop, (Figure 1.2B) and an Asp residue in the otherwise hydrophobic αF helix (Figure 1.2A).

A

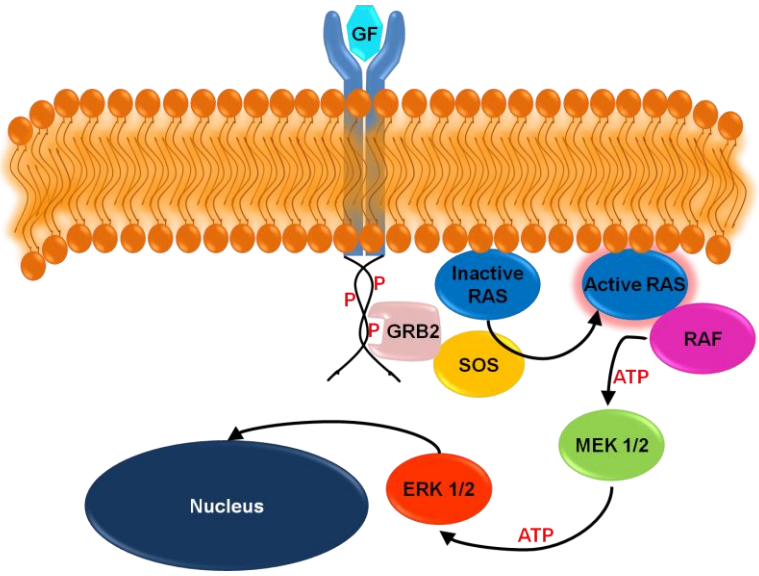

B

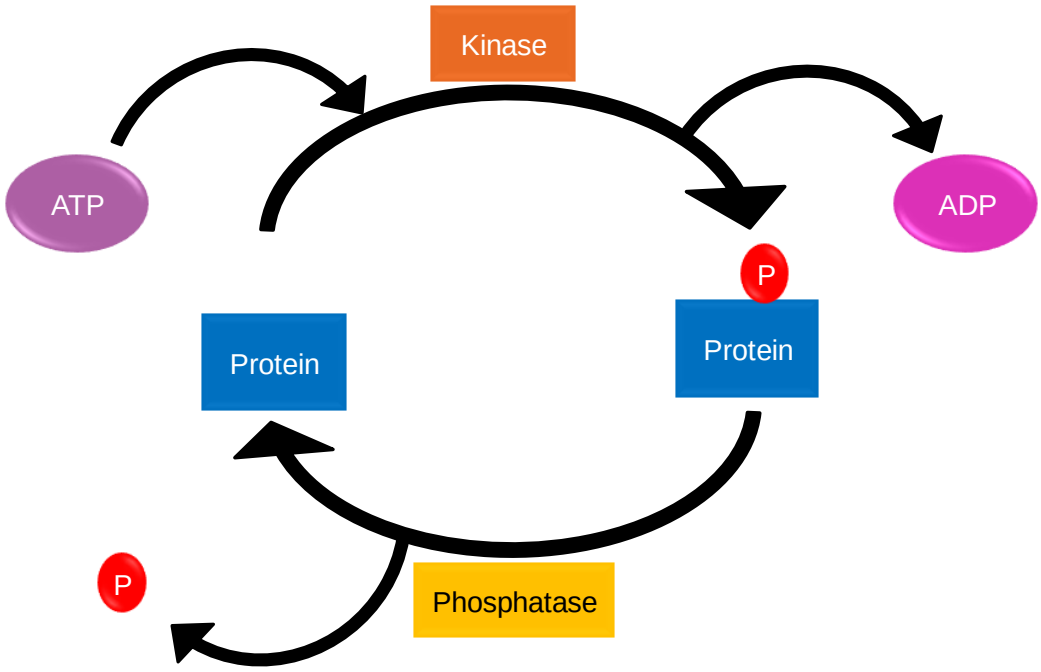

Figure 1.1 Protein kinases phosphorylate substrates and trigger kinase cascades A) A cartoon of the ERK pathway stimulated by the binding of a growth factor (GF) to a monomeric RPTK, which dimerises and stimulates trans-receptor autophosphorylation, causing interacting proteins to bind, which activates further intracellular proteins and kinases, propagating the signal into the cell and often towards the nucleus. B) A simplified diagram showing the opposing functions of protein kinases and phosphatases.

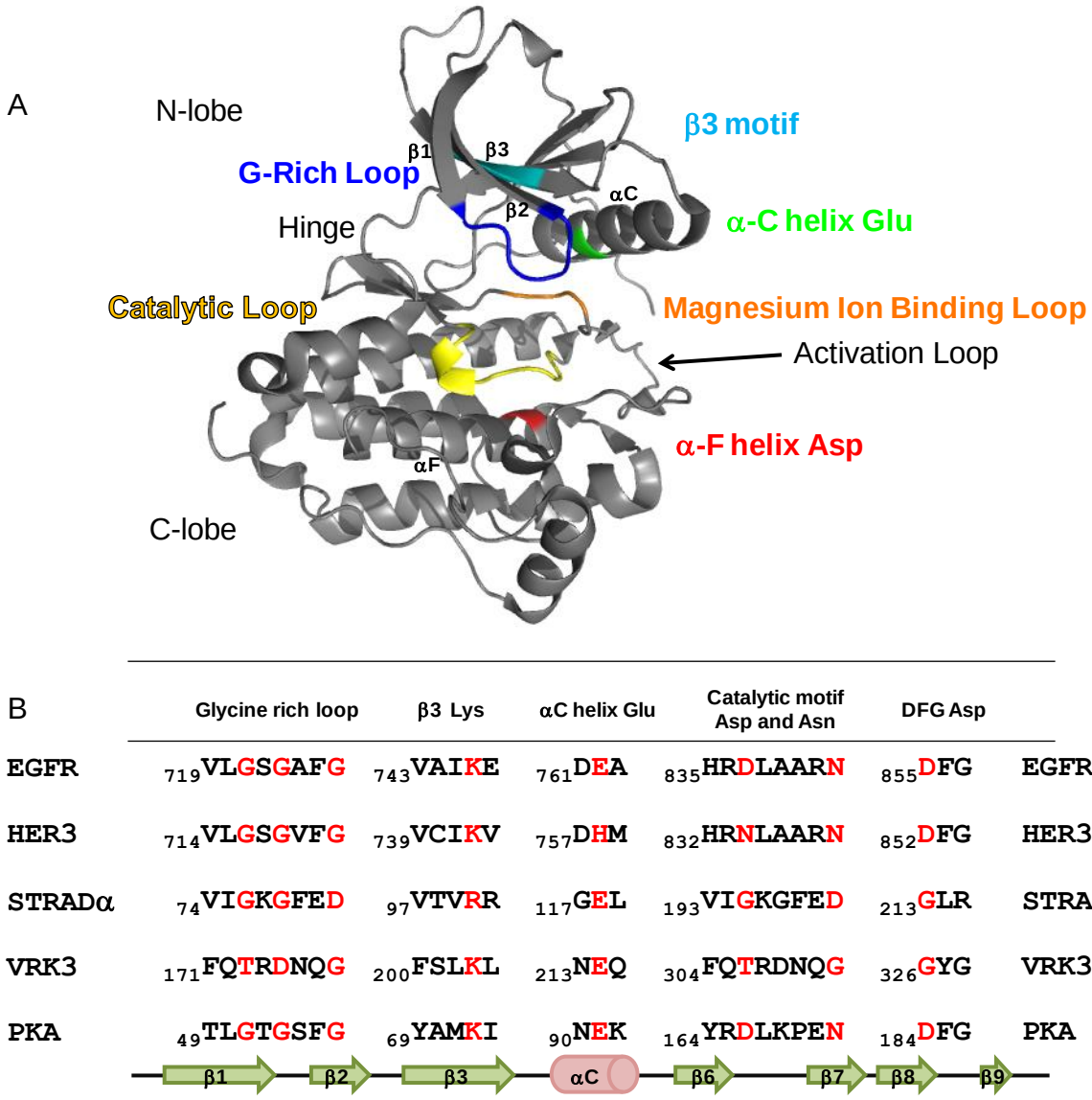

Figure 1.2 Conserved kinase residues annotated on the kinase domain of EGFR A) The EGFR kinase domain (PDB ID 1M14) with the glycine-rich loop highlighted in blue, the β3 motif highlighted in cyan, the conserved glutamate residue in the C helix in green, the catalytic loop in yellow, the magnesium ion binding residue in orange and the Asp of the F helix in red. The activation loop situated between the DFG and APE motifs is marked by the arrow and the helices and sheets are numbered accordingly B) A comparison of the conserved kinase domain motifs for the two canonical kinases PKA and EGFR, and the three pseudokinases HER3 STRADα and VRK3. The conserved residues are highlighted in red and the secondary structures represented above the sequences. Beta sheets are a green arrow and helices are pink cylinders.

1.2.1. The glycine-rich loop

The consensus sequence of GxGxxG forms part of a β-turn-β motif between the β1 and β2 strands, with the second Gly residue considered to be the most important for functional ATP binding. The purpose of the glycine-rich loop is to bind and expose the γ-phosphate of ATP to the solvent for catalysis. The glycine-rich loop is inherently flexible and the presence of the Gly residues minimizes steric hindrance so that the loop can clamp down on ATP, placing the gamma phosphate in an accessible position for phosphotransfer. The flexibility of the loop also enables hydrogen bonds to form between the backbone and ATP, orientating it in the binding pocket. By correctly orientating ATP, the glycine-rich loop can control the rate of phosphotransfer and directly affect ATP affinity (Barouch-Bentov *et al.*, 2009, Scheeff *et al.*, 2009, Taylor and Kornev, 2010).

1.2.2 The β3 motif conserved lysine

A positively charged Lys residue that is conserved in the β3 sheet of canonical kinases coordinates the α and β phosphate groups of ATP, which stabilizes and correctly aligns ATP (Hanks and Hunter, 1995). Mutation of this Lys to Arg, or more effectively, an uncharged side chain reduces the activity of many protein kinases (Iyer *et al.*, 2005b), and is often used to create inactive protein kinase mutants. The hydrophobic motif, in which the conserved Lys is typically located (VAIK) also stabilises the adenine ring of ATP (Taylor and Kornev, 2010), however, it has been hypothesised that the lysine might be involved with catalysis rather than ATP binding because a β3 lysine mutation in pp56lck could still bind to ATP but transfer of the phosphate group to a substrate was impaired (Carrera *et al.*, 1993). Currently, the lysine residue is thought to be involved in an ionic interaction with ATP in most protein kinases (Adams, 2001), in addition to the formation of a critical salt bridge (see below).

1.2.3 A conserved glutamate in the αC helix

The C helix of many kinase domains contains a conserved glutamate residue, which forms a salt-bridge with the conserved β3 Lys residue only when the kinase is in a catalytically active conformation. This alignment of residues also aids the correct positioning of the ATP into the correct orientation for catalysis (Huse and Kuriyan, 2002, Taylor and Kornev, 2011). The conserved Glu residue is present in most, but not all, kinases with catalytic activity, although its precise position in the

N-terminal αC helix varies, and it is not embedded in a specific amino acid motif, making it hard to identify specifically using bioinformatics.

1.2.4 The catalytic loop

The motif that contains the amino acid residues HxDxxxxN is termed the catalytic loop. The Asp residue in this motif acts as the catalytic base and accepts a proton from the OH group of the protein substrate phosphate acceptor group (typically Tyr/Ser/Thr) (Huse and Kuriyan, 2002). The catalytic Asp is, in part, orientated by the Asn at the end of the motif, which also helps to coordinate one or two Mg^{2+} ions in collaboration with the DFG motif (see below). Mutations in the Asn residue have historically been used to create inactive kinases, often by mutating the residue to Ala, since the divalent cation(s) also stabilise the highly negative charge of the three ATP phosphate groups and loss of this interaction abolishes kinase activity (Hanks and Hunter, 1995). In addition, the His that begins the motif (HxD) makes hydrophobic contacts between the Phe from the DFG motif (and builds the hydrophobic spine of active kinases) and also interacts with the DFG Asp (Kornev *et al.*, 2006). Finally, the 'x' residue in the HxD motif is often an Arg, especially in active kinases that are regulated by phosphorylation, since it interacts with phosphorylated amino acids in the activation loop (Bayliss *et al.*, 2012).

1.2.5 The magnesium ion binding loop or 'DFG' motif

The main role of the Mg^{2+} ion binding loop, which is also termed the DFG motif, is to coordinate a second Mg^{2+} ion, which has the same role as the first bound by the Asn described above, to stabilize the negatively charged phosphates of ATP. Mutation of the Asp in the DFG motif to either Asn or Ala (both uncharged and unable to bind metals), is perhaps the best way to inactivate canonical protein kinases, which usually require ATP/Mg complexes for activity (Haydon *et al.*, 2003). In addition, the conserved Phe in the DFG motif also makes hydrophobic contacts with the residues in the catalytic loop, and helps to position the αC helix correctly to stimulate formation of the Lys-Glu salt bridge (Kannan and Neuwald, 2005). The Gly of DFG helps facilitate the correct positioning of the Asp of the DFG motif, explaining the very strong conservation of the complete DFG motif in most active kinases. When the kinase is in an inactive conformation, a hydrogen bond between the Gly and the Asp is disrupted and the Asp can move by as much as 140˚ without steric hindrance and in this position is unable to coordinate magnesium ions (Kornev *et al.*, 2006). Rotational movement of the kinase domain is a way of

switching the kinase from an inactive conformation to an active one. The 'DFG-in' conformation, when the Phe is placed in the ATP binding pocket, is typically the conformation found in an 'active' kinase, whereas an 'inactive' kinase, 'DFG-out' conformation does not have the Phe residue within the ATP binding site, but it has been "flipped" out (Taylor and Kornev, 2010, Xu *et al.*, 2011, D'Abramo *et al.*, 2014).

1.2.6 The αF helix

The Regulatory (Reg) spine of the kinase domain is made up of hydrophobic amino acids that are not related in sequence, but form a column-type structure in three dimensions (Taylor and Kornev, 2010). The Reg spine is anchored to the N terminus of the hydrophobic F-helix, whilst the Catalytic (Cat) spine terminates at the C terminus of the F-helix. The spines constitute hydrophobic spatial motifs and the Reg spine can be assembled or disassembled by varying the flexibility of the αC helix and activation loop. The Cat spine is formed from the Ala residue in the VAIK motif in the β3 sheet and this interacts with the adenine ring of ATP which forms part of the Cat spine. The catalytic loop is kept rigid by its interactions with the F-helix. The αF helix contains only one charged Asp residue, and this interacts with the backbone of the catalytic loop. The F-helix and the two spines coordinate and connect the different segments of the kinase and are therefore key during activation and inactivation cycles undergone by the kinase domain (Taylor and Kornev, 2010, Kornev *et al.*, 2008).

1.2 Common phosphate acceptor residues of protein substrates

The most widely studied protein kinases phosphorylate either tyrosine (Tyr) or serine and threonine (Ser/Thr) residues, or Ser, Thr *and* Tyr residues (dual-specificity kinases) (Douville *et al.*, 1994), although there are examples of kinases that phosphorylate arginine or histidine residues as substrates *in vitro*, these are not closely related to the eukaryotic protein kinases (Cheek *et al.*, 2002). The diverse loops on the surface of the kinase are what provides the conserved fold with its different substrate specificities (Taylor and Radzioandzelm, 1994). For example, simple analysis of the catalytic loop sequences from human kinases can be used to help determine whether phosphorylation substrates are likely to be Tyr residues or Ser/Thr residues. The catalytic motif of tyrosine kinases have the common consensus sequence of RDx(A/R)A(A/R)N, whilst Ser/Thr kinases often possess an RDxKxxN

motif, which also resembles the consensus motif of dual-specificity kinases (Okamoto *et al.*, 2014, Hanks *et al.*, 1988, Lindberg *et al.*, 1992).

1.3 **Kinase domain activation**

There are a variety of methods that kinases use to become fully active. cAMP-dependent protein kinase (PKA), which is termed an 'RD kinase,' due to the Arg residue that is adjacent to the catalytic Asp in the HRD motif, is activated by the phosphorylation of a Thr197 residue located within its activation loop. The activation loop is a highly flexible loop that is situated between the two tripeptide sequences DFG and APE in catalytic subdomain VII and VIII, and a key site of phosphoregulation. Following phosphorylation of Thr197, the phosphate group coordinates the C helix (His 87), the Catalytic loop (Arg165), the β9 sheet (Lys189) and the activation loop (Thr195) and the K_m for ATP decreases 7 fold (Steichen *et al.*, 2010), reflecting the appearance of the active conformation.

Tyrosine kinases are also activated by phosphorylation. For example, both the Fibroblast Growth Factor Receptor (FGFR) and Insulin-like Growth Factor Receptors autophosphorylate following dimerisation of the receptor domains. The autophosphorylation relieves the inhibition caused by the activation loop, which occludes the active site for the protein substrate to bind to (Lemmon and Schlessinger, 2010). PDGFR family member, c-Kit is inhibited by its juxtamembrane domain, not its activation loop. It is not phosphorylation of a Tyr residue in the activation loop of c-Kit that destabilises the autoinhibitory interactions but instead the phosphorylation of 14-22 Tyr residues in the c-Kit juxtamembrane domain, the kinase insert domain (a variable length of sequence between the αC and αD helices in the C-terminal domain found in many RPTKs), the C-terminal domain and the activation loop (DiNitto *et al.*, 2010, Lemmon and Schlessinger, 2010). It is not one phosphorylation event that causes this dynamic shift, as observed for FGFR, but a combination of phosphorylation events that together causes activation. The equivalent residue in c-Kit (Y823) to the FGFR activating tyrosine is phosphorylated, but only after the kinase has been 90% activated by phosphorylation elsewhere.

Kinase domains can also be autoinhibited, not by occlusion of the substrate binding site with the C-terminal tail (a region outside the catalytic domain), but through binding interactions that lock the protein into an inactive conformation. For

example, the tyrosine kinase Src has an SH2 group that binds to phosphorylated Tyr527, which is phosphorylated by Csk. An SH3 group in the C-terminal tail of Src binds to a polyproline type-II helix which is located between the kinase domain and the SH2. This positions the αC helix in a conformation where a salt bridge cannot form between the conserved C-helix Glu residue and the β3 sheet conserved Lys, and so ATP is incorrectly orientated. The SH2 interaction with phosphotyrosine stabilizes this conformation (Hubbard, 1999).

Other kinases require the presence of separately encoded interacting proteins to attain full catalytic activity along with phosphorylation. Cyclin-dependent kinases for instance, require a specific cyclin protein to become activated. In cells, monomeric CDK2 is inactive and requires cyclin E at the G1/S transition and cyclin A throughout S phase for activity. CDK2 activity is inhibited by phosphorylation of either Tyr15 or Thr14 by Wee1 and this is independent of cyclin status, whereas the activating phosphorylation of Thr 160, in the activation loop, requires the presence of the cognate cyclin molecule. However, the phosphorylated complex is inactive until the inhibitory phosphates at either Thr14 or Tyr15 are removed by the CDC25 phosphatases (Bartova *et al.*, 2004).

Another protein that requires the presence of an additional protein to achieve full catalytic activity is Aurora A. Phosphorylation of Aurora A Thr288 in the activation loop is crucial for catalytic activity (Bayliss *et al.*, 2003), however catalytic activity is increased *in vitro* following TPX2 binding (Eyers *et al.*, 2003) with the presence of TPX2 and phosphorylation of Thr288 acting synergistically to activate Aurora A (Dodson and Bayliss, 2012). The phosphorylated activation segment of Aurora A lies in an inactive conformation when TPX2 is absent and binding to TPX2 induces a 10 Å shift of the phosphorylated Thr288 from an exposed to a buried position, which prevents dephosphorylation of the activating phosphate group by protein phosphatases (Bayliss *et al.*, 2003).

Other kinases however, such as the EGFR family, do not employ phosphorylation-mediated switches for catalytic activation but are moved into an active conformation by allosteric interactions following asymmetrical dimerisation after EGF binding. The juxtamembrane domains of each EGFR member of the dimer form a ‘juxtamembrane latch’ between the C-terminal half of the juxtamembrane segment (JM-B) from the ‘receiver kinase’ N-lobe to the ‘activator kinase’ C-

terminal lobe along with short anti-parallel helices forming by both the activator and receiver JM-A segments (N-terminal sections of the juxtamembrane domains) that link to the C terminal sides of the dimeric transmembrane helices. Extracellular ligand binding induced dimerisation stabilizes the helical JM-A dimer, which in turn stabilizes the kinase domain dimer, activating the kinase domain. Ligand-independent activation by alternative dimers can be prevented by the C-terminal tails inhibiting the formation of the 'juxtamembrane latch' creating a dimer of inactive kinase domains (Jura *et al.*, 2009a).

1.4 Protein kinases and cancer

Most tumors appear after more than one genetic mutation has accumulated in a cell. However, a single mutation in a gene that encodes a protein kinase domain can significantly increase the oncogenicity of the cells by either promoting cell proliferation or reducing tumour suppressor function (Tsatsanis and Spandidos, 2000). A few of the many kinases implicated in human cancers are briefly described below.

ErbB2 is a Receptor Protein Tyrosine Kinase that is overexpressed in ~30% breast cancers and these often have poor clinical outcomes, with overexpression of ErbB2 implicated in increased metastasis of tumors and therapeutic resistance (Yu and Hung, 2000). The extracellular portion of ErbB2, whose kinase activity is regulated in conjunction with the pseudokinase ErbB3 (HER3, see below) is a target for the therapeutic antibody Herceptin (Nahta and Esteva, 2006).

The fusion protein BCR-Abl drives the development of chronic myelogenous leukemia (CML). The fusion is caused by the translocation of the Abl locus on chromosome 9 to the BCR locus on chromosome 22, t(9;22)(q34;q11) (Cilloni and Saglio, 2012). This fusion halts the translocation of BCR-Abl to the nucleus and prevents Abl induced apoptosis (Vigneri and Wang, 2001). The fusion kinase initiates downstream proliferative pathways by being in a constitutively active conformation and so phosphorylates more substrates and also increasing autophosphorylation, which subsequently recruits more adapter molecules leading to feed-forward activation (Salesse and Verfaillie, 2002).

BRAF is a Ser/Thr kinase that lies at the head of the ERK signaling pathway (Figure 1.1A) and phosphorylates the dual-specificity kinases MEK1/2, which in turn activates ERK1/2 by phosphorylation on Tyr and Thr residues. Multiple ERK targets are known, and include other kinases and transcriptional programmes

associated with proliferation. Inappropriate regulation of this pathway can trigger the onset of tumourigenesis, due to uncontrolled cell growth and/or lack of apoptosis. Ninety percent of BRAF mutations that drive cancers occur in the residue Val 600, which is commonly mutated to a glutamate in melanoma patients (Qin *et al.*, 2012). This can increase its activation 500 fold, causing constitutive downstream activation of the MEK/ERK even in the absence of extracellular signals (Cantwell-Dorris *et al.*, 2011). This example of kinase activation by mutation vividly illustrates how subtle changes in the composition of kinase catalytic domains can change their activity so markedly, and not surprisingly, these mutant kinases are excellent drug targets.

1.5 Protein kinases as drug targets

Small molecules that target kinases have become a major research focus for developing new cancer therapeutics, with ~150 being developed for clinical exploitiaton (Fabbro *et al.*, 2012). Small molecules that target the ATP binding pocket can be classified as either Type I or Type II inhibitors. Type I inhibitors bind to the ATP binding site when it is in an 'active' conformation and the DFG motif can coordinate a magnesium ion and the Phe places the αC helix and activation loop into a position primed for catalysis (Fabbro *et al.*, 2012). The inhibitor mimics the binding of the adenine ring of ATP by forming between 1-3 hydrogen bonds with the hinge region residues (Zhang *et al.*, 2009, Liu and Gray, 2006). Dasatinib is a type I inhibitor, which binds to the ATP binding site of the active Abl kinase domain. The aminothyazole of Dasatinib sits into the space that is normally occupied by the ATP adenine ring, whilst two hydrogen bonds form between Dasatinib and Met318 (one to the carbonyl oxygen and one to the amide nitrogen), whilst another hydrogen bond forms between the oxygen hydroxyl oxygen from the Thr315 sidechain (Tokarski *et al.*, 2006) which is the Abl gatekeeper residue (Weisberg *et al.*, 2010), and Dasatinib can bind to the majority of Abl mutants apart from the Abl T315I gatekeeper residue mutation (Tokarski *et al.*, 2006).

Another example of an inhibitor that binds to BCR-Abl is Imatinib (Glivec/Gleevec), which in 2001 was the first kinase inhibitor to be clinically approved. Imatinib is a Type II inhibitor that can only bind to the ATP active site and gain access to the adjacent hydrophobic pocket when the DFG motif is in an 'inactive' conformation (DFG-out) (Treiber and Shah, 2013, Kufareva and Abagyan, 2008). Hydrogen bonds formed between Imatinib and the hinge region Met318

backbone NH, the gatekeeper Thr315 side-chain hydroxyl, the αC helix Glu286 and the backbone Asp381 from the DFG motif. Ile360 and His361 make contacts with the tail of imatinib and the pyrimidine ring forms π-stacking interactions with the P-loop Tyr253 and the DFG Phe382. Hydrophobic residues are exposed following the movement of the DFG motif into the 'out' conformation and the benzamide group of Imatinib sits in this pocket (Blanc *et al.*, 2013), preventing kinase activation and activity.

1.6 **Protein pseudokinases**

Pseudokinases are so called because they lack one or more of the motifs discussed above that are generally conserved throughout kinase domains, and which are found in nearly all catalytically active protein kinases (Manning *et al.*, 2002). Approximately 10% of the human kinome are termed pseudokinases, with approximately 50 being documented (Eyers and Murphy, 2013, Reiterer *et al.*, 2014). When their locations are highlighted on the human kinome phylogenetic tree, it can be seen that each of the ~7 major subfamilies of kinases contains at least 1 pseudokinase (Boudeau *et al.*, 2006). This suggests that pseudokinases evolved independently from one another and explains why different pseudokinases have evolved deviations in the different motifs that are associated with ATP binding and catalysis (Manning *et al.*, 2002, Boudeau *et al.*, 2006).

Pseudokinases were initially predicted to be 'catalytically inactive' because they lacked either the β3-sheet Lys residue, the catalytic Asp of the catalytic loop, or the Asp residue located within the DFG motif that usually binds a magnesium ion (Boudeau *et al.*, 2006). Depending upon their polypeptide sequence, pseudokinases were grouped as either modulators of other catalytic domains, which included proteins that contained a pseudokinase domain alongside a second 'active' domain (such as the JAK kinases), or if the pseudokinases retained a high similarity to a protein kinase domain, then they were grouped together. A final group consisted of polypeptides that all had a lower sequence similarity to canonical protein kinases, and were considered to be inactive based on this difference (Manning *et al.*, 2002).

Following initial annotation and analysis of the human genome in 2001, the human kinome was loosely divided into kinases and pseudokinases in 2002 (Manning *et al.*, 2002). However, additional sub-groups of pseudokinases have recently been added, based on further sets of experimentally-identifiable criteria. For

example, pseudokinases have been grouped together depending upon which of the important catalytic residues they lack, either individually, or in combination, amongst the DFG Asp, HxD catalytic Asp, and the conserved Lys in the β3 sheet (Boudeau *et al.,* 2006). Throughout the eukaryotic protein kinome, each of these motifs are highly conserved but the conservation does vary slightly amongst known active kinases, with the Lys in the β3 'VAIK' motif conserved amongst 98% of canonical kinases, but the catalytic Asp being present in a slightly smaller proportion of kinases (93%) and leaving only 3% of the eukaryotic kinome having evolved a non-classical DFG metal- binding Asp residue (Kannan *et al.*, 2007). Table 1.1 summarizes the human complement of pseudokinases and the sequence deviations found upon comparison with typical kinases (Eyers and Murphy, 2013).

Pseudokinase	Motif(s) Mutated
Consensus	**D**FG
CASK	GFG
PTK7	ALG
SgK223	NFL
SgK269	NFS
SgK495	NFC
NOK	GLG
RSKL1	YFS
RSKL2	YFG
Titin	EFG
Trib1	SLE
Trib2	SLE
Trib3	NLE
Consensus	HX**D**
ANPα	HGN
ANPβ	HGS
HSER	HGR
CYGD	HGR
CYGF	HGR
HER3	HRN
ILK	RHA
IRAK3	CQS
JAK1 (JH2)	HGN
JAK2 (JH2)	HGN
JAK3 (JH2)	HGN
TYK2 (JH2)	HGN
PSKH2	HRN
SgK071	HRN
SgK396	HGS
VACMKL	HRN
Consensus	β3 K
WNK	C
KSR1	R
KSR2	R
Consensus	β3 K/HX**D**
GCN2	Y/HKV
PXK	S/YGH
Consensus	β3 K/**D**FG
ULK	L/NFC
Consensus	HX**D**/**D**FG
IRAK2	HSN/HPM
MLKL	HGK/GFE
SgK307	HRS/NLE
Pseudokinase	**Motif(s) Mutated**
Consensus	β3 K/HX**D**/**D**FG
EphA10	H/HRG/GFG
EphB6	Q/HRS/RLG
NRBP1	N/HGN/SVA
NRBP2	N/HGN/SVW
SCYL1	F/HNN/GLD
SCYL2	F/HGN/GFD
SCYL3	F/HNN/GME
SgK196	S/TRV/NFS
STRADa	R/HRS/GLR
TBCK	N/HRA/KFG
TRRAP	M/LNR/YFR

Table 1.1 A summary of the human pseudokinases and their deviant motifs A compilation of human pseudokinases grouped by their non-canonical kinase motifs (adapted from (Eyers and Murphy, 2013)).

Following biochemical and structural studies, it became apparent that some pseudokinases were actually catalytically active, and able to transfer phosphate from ATP to a substrate at a rate above background levels detected with non-kinase proteins, or that of canonical protein kinases that had been inactivated by mutation (Eyers and Murphy, 2013). Moreover, during the past twenty years a selection of pseudokinases have been shown to bind to ATP but have so far not demonstrated the ability to transfer the gamma phosphate group to a substrate in the conditions tested, whilst some have been proven to lack ATP binding altogether (Scheeff *et al.*, 2009). Therefore, a new pseudokinase grouping system was suggested by Zeqiraj and van Aalten in 2010, which segregated pseudokinases into one of four groups. Group 1, predicted pseudokinases, pseudokinases for which there is currently no structural or biochemical evidence that can help define whether they are able to bind ATP. Group 2, pseudokinases, this group contains pseudokinases that cannot bind to ATP, or which do bind ATP (often weakly), but for which no catalytic activity has been determined. Group 3, for 'low activity pseudokinases,' which are pseudokinases that do phosphorylate a substrate but whose activity is much lower than that of typical kinases, and Group 4 'active pseudokinases' are pseudokinases that are catalytically active, with high activity comparable to classically-active kinases even though they lack the 'full' complement of canonical kinase domain residues (Zeqiraj and van Aalten, 2010). Although this classification is useful, it does not really separate kinases based on their intrinsic ability to regulate a cellular function dependent on nucleotide binding, and places pseudokinases that can and cannot bind ATP into the same grouping. Recently, a fluorescence based thermal denaturation assay was utilized to further stratify pseudokinase domains into 4 groups based upon their nucleotide and cation-binding abilities. According to this nomenclature, Class 1 pseudokinases do not bind to either a nucleotide or divalent cations, Class 2 pseudokinases bind to nucleotides, whilst Class 3 bind to divalent cations (but not detectably to nucleotides). Finally, Class 4 pseudokinases, on the other hand, demonstrate the ability to bind to both nucleotides and divalent cations (*i.e.* $Mg^{2+/}$ATP), similar to the conventional protein kinases (Murphy *et al.*, 2014b).

As more biochemical and structural evidence concerning ATP binding and catalytic activity is generated, the 'classes' that the pseudokinases have been somewhat arbitrarily grouped into will undoubtedly alter depending upon the type (and nature) of the evidence obtained. Current classifications for a selection of

pseudokinases and the supporting evidence based on the current literature have been summarized in Table 1.2.

There are a variety of methods discussed in the literature that have been used to detect ATP binding. Structural methods, such as X-ray crystallography, initially require high concentrations of protein and the identification of appropriate buffers that facilitate the formation of protein crystals. Radiometric kinase assays are highly sensitive but require the use of radioactive nuclides (Lilienthal *et al.*, 2010) and require the covalent incorporation of the γ-phosphate for detection, and as discussed previously, pseudokinases such as STRADα (Zeqiraj *et al.*, 2009b), bind but do not hydrolyse ATP and therefore radioactive assays are not always suitable. One alternative method utilises fluorescent ATP analogues such as 2',3'-*O*-(2,4,6-Trinitrophenyl)ATP (TNP-ATP) or 2'(3')-*O*-(N-methylanthraniloyl)ATP (mant-ATP). When either of these analogues enters a hydrophobic environment (such as an ATP binding pocket), the fluorescence increases (Lucet *et al.*, 2013), allowing for easy detection. Alongside DAP, these ligands have been used for the analysis of the nucleotide binding properties of the pseudokinases STRADα (Zeqiraj *et al.*, 2009a, Zeqiraj *et al.*, 2009b), CASK (Mukherjee *et al.*, 2008), JAK2 (Ungureanu *et al.*, 2011) and HER3 (Shi *et al.*, 2010). However, following the analysis of the binding affinities of a variety of nucleotide binding proteins with TNP-ATP, including to the histidine kinase CheA (Stewart *et al.*, 1998), it was revealed that some (non-kinase) proteins bind to TNP-ATP with an affinity that is 1-3 orders of magnitude greater than ATP (Hiratsuka, 2003, Weber and Senior, 1997, Murphy *et al.*, 2014b, Bilwes *et al.*, 2001). ATP can also be immobilized upon an agarose or Sepharose affinity matrix, and these pull-down experiments using purified protein are relatively simple and inexpensive to perform. ROP5 (*T. gondii*) and HSER (GUCY2C) were both identified as ATP binding pseudokinases using this method (Reese and Boothroyd, 2011, Jaleel *et al.*, 2006). The pseudokinase ILK can also bind to ATP and this has been demonstrated not only by using an ATP affinity matrix (Becher *et al.*, 2013) but also by isothermal titration calorimetry (ITC) (Fukuda *et al.*, 2009). ITC confirmed that human MLKL could bind to ATP, and the K_d value determined in this experiment was comparable to the value obtained by differential scanning fluorimetry (DSF) (Murphy *et al.*, 2014b). One limitation for ITC compared to DSF is the need for large amounts of purified protein, but for DSF only 2-5 μg protein is required, and providing the kinase/pseudokinase of interest is the major species in

the assay mixture then the signal is not affected (Murphy *et al.*, 2014b). This technique is also applicable to rapid, high throughput screening by using either 96 or 384 well plates (Murphy *et al.*, 2014b, Niesen *et al.*, 2007, Lucet *et al.*, 2013).

In the next section, I discuss the available literature on pseudokinases, which includes members of the Tribbles pseudokinase family and the NOK pseudokinase, which are the subject of this thesis.

Pseudokinase nomenclature	Evidence in the literature for ATP binding/hydrolysis?	Pseudokinase class	Pseudokinase group
CASK	Yes, crystal structure and phosphorylation (Mukherjee *et al.*, 2008)	Class 2	Low activity pseudokinase
EphB6	Yes, binds to ATP (+GTP) (Murphy *et al.*, 2014b)	Class 2	Pseudokinase
ErbB3	Yes, phosphorylation and crystal structure with ATP mimetic (Shi *et al.*, 2010)	Class 4	Low activity pseudokinsae
GCN2	No thermal protective effect imparted by ATP (Murphy *et al.*, 2014b)	Class 1	Pseudokinase
GUCY2C/HSER	Yes, binds to ATP-agarose (Jaleel *et al.*, 2006)	Class 2	Pseudokinase
ILK	Yes, binds ATP but is not hydrolysed (Fukuda *et al.*, 2009)	Class 2	Pseudokinase
IRAK2	Possible autophosphorylation (Wesche *et al.*, 1999)but queried (Pauls *et al.*, 2013), binds ATP and cation (Murphy *et al.*, 2014b)	Class 4	Pseudokinase
IRAK3	Possible autophosphorylation (Wesche *et al.*, 1999) but queried (Pauls *et al.*, 2013)	Class 1	Pseudokinase
JAK1 JH2	No autophosphorylation detected and structural study suggests activation loop blocks phosphoacceptor (Toms *et al.*, 2013) but binds ATP and divalent cation (Murphy *et al.*, 2014b)	Class 4	Pseudokinase
JAK2 JH2	Yes, autophosphorylates (Ungureanu *et al.*, 2011)	Class 4	Low activity pseudokinase
KSR1	Yes, binds ATP and suggestion it can phosphorylate MEK (Hu *et al.*, 2011a)	Class 4	Low activity pseudokinase
KSR2	Yes, phosphorylation of MEK1 and crystal structure bound to ATP (Brennan *et al.*, 2011)	Class 4	Low activity pseudokinase
MLKL	Binds to ATP but is catalytically inactive (Murphy *et al.*, 2014a)	Class 2	Pseudokinase
NRBP1	Does not detectably bind to ATP/ions (Murphy *et al.*, 2014b)	Class 1	Pseudokinase
PEAK1/SgK269	Binds to divalent cations only (Murphy *et al.*, 2014b), contrasting catalytic behavior reported (Kelber *et al.*, 2012)	Class 3	Pseudokinase
PTK7	Not catalytically active (murine) when assayed *in vitro* (Jung *et al.*, 2004). Does not bind ATP/ions (Murphy *et al.*, 2014b)	Class 1	Pseudokinase
RYK	Catalytically inactive (Hovens *et al.*, 1992). Does not bind ATP/ions (Murphy *et al.*, 2014b)	Class 1	Pseudokinase
SCYL1	No detectable ion or nucleotide binding ability (Murphy *et al.*, 2014b)	Class 1	Pseudokinase
SgK071	Binds to ATP + divalent cations (Murphy *et al.*, 2014b)	Class 4	Pseudokinase
SgK196	Yes, phosphorylates O-mannose (Yoshida-Moriguchi *et al.*, 2013)	Class 4	Low activity pseudokinase
SgK223/Pragmin	No detectable ATP or cation interaction (Murphy *et al.*, 2014b)	Class 1	Pseudokinase
SgK495	Yes, binds ATP in absence of divalent cations (Chapter 4). Not catalytically active	Class 2	Pseudokinase
STRADα	Yes, structurally shown to bind to ATP (Zeqiraj *et al.*, 2009b)	Class 2	Pseudokinase
Trib2	Yes, autophosphorylates and binds to ATP in the absence of divalent cations (Chapters 3 and 4)	Class 2	Low activity pseudokinase
Trib3	Yes, evidence for autophosphorylation (Chapter 3)	Class 2	Low activity pseudokinase
TYK2	ATP binding not detected (Murphy *et al.*, 2014b), but a crystal structure of TYK2 pseudokinase domain bound to an ATP competitive inhibitor has been deposited in PDB (3ZON)	Class 1	Pseudokinase
ULK4	Binds to ATP in the absence of divalent cations (Murphy *et al.*, 2014b). Catalytic behavior unknown	Class 2	Pseudokinase
VRK3	No, crystal structure shows ATP cannot access binding pocket (Scheeff *et al.*, 2009)	Class 1	Pseudokinase

Table 1.2 A summary of the ATP binding properties of individual pseudokinase domains. The pseudokinases have been arranged in alphabetical order and the classes, described by Murphy and colleagues (Murphy *et al.*, 2014b) and by Zeqiraj and van Aalten (Zeqiraj and van Aalten, 2010) based on experimental evidence reported in the literature describing the presence or absence of ATP binding using recognized reliable assays, listed.

1.7 Pseudokinases act in a variety of ways to alter cell signaling

Following a recent review of pseudokinase (and pseudophosphatase) biology (Reiterer *et al.*, 2014), and the implications of these physiological and disease functions, mechanistic effects that pseudokinases might employ have been summarized into 5 distinct categories and it has been suggested that all pseudokinases function in at least one of these roles:

- Modulator: Regulates activity of a partner kinase by dimerisation and allostery.
- Competitor: Binds to the substrates of canonical kinases reducing the free concentration of substrate available for a reaction.
- Spatial anchor: When the pseudokinase is localized to a particular subcellular compartment, it binds to a 'substrate' and effectively traps it in this location.
- Integrator: Many pseudokinases contain more than one functional domain and so can act as scaffolds, which bring substrates from one pathway into close proximity with the components from another pathway or substrates for a neighboring domain, initiating a new signaling cascade (Figure 1.3).
- Activator: Pseudokinase is catalytically active, and can drive a signaling pathway.

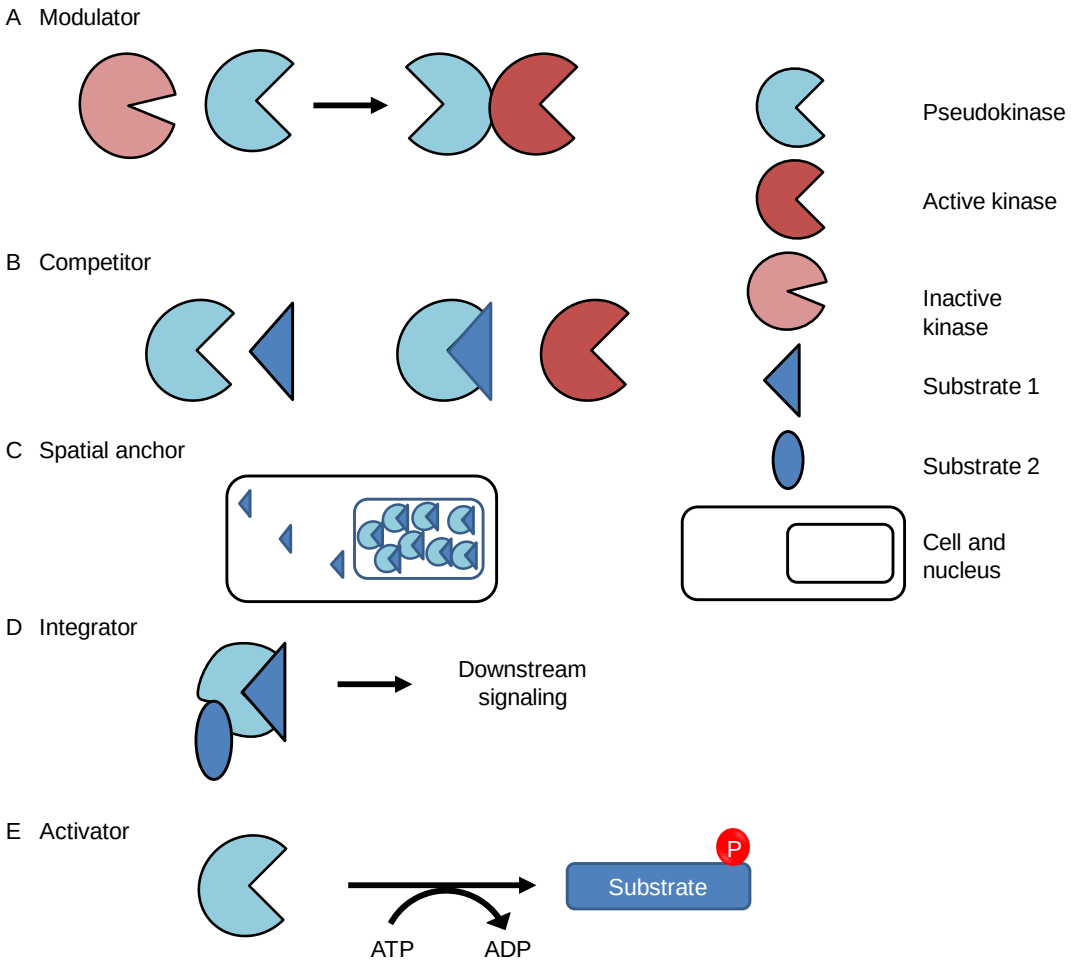

Figure 1.3 Four mechanisms employed by pseudokinases that might modulate a cell signaling pathway without transferring a phosphate group to a substrate A-D) Illustrative examples of the different ways pseudokinases might mediate or perturb the signaling processes in a cell, any one of which might still be regulated by ATP binding. E) The fifth category shows the pseudokinase acting as a catalytic kinase, hydrolyzing ATP and transferring the phosphate group to a protein substrate. Adapted from Reiterer et al., 2014.

1.8 **CASK**

CASK (Calcium and Calmodulin-activated Serine-threonine Kinase) is a pseudokinase that does not have either of the kinase domain canonical divalent cation binding residues (DFG or N) and so was originally termed a pseudokinase, when the meaning of pseudokinase was meant to be interpreted to suggest a complete lack of catalytic activity, even though, in most cases, this had yet to be experimentally tested (Manning *et al.*, 2002). In CASK, the canonical kinase catalytic motif Asn is replaced with a Cys residue, and the magnesium ion binding Asp residue located in the 'DFG' motif of typical kinases is swapped for a Gly (Mukherjee *et al.*, 2010, Mukherjee *et al.*, 2008). CASK has 44% sequence homology with the related (active) kinase CAMKII and in addition to the mutations discussed above, His145 is present in the catalytic motif of CASK whereas the 'classical' CAMK related proteins have a Glu. In addition CASK Pro22 is an Ala residue in CAMK proteins, with both amino acids lining the nucleotide-binding pocket. (Mukherjee *et al.*, 2010). In a very important finding, CASK was shown to autophosphorylate weakly and to directly phosphorylate the substrate neurexin-1 *in vitro*, suggesting that it belonged to the low activity pseudokinase group (Zeqiraj and van Aalten, 2010). However, because of its weak affinity for ATP (K_m[ATP] measured at 0.563 mM), its thermal stability was not increased in the presence of ATP when analysed in a fluorescence-based assay (Table 1), which has become a standard technique in the field to help understand isolated pseudokinase domain binding to ligands such as ATP (Scheeff *et al.*, 2009, Murphy *et al.*, 2014b). This has now led to CASK being designated as a group 1 pseudokinase: 'Does not bind detectably bind to nucleotides or cations' in a very recent study (Murphy *et al.*, 2014b), despite biochemical evidence to the contrary when a radioactive isotope (^{32}P) or a fluorescent reporter (TNP-ATP) was employed to evaluate ATP binding to CASK by a separate group (Mukherjee *et al.*, 2010). This issue aptly demonstrates the requirement of a combination of methods to resolve whether a pseudokinase is catalytically active or can bind to ATP *in vitro* and does not even begin to address the biological relevance of CASK signaling potential in cells.

In a second remarkable finding, and unlike all other active kinases that have been tested, the catalytic activity of CASK was inhibited in the presence of metal ions, which are nearly always added in kinase assays alongside ATP, and no metal ions have been detected in crystallographic structures, including those bound to an

ATP-mimetic, which contain a sodium ion at this site (Mukherjee *et al.*, 2008). However, metal-dependent inhibition can be relieved by multiple 'back' mutations to absent Mg^{2+} ion binding residues in the pseudokinase domain. To achieve this, the Cys in the catalytic loop was mutated back to an Asn and the Gly in the 'DFG' motif was mutated to the canonical Asp (GFG becomes DFG). Other residues that align with the most closely related active kinase (CAMKII) were also reverted, so that the CASK His residue in the catalytic motif was mutated to the CAMKII Glu, and a Pro in the CASK Gly Rich loop was mutated to an Ala. When all of these residues were mutated simultaneously, the rate of CASK autophosphorylation was stimulated enormously, and the enzyme was no longer inhibited in the presence of Mg^{2+} ions (Mukherjee *et al.*, 2010). The only known CASK substrates are itself (an autophosphorylation site within the catalytic domain) as well as the synaptic protein neurexin-1, with which it is thought to co-localise in the nerve terminals of neurons.

Structural analysis revealed that the catalytic domain of CASK crystallized in an active conformation, and the ATP binding site was not occluded by residue side chains (Mukherjee *et al.*, 2008), consistent with its detectable phosphotransferase activity. These studies, alongside several others discussed below, demonstrated that pseudokinases have the ability to be catalytically active in some cases, and this work has stimulated the pseudokinase field to move ahead with the analysis of many other pseudokinases, with the realization that each separate pseudokinase needs to be functionally evaluated *in vitro* and in cells prior to its classification as either inert or 'devoid of activity.'

1.9 **ErbB3**

The Receptor Protein Tyrosine Kinase (RPTK)-related pseudokinase HER3 (ErbB3) has evolved an uncharged Asn amino acid instead of a putative catalytic Asp residue in its unusual 'HRD' motif, and also possesses a His residue in the αC helix in the region where the canonical Lys-interacting Glu residue might be expected to be present. HER3 is closely related to the ErbB family of RPTKs, of which there are four members, including model active kinases such as EGFR and ErbB2, which phosphorylate proteins containing Tyr residues.

Interestingly, despite not having the catalytic Asp residue or the conserved Glu, as part of its catalytic domain, HER3 has demonstrated weak phosphotransferase activity *in vitro* (approximately $1/1000^{th}$ the activity of the closely related EGFR when assayed side-by-side) (Shi *et al.*, 2010) and so HER3

was re-classified as a ‘low activity pseudokinase’ (Zeqiraj and van Aalten, 2010). Crystal structures of HER3 show that it resembles an ‘inactive’ tyrosine kinase conformation (Jura *et al.*, 2009b, Shi *et al.*, 2010), however, despite this HER3 binds ATP with high affinity (Shi et al., 2010), and in cells can activate a ‘trans-receptor’ partner as part of a heterodimer (e.g. other ErbB family members). Whether ATP binding is required for HER3 cellular function is not known, but in the presence of the clinically approved kinase inhibitor Bosutinib, a drug that binds strongly to the ATP-binding pocket of HER3 (K_d ~1 nM) (Davis *et al.*, 2011), the trans-activation of EGFR actually increases because the presence of the small molecule increased the binding affinity of the dimer constituents (Littlefield *et al.*, 2014). This suggests that small molecules that mimic the ATP site of this pseudokinase will not necessarily function as inhibitors, and might actually be allosteric activators depending upon the binding mode (Klaus *et al.*, 2013).

For kinase-driven phosphoryl transfer, the conserved kinase catalytic Asp (corresponding to the Asn in HER3 pseudokinase) extracts the proton from the substrate Tyr OH group, which facilitates nucleophilic attack of the phosphate group by the Tyr O^- substrate acceptor. HER3 must therefore utilize a different pathway, or residue, for phosphoryl transfer because it does not possess the Asp residue. It has been suggested that HER3 transfers the labile proton of the phenolic tyrosine to the O1γ and then to O2β oxygens of ATP, and that phosphoryl transference occurs concurrently with this step (Shi *et al.*, 2010).

1.10 **STRADα**

STRADα (Ste-20-related adaptor protein) is a pseudokinase that has a partially conserved Gly-rich loop, but does not contain the canonical β3 Lys, the catalytic Asp or magnesium binding Asn in the catalytic motif, nor the magnesium ion binding Asp residue in the DFG motif. Instead the respective residues in vertebrate STRADα homologues are Arg, Ser, His and Gly (Zeqiraj *et al.*, 2009b). Despite these major differences (compared to the residues observed in standard kinase domains), STRADα can bind with high affinity to ATP, a process that is stimulated by the auxiliary protein MO25α (Zeqiraj *et al.*, 2009b), but there has been no evidence presented that it is catalytically active, indeed no ATP turnover has ever been detected by STRADα *in vitro*, and it is therefore listed as a member of the inactive pseudokinase group as defined by Zeqiraj and van Aalten 2010., but

because it can bind to nucleotides it has also been re-classed recently by Murphy and colleagues as a group 2 pseudokinase (Murphy *et al.*, 2014b).

STRADα binds to the active kinase LKB1 and the scaffolding protein MO25α with a 1:1:1 stoichiometry. Following binding, the conformation of LKB1 alters and it becomes activated independently of phosphorylation. STRADα is in an active/closed conformation when it binds to LKB1. The activation loop of LKB1 is not phosphorylated, but the αC helix is rotated akin to that of an active kinase, which allows the typical salt bridge to form between the conserved Glu and β3-Lys. Both MO25 and STRADα are required for this event (Zeqiraj *et al.*, 2009a). STRADα is therefore an example of a pseudokinase that modulates the activity of an independent protein kinase, and by association the downstream pathways controlled by LKB1 (Lizcano *et al.*, 2004) by an allosteric interaction driven by ATP (and metal) binding, rather than by direct substrate phosphorylation.

1.11 The 'With No Lysine' (WNK) family of kinases

The WNK family comprises four kinases (WNK1-4), none of which contain the conserved lysine situated in the β3 'VAIK' motif that coordinates the α- and β phosphates of ATP in model protein kinases. However, the WNK kinases are catalytically active (Lenertz *et al.*, 2005) and are members of the 'Active Pseudokinase' grouping (Zeqiraj and van Aalten, 2010). The terminal residue in the glycine-rich loop is normally a Gly in kinases, however, for the WNK family it is a Lys residue and this performs the same role as the 'missing' Lys residue in the VAIK motif (Verissimo and Jordan, 2001, Xu *et al.*, 2000). Remarkably, the molecular basis for the absence of the Lys in the VAIK motif has recently been revealed by the publication of the structure of WNK1, which shows a chloride ion bound adjacent to the site that would normally be occupied by the lysine, stabilizing an inactive conformation and inhibiting WNK1 activation. This permits WNK1 activity to be regulated by physiologically-relevant chloride ion sensing (Piala *et al.*, 2014).

1.12 JAK2 JH2 pseudokinase domain

STAT proteins can bind to cytokine receptors following JAK phosphorylation, which occurs in response to ligand binding. This activates the STATs, which are a series of transcription factors. There are four mammalian JAK-containing polypeptides (JAK1-3 and Tyk2) and all contain related JAK homology

(JH) domains 1-7. The JH1 domain is an active canonical kinase domain but the 'JH2' domain is a pseudokinase that lacks the catalytic Asp, possessing an invariant Asn residue instead in the JAKs. This led to the assumption that the pseudokinase domain of JAK kinases were catalytically inactive. However, Saharinen and colleagues demonstrated that JAK2 JH1 kinase activity was inhibited by the presence of the JAK2 JH2 (pseudokinase domain) (Saharinen *et al.*, 2000) with the JH2 Cys618 residue that sits in a loop between the two N lobe β strands reduces the activity of the JH1 domain by restricting the conformational flexibility of the JH1 activation loop by interacting with the JH1 residues Val1000 and Pro1002 (Lindauer *et al.*, 2001). Moreover, a mutation in the JAK2 JH2 domain next to this site (V617F) is a very common oncogenic driver in the bone marrow disorder polycythemia vera (Scott *et al.*, 2007). Intriguingly, it has recently been demonstrated that the JH2 domain of JAK2 is actually catalytically active and autophosphorylates the JH2 residues Ser523 and Tyr570, indicating that the JH2 domain is a dual specific kinase, the phosphorylation of Tyr residues by JH2 is however dependent upon prior Ser523 phosphorylation. Moreover, the phosphorylation of Ser523 or Tyr570 had an autoinhibitory effect upon the activation of the JAK2 JH1 domain and when either Ser523 or Tyr570 were mutated, the levels of JH1 activation loop phosphorylation increased (Ungureanu *et al.*, 2011).

1.13 **VRK3**

VRK3, a pseudokinase of the *Vaccinia* Related Kinase (VRK) family, which has several paralogues in the human kinome (Scheeff *et al.*, 2009). VRK3 contains a glycine-rich loop that consists of residues with much larger and acidic side chains than those found in active kinases, and that are required for ATP binding. Instead of the consensus GxGxxG, the sequence is TRDNQG in VRK3. These disrupt the interactions between ATP and the kinase by increasing the steric hindrance. In addition, the nucleotide binding site is, unusually, highly acidic in VRK3, which might repel, rather than stabilize, the negatively charged ATP co-factor in cells. This, and other mutations, clearly prevent VRK3 from binding ATP (and chemical analogues of ATP) and so it is the founding member of the Class 1 of pseudokinases that does not bind to ATP or cations (Murphy *et al.*, 2014b) and a 'catalytically inactive pseudokinase' (Zeqiraj and van Aalten, 2010). Despite deviations from the catalytic domain of VRK3, the crystal structure of VRK3 strongly resembles the crystal structure of VRK2, with the retention of key VRK structural residues but not

catalytic residues, however, the activation loop and Gly-rich loop are much more rigid in the pseudokinase than its active counterpart (Scheeff *et al.*, 2009), meaning that ATP is physically occluded from the catalytic site.

1.14 **KSR1/2**

KSR1 (kinase suppressor of RAS1) and KSR2 are pseudokinases that lack the highly conserved lysine in the kinase domain β3 sheet. KSR1 has recently confirmed to act as both as a catalytically 'active' pseudokinase and as a scaffolding protein for the ERK signaling pathway (Zhang *et al.*, 2013). To distinguish between the scaffolding functions of KSR1 and its intrinsic ATP-dependent activity, a KSR1 mutant was generated that stabilized the 'closed' active conformation of the protein that could not bind ATP. In Ras-transformed cells, the induction of dimerisation between active B- and C-RAF by the presence of B-RAF specific inhibitors leads to the activation of C-RAF and the MEK/ERK pathway. Also, following treatment with PLX4720 (Vemurafenib), MEK/ERK signaling is induced in RAS-transformed cells, even though B/C-RAF dimers do not form. KSR1 was implicated in activating MEK via C-RAF because it forms dimers with both C and B-RAF. Following the induction of C-RAF/KSR1 dimers, by the addition of PLX4720 or GDC0879, MEK and ERK were activated (Hu *et al.*, 2011a, Hatzivassiliou *et al.*, 2010). However, following mutation of KSR1 to a mutant (A587F) that could not bind ATP, but could still dimerise constitutively with C-RAF, downstream pathway activation was reduced, which indicates that the KSR1-mediated pathway activation was reliant upon ATP binding by the pseudokinase. Even more interestingly, *in vitro* kinase activity was detected when KSR1 and C-RAF were co-expressed and dimerisation was induced following the addition of 10 μM PLX4720, and this activity could be traced by chemical genetics specifically to the pseudokinase protomer when a similar experiment was performed with the closely related KSR2 pseudokinase (Brennan *et al.*, 2011). Furthermore, KSR1 immunoprecipitates were assayed in the presence of a C-RAF inhibitory concentration of PLX4720, and KSR1 phosphorylation of MEK was detected, but only when dimerisation of KSR1 and C-RAF had been induced, and the *in vitro* phosphorylation of MEK was not observed when the KSR1 ATP binding mutant (A587F) was assayed (Hu *et al.*, 2011a).

1.15 **MLKL**

Mixed lineage kinase domain-like (MLKL) has recently been analysed and revealed to be a catalytically 'inactive' pseudokinase with multiple biological roles. It not only lacks the G-rich loop, but also the two conserved Asp residues, one that typically acts as the catalytic base and one that binds a magnesium ion (Murphy *et al.*, 2013, Murphy *et al.*, 2014a). MLKL is required for TNF-induced necroptosis and acts downstream of the kinase RIP-3 in this process (Sun *et al.*, 2012). The thermal stability of MLKL in the presence or absence of ATP is markedly different, and confirms that despite a highly-degraded catalytic domain, this pseudokinase does indeed bind to the nucleotide with high affinity. Interestingly, the affinity of binding is reduced in the presence of divalent cations, contrary to the behavior of most 'standard' kinases. To investigate this structurally, the crystal structure of MLKL was solved at a resolution of 1.7 Å, and confirmed that it retained the overall topology of a bilobial kinase domain. The crystal structure revealed that the only residue that could potentially block ATP from accessing the binding site was an Arg residue located in the Gly rich loop. It also confirmed that MLKL was in an 'active' conformation, with the β3 lysine coordinating a conserved Glu residue in the αC helix. Consistently, the Glu from the GLE 'substitution' in the DFG motif was not in a position conducive for metal binding, which supported the finding that binding is metal-independent. The catalytic motif of MLKL contains an HGK, in place of the typical HRD motif. Lys 331 in this motif resides in the position of the canonical catalytic Asp and protrudes into the ATP binding cleft. Mutation of this Lys (K331N) reduced the affinity for ATP 3-fold, compared to the WT, indicating that the Lys might be involved in the coordination of ATP (Murphy *et al.*, 2014a). This may be a similar situation to the WNK kinases, where a Lys residue had evolved in a different conserved motif (not the VAIK motif) to aid ATP binding, but unlike the WNKs, MLKL is catalytically inactive because the remaining motifs important for function are very highly degraded.

1.16 **Tribbles pseudokinases**

The blastoderm in the *Drosophila* embryo develops by groups of cells progressing through mitosis in a coordinated and tightly regulated sequence of divisions. These cells or 'mitotic domains' only proceed through mitosis after the String/CDC25 phosphatase is expressed. String removes inhibitory (Tyr 15)

phosphates on *Drosophila* CDK1, which relieves a block on G2 progression, with mitosis being initiated immediately (Figure 1.4A). The first domain to express String is the mesoderm, however in contrast to the other domains, this does not initiate mitosis immediately following String expression, but the cell cycle is halted until nine other domains have passed through the G2/M checkpoint. This pause in the cell cycle allows mesoderm invagination to occur by a controlled change in cell shape and mitotic progression disrupts this process (Seher and Leptin, 2000). Upon overexpression in the embryo, the Tribbles (Trbl) gene, which encodes a pseudokinase in flies lacking the canonical DFG motif, promotes the G2-phase of the cell cycle in wing imaginal disc cells and modulates the levels of String and Twine (a second CDK1 phosphatase) by targeting them for proteasomal degradation, thus decreasing protein levels and slowing mitotic progression. This allows the correct arrangement of cell morphologies prior to cell division, and loss of Tribbles underlies phenotypic defects in mitotic timing and its coordination with development (Mata *et al.*, 2000).

Trbl has 3 closely-related human homologues (Manning *et al.*, 2002), and in flies also regulates the turnover of the human C/EBP transcription factor homolog termed slbo, which promotes migration of border cells in the *Drosophila* ovary (Rorth *et al.*, 2000). In these cells, Trbl opposes slbo and halts border cell migration; the pseudokinase domain of Trbl is required for this phenotype. Mechanisticly, Trbl controls the levels of slbo by interacting with an E3 ligase and targeting slbo for proteasomal degradation. The ubiquitin hydrolase Ubp64 can stabilize slbo protein levels (Rorth *et al.*, 2000, Masoner *et al.*, 2013) (Figure 1.4B).

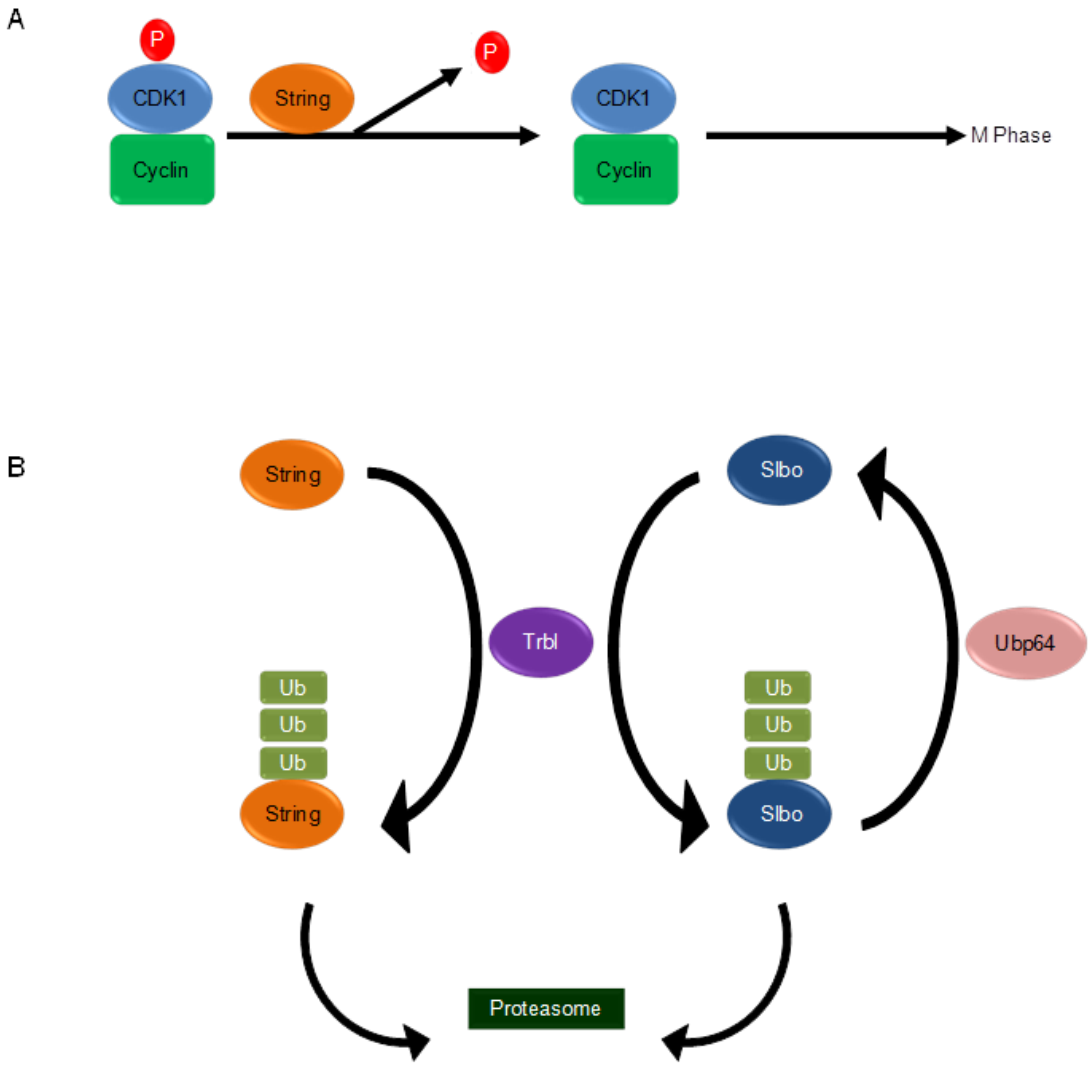

Figure 1.4 The biochemical function of *Drosophila* Trbl. A) A cartoon of the action of String (equivalent to CDC25 in yeast and vertebrates, which helps drive cells through mitosis by removing an inhibitory phosphorylation on CDK1. B) Trbl interacts with both String and slbo, targeting them for proteasomal degradation and thereby preventing M-phase progression.

1.17 **Trib2**

The major focus of this thesis is an analysis of the human pseudokinase Trib2 (also known as C5FW/SKIP2/SINK and TRB2). Bioinformatic analysis of the human Trib2 sequence predicted the presence of a kinase-domain fold between amino acid residues 64 and 308 (Simple Modular Architecture Research Tool), and further alignments with other vertebrate Trib2 orthologues (Figure 1.5 A) confirm an almost 100% identity between human Trib2 in the catalytic domain, in a region lying N-terminal to the kinase domain (termed 1-63) (Figure 1.5 B) and in the C-terminal region (termed 309-343) (Figure 1.5C). The predicted secondary structure elements of human Trib2 are shown beneath the protein sequence, with green arrows representing β-sheets, and α-helices depicted by red ovals. However, it should be noted that these are bioinformatic-based predictions and may not necessarily totally accurate because they rely upon comparisons with canonical kinases, and currently, there are no published structures of any Tribbles-related kinases to permit structural analysis of the kinase fold.

The presence of the kinase-like domain in Trib2 led to its inclusion in the human kinome dendrogram, and its denotation as a pseudokinase (Figure 1.6 adapted from (Manning *et al.*, 2002)). The dendrogram is a compilation of the 518 distinct, evolutionally-related protein kinases. On the same 'evolutionary branch' as Trib2 are the closely-related pseudokinases Trib1 (also termed TRB1, SKIP1, C8FW and GIG2) and Trib3 (also termed NIPK, SKIP3, SINK, TRB3 and LOC57761) and the more distant pseudokinase SgK495 (also termed SHIK and STK40). Trib2 location is highlighted in red, and it is most closely related to the CAMK and CGMC sub-families of protein kinases, although it does not formally reside in either.

An alignment of the full-length human pseudokinases Trib2, Trib1, Trib3, SgK495, the *Drosophila* orthologue Tribbles and the model active human kinase PKA (Figure 1.7) clearly demonstrates that the N-terminal and C-terminal segments of the Trib proteins are the most divergent. However, in the C-terminal regions of both Trib2, Trib1, Trib3 and *Drosophila* Tribbles there is a conserved sequence of amino acids [D/E/A]QxVP[D/E/A]. The presence of this sequence is known to facilitate the binding of an E3 ubiqutin ligase termed COP-1 to Trib2, Trib3 and Trib1 (Keeshan *et al.*, 2010, Qi *et al.*, 2006, Yokoyama *et al.*, 2010).

Another protein-protein interaction sequence observed throughout the C-terminal region of the Trib family, including *Drosophila* Tribbles, has been suggested to drive binding to MEK1, the major target of RAF in the ERK pathway (Figure 1.1A), and all 3 human Tribs have been shown to interact biochemically with this MAPKK *in vitro*. Indeed, following deletion of the IL(D/L)HPWF(F/L) binding motif, the interaction of Trib1 with MEK1 was abrogated (Yokoyama *et al.*, 2010). Human Tribbles proteins are also reported to interact with other MAPKKs, including the JNK upstream kinases MKK4 and MKK7 (Eder *et al.*, 2008, Kiss-Toth *et al.*, 2004). Through these interactions, the stability of MAPKKs can be controlled (Kiss-Toth *et al.*, 2004) and monocytic innate immune responses regulated, although as discussed in the literature, it still remains to be determined how the Tribbles family of proteins can alter the activity of its partner kinases at the molecular level (Eder *et al.*, 2008).

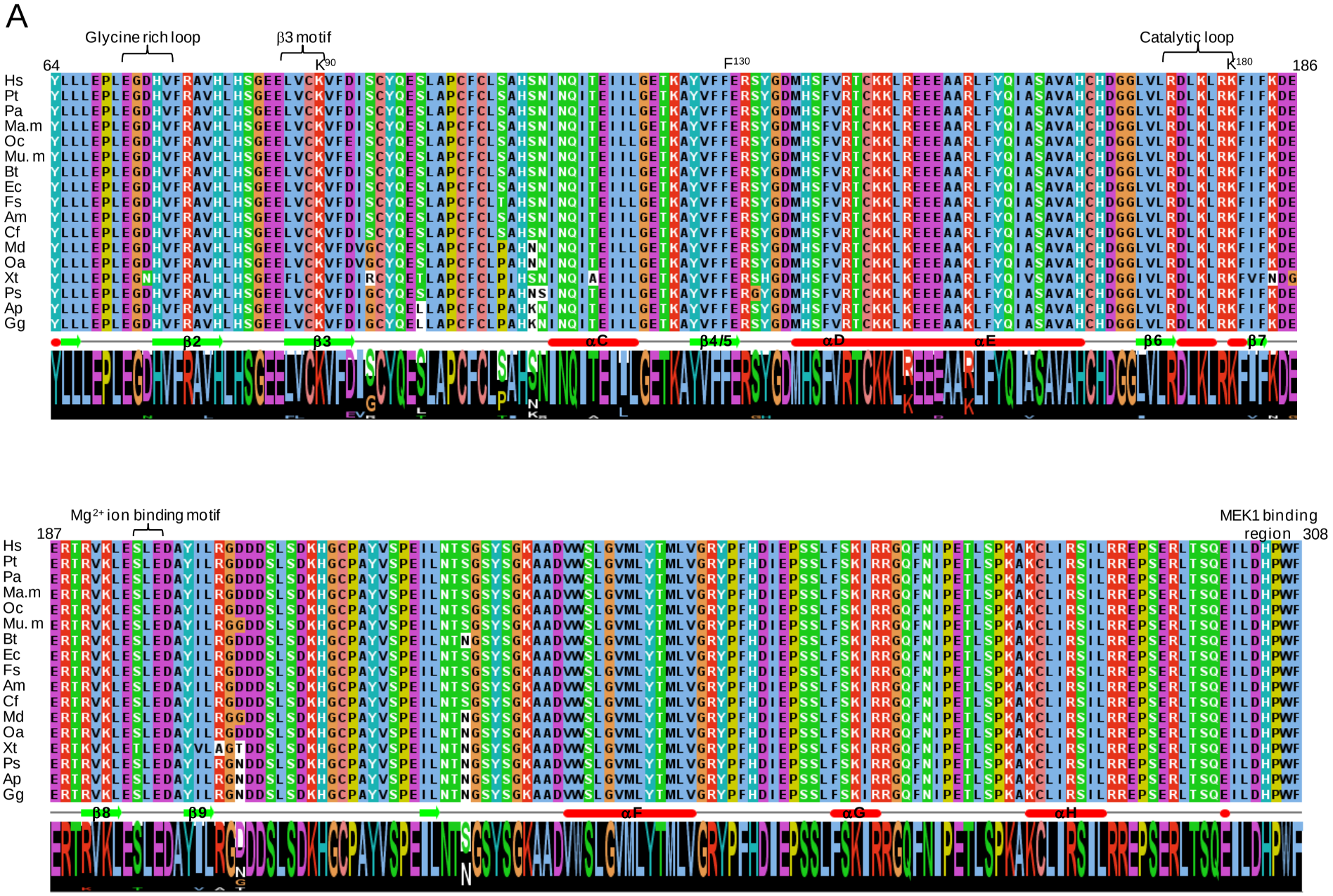
A
Glycine rich loop
β3 motif
Catalytic loop
64
K90
F130
K180
186
Hs
Pt
Pa
Ma.m
Oc
Mu. m
Bt
Ec
Fs
Am
Cf
Md
Oa
Xt
Ps
Ap
Gg
β2
β3
αC
β4/5
αD
αE
β6
β7
Mg2+ ion binding motif
MEK1 binding region
187
308
β8
β9
αF
αG
αH

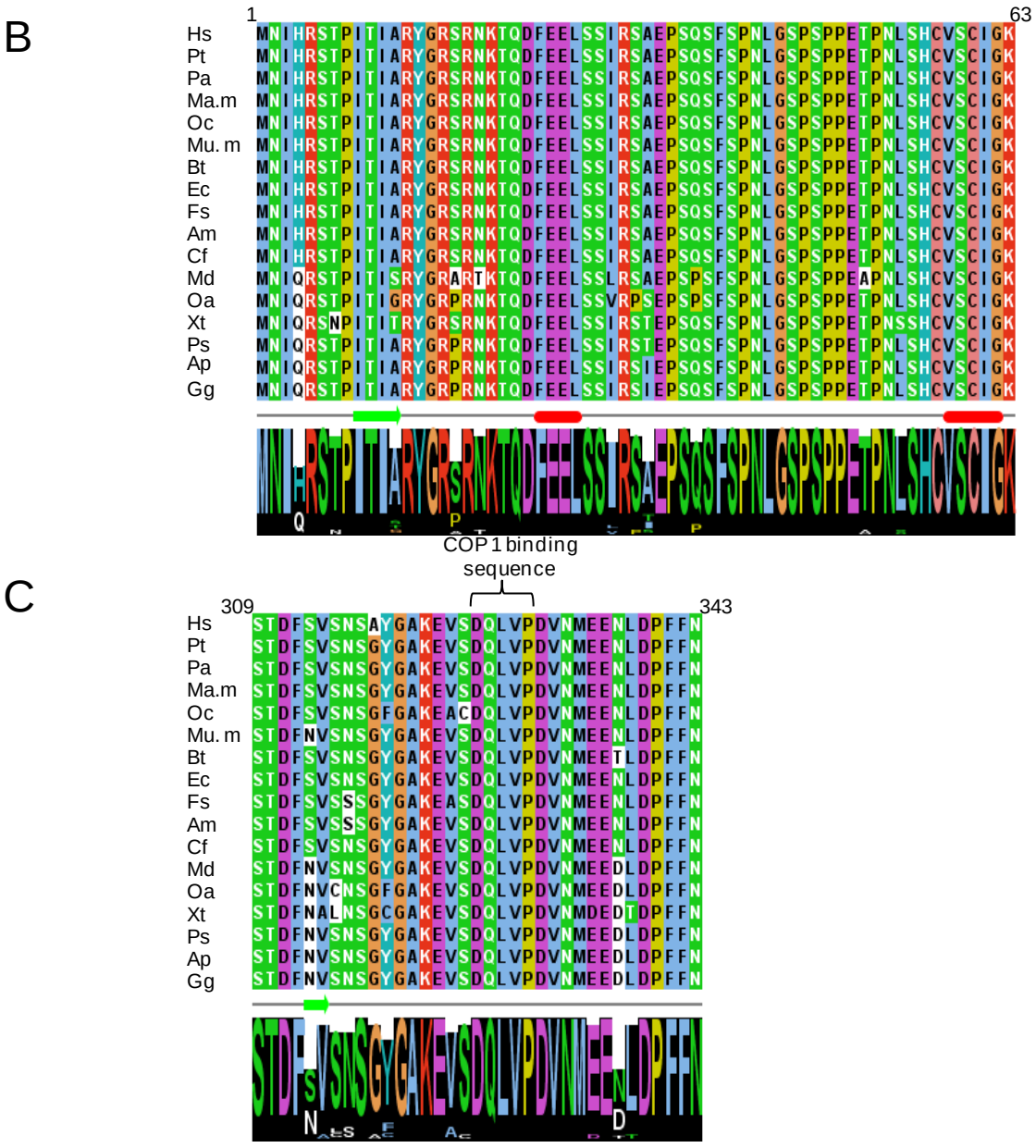

Figure 1.5 Trib2 amino acid conservation in vertebrates Alignments were performed in Jalview, using the Muscle alignment tool with the residues shaded using the Clustal colour scheme for clearer visualisation of levels of conservation. The secondary structure prediction was also performed in Jalview using the Jnet Secondary Structure Prediction tool (helices: red ovals, βsheets: red arrows). Hs *Homo sapiens*, Pt *Pan troglodytes*, Pa *Pongo abelii*, Ma.m *Macaca mulatta*, Oc *Oryctologus cuniculus*, Mu. m *Mus musculus*, Bt *Bos taurus*, Ec *Equus caballus*, Fs *Felis silvestris*, Am *Ailuropoda melanoleuca*, Cf *Canis familiaris*, Md *Monodelphis domestica*, Oa *Ornithorhynchus anatinus*, Xt *Xenopus tropicalis*, Ps *Pelodiscus sinensis*, Ap *Anas platyrhinchos*, Gg *Gallus gallus*. A) Trib2 catalytic domain. Numbered in relation to human Trib2 (catalytic domain between 64-308). B) Trib2 'N-terminal domain', labelled in relation to human Trib2 1-63 C) Trib2 'C-terminal domain' numbered in relation to human Trib2 309-343.

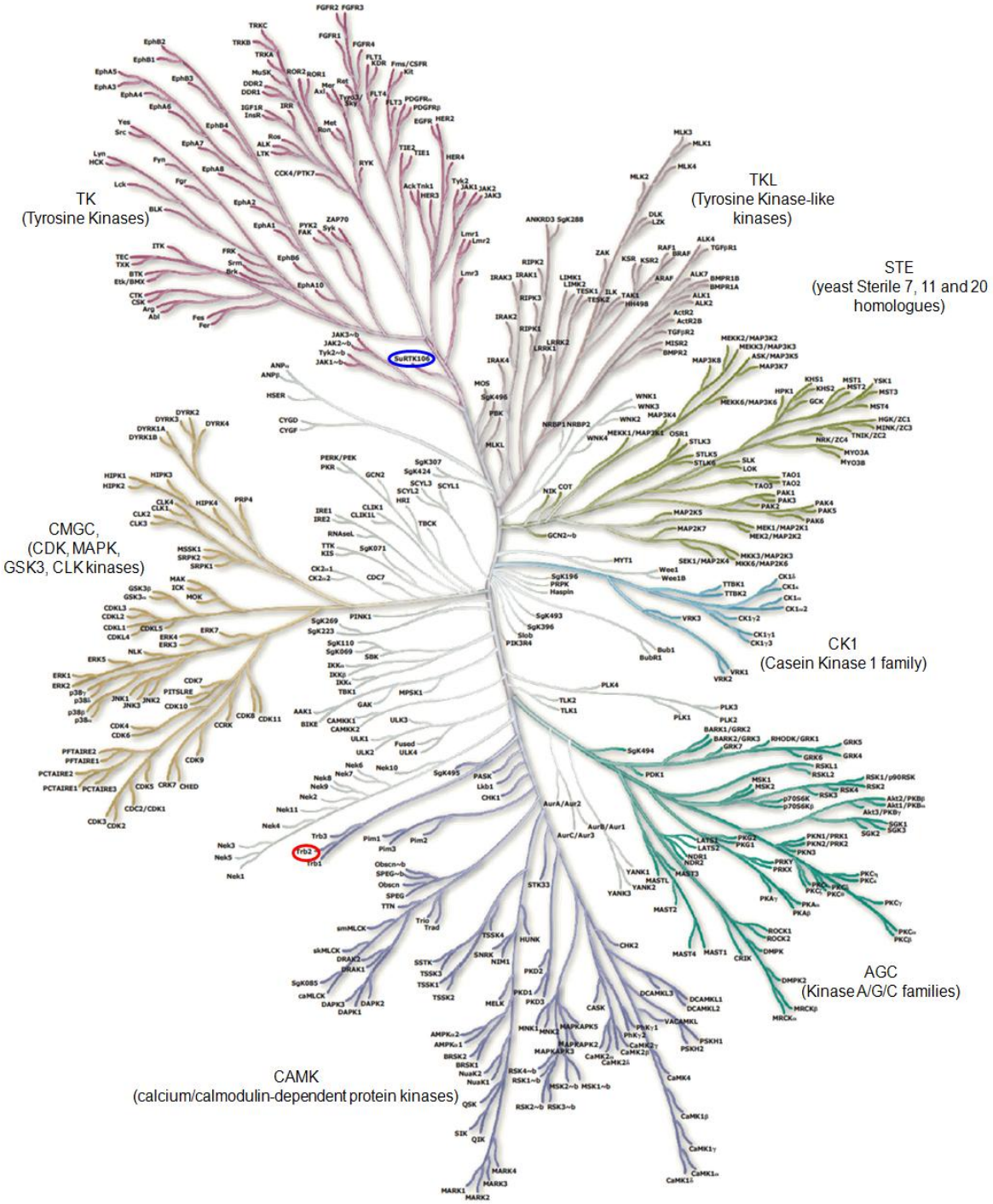

Figure 1.6 The human kinome dendrogram. The human kinome (Illustration reproduced courtesy of Cell Signaling Technology, Inc. (www.cellsignal.com) depicts the evolutionary relationship between proteins that contain the highly conserved kinase fold. The human Trib2 protein, closely flanked by its human homologues Trib1, Trib3 and the more distant SgK495, is marked by a red circle and is termed Trb2. NOK, labeled as SURTK106 in this figure, is highlighted by a blue circle.

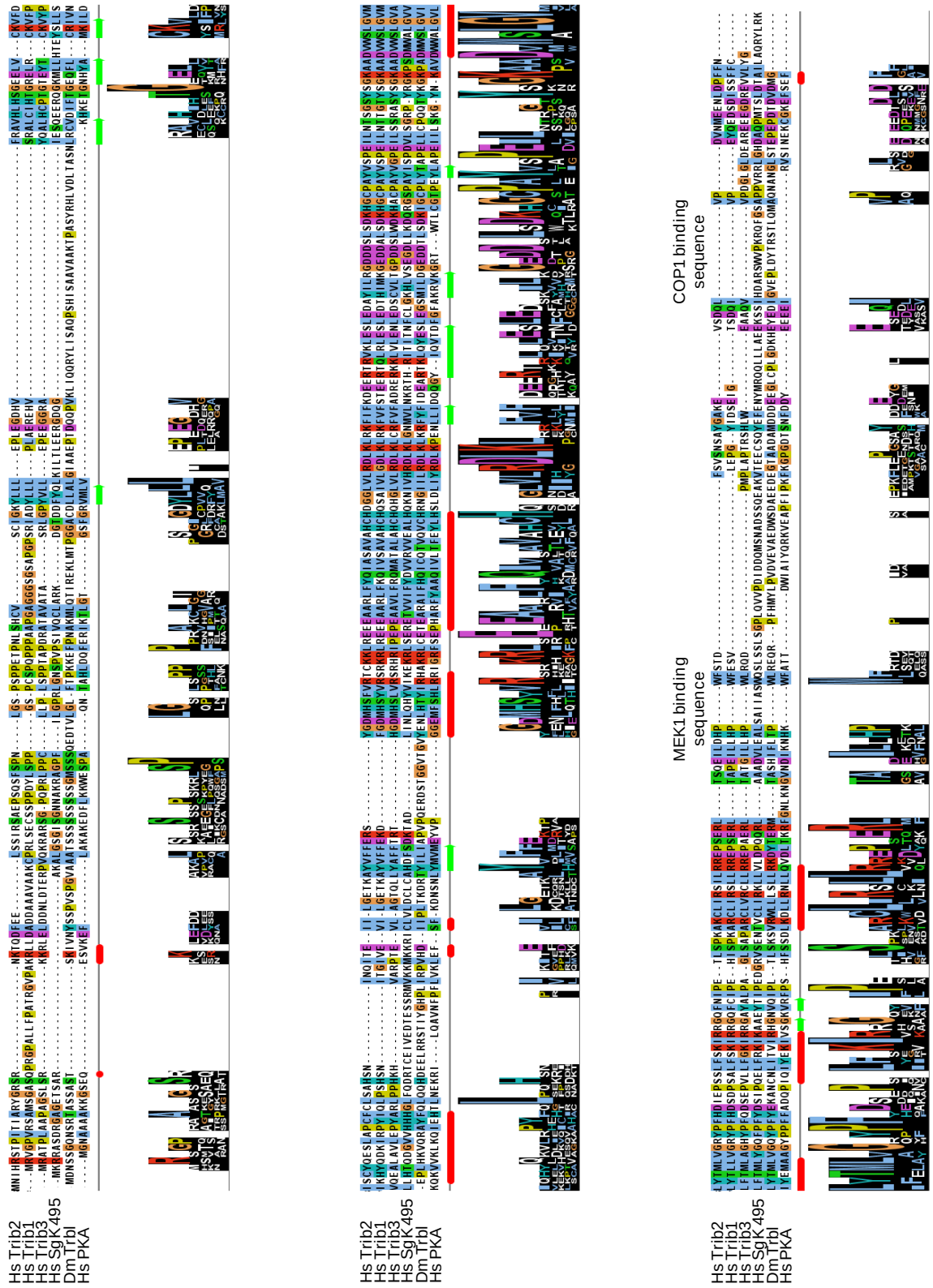

Figure 1.7 Alignment of the human Trib orthologues. Full length (1-343) Trib2 (Uniprot Q92519), Trib1 (1-372 Uniprot Q96RU8), Trib3 (1-358, Uniprot Q96RU7) SgK495 (1-435, Uniprot Q8N2I9), and Drosophila melanogaster Trbl (1-484, Uniprot Q9V3Z1) were aligned against the classical kinase PKA. The alignment was performed using the MUSCLE tool in JALVIEW and the secondary structure was predicted using the JNETPRED tool. The colours correspond to the CLUSTAL colour scheme.

1.18 Predicted structure of Trib2 in three dimensions

As of 2014, no structural coordinates for any of the Trib proteins have been deposited in the RCSB Protein Data Bank (PDB) or the Biological Magnetic Resonance Bank (BMRB). One of the goals of this thesis is to generate high-quality pseudokinases that can be analysed using X-ray or NMR-based approaches, but until this is achieved, structural analysis is based largely on prediction. As shown in Figure 1.8A, a model of the Trib2 catalytic domain indicates that it does maintain (as is predicted by sequence analysis) the classical bilobal kinase fold, with the catalytic site at the interface of the N and C lobes. The conserved kinase domain residues are highlighted. The Trib2 residues that align with the glycine-rich loop (Figure 1.8 B) do not follow the consensus GxGxxG sequence, and are instead EGDHVF (blue). This sequence is predicted to be much more rigid because of increased steric hindrance caused by the presence bulkier residues and contains several acidic residues akin to the equivalent motif in the non-ATP binding pseudokinase VRK3 (Scheeff *et al.*, 2009). The β3 motif of Trib2, LVCK, consists of a canonical Lys (K90-cyan) preceded by hydrophobic residues that would normally pack against the adenine ring of ATP in canonical kinases (Taylor and Kornev, 2010); this Lys normally coordinates the phosphate residues of ATP that are not transferred to substrate (α- and β-) and forms a salt bridge with the conserved glutamate in the α-C helix. However, in Trib2, the predicted Trib2 Glu (E99-orange) that is nearest to the conserved Glu in PKA (E90) when sequences are compared (Figure 1.8), points away from the catalytic domain. The lack of conservation of Trib2 E99 with the other Trib family members suggests (but does not prove) that this Glu is not the residue that interacts with Lys 90, should one exist. The predicted 'gatekeeper' residue, which lies at the back of the ATP pocket, but is not involved in ATP binding, is a Phe in Trib2. F130 is coloured green and points into the ATP binding pocket between the two lobes of the kinase, where it controls access of adenine-substituted kinase inhibitor mimetics in classical kinases. The gatekeeper residue is a Met in the closely related kinase CAMK1, a Met in the archetypal kinase PKA, and a Phe in the related CDK1 and CDK2 kinases. No human kinases have a Gly or Ala at this position (Garske *et al.*, 2011), although the exploitation of the gatekeeper in chemical genetics will be discussed in Chapter 4 of this thesis. Trib2 has retained putative canonical Arg and catalytic Asp residues in the motif LRDLKLRK, however, the terminal lysine of this sequence and the serine in the SLE (DFG) motif,

are typically Asn and Asp in active kinases (Kannan and Taylor, 2008), and the importance of this atypical sequence in human Tribbles pseudokinases (as in *Drosophila* Tribbles) is not yet understood.

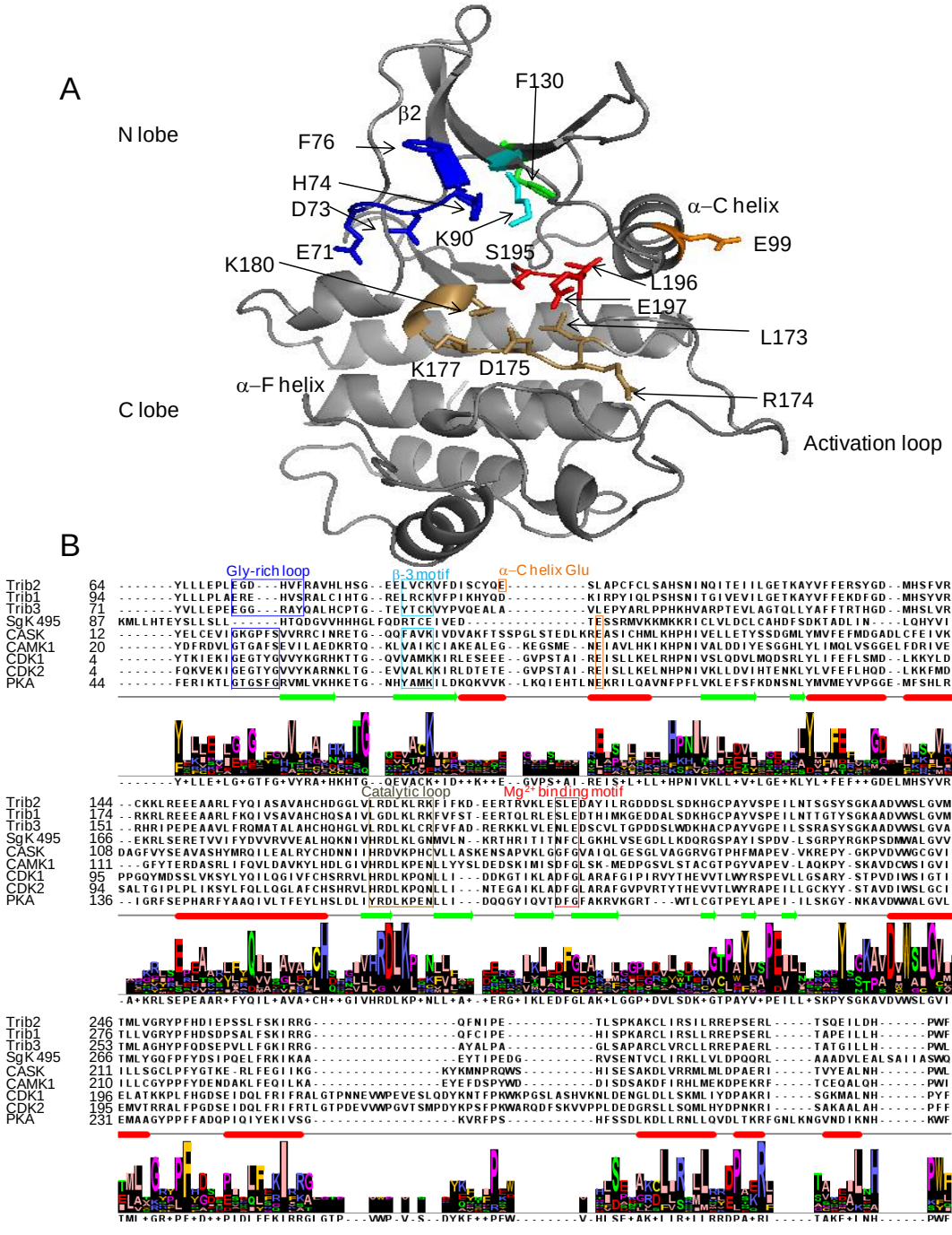

Figure 1.8 A model of the Trib2 catalytic domain, which retains the kinase fold. A) A predicted model structure of Trib2 visualised in Pymol, based on the crystal structure of p38γ (PDB ID:1CM8) is shown in dark grey ribbons. The conserved kinase motifs have the sidechains displayed in 'stick' format and are colour coded. In the N lobe, the glycine-rich loop is blue and stretches from E71-F76 prior to the β2 sheet. The conserved lysine in the β3 sheet (K90) is turquoise. The orange side chain in the αC helix, points away from the catalytic domain (E99). This is the closest Trib2 Glu residue to the conserved Glu residue found throughout the canonical kinases (highlighted in orange in panel B). The green Phe residue at 130 is the Trib2 gatekeeper residue and aligns with the classical kinase gatekeeper residues in the alignment below. L173-L180, which corresponds to the Trib2 catalytic loop, highlighted in gold in the C lobe of the modelled kinase domain and is followed by the Mg^{2+} binding loop (red). B) A MUSCLE alignment of Trib2 with the human Trib related proteins, Trib1, Trib3 and SgK495, as well as the pseudokinase CASK, that also lacks dthe metal ion binding residues (brown and red) like the Trib family and has demonstrated catalytic activity in vitro. The other proteins in this alignment include the canonical kinases CAMK1 and PKA, and also kinases CDK1 and CDK2 that, like Trib2 possess a Phe 'gatekeeper' residue (green).

1.19 **Trib2 is predicted to assemble Regulatory and Catalytic 'spines'**

Upon alignment with the kinase domain of PKA (Figure 1.9 A), structural residues that constitute the Regulatory (red) and Catalytic spines (blue) (Taylor and Kornev, 2010) are highlighted and the corresponding Trib2 residues can be identified (Figure 1.9). The same residues were then highlighted on the 3D catalytic domain model of Trib2 and the known crystal structure of PKA (PDB 1ATP) (Figure 1.9 B). As discussed above, both 'spines' are anchored to the hydrophobic F helix in known kinases and pseudokinases. At its N terminus, the F-helix binds the Reg spine and at the C terminus binds the Cat spine of the kinase. The Regulatory (Reg spine) is a hydrophobic configuration of residues that controls the catalytic activity of the kinase domain because it is either assembled or disassembled by the mobility of the αC helix and activation loop, of which (PKA) Leu95 and Tyr164 are members. The Catalytic (Cat) spine is also very hydrophobic and is completed by the presence of the ATP adenine ring with which the Ala from the β-3 VAIK motif interacts. The F-helix forms the base of both spines to structurally organise and connect the different segments of the kinase together (Taylor and Kornev, 2010). Despite deviations between the residues found in canonical kinase domains and Trib2, the Reg and Cat spines appear to remain intact when modelled and all but the conserved Asp located within the F-helix (PKA220/Trib2236) are hydrophobic, as observed for PKA. Mutations to spine residues can alter the behavior of a kinase. As discussed above, a catalytically inactive form of B-RAF that could allosterically activate ERK was generated by the Cat-spine mutation A481F. The Phe residue blocked catalytic activity by preventing ATP from binding in the ATP binding pocket, but locked the kinase domain in a constitutively active conformation, which activated the downstream pathway in a B-RAF ATP independent manner (Shaw *et al.*, 2014).

There is currently no evidence that any of the Tribbles-related (Trib-related) pseudokinases are able to bind to ATP or are catalytically active. However, one published study indicated that following *in vitro* assay of immunoprecipitated Trib3 from U2OS cell lysates, no autophosphorylation or phosphorylation of MBP, α/β casein, or Histone H1 could be detected (Bowers *et al.*, 2003), raising the possibility that Trib-related pseudokinases are indeed catalytically inactive. Moreover, the high degree of conservation observed within key areas of the catalytic domains of

vertebrate Trib-related proteins does indicate that they have an important function that has been selected for during molecular evolution.

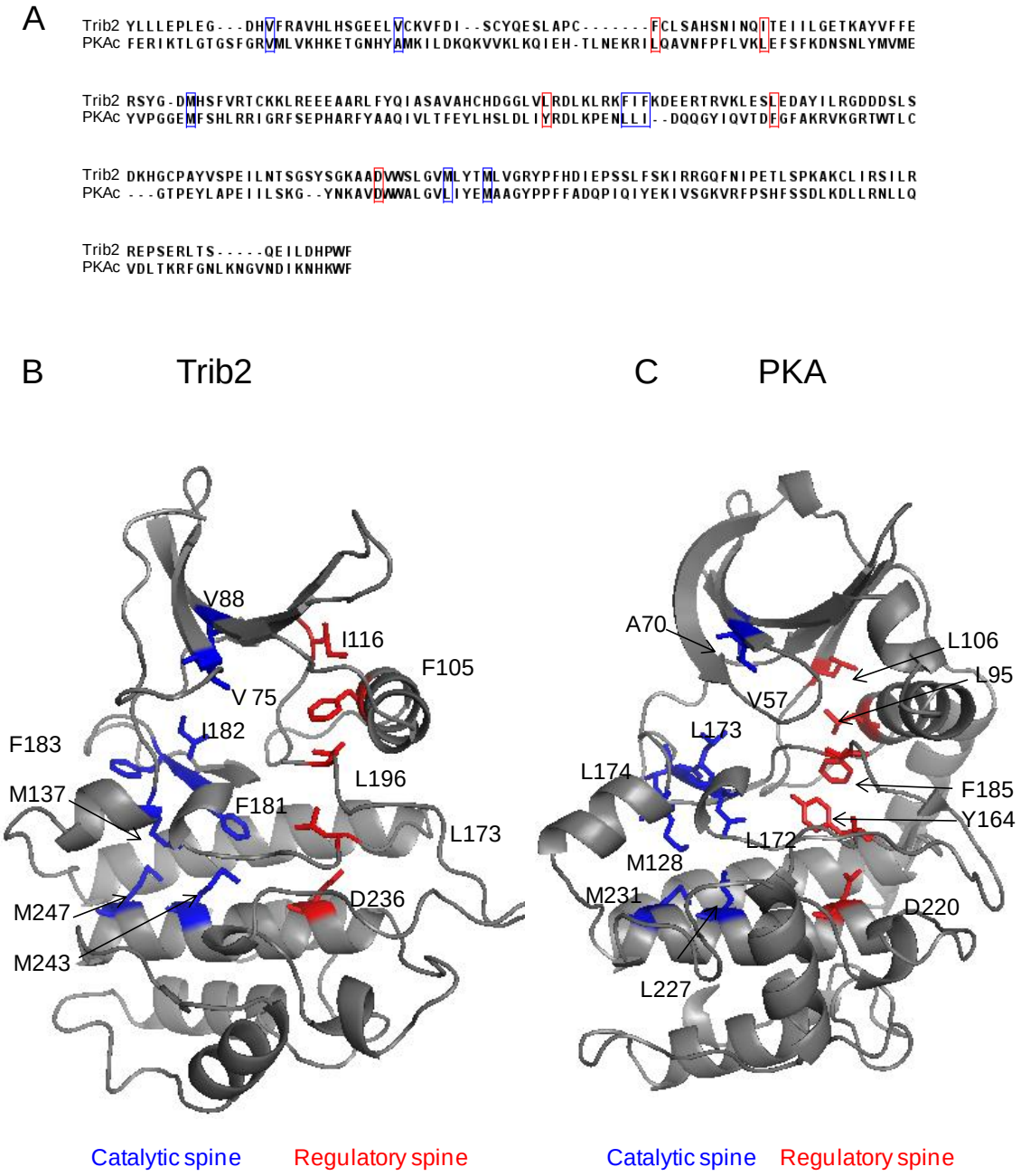

Figure 1.9 A comparison of the kinase core hydrophobic spines highlighted in a model of the Trib2 catalytic domain compared with PKA A) A MUSCLE alignment of the Trib2 and PKA catalytic domains with the catalytic spine residues highlighted in blue and the regulatory spine constituent residues highlighted in red. B) The residues that align with the PKA spine residues are annotated on the structural model of Trib2 (using the closest available kinase for which a structure is known; p38γ (PDB ID:1CM8) as a model) and displayed using Pymol. The catalytic spine is blue and the residues that comprise the catalytic spin are red. C) The corresponding PKA crystal structure (PDB ID:1ATP) with the annotated spines shown in the same colours. The PKA spine residues were obtained from Taylor *et al.,* 2010 (Figure 3).

1.20 Trib2 is not essential for mouse development

All individual homozygous "knock-out" mice for the Trib1, Trib2 and Trib3 genes are viable (Burkhardt *et al.*, 2010, Okamoto *et al.*, 2007, Takasato *et al.*, 2008) and following Trib3 knockout no clear phenotypic changes between the parameters tested could be found (Okamoto *et al.*, 2007). Homozygous Trib2 knock-out mice also demonstrated no developmental changes, with no significant differences observed between the litter sizes or incidence of premature death. As well as this, all organs appeared to develop normally and it was therefore concluded that Trib2 was not required for embryonic development or organogenesis (Takasato *et al.*, 2008). Interestingly, elevated levels of ACC expression were observed in Trib1 knockout mice (Burkhardt *et al.*, 2010). However, because of the marked similarities between the three Trib proteins, and lack of discernible phenotypes observed following individual knock-out, there might be some redundancy between each of the proteins. Creating multiple Trib knock out mice could help investigate this further, although discovery of specific small molecule regulators of Trib proteins would be even more useful.

1.21 Trib2 is associated with COP1-mediated protein degradation

Trib2 contains a COP1 (Constitutive Photomorphogenesis-1) binding domain as part of a motif in the C-terminus, and Trib2 binding to COP1 has been reported to be required for the degradation of the transcription factor C/EBPα (Keeshan *et al.*, 2010). The COP1 E3 ubiquitin ligase has a RING-finger motif, a coiled coil domain and seven WD40 repeats (Kato *et al.*, 2008). Not only does Trib2 bind to COP1 to degrade C/EBPα, but Trib2 mediated degradation of CEBP/α has also been associated with two other E3 ubiquitin ligases, βTrCP and TRIM21 in oncogenic environments (Wang *et al.*, 2013b, Grandinetti *et al.*, 2011).

1.22 Trib2 binding to COP1 is required for C/EBPα degradation and AML onset

Trib2 was associated with the development of AML (acute myeloid leukemia) in mouse models. When mice were reconstituted with bone marrow cells that expressed Trib2, they died prematurely and displayed enlarged spleen and lymph nodes. Analysis of the bone marrow and blood sampled prior to death showed

that there was extensive involvement (greater than 80%) of myeloblasts and immature myelomonocytic cells, and because the proportion of the cellular population was greater than 20% blast cells, AML was diagnosed. The immature phenotype was further validated by flow cytometry (Keeshan *et al.*, 2006). Further investigation of Trib2 induced AML, identified that HOXA9 worked synergystically with Trib2 in mice, advancing mortality from 152 and 169 days, respectively, to just 79 days for the co-transduced mice (Keeshan *et al.*, 2008). To ascertain which regions of the Trib2 polypeptide prevented the differentiation of granulocytes, a myeloid cell line, 32D, was engineered to express a variety of Trib2 protein truncations, including amino acids at the N-terminus, C-terminus or a combination of both. Fl Trib2 blocked G-CSF induced granulocyte differentiation and promoted the degradation of C/EBPα. Cells expressing the N-terminal deletion variants (namely Δ63, Δ55 or Δ32) also displayed this Trib2-driven blockade of cellular differentiation. However, cells expressing Trib2 that was mutated in the C-terminal domain or the kinase domain, or had the COP-1 binding site removed, were able to differentiate under these conditions unlike control cells expressing WT Trib2.

Furthermore, degradation of C/EBPα was impeded by the deletion of either the COP-1 binding site or a mutation within the kinase domain, whereas an N-terminal mutant, which had a complete catalytic domain and total COP1 binding sequence integrity, could still reduce C/EBPα protein levels. The N terminal deletion mutant of Trib2, and WT Trib2 could both promote serial replating of transduced cells, compared to the cells expressing the C-terminal or catalytic domain mutant Trib2. These cells lost the transformed phenotypes observed for the deleted N-terminal or WT cells (Keeshan *et al.*, 2010).

Interestingly, mutation of the Trib2 $D^{326}QLVP^{331}$ sequence to an AQLAA (Trib3 also binds to COP1 via this sequence (Qi *et al.*, 2006)), as well as a very subtle mutation of the conserved Lys in the catalytic motif (K177R, the analogous point mutation to *Drosophila* K266R (Grosshans and Wieschaus, 2000)) failed to provoke C/EBPα degradation with the same efficiency as in WT Trib2 expressing cells, and cells expressing these mutations were unable to be serially replated. Critically, mice transplanted with cells expressing both HoxA9 and Trib2 COP1 binding mutants survived for the same duration as mice transplanted with only HoxA9 cells. However, mice that had been transplanted with the N-terminal deletion

Trib2 expressing cells, had a latency period similar to that of WT Trib2 + HoxA9 (79 ±12 and 83± 3 days respectively) (Keeshan *et al.*, 2010). This proved that the ability of Trib2 to mediate leukemogenesis was dependent upon its ability to bind to COP1 and to degrade the putative tumor suppressor C/EBPα (Figure 1.10).

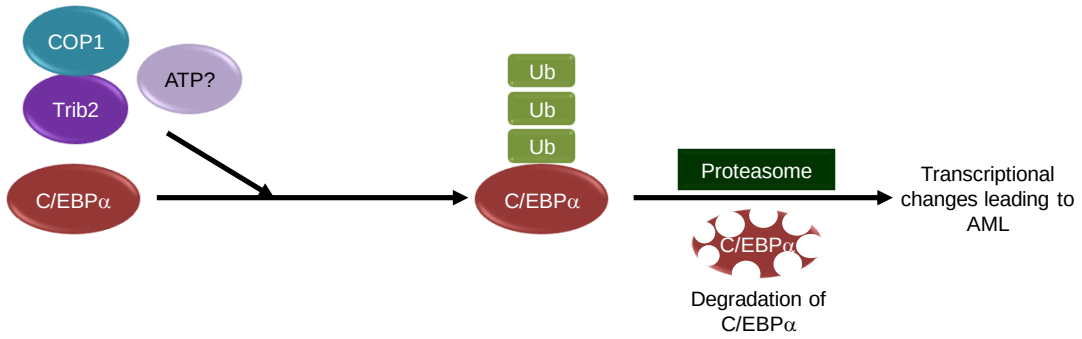

Figure 1.10 The induction of AML by Trib2-mediated C/EBPα degradation. A flow diagram showing how the putative tumour suppressor C/EBPα is targeted for degradation by COP1 binding to Trib2, which stimulates the Ubiquitination of C/EBPα and therefore targets it for proteasomal degradation, which presumably contributes to AML by a change in the transcriptional profile of the cell (Keeshan *et al.*, 2010). A requirement for ATP binding and/or hydrolysis by Trib2 in this process in cells is unknown, as shown by the '?'

In Trib2 leukemia samples, the expression of C/EBPαp30 was high compared to the p42 isoform, a characteristic of AML (Keeshan *et al.*, 2006). C/EBPαp30 lacks the mitotic inhibitory, transactivation domain in the N-teminus of the protein and this domain inhibits the activation of the c-Myc promoter by E2F1. E2F1, 2, 3 and 4, but not E2F5 activated the Trib2 promoter and following overexpression of E2F1, Trib2 mRNA increased. Adjacent to the E2F1 binding sites in the Trib2 promoter a C/EBP binding site was detected, which both isoforms of C/EBPα were predicted to bind. There was an inverse correlation between Trib2 promoter activity and the levels of C/EBPαp42 when cotransfected with E2F1. The opposite was observed when C/EBPα p30 was co-transfected with E2F1, it increased Trib2 promoter activation raising the levels of Trib2 mRNA expression. In normal cells E2F1 is inhibited by the recruitment of C/EBPαp42 on to the promoter region of Trib2, however when C/EBPαp30 is in excess the levels of Trib2 mRNA increase, which indicates that the different C/EBPα isoforms regulate the expression levels of Trib2 by modulating the promoter activities of E2F1. In AML samples derived from patients, high Trib2 and high E2F1 expression levels were apparent (Rishi *et al.*, 2014).

Both Trib2 and Trib1 are overexpressed in AML and following transplantation of Trib1- or 2-expressing bone marrow cells, transplantable-AML was induced in mouse models. However, Trib3 expressing cell-transplants did not promote leukemogenesis, consistent with its inability to degrade C/EBPα, and its lower binding ability, compared to Trib1 and 2. In domain swap experiments, when the Trib3 C-terminal domain was fused to the N/kinase domain of Trib1, C/EBPα was degraded, however the Trib3 N- and catalytic domains bound to the Trib1 C-terminal region could not degrade C/EBPα. All three human Trib proteins could bind and degrade the fatty acid-synthetic enzyme acetyl CoA carboxylase (Dedhia *et al.*, 2010), which indicates redundancy of Trib proteins is tissue specific, and a report has recently described that following Trib1 knockdown in mice, the *ACC-1* gene was upregulated, whereas in Trib1 overexpressing mice, it was downregulated (Burkhardt *et al.*, 2010). It will be interesting to observe the double Trib2/1 knockout mouse, because both of these proteins, unlike the 3rd member of the family Trib3, are thought to promote oncogenesis through the degradation of C/EBPα.

1.23 Trib2 and ALL

Trib2 is also associated with lymphoid associated leukaemia (T-ALL) and is regulated by the transmembrane receptor NOTCH1 following proteolytic cleavage. The levels of NOTCH1 protein are controlled by ubiquitination through FBXW7 (Wouters *et al.*, 2007, Hannon *et al.*, 2012, Keeshan *et al.*, 2006). Interestingly, when samples from 60 paediatric ALL patients with either NOTCH1 or FBX7W mutations were analysed, Trib2 expression was increased, with the highest expression seen in patients that have a mutation to the PEST domain of NOTCH1, which controls its rate of turnover. Trib2 was identified in particular subsets of ALL. Compared to controls, T-ALL that had a normal karyotype and pre B-ALL t(1:19) both expressed Trib2 to a significantly high level, however, pre B-ALL t(12:21) in contrast had reduced Trib2 expression. In Trib2 high expressing ALL, other genes significantly expressed were associated with T-cell signaling and this indicates that the role of Trib2 could be involved with lineage determination of T/B cells (Hannon *et al.*, 2012).

1.24 Trib2 regulates the stability of C/EBPα in NSCLC

Trib2 mediated degradation of the transcription factor C/EBPα has also been associated with driving the development of non-small cell lung cancers (Grandinetti *et al.*, 2011). NCI-H1650 lung cancer cells that had either been cultured as a monolayer or in non-adherent conditions (which increases their tumorigenesis abilities) were injected into NOD/SCID mice. By comparing the gene expression profiles of the tumors that formed in the mice derived from spheroids with tumors derived from the monolayer, Trib2 expression increased by as much as 76 fold. Furthermore, Trib2 was overexpressed in ~ 1/3rd (20/68) of primary tumor samples tested. SNP analysis and qPCR identified that Trib2 gene amplification had occurred in 12% (8/68) of the tumors.

Following shRNA knockdown in two different cell lines, cell proliferation of transformed cells and the ability to grow in non-adherent conditions was reduced, indicating that without Trib2 expression, the oncogenicity of the cells was hindered. This was confirmed further by the injection of NOD/SCID mice with either Trib2 shRNA expressing cancer cell lines, or controls. The Trib2-silenced cells failed to initiate tumor growth, in comparison, tumorigenesis was prevalent in mice that were injected with cells that still expressed Trib2. Following Trib2

depletion the levels of C/EBPα rose. Cells that had higher C/EBPα levels matured defined lineages. However, Trib2 expressing cells maintained an immature, undifferentiated phenotype. In primary tissues, it was confirmed that samples with a high Trib2 expression had low levels of C/EBPα. TRIM 21 was the E3 ligase required for C/EBPα degradation in lung tissues. Despite COP1 expression, it was not identified bound to Trib2, which indicates cell-specific E3-ligases are involed with Trib2-mediated C/EBPα degradation regulation by ubiquitination (Grandinetti *et al.*, 2011). When A549 cells, a lung cancer cell line was transfected with either of the microRNAs miR511 or miR 1297 that target the 3'UTR of Trib2, the expression of Trib2 reduced and as a result of this levels of C/EBPα rose and the rate of proliferation decreased. A549 cells transfected with the miRNAs were transplanted into the mice. The tumors that developed were smaller than the control Trib2 expressing tumors (Zhang *et al.*, 2012).

1.25 Trib2 levels are regulated by β-TRCP and Smurf1

Trib2 has been associated with the E3 ubiquitin ligases β-TRCP and Smurf1 in liver cancer cells (Wang *et al.*, 2013c, Qiao *et al.*, 2013), however, in this instance C/EBPα is not the intended target of degradation, but Trib2 itself. Both of these ligases interact with Trib2 at the N-terminus of the protein in what has been termed the 'Trib2 Degradation Domain' (Trib2 1-5) (Qiao *et al.*, 2013), however, the removal of the Trib2 C-terminus also reduced Trib2 interaction with β-TRCP, albeit incompletely (Wang *et al.*, 2013b). Overexpression of β-TRCP increased the ubiquitination of Trib2. Other β-TRCP substrates include the protein PERIOD which contains a phosphodegron that has a phospho-Thr as the N-terminal residue in this motif (TSGSYS). Trib2 also has this motif but it has yet to be functionally analysed (Qiao *et al.*, 2013) and it is not known if these Ser residues are phosphorylated. Interestingly, p70S6K phosphorylated Trib2 at Ser83, and this was recently shown to be required for Trib2 degradation by Smurf1 (Wang *et al.*, 2013c). Consistently, when p70S6K is silenced, Trib2 is not targeted for degradation and the presence of Trib2 protects the oncogene YAP from β-TRCP mediated degradation. An indication that Trib2 also regulates C/EBPα in hepatic cancers was observed when the expression of the transcription factor increased following Trib2 knockdown (Wang *et al.*, 2013c), which resembled data observed in lung tumors and AML (Keeshan *et al.*, 2010, Grandinetti *et al.*, 2011). The regulation of C/EBPα was independent of β-

TRCP. Interestingly, high C/EBPα levels prevented the YAP-TEAD interaction, which is important for YAP mediated transcriptional activation. In this context, Trib2 acts as an apparent mediator, or 'hub' interlinking the three signaling pathways; Wnt, YAP, and C/EBPα in liver tumorigenesis (Wang *et al.*, 2013b).

1.26 Trib2 regulates FOXO activity in malignant melanoma

Trib2 was identified as a regulator of FOXO (forkhead/winged helix class O transcription factor) activity following a large-scale siRNA screen. When Trib2 was knocked down, the activity of FOXO, a tumor suppressor, increased. Trib2 mRNA expression was upregulated in 70% of matched skin cancer samples tested compared to normal, and all of these positive hits were from malignant melanomas. Further analysis observed the presence of overexpressed Trib2 mRNA in stage III/IV lesions, and immortalised lines derived from high grade skin malignancies also exhibited high levels of Trib2 mRNA, compared to 'normal,' non-cancerous cell lines. Moreover the expression level of Trib2 inversely correlated with the FOXO-regulated protein, Bim, which is involved in apoptosis. Following knockdown of Trib2 in a melanoma cell line (G-361), the cells were less invasive than the control cells and growth was inhibited by cell-cell contact. Trib2 knockdown cells were transplanted into ZSCID mice and the tumors that formed in the absence of Trib2 were on average smaller than the Trib2-expressing cells (Zanella *et al.*, 2010).

1.27 Mutational analysis of Trib2 confirms a cancer association

Somatic cancer-driving mutations are commonly observed in kinases. Examples include BRAF V600E (He *et al.*, 2013) and JAK2 V617F (Griner *et al.*, 2013). To identify pseudokinases that are potential drivers of cancer, we analyzed the total frequency of somatic mutations that occur in a multitude of independent samples (Bailey, Byrne and Eyers, In Press). By mining the Catalogue of Somatic Mutations in Cancer database (COSMIC V.68), we identified the frequency of missense point mutations that occurred in each human pseudokinase domain. We assumed that if a somatic mutation occurred more than once in a pseudokinase domain then it potentially provides a survival advantage to the cell. The background (spontaneous) mutation rate was filtered by dividing the total number of missense point mutations by the protein length. This created a very basic Mutation Rate (MR) for each (pseudo)kinase. An arbitrary cut-off value of 1.0 was employed, below which significance was assumed, and the greater the number of point mutations

detected in the analyzed samples, the smaller the MR value. This held true for the cancer-associated kinases BRAF, EGFR and JAK2, which had very low MR values, 0.04, 0.02 and 0.03, respectively. Interestingly, several cancer-associated pseudokinases also had low MR values. The pseudokinases with the highest rate of mutation was HER3 (MR=0.66), which binds to ATP, exhibits vestigial kinase activity (see above) and has previously been identified to be mutated in 11% of gastric tumors sampled, and these mutations were capable of transforming normal epithelial cells, independent of ligand stimulation (Jaiswal *et al.*, 2013). Excitingly, Trib2 also had a relatively low MR value of 0.88, and therefore was more highly mutated (in respect to its size) in selected tumor samples. Trib2 point mutations that have been identified in more than one cancer sample include D211N, R251W and R286Q. Both D211N (2 occurrences) and R251W (1 occurrence) have been identified following analysis of 781 large intestine carcinomas. Out of the 781 large intestince cancer samples analysed, Trib2 was mutated 10 times (1.28%) in total. Trib2 R251W was also detected in an endometrium carcinoma sample, as was Trib2 R286Q and this Arg to Gln mutation also arose in both a breast cancer and a pancreatic cancer sample. In the database, there were 505 endometrium carncinomas sequenced and Trib2 was mutated in 6 of these (1.19%) whilst there were 905 pancreatic carcinoma samples sequenced and Trib2 was mutated in only 2 of these samples (0.22%). Interestingly, out of 1220 central nervous system carcinoma samples there were no instances of mutant Trib2 proteins detected. The total number of samples per tissue type that were analysed along with the number of samples that contained a mutated variant of Trib2 and the corresponding percentage are listed in Table A (Appendix), and future work might focus on detailing the effects of such mutations on Trib2 function.

Other pseudokinases with high mutation rates include PSKH2 (MR=0.66), JAK3 (MR=0.81) and EphB6 (MR=0.87), although the mechanistic importance of these mutations remains unknown (Table 1.3).

Kinase/ Pseudokinase Nomenclature	Uniprot ID	Poly-peptide (total amino acids)	(pseudo) kinase domain boundaries	Examples of enriched somatic mutations	Mutation Rate (%)	Normalised Mutation Rate (MR)
BRAF	**P15056**	**766**	**457-717**	**G469A, V600E**	**19.4**	**0.04**
EGFR	**P00533**	**1210**	**712-979**	**T790M, L858R**	**9.7**	**0.12**
BubR1	*O60566*	*1050*	*766-1050*	*S913F, F996L*	*0.52*	*2.02*
Ror1	*Q01973*	*937*	*473-746*	*F150L, G590R*	*0.80*	*1.17*
RYK	*P34925*	*604*	*327-600*	*R146C, R561Q*	*0.23*	*2.62*
KSR1	Q81VT5	921	611-881	V676A	0.47	1.96
KSR2	Q6VAB6	950	666-931	T778M	0.91	1.04
WNK1	Q9H4A3	2382	221-479	I1172M	1.35	1.76
WNK4	Q96J92	1243	174-432	R669W	0.61	2.04
ErbB3/HER3	P21860	1342	709-966	V438A, E928G	2.04	0.66
GUCY2A	P16066	1061	528-805	G541S, A887V	0.82	1.29
GUCY2B	P20594	1047	513-786	E567K	0.68	1.54
GUCY2C	P25092	1073	489-749	D509N, G944R	0.90	1.19
GUCY2D	Q02846	1103	525-808	R331P	0.61	1.81
GUCY2F	P51841	1108	532-812	R493H, R980L	1.21	0.95
ILK	Q13418	452	193-446	F342L, R349H	0.45	1.00
IRAK3	Q9Y616	596	165-452	R267Q, D493N	0.48	1.24
JAK1 (JH2)	P23458	1154	583-855	V658F, R742H	0.99	1.17
JAK2 (JH2)	O60674	1132	545-809	K539L, V617F	33.8	0.03
JAK3 (JH2)	P52333	1124	521-781	A572T, R657Q	1.39	0.81
PSKH2	Q96QS6	385	63-320	G312D, R338Q	0.63	0.61
SgK071	Q8NE28	680	28-297	R198C, R246H	0.38	1.79
SgK396	Q9BXU1	1019	710-1019	M804L, V860L	1.32	0.77
TYK2 (JH2)	P29597	1187	589-875	R565W, I684S	0.87	1.36
VACAMKL	Q8NCB2	501	24-286	G182R, S364T	0.39	1.28
CASK	O14396	926	12-276	R28Q, R489W	0.52	1.78
PTK7/CCK4	Q13308	1070	796-1066	E743D, A933V	0.63	1.70
NOK	Q6J9G0	422	114-384	G313V, L316F	0.43	0.98
RSKL1	Q96S38	1066	794-1056	G401S, E1022K	0.79	1.35
RSKL2	Q9Y6S9	572	145-539	-	0.26	2.20
Titin	Q8WZ42	34350	32178-32432	-	12.8	2.68

Trib1	Q96RU8	372	94-338	R178W, F371S	0.32	1.16
Trib2	Q92519	343	61-308	D211N	0.39	0.88
Trib3	Q96RU7	358	68-316	R29H	0.32	1.12
SgK223	Q86YV5	1402	976-1325	G758S	0.46	3.05
SgK269	Q9H792	1746	1313-1675	H611R, A1341V	0.95	1.84
SgK495	Q8N219	435	35-331	V121A, M133V	0.36	1.21
GCN2	Q9P2K8	1649	296-539	H939Y	1.13	1.46
SLOB	Q32NE9	578	149-396	-	0.34	1.70
PTK7	Q96C45	1275	4-280	D295Y, C384Y	0.78	1.63
IRAK2	O43187	625	210-489	V446M, G561K	0.50	1.25
MLKL	Q8NB16	471	194-469	E258K, G330E	0.37	1.27
SgK307	Q81WB6	1497	227-518	R369C, E627K	1.11	1.35
STRADβ	Q9C0K7	418	58-369	G155E, K356N	0.24	1.75
VRK3	Q8IV63	474	166-457	S91F, R461C	0.41	1.16
EphA10	Q5JZY3	1008	645-900	R150H, V1007M	0.9	1.27
EphB6	O15197	1021	670-919	K154N, R719W	1.17	0.87
NRBP1	Q9UHY1	535	68-327	T421I	0.34	1.57
NRBP2	Q9NSY0	501	38-306	-	0.13	3.85
SCYL1	Q96KG9	808	14-314	R271H, R368C	0.34	2.38
SCYL2/PACE 1	Q6P3W7	933	32-327	R301C, G355R	0.76	1.23
SCYL3	Q81ZE3	742	2-245	R61C, K307E	0.47	1.58
SgK196	Q9H5K3	350	81-350	-	0.13	2.69
STRADα	Q7RTN6	431	69-379	-	0.21	2.05
TBCK	Q8TEA7	893	1-273	R41C, F256L	0.65	1.37
TRRAP	Q9Y485	3877	3514-3839	S722F, R3486W	2.75	1.41

Table 1.3 Identifying potential cancer-driving pseudokinases. Data has been compiled from online resources (www.uniprot.org, www.kinase.com/kinbase and cancer.sanger.ac.uk/cancergenome/projects/cosmic). The mutation ratio (MR) of the canonical kinases BRAF and EFGR (bold), and a panel of pseudokinases were determined by normalizing the total frequency of somatic mutations to the length of the peptide. The MR of the BuBR1, Ror1 and RYK atypical kinases (italicized) were determined along with all human pseudokinases originally described during kinome annotaion. Trib2 is shown in red. The size of each pseudokinase-containing polypeptide, the position of the pseudokinase domain, the normalized mutation rate (polypeptide size divided by frequency (%) of samples in COSMIC v.68 containing a missense mutation, divided by 1000 for easy comparison) and examples of enriched mutations are listed in the table. Note that a lower MR indicates an increased average number of somatic mutations (normalized to polypeptide length), with enriched (≥2) mutations, many embedded in the pseudokinase domain, being noted where appropriate.

1.28 Trib2 and Inflammatory Bowel Disease

Immunohistochemical staining of Trib2 in tissue samples of Inflammatory Bowel Disease (IBD) was reduced in inflamed epithelium compared to controls. By stimulating the TLR receptors 2, 3, 5 and 9 with their cognate ligands, it was observed that the TLR5 activator flagellin increased the expression of Trib2 mRNA 2 fold higher than controls and Trib2 upregulation was not observed following TLR5 knockdown. When Trib2 was knocked down by siRNA, the activation of NFκB by flagellin-stimulated TLR5 was increased, and the levels of phospho-IKKα/β and p65 also increased, whilst the levels of phosphorylated JNK and p-38 decreased. There were no changes detected to the activation levels of the MAPK/ERK pathway. Trib2 mediates NFκB (p100/p52) activation by binding directly and reducing its phosphorylation. The Trib2 residues 158-177 were required for this effect (Wei *et al.*, 2012). Incidentally this is part of the catalytic motif and the nature of the residue at position 177 has also been identified as important for COP1-mediated C/EBPα degradation (Keeshan *et al.*, 2010).

1.29 Trib2 and Trib3 target multiple proteins for degradation

In murine pre-adipocyte cell lines that overexpressed Trib2 or Trib3, the levels of C/EBPα mRNA were reduced, indicating that Trib2/3 are required for modulation of C/EBPα expression. In contrast, the levels of C/EBPβ remained constant. As well as an observed decrease in C/EBPα levels, the mRNA levels of a second transcription factor required for adipocyte differentiation, PPARγ was also reduced. Despite both proteins reducing the levels of PPARγ and C/EBPα, Trib3 (but not Trib2) blocked the phosphorylation of AKT, indicating that they operate using two distinct mechanisms. For example, Trib2 degrades LAP protein, a C/EBPβ isoform, but not LIP, another C/EBPβ isoform that lacks the transactivation domain. The degradation is prevented by treatment with the proteasome inhibitor MG132 (Naiki *et al.*, 2007, Han *et al.*, 2009), which demonstrates that Trib2 mediated LAP levels are also regulated in a proteasome-dependent manner, although this does not require the Trib2 C-terminal region. Finally, Trib2 mediated LAP degradation prevented adipogensis (Naiki *et al.*, 2007).

1.30 Trib2 autoantigens are linked to narcolepsy

High levels of anti- Trib2 antibodies in the hypocretin producing neurons have been associated with the disease, narcolepsy. Three independent groups have noted this association in geographically distant cohorts: European, Northern American and Japanese (Cvetkovic-Lopes *et al.*, 2010, Toyoda *et al.*, 2010, Kawashima *et al.*, 2010). However, the specificity or biological role of these antibodies has yet to elucidated (Lim and Scammell, 2010). As discussed in Chapter 4, Oncomine analysis of differential Trib2 expression between cancer and non-cancer tissues highlighted the brain as site of high Trib2 expression in a variety of brain tumors. The prevalence of Trib2 protein and Trib2 reactive antibodies in brain tissue associated diseases indicates that Trib2 expression here is deleterious to health.

1.31 Trib2 autoantibodies associated with uveitis

Trib2 auto antibodies have also been associated in uveitis, inflammation of the eye, and increased levels of Trib2 reactive auto antibodies were detected in 30% of uveitis patients tested (Zhang *et al.*, 2005b). Currently, to my knowledge, there have been no other correlations discovered between Trib2 and ocular tissues.

1.32 Trib2 can inhibit MKK7 and MEK1 activity

Both acetylated low density lipoprotein (AcLDL) and LPS-treated monocytes (THP-1 cell line) caused a reduction of Trib2 expression, and when both were added to monocytes at the same time, maximum IL8 production was stimulated. IL8 stimulates the MAPK and JNK pathways, and when Trib2 levels were knocked down, the IL8 stimulated MAPK and JNK pathways were further induced. Trib2 inhibits the MAPK pathway by binding to MKK7 and MEK1 through its pseudokinase domain. This effect is observed because exposure to AcLDL reduces the expression of Trib2, and this relieves the inhibitory effect on MEK1 and MKK7, causing LPS-stimulated THP-1 cells to increase the release of IL8. The inhibitory effect of Trib2 upon MKK7 and MEK1, which activate the JNK and MAPK pathways respectively, is by a direct, binding effect (Eder *et al.*, 2008) mediated through the Trib2 sequence IL(D/L)HPWF(F/L), which is found in the pseudokinase domain between amino acids 302 and 308 in human Trib2, and is conserved in all vertebrate Trib2 homologues (Yokoyama *et al.*, 2010).

1.33 Trib1 can hyperactivate the ERK pathway

Trib1, like Trib2 can bind to MEK1, and it can also bind to the JNK-specific activator MKK4 (Yokoyama *et al.*, 2010), which Trib2 does not (Eder *et al.*, 2008). Following the binding of MEK1/MKK4 via the Trib C-terminal MEK1 interaction sequence (ILLHPWF), ERK phosphorylation/activation was increased and this interaction was crucial for Trib1 mediated leukemogeneis in murine models. Trib1 mediated disease progression was accelerated when HoxA9/Meis1 was co-expressed (Yokoyama *et al.*, 2010, Jin *et al.*, 2007), a similar synergistic effect was observed between Trib2 and HOXA9 (Keeshan *et al.*, 2008). ERK phosphorylation increased in HeLa cells (non-bone marrow derived), and in bone marrow-leukemaia cells when HOXA9/Meis1 and Trib1 were coexpressed. A Trib1 mutant that loses the ability to bind MEK1 reduced the level of ERK phosphorylation. Only Trib1 that could bind to MEK1, when co-expressed with HOXA9 activated the MAPK pathway in the absence of IL3 (Jin *et al.*, 2007, Yokoyama *et al.*, 2010). This is in contrast to Trib2, which has an inhibitory effect on MAPK signaling following exposure to AcLDL in monocytic cells (Eder *et al.*, 2008). Trib1 that was unable to bind to MEK1 could, however, still bind to C/EBPα. However, when AML cells overexpressed both C/EBPα and the Trib1 MEK1 binding mutant, the degradation of C/EBPαp42, which is mediated by both Trib1 and Trib2 expressing leukemia cells (Keeshan *et al.*, 2006), was reduced, demonstrating that C/EBPα regulation by Trib1 involved the MAPK pathway, although it is not thought that this is *via* phosphorylation of C/EBPα Ser21, an ERK1/2 phosphorylation substrate (Yokoyama *et al.*, 2010). Finally, in trisomy-21 associated leukemias a Trib1 mutation at R107 (R107L), has been observed. This mutation stimulated greater ERK1/2 phosphorylation in murine AML compared to WT upon cellular expression (Yokoyama *et al.*, 2012).

1.34 Trib1 and fatty liver disease

Trib1 is implicated in oncogenic progression of AML, and is also strongly implicated in fatty disease of the liver. For example, Trib1 knockout mice had upregulated ACC expression levels (Burkhardt *et al.*, 2010) and Trib1, along with other family members, could target ACC for COP1-mediated degradation (Dedhia *et al.*, 2010), Trib1 has been associated with the development of (nonalcoholic) fatty liver disease (Kitamoto *et al.*, 2014) and Trib1 heterozygous

knockout mice have an aberrant cytokine gene expression but are protected from obesity, intolerance to glucose and are insulin resistant, and by associating with the NFκB RelA subunit, Trib1 is thought to promote proinflammatory cytokine production (Ostertag *et al.*, 2010).

1.35 Trib3 does not induce AML, but is a cancer-associated protein

In vitro, Trib3 demonstrated an inability to degrade C/EBPα and promote AML (Dedhia *et al.*, 2010) however expression analysis in colorectal cancer showed that high Trib3 expression was observed in CRC cancers that had metastasised to the liver, lung, brain and bone, and the overall survival rate of high Trib3 expressing patients was low compared to the other groups. Following Trib3 siRNA knockdown in CRC cell lines there was a reduction in cell proliferation (Miyoshi *et al.*, 2009). High Trib3 mRNA levels indicated a poor prognosis in breast cancers (particularly the triple negative phenotype) by association with the Unfolded Protein Response (UPR) PERK/ATF4/CHOP pathway (Wennemers *et al.*, 2011b). In contrast, patients with high Trib3 protein expression in tumor samples had a longer mean overall survival compared to lower expressing tumors, although the detected protein levels did not correlate with the levels of Trib3 mRNA expression in breast cancer cell lines and patient samples. High Trib3 protein expression reduced the levels of cells that survived following hypoxic conditions but when Trib3 was knocked down, cells were more resistant to hypoxia. Typically, tumors that are tolerant to hypoxic conditions are more resistant to radiotherapy (Wennemers *et al.*, 2011a, Rouschop *et al.*, 2010). The deviations between Trib3 mRNA expression levels and Trib3 protein levels indicates that Trib3 is not just regulated at the level of transcription, but further translational regulatory events, possibly associated with hypoxia are required to modify the protein (Wennemers *et al.*, 2011a).

Overexpression of Trib3 inhibited the insulin-, but not nutrient- activation of AKT, mTOR and p70S6K, and in the livers of fed mice there was an increased level of glucose and insulin. On further analysis, the mice were insulin resistant. Trib3 inhibits Akt activation by binding to the unphosphorylated form (Matsushima *et al.*, 2006). Reduced Trib3 Akt activation, and ERK1/2 phosphorylation has also been identified in other studies (Liu *et al.*, 2010, Kiss-Toth *et al.*, 2004)

1.36 C/EBPα regulation is evolutionary conserved in Trib proteins

Drosophila Tribbles (Trbl), the founding member of the Tribbles pseudokinases is also involved in regulating the turnover of the fly C/EBP homolog: slbo. Slbo is required for the migration of border cells in the ovary of *Drosophila* (Rorth *et al.*, 2000). In the border cells Slbo and Trbl have opposing activities and the kinase domain of Trbl is required for halting border cell migration. Following individual mutations to the β3 motif (FCLR to FCLA), the catalytic Asp (to Asn) and to the Mg^{2+} ion binding loop, showed that, the FLCA mutant and the Mg^{2+} binding mutants behaved like the Tribbles-associated phenotype, but WT-mediated border cell migration pause was attenuated upon expression of the catalytic Asp mutant. This mutant also had a reduced ability to bind slbo, and suggests that the catalytic motif is functionally important for slbo degradation, which is mediated by an E3 ubiquitin ligase (Rorth *et al.*, 2000, Masoner *et al.*, 2013). In *Drosophila*, String/CDC25 is required for the mitotic progression of the cells in the blastoderm through the G2/M checkpoint (Seher and Leptin, 2000), and a loss of function mutation to String in the imaginal disc cells slows the G2 phase, causing cells to increase in size, akin to the phenotype observed from Trbl overexpression. When Trbl and String were overexpressed together, a normal phenotype was observed, which indicated that String and Trbl opposed each other and Trbl regulated String/CDC25 levels by degradation and this delayed mitosis, allowing gastrulation to complete (Mata *et al.*, 2000). A K266R mutation which is located in the catalytic loop of Trbl does not cause any phenotypic changes in the progression of cells through the cell cycle when compared to WT and it indicates that whilst the catalytic loop is important for Slbo binding, it is not the relevant binding site for String/CDC25 (Grosshans and Wieschaus, 2000).

1.37 SgK495 is required for lung development in murine embryos

In contrast to Trib1, 2 and 3 knockout mice, which are all viable and born at normal Mendelian ratios, the related pseudokinase SgK495 knockout (*STK40*$^{-/-}$) mice die within 12 hours of birth and exhibit a reduced body weight and size. Their determined cause of death was a failure to initiate breathing. Analysis of the lungs of SgK495 (-/-) mice showed that lung development was severely stunted. The small lobes contained fissures and displayed many of the phenotypes associated with

immature lungs, which included an increased glycogen level. Heterozygous mice with one functional copy of the gene (*STK40*$^{+/-}$) did not demonstrate any obvious phenotypic changes from their WT littermates (+/+). Analysis of gene expression changes following *STK40* homozygous deletion has highlighted a panel of genes that were significantly altered, and these included the genes *FGF-18*, *FGF-1*, *Shh*, *Wnt2* and interestingly, *C/EBPα*, which are known to be important for lung development (Yu *et al.*, 2013). SgK495 expression in mouse embryonic stem cells (ESCs) is inhibited by the transcription factor Oct4, when Oct4 is depleted SgK495 levels rise. SgK495 is able to signal through the MAPK pathway and activates ERK1/2 by interacting with RCN2, a Ca^{2+} binding protein to induce embryonic stem cell differentiation into the extraembryonic endoderm (ExEn) lineage (Li *et al.*, 2010). Conversely, overexpression of other Tribbles-related proteins, drive cells into an undifferentiated or more immature state, an example being Trib2 overexpression in lung tissues (Grandinetti *et al.*, 2011).

As described above, Trib2 is an important regulator of multiple, divergent, signaling pathways associated with proliferation, cell size and disease, which includes the classical MAPK pathway, the JNK pathway, the HIPPO/YAP pathway, and the Wnt signaling pathway. There is clear evidence that Trib2, and other closely related Trib family members target specific proteins for degradation, and that aberrant regulation of this process is strongly associated with cancers, especially for Trib2 and Trib1, which can both appear to regulate the stability of the transcription faction C/EBPα. However, it is as yet unclear whether the Tribbles proteins, which have all evolved a pseudokinase domain, can act catalytically to phosphorylate protein substrates, or whether they function in cells as 'inert' scaffolding proteins, whose role is to bring together various signaling complexes.

1.38 NOK (Novel Oncogene with Kinase domain)

NOK (Novel Oncogene with Kinase domain)/SuRTK106 Sugen Receptor Tyrosine Kinase 106)/STYK1 (Serine Threonine Tyrosine Kinase1), is a pseudokinase whose analysis constitutes Chapter 5 of this thesis. NOK, like the pseudokinases ErBb3 (HER3), PTK7, Ror1, Ror2, Ryk and NOK contains a (predicted) single-pass transmembrane domain found between residues 26-49 (Figure 5.2) in its N-terminal region and an intracellular pseudokinase domain (Mendrola *et al.*, 2013). NOK is a 422 amino acid polypeptide whose pseudokinase domain contains a partially conserved glycine-rich loop with the (CSGSCG), a canonical β3 motif which has the conserved lysine (K147) important for typical kinase coordination of the α- and β- phosphates of ATP. A 'complete' (canonical) catalytic motif is present in vertebrate NOK polypeptides, which contains the putative catalytic Asp residue and the Mg^{2+} ion-binding Asn at the end of the loop. The second metal-binding residue, the Asp of the DFG motif, is changed to a Gly in NOK, suggesting that NOK will not be able to phosphorylate substrates in a metal/ATP-dependent manner. These deviations from canonical kinase domains are conserved throughout NOK vertebrates, including in *Xenopus tropicalis*, which despite containing a canonical GxGxxG motif in the glycine loop, still lacks a canonical 'DFG' motif (Figure 1.11 B). Rather like the Trib-related pseudokinases, the presence of these unusual motifs has cast doubt upon the ability of NOK to bind to ATP or to phosphorylate a substrate protein, and the mechanism by which NOK signals in cells remains unknown.

A

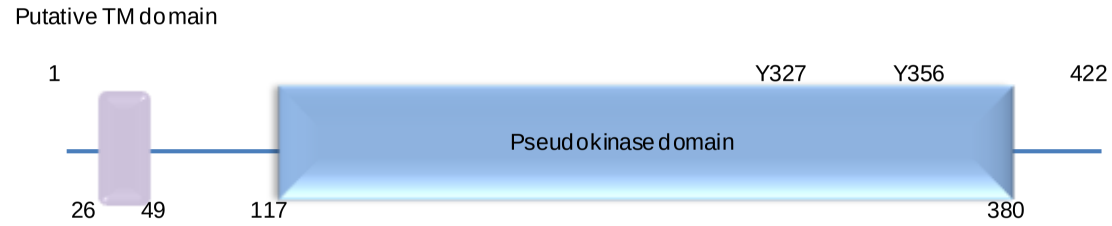
Putative TM domain
1
Y327
Y356
422
Pseudokinase domain
26
49
117
380

B

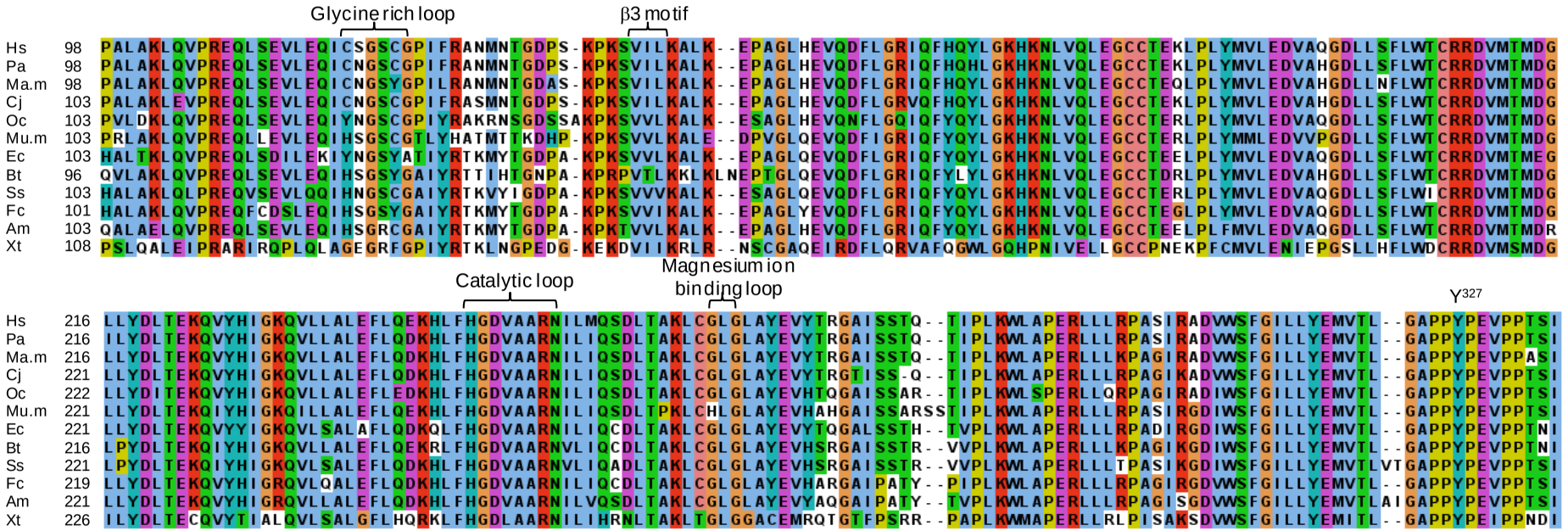
Glycine rich loop
β3 motif
Catalytic loop
Magnesium ion binding loop
Y327
Hs 98 PALAKLQVPREQLSEVLEQICSGSCGPIFRANMNTGDPS-KPKSVILKALK--EPAGLHEVQDFLGRIQFHQYLGKHKNLVQLEGCCTEKLPLYMVLEDVAQGDLLSFLWTCRRDVMTMDG
Pa 98 PALAKLQVPREQLSEVLEQICNGSCGPIFRANMNTGDPS-KPKSVILKALK--EPAGLHEVQDFLGRIQFHQHLGKHKNLVQLEGCCTEKLPLYMVLEDVAHGDLLSFLWTCRRDVMTMDG
Ma.m 98 PALAKLQVPREQLSEVLEQICNGSYGPILRANMNTGDAS-KPKSVILKALK--EPAGLHEVQDFLGRIQFHQYLGKHKNLVQLEGCCTEQLPLYMVLEDVAHGDLLNFLWTCRRDVMTMDG
Cj 103 PALAKLEVPREQLSEVLEQICNGSCGPIFRASMNTGDPS-KPKSVILKALK--EPAGLHEVQDFLGRVQFHQYLGKHKNLVQLEGCCTEKLPLYMVLEDVAHGDLLSFLWTCRRDVMTMDG
Oc 103 PVLDKLQVPREQLSEVLEQIYNGSCGPIYRAKRNSGDSSAKPKSVVLKALK--ESAGLHEVQNFLGQIQFYQYLGKHKNLVQLEGCCTERLPLYMVLEDVAQGDLLSFLWTCRRDVMTMDG
Mu.m 103 PRLAKLQVPREQLLEVLEQIHSGSCGTLYHATMTTKDHP-KPKSVVLKALE--DPVGLQEVQDFIGRIQFYQYLGKHKNLVQLEGCCTERLPLYMMLEDVVPGDLLSFLWTCRRDVMTMDG
Ec 103 HALTKLQVPREQLSDILEKIYNGSYATIYRTKMYTGDPA-KPKSVVLKALK--EPAGLQEVQDFLGRIQFYQYLGKHKNLVQLEGCCTEELPLYMVLEDVAQGDLLSFLWTCRRDVMTMEG
Bt 96 QVLAKLQVPREQLSEVLEQIHSGSYGAIYRTTIHTGNPA-KPRPVTLKKLKLNEPTGLQEVQDFLGRIQFYLYLGKHKNLVQLEGCCTDRLPLYMVLEDVAHGDLLSFLWTCRRDVMTMDG
Ss 103 HALAKLQLPREQVSEVLQQIHNGSCGAIYRTKVYIGDPA-KPKSVVVKALK--ESAGLQEVQDFLGRIQFYQYLGKHKNLVQLEGCCTERLPLYMVLEDVAQGDLLSFLWICRRDVMTMDG
Fc 101 HALAKLQVPREQFCDSLEQIHSGSYGAIYRTKMYTGDPA-KPKSVVIKALK--EPAGLYEVQDFLGRIQFYQYLGKHKNLVQLEGCCTEGLPLYMVLEDVAQGDLLSFLWTCRRDVMTMDG
Am 103 QALAELQVPREQLSEVLEQIHSGRCGAIYRTKMYTGDPA-KPKTVVLKALK--EPAGLHEVQDFLGRIQFYQYLGKHKNLVQLEGCCTEELPLFMVLEDVAQGDLLSFLWTCRRDVMTMDR
Xt 108 PSLQALEIPRARIRQPLQLAGEGRFGPIYRTKLNGPEDG-KEKDVIIKRLR--NSCGAQEIRDFLQRVAFQGWLGQHPNIVELLGCCPNEKPFCMVLENIEPGSLLHFLWDCRRDVMSMDG
Hs 216 LLYDLTEKQVYHIGKQVLLALEFLQEKHLFHGDVAARNILMQSDLTAKLCGLGLAYEVYTRGAISSTQ--TIPLKWLAPERLLLRPASIRADVWSFGILLYEMVTL--GAPPYPEVPPTSI
Pa 216 ILYDLTEKQVYHIGKQVLLALEFLQDKHLFHGDVAARNILIQSDLTAKLCGLGLAYEVYTRGAISSTQ--TIPLKWLAPERLLLRPASIRADVWSFGILLYEMVTL--GAPPYPEVPPTSI
Ma.m 216 LLYDLTEKQVYHIGKQVLLALEFLQDKHLFHGDVAARNILIQSDLTAKLCGLGLAYEVYTRGAISSTQ--TIPLKWLAPERLLLKPAGIRADVWSFGILLYEMVTL--GAPPYPEVPPASI
Cj 221 LLYDLTEKQVYHIGKQVLLALEFLQDKHLFHGDVAARNILIQSDLTAKLCGLGLAYEVYTRGTISS-Q--TIPLKWLAPERLLLRPAGIKADVWSFGILLYEMVTL--GAPPYPEVPPTSI
Oc 222 LLYDITEKQVYHIGKQVLLALEFLEDKHLFHGDVAARNILIQSDLTAKLCGLGLAYEVHTQGAISSAR--TIPLKWLSPERLLQRPAGIRADIWSFGILLYEMVTL--GAPPYPEVPPTSI
Mu.m 221 LLYDLTEKQIYHIGKQILLALEFLQEKHLFHGDVAARNILIQSDLTPKLCHLGLAYEVHAHGAISSARSSTIPLKWLAPERLLLRPASIRGDIWSFGILLYEMVTL--GAPPYPEVPPTSI
Ec 221 LLYDLTEKQVYYIGKQVLSALAFLQDKQLFHGDVAARNILIQCDLTAKLCGLGLAYEVYTQGALSSTH--TVPLKWLAPERLLLRPADIRGDIWSFGILLYEMVTL--GAPPYPEVPPTNI
Bt 216 LPYDLTEKQIYHIGKQVLLALEFLQEKRLFHGDVAARNVLIQCDLTAKLCGLGLAYEVHSRGAISSTR--VVPLKWLAPERLLLKPAGIKGDIWSFGILLYEMVTL--GAPPYPEVPPTNI
Ss 221 LPYDLTEKQIYHIGKQVLSALEFLQDKHLFHGDVAARNVLIQADLTAKLCGLGLAYEVHSRGAISSTR--VVPLKWLAPERLLLTPASIKGDIWSFGILLYEMVTLVTGAPPYPEVPPTSI
Fc 219 LLYDLTEKQVYHIGRQVLQALEFLQDKHLFHGDVAARNILIQCDLTAKLCGLGLAYEVHARGAIPATY--PIPLKWLAPERLLLRPAGIRGDVWSFGILLYEMVTL--GAPPYPEVPPTSI
Am 221 LLYDLTEKQVYHIGRQVLLALEFLQDKHLFHGDVAARNILVQSDLTAKLCGLGLAYEVYAQGAIPATY--TVPLKWLAPERLLLRPAGISGDVWSFGILLYEMVTLAIGAPPYPEVPPTSI
Xt 226 ILYDLTECQVYTIALQVLSALGFLHQRKLFHGDLAARNILIHRNLTAKLTGLGGACEMRQTGTFPSRR--PAPLKWMAPERLLRLPISAKSDVWSFGILLYEMITL--GAPPYPEIPPNDI

Figure 1.11 NOK vertebrates lack the canonical DFG motif. A) A cartoon of the NOK polypeptide domain structure with the predicted transmembrane and pseudokinase domains highlighted, along with the conserved Tyr residues Y327 and Y356. B) An alignment of human 98-335, with vertebrate NOK polypeptides, which contains conserved kinase domain residues performed in Jalview, using the Muscle alignment tool with the residues shaded in the Clustal colour scheme. Hs *Homo sapiens*, Pa *Pongo abelii*, Ma.m *Macaca mulatta*, Cj *Callithrix jacchus*, Oc *Oryctologus cuniculus*, Mu. M *Mus musculus*, Ec *Equus caballus*, Bt *Bos taurus*, Ss *Sus scrofa*, Fc *Felis catus*, Cf *Canis familiaris*, Am *Ailuropoda melanoleuca*, Xt *Xenopus tropicalis*.

1.39 NOK catalytic activity has not been demonstrated convincingly

There is currently no clear and conclusive evidence confirming whether NOK is an active kinase or a pseudokinase, and whether it autophosphorylates or can phosphorylate an exogenous substrate, perhaps including a canonical receptor tyrosine kinase. Although there are suggestions that it is catalytically active, the supporting Figures in several papers do not adequately control for potential protein kinase contaminants in the assay (Chen *et al.*, 2005b, Chung *et al.*, 2009). There is further evidence to suggest that an EPOR/NOK-transmembrane-and-intracellular domain artificial fusion protein that 'dimerises' and 'autophosphorylates' is constitutively active (Liu *et al.*, 2004). The fusion protein consists of the NOK transmembrane (TM) and intracellular domain attached to the extracellular domain of the mouse erythropoietin receptor. Human NOK does not contain such a receptor domain and so any activity observed by this fusion protein may not be reconstituted *in vivo* in a wild-type configuration and cellular environment, because it may not be able to receive any ligand stimulation. Potentially, NOK could be constitutively active in the absence of a bound ligand, or dimerise with another receptor that binds ligands, autophosphorylating NOK Tyr residues, in a similar fashion to ErbB2/ErbB3 (HER3) receptor heterodimer activity (Citri *et al.*, 2003).

1.40 NOK activates the Akt and MAPK pathways

Despite questions relating to its catalytic activity, the NOK pseudokinase has been implicated in both the Akt and MAPK pathways in cell-based studies. NOK physically interacts with Akt and in doing so, the phosphorylation of Akt-308 (the PDK1-activating site in Akt) increases, which leads to an increase in activity and downstream GSK3β phosphorylation on Ser9 (Li *et al.*, 2012). Phosphorylation at Ser9 by Akt reduces GSK3β activity by approximately 50%, but because GSK3β is constitutively active, this is sufficient to trigger changes in GSK3β-dependent signaling (Cross *et al.*, 1995). NOK has also been reported to activate the MAPK pathway and interestingly, this activation was increased further following removal of the putative NOK transmembrane domain, indication that the presence of this TM domain might regulate the ability of NOK to activate signaling pathways, or lead to constitutive NOK activation (Li *et al.*, 2009). Another example of NOK autoinhibiting the ability to activate the ERK pathway was observed following

mutation of Y417F, a tyrosine located within the C-terminal tail of NOK. When this residue was mutated to Phe, cellular proliferation increased, accompanied by increased levels of phosphorylated ERK and STAT1 (Li *et al.*, 2007). Altogether, these studies indicate that NOK has evolved a variety of mechanisms to regulate its activity, perhaps suggesting that if these are deregulated there could be detrimental consequences in terms of normal cell control pathways.

1.41 **NOK is implicated in cancer progression**

Evidence of aberrant activation of the NOK-mediated MAPK and other signaling pathways is revealed by the reported oncogenic association of NOK expression in cancers, which led to it being given the name NOK, which I have employed in this thesis. For example, BaF3 cells expressing NOK were subcutaneously injected into nude mice and this induced tumor formation and subsequent metastasis in a variety of organs distant from the point of injection, including the spleen, liver, kidney and skeletal muscle. The life span of NOK-expressing mice was reduced to just 30 days from the time of injection. Further analysis of the BaF3-NOK cells demonstrated that both the PI3K and MAPK pathways had been activated (Liu *et al.*, 2004), which is consistent with an anti-apoptotic, proliferative effect. Interestingly, NOK-mediated tumorigenesis could be prevented by mutation of either Y327 or Y356. These corresponding Tyr residues in FGFR1 (Y701 and Y724), which are conserved in a variety of RPTKs, are required for FRS2-mediated ERK activation (Chen *et al.*, 2005b). The association of NOK with human cancers has been observed by analysis of mRNA levels in patient samples. For example, elevated NOK mRNA was observed in 16/20 acute leukaemia patients and following chemotherapy, the amount of NOK mRNA detected reduced (Kondoh *et al.*, 2009). Other tumor types where NOK mRNA expression has been detected are lung (Amachika *et al.*, 2007), ovarian (Jackson *et al.*, 2009), prostate (Chung *et al.*, 2009) and breast (Kimbro *et al.*, 2008). Interestingly, NOK subcellular localization has been reported in both the cytoplasm (Liu *et al.*, 2004, Li *et al.*, 2009), and in internalised EGFR-containing endosomes (Ding *et al.*, 2012), although the function of its transmembrane domain in localization has not been investigated.

1.42 **Aims of this Thesis**

The thesis is divided into two major experimental sections. In order to help understand the biochemistry of Trib2 and the related human pseudokinases Trib3 and SgK495, I devoted the majority of my studies to analyzing these three pseudokinases, which are described in Chapters 3 and 4.

The major aims of this part of my project were to:

- Optimize the purification of recombinant, soluble human Trib2 and Trib3
- Develop a protocol that would permit the purification of large quantities of Trib2 sufficient for biochemical analysis and crystallization studies
- Identify whether Trib2 and/or Trib3 pseudokinase domains are catalytically active *in vitro*
- Analyse the metal ion sensitivity of Trib2
- Adapt a fluorescence based assay for Trib2 ligand-binding analysis
- Discover ligands that can bind to Trib2
- Generate tools to facilitate translation of recombinant Trib2 biochemical work into human cell models
- Identify novel binding partners of Trib2 in model human cells.

In addition, I was interested in understanding the biological function of a separate pseudokinase that, like Tribbles pseudokinases, lacks a canonical 'DFG' motif. The putative tyrosine kinase-like pseudokinase termed NOK has demonstrated the ability to alter several signaling pathways when overexpressed. However very little is known about its cellular role or its biochemical functions and to improve our understanding of this interesting cancer-associated pseudokinase, I have begun to evaluate its function (Chapter 5). The goals of this work were:

- Generate inducible NOK-expressing human cell lines
- Determine the subcellular localization of NOK by microscopy
- Identify signaling sequences in the polypeptide that might target NOK in cells
- Determine whether NOK pseudokinase domain mutants affect downstream signaling pathways
- Identify optimum expression conditions for expression and purification of recombinant tagged versions of NOK

CHAPTER 2. Materials and Methods

2.1 Chemicals and Reagents

All chemicals (unless otherwise stated) were purchased from either Melford or Sigma and were of the highest quality available. The pET Ek/LIC vectors were purchased from Novagen and the Flp-In T-REx system including parental cells and plasmids were purchased from Invitrogen. The pGEx-6P-1 vector containing C/EBPα, was a kind gift from K. Keeshan. All restriction enzymes used were from New England Biolabs as was the Deep Vent polymerase. Taq polymerase was sourced from Invitrogen, KOD polymerase was from Novagen. All buffers were made using RO (reverse osmosis) water and filter sterilized or autoclaved.

2.2 Antibodies described in this thesis

Antibody	Dilution for Western Blotting	Dilution for IF	Species	Source
Anti-Myc (9E10)	1:5000	1:200	Mouse	CR-UK
Anti FLAG M2	1:5000	1:200	Mouse	Sigma
Anti Trib2	1:200	NT	Rat	Si Biologics
Anti NOK	1:1000	NT	Rabbit	Abcam
Anti phospho Ser10 Histone H3	1:1000	NT	Rabbit	Upstate
Anti p44/42 (ERK1/2)	1:1000	NT	Rabbit	Cell Signaling technology
Anti phospho-p44/42 (phospho ERK1/2)	1:1000	NT	Mouse	Cell Signaling Technology
Anti Phosphotyrosine A4310	1:5000	NT	Mouse	Millipore
Anti polyHis-HRP	1:10,000	NT	Mouse	Sigma
Anti Lamin B1	NT	1:10,000		Abcam
Anti TAT-1 Tubulin	1:10,000	NT	Mouse	CRUK

Table 2.1 Primary antibodies used in this thesis. A list of the primary antibodies used for western blotting and immunofluorescence throughout this thesis. NT=Not Tested

The corresponding mouse HRP conjugated secondary antibody was purchased from Cell Signaling, and the rat HRP antibody was obtained from SI Biologics. The secondary antibodies for immunofluorescence were conjugated to the fluorophorore (either FITC or Cy3) as determined in the experiment.

2.3 Plasmid vectors

The Ligation Independent Cloning (LIC) system (Haun *et al.*, 1992) was employed to clone full length Trib2, Trib3, SgK495, Aurora A, NOK 98-422, NOK 98-415, and NOK 98-400 cDNA from appropriate templates into the pET-30Ek/LIC vector (Novagen), which leads to the expression of an N-terminal fusion protein containing 43 amino acids, a 6His tag, and an enterokinase cleavage site immediately adjacent to the cDNA. NOK and CASK were cloned into pET-41Ek/LIC vector (Novagen), which encodes a GST and 6His tag N-terminal to the cDNA, whilst Trib2 and NOK 98-422 were cloned into the baculoviral expression plasmid pBAC-2cp Ek/LIC (Novagen), which encodes an N-terminal 6His tagged fusion protein. Following ligation, the plasmids were transformed into the *E. coli* strain 'NovaBlue' (GigaSingle size) and plasmids were purified from single colonies that had been expanded overnight in 3 ml LB that contained Kanamycin (50 μg/ml), using a QIAprep Spin Miniprep kit according to manufacturer's instructions (Qiagen). Correct ligation and transformation were confirmed by restriction digestion of the plasmid and/or automated DNA sequencing using the dye-terminator method (University of Sheffield, DNA Sequencing core facility). Each DNA sequencing reaction required ~0.5 μg of plasmid DNA and employed appropriate primers to generate between 500 and 1200 bp of readable sequence.

pET-30Ek/LIC and pET-41Ek/LIC vectors were employed for the expression of recombinant proteins with N-terminal 6His or dual N-terminal GST-6His affinity tags respectively, following transformation into the BL21(DE3)pLysS (Novagen) strain of *E. coli*. Successful transformants were selected on LB-Agar plates that contained the antibiotic Kanamycin (50 μg/ml). The following three vectors were selected for, following successful transformation on LB-agar plates containing Carbenicillin (100 μg/ml). LB (Melford) was made as directed by the manufacturer and autoclaved for 15 minutes at 121°C.

The pBAC-2cp Ek/LIC (Novagen) vector was used for baculoviral protein synthesis of either 6His tagged NOK or 6His tagged Trib2 in Sf9 cells derived from *Spodoptera frugiperda* pupal ovarian tissue.

Recombinant C/EBPα was supplied in the bacterial GST-fusion vector pGEx-6P-1 (kind gift from Dr K. Keeshan) and was transformed into BL21(DE3)pLysS prior to expression as described below.

Inducible isogenic expression of FLAG tagged Trib2, or FLAG tagged or Myc tagged NOK was facilitated following the transfection of the vector pcDNA5/FRT/TO (Invitrogen) that contained either the Trib2 or the NOK gene into human Flp-In T-REx cell lines, which were selected, and maintained, using appropriate antibiotics (Scutt *et al.*, 2009).

2.4 Primer design

To clone the amplified cDNA into epitope fusion bacterial expression plasmids, the primers used were designed for Ligation Independent Cloning and generated overhangs that were complementary to the Ek/LIC plasmids used (sequences are underlined in Tables 2.2 A and B). The reverse primers were also engineered to have an additional STOP codon immediately after the cDNA (BOLD)

The PCR primers for the cloning of NOK or Trib2 into BamHI-NotI digested pcDNA5/FRT/TO, encoded a BamHI site (GGATCC) 5’ to the N-terminus of the insert, or a NotI (GCGGCCGC) recognition sequence 3’ to the insert, which facilitated vector ligation (Restriction sites are underlined with a dashed line in Tables 2.2 A and B).

Site-directed mutagenesis required the primers shaded in Tables 2.2 A and B.

A

Description	Direction	Primer Sequence 5' – 3'
LIC end + TRB2 N terminus	Forward	*GACGACGACAAGATG*AACATACACAGGTCTACC
TRB2 C-Terminus + LIC ends	Reverse	*GAGGAGAAGCCCGGT***TCA**GTTAAAGAAAGGGTCC
BamHI +TRB2	Forward	GGGGATCCATGAACATACACAGGTCTACCC
NotI +C-Terminal TRB2+FLAG tag	Reverse	GCGGCCGC**TCA**CTTGTCATCGTCGTCCTTGTAGTCCATGTTAAAGAAA GGGTCCAAGTTCTC
K90A	Forward	GGAGAGGAGCTGGTGTGCGCGGTGTTTGATATCAGCTGC
K90A	Reverse	GCAGCTGATATCAAACACCGCGCACACCAGCTCCTCTCC
K90M	Forward	GGAGAGGAGCTGGTGTGCATGGTGTTTGATATCAGCTGC
K90M	Reverse	GCAGCTGATATCAAACACCTTGCACACCAGCTCCTCTCC
K90R	Forward	GGAGAGGAGCTGGTGTGCAGGGTGTTTGATATCAGCTGC
K90R	Reverse	GCAGCTGATATCAAACACCCTGCACACCAGCTCCTCTCC
K180N	Forward	CGGGACCTCAAGCTGCGGAACTTCATCTTTAAGGACGAAG
K180N	Reverse	CTTCGTCCTTAAAGATGAAGTTCCGCAGCTTGAGGTCCCG
S195D L196F E197G	Forward	CTCGGGTCAAGCTGGAAGACTTCGGAGACGCCTACATTCTGCGG
S195D L196F E197G	Reverse	CCGCAGAATGTAGGCGTCTCCGAAGTCTTCCAGCTTGACCCGAG
K177A	Forward	CTGGTGCTGCGGGACCTCGCGCTGCGGAAATTCATCTTT
K177A	Reverse	AAAGATGAATTTCCGCAGCGCGAGGTCCCGCAGCACCAC
F129A	Forward	GAGACCAAAGCCTATGTGGCCTTTGAGCGAAGCTATGGG
F129A	Reverse	CCCATAGCTTCGCTCAAAGGCCACATAGGCTTTGGTCTC
F129G	Forward	GAGACCAAAGCCTATGTGGGCTTTGAGCGAAGCTATGGG
F129G	Reverse	CCCATAGCTTCGCTCAAAGCCCACATAGGCTTTGGTCTC
F130A	Forward	ACCAAAGCCTATGTGTTCGCTGAGCGAAGCTATGGGGAC
F130A	Reverse	GTCCCCATAGCTTCGCTCAGCGAACACATAGGCTTTGGT
F130G	Forward	ACCAAAGCCTATGTGTTCGGTGAGCGAAGCTATGGGGAC
F130G	Reverse	GTCCCCATAGCTTCGCTCACCGAACACATAGGCTTTGGT

B

Description	Direction	Primer Sequence 5' – 3'
NOK Residue 98 + LIC ends	Forward	*GACGACGACAAGATG*GCTACCACACCTGCCCTGGCTAAGC
NOK C-Terminus + LIC ends	Reverse	*GAGGAGAAGCCCGGT***TCA**AAGCATGCTATAGTTG
NOK C-Terminus Δ residues 401-422 + LIC ends	Reverse	*GAGGAGAAGCCCGGT***TCA**TACCACCAACTCTGGTACTTGTAACAC
NOK C-Terminus Δ residues 416-422 + LIC ends	Reverse	*GAGGAGAAGCCCGGT***TCA**GAGGCTCTCCACTCTGATGCC
BamHI + Myc Tag N-terminal NOK	Forward	GGATCC**ATG**GAACAAAAACTTATTTCTGAAGAAGATCTGATGGGCATG ACACGGATGCTCCTG
NotI +C-Terminal NOK	Reverse	GCGGCCGC**TCA**AAGCATGCTATAGTTGTAG
BamHI +NOK N-Terminus	Forward	GGGGATCC**ATG**GGCATGACACGGATGCTCCTG
NOK + FLAG + Stop+ NotI	Reverse	GCGGCCGC**TGA**CTTGTCATCGTCGTCCTTGTAGTCCATAAGCATGCTA TAGTTGTAG
NOK ΔBamHI	Forward	GCAGATGTCTGGTCTTTTGGCATCCTGCTCTATGAGATG
NOK ΔBamHI	Reverse	CATCTCATAGAGCAGGATGCCAAAAGACCAGACATCTGC
R377A	Forward	CCCTCACCTAGAGAGCTGGCCTTGCGCCTAGAAGCTGCC
R377A	Reverse	GGCAGCTTCTAGGCGCAAGGCCAGCTCTCTAGGTGAGGG
R379A	Forward	CACCTAGAGAGCTGCGCTTGGCCCTAGAAGCTGCCATTAAAAC
R379A	Reverse	GTTTTAATGGCAGCTTCTAGGGCCAAGCGCAGCTCTCTAGGTG
K147M	Forward	GCCCAAGAGTGTTATTCTCATGGCTTTAAAAGAACCAG
K147M	Reverse	CTGGTTCTTTTAAAGCCATGAGAATAACACTCTTGGGC
G269D AND L270F	Forward	CTCACTGCTAACATCTGTGACTTCGGCCTGGCTTATGAACTTTAC
G269D AND L270F	Reverse	GTAAACTTCATAAGCCAGGCCGAAGTCACAGAGCTTAGCAGTGAG

Table 2.2 Primers used for the generation of constructs used in this thesis. The sequences of the primers used for the amplification/mutation of A) Trib2-containing plasmids or B) NOK containing plasmids are listed in the table. The shaded primers were used for site-directed mutagenesis of the template cDNA, whereas the primers used for LIC cloning, have the required LIC sequences and these are in *italics*. The C-terminal LIC primers encode an extra STOP codon (bold). The restriction digestion recognition sequences (BAMHI and NOTI) are underlined with a dashed line and the sequences that encode the Myc (EQKLISEEDL) or FLAG epitope tags (DYKDDDDK) are underlined with a solid line.

2.5 PCR cycling parameters used to generate LIC-compatible ends

Reaction Mixture:

~100 ng DNA template cloned in a plasmid

1 µl Forward Primer (1 mg/ml stock, contains GAC GAC GAC AAC AAG ATG added to the cDNA sequence for LIC cloning, with the underlined ATG corresponding to the first Met residue)

1 µl Reverse Primer (1 mg/ml stock contains GAG GAG AAG CCC GGT TCA sequence for LIC cloning, with TCA encoding the reverse orientation stop codon TAG)

1 µl Deep Vent DNA Polymerase (2000 U/ml)

5 µl 10x ThermoPol Reaction Buffer (NEB)

5 µl 10x dNTP mixture (Final concentration 50 µM dATP, dTTP, dCTP, dGTP)

H_2O to a total of 50 µl

PCR Cycle Parameters:

Hot Start 94°C

94°C 30s
55°C 60s
72°C 240s
} 30 cycles

72°C 10 min

Hold 4°C

2.6 PCR products for blunt-end ligation into pCR2.1-TOPO vector using an overhanging adenine and Topoisomerase I ('TOPO' cloning)

>100 ng Template

1 µl Forward Primer (1 mg/ml stock) (containing a BamHI sequence)

1 µl Reverse Primer (1mg/ml stock) (containing a NotI sequence)

1 µl Taq DNA Polymerase (5U/µl) (Invitrogen)

5 µl 10x PCR Buffer

1.5 µl 50mM $MgCl_2$ (Final concentration 10 mM Mg^{2+} ions)

5 µl 10x dNTP mixture (Final concentration 50 µM each dATP, dTTP, dCTP, dGTP)

H_2O to a total of 50 µl

PCR Program:

Hot Start 94°C

	94°C 30s	30 cycles
	55°C 60s	
	72°C 240s	
	72°C 10 min	
Hold 4°C		

2.7 Site-Directed Mutagenesis PCR procedure

~100 ng Template

1 µl Forward Primer (1mg/ml stock)

1 µl Reverse Primer (1mg/ml stock)

1 µl Deep Vent (NEB) polymerase (2000 U/ml)

5 µl 10x ThermoPol Buffer (NEB) containing 10 mM Mg^{2+} ions

5 µl 10x dNTP mixture (Final concentration 50 µM of each dATP, dTTP, dCTP, dGTP)

H_2O to a total of 50 µl

PCR Cycle Parameters:

Hot Start 94°C

	95°C 30s	30 cycles
	50°C 60s	
	68°C 18 min	
	68°C 10 min	
Hold	4°C	

After PCR completion 20U DpnI was added to each PCR reaction tube and incubated for 1h at 37°C to fully digest double-stranded methylated DNA template. PCR products were checked by gel electrophoresis prior to transformation.

2.8 Ligation-Independent Cloning (LIC)

PCR products that contained LIC overhangs were gel purified and 0.2 pmol were treated with 0.6 µl T4 DNA polymerase (3000 U/ml) in the presence of DTT, dATP and T4 DNA polymerase buffer for 30 min at room temperature. The T4 DNA

polymerase was then heat-inactivated at 75°C for 20 min. The T4 polymerase treated, heat inactivated DNA fragments were incubated with the Ek/LIC vectors in a ratio of 5:1 for 5 minutes before 1 µl EDTA (1 mM) was added. After a 5 minute incubation, 2 µl of the annealed plasmid containing the LIC-PCR product was transformed into NovaBlue GigaSingle *E. coli* strain (*endA1 hsdR17*(r_{K12}^{-} m_{K12}^{+}) *supE44 thi-1 recA1 gyrA96 relA1 lac* F'[*proA*$^{+}$*B*$^{+}$ *lacI*^{q}*ZΔM15*::Tn*10* (Tc^{R})] > 1 × 10^{9} cfu/µg).

2.9 Vectors for generation of Tet-inducible stable human cell lines

To engineer Tetracycline-controlled expression of tagged full length proteins in human Flp-In T-REx cell lines (commercially available HeLa and 293, Invitrogen), the host plasmid pcDNA5/FRT/TO was employed.

N-terminal Myc epitope tagged NOK or C-terminal FLAG epitope tagged NOK or Trib2 constructs were amplified by PCR and a Bam HI site was added 5' and a NotI restriction site was added 3' to the construct DNA, which permitted rapid ligation and cloning.

2.10 Cloning of cDNA in Human expression Vectors

The pcDNA5/FRT/TO vector (100 ng/µl) was digested using the restriction enzymes BamHI (10U) and NotI (5U) (New England Biolabs).

BamHI/NotI PCR products that had a single (non-template) A on the 3' end (a by-product of using Taq-polymerase in the PCR reaction) were first cloned into the 'general purpose' pCR2.1-TOPO cloning vector (can be selected by either 50 µg/ml Kanamycin or 100 µg/ml Carbenicillin) using the TOPO-TA cloning kit (Invitrogen). The pCR2.1-TOPO was supplied linearized with a single 3' T overhang and a covalently bound Topoisomerase I, which facilitated the ligation of the Taq amplified PCR products into the plasmid. The ligated plasmid was then transformed into chemically competent OneShot TOP10 *E. coli* cells following the protocol provided by the manufacturer (Invitrogen). The pCR2.1-TOPO vector containing the recombinant NOK/ Trib2 inserts were isolated using a QIAprep spin Miniprep kit (Qiagen) and the isolated DNA was then treated with BamHI (10U) and NotI (5U) restriction enzymes and gel purified using a QIAquick Gel Extraction kit (Qiagen). Purified BamHI and NotI digested DNA inserts were ligated into the BamHI, NotI treated pcDNA5/FRT/TO vector using 400U T4 DNA Ligase (New England

Biolabs) and a ratio of vector to insert 1:5, ensuring the T4 DNA ligase was not added to the reaction mixture before the inserts were added. To observe successful ligation, ligation products were subjected to gel electrophoresis as described in the agarose gel purification section after treatment with 10U BamHI to relieve supercoiling of the plasmid alongside the nicked pcDNA5/FRT/TO that had not had the cDNA ligated into it. By analysis of the differences in migrated distance during electrophoresis it was possible to predict whether the ligation had occurred correctly. This was confirmed by dye terminator sequencing following transformation of the plasmids into GigaBlue Singles or TOP10 strains of *E. coli*, which were expanded in 3 ml selective LB overnight, and the plasmids isolated by using a QIA Spin Miniprep Kit (Qiagen) as described below and in the Manufacturer's instructions. This procedure allowed for the insertion of FLAG-tagged Trib2 or NOK and Myc-tagged NOK into this mammalian expression vector prior to generation of stable cell lines.

The NOK template cDNA used in this procedure had already undergone mutagenic PCR using the 'NOK ΔBamHI' primers listed in Table 2.2B and treatment with DpnI (as described below) to remove an internal BamHI site situated within its coding sequence, prior to amplification with BamHI/NotI NOK primers.

2.11 Plasmid DNA preparation

The plasmids from transformed GigaBlue singles, or TOP10 cells could be purified from 3 ml LB that had been inoculated with transformed cells 18 hours previously. The cells were pelleted by centrifugation and then were treated sequentially by the constituents of the QIA Spin Miniprep kit, as described in the Manufacturer's instructions (Qiagen).

2.12 Site-Directed Mutagenesis

To specifically mutate a residue in Trib2 or NOK, primers were used that introduce specified mutation(s) into the Trib2 or NOK coding sequence, but do not affect the remaining sequence integrity of the plasmid. To remove the template DNA, DpnI (20U) was added to the reaction mixtures following PCR, which were incubated at 37°C for 1hr. DpnI is able to distinguish between template DNA and PCR products due to purine methylation of the template DNA in the original host strain from which the plasmid was purified (Weiner and Costa, 1994). The PCR

products were then transformed into the NovaBlue GigaSingles strain of *E. coli*. The mutated plasmids were isolated using a QIA miniprep QuickSpin Kit (Qiagen) from one colony that had been expanded overnight in 3 ml LB. Successful mutagenesis was determined by dye terminator sequencing (University of Sheffield).

2.13 Agarose gel Purification of DNA fragments

After PCR amplification or digestion with restriction enzymes, the DNA products were isolated using electrophoresis in 0.8% (w/v) agarose gels (solid agarose was dissolved in 1x TAE in a microwave), which contained the intercalating DNA stain ethidium bromide (final concentration 5μg/ml). The DNA was electrophoresed at a constant field strength of 6.7 Vcm^{-1} for ~45 min. The DNA was then viewed on a UV transilluminator and DNA migrating at the predicted size (when compared to a 1-10 kb DNA marker ladder, New England Biolabs) was extracted using the QIAquick Gel Extraction kit, as described in the manufacturer's protocol (Qiagen). Briefly, this involved adding 900 μl QG buffer to the gel fragment which was melted by incubating the solution in a water bath at 50°C. After the gel had dissolved, 200 μl isopropanol was added and the solution was applied to the QIA quick spin column provided in the kit. Following centrifugation at 16162 *x g* for 1 minute the flow through was discarded. This process was repeated until all the solution had passed through the QIA quick spin column. To the column, 750 μl Buffer PE (containing ethanol) was added and the column was centrifuged as before. The flow through was discarded and a further 1 minute centrifugation step performed after 2 minutes later had elapsed. The DNA was eluted in 40 μl of sterile, distilled H_2O that had been applied to the centre of the silica membrane in the column. After 1 minute the DNA was spin-eluted and stored at -20°C and 4 μl of the purified plasmid were re-examined by gel electrophoresis, and if the presence of the plasmid is visible by UV, a sample is sequenced and the remainder frozen at -20°C.

2.14 General protocol for chemical transformation of *E. coli*.

Approximately 20 ng of plasmid DNA containing Trib2/NOK constructs were added to 50 μl aliquots of Novablue Gigasingles (for plasmid generation) or 10 μl BL21(DE3)pLysS (for protein expression) strains of competent *E. coli* cells and incubated on ice for 30 minutes. The mixtures were then transferred to a 42°C water bath for a 30s heat shock and immediately placed back on ice for a further 2 min.

Two hundered of pre-warmed (37°C) SOC media (2% tryptone, 0.5% yeast extract, 10 mM NaCl, 2.5 mM KCl, 10 mM $MgCl_2$, 10 mM $MgSO_4$, 20 mM glucose) was added to the transformation mixture and incubated for 2 hours in a heated shaker at 37°C. The mixtures were plated onto pre-warmed Luria-Bertani (LB) media and agar plates that contained antibiotics for selection. The plates were incubated for 18 h at 37°C. Upon growth of colonies, individual clones were picked and expanded in 3ml of selective LB broth at 37°C for 18 h. Plasmids were purified from Novablue Gigasingles using the QIAprep spin Miniprep kit and stored at -20°C or protein was expressed from the BL21(DE3)pLysS cells. Glycerol stocks were created by adding glycerol (to a final concentration of 15% v/v) to the transformed cells in LB broth and stored at -80°C.

2.15 Optimising protein expression in BL21 (DE3) pLysS *E. coli* strain

Trib2 expression:

Two autoclaved 2 litre flasks containing 1 litre sterile LB (supplemented with 50 μg/ml filtered kanamycin) was inoculated with 500 μl of an overnight culture of *E. coli* BL21(DE3)plysS that had been transformed with pET-30 Ek/LIC Trib2. The flasks were incubated at 37°C whilst rotating at 1 *x g*. When the A_{600nm} reached 0.8, protein expression in both flasks was induced by the addition of sterile Isopropyl-1-thio-β-D-galactosidase (IPTG) at a final concentration of 0.5 mM.

One flask was incubated for 3 hours at 37°C, whilst the other was incubated for 18 hours at 18°C. The cells were pelleted and lysed as described below. Induction for 18 hours at 18°C was routinely used when expressing pET-30 Ek/LIC Trib2, Trib3, SgK495, STRADα, pET-41 Ek/LIC CASK and C/EBPα pGEX-6P-1

NOK expression:

Three mililitres of autoclaved LB broth supplemented with Kanamycin (50 μg/ml) was inoculated with BL21(DE3)pLysS strains transformed with either pET-30Ek/LIC or pET-41Ek/LIC vectors ligated to NOK DNA corresponding to residues 98-400, 98-415 or 98-422 in sterile 15 ml Falcon tubes. To induce protein expression IPTG was added in a sterile environment, once the cells reached mid-log phase (A_{600nm} 0.8) and the cultures were incubated at 37°C for 3 h or 18°C for 18 h. Subsequently, the cultures were centrifuged at 21036 *x g* for 20 min. The media was discarded and the cell pellet resuspended in sodium dodecyl sulphate (SDS) sample

buffer (5x SDS sample buffer: 10% SDS, 10mM β-mercaptoethanol, 20% glycerol, 0.2M Tris 6.8, 0.05% Bromophenol Blue.). The proteins were boiled for 5-8 min and then resolved using SDS-PAGE (See SDS-PAGE below).

2.16 Lysis of *E. coli* cells

Two litres of autoclaved LB were inoculated from -80°C glycerol stocks of His tagged Trib2, Trib3, Aurora A, SgK495, STRADα, GST-His tagged CASK and GST C/EBPα transformed BL21(DE3)pLysS and incubated at 37°C, 1 *x g*, until the A_{600nm} reached 0.8 at which point a sample was taken and stored at -20°C. Recombinant protein expression was induced by the addition of 0.5 mM IPTG and the flasks were incubated for a further 18 hours at 18°C on a shaking platform.

To purify 6His-tagged proteins, the cells were pelleted and ice-cold lysis buffer (50 mM Tris-HCl pH 7.4, 300 mM NaCl, 0.1% Triton X-100, 10 mM imidazole, 1 mM DTT, 0.1mM Na-vanadate, 10 mM NaF, 10 mM β-glycerophosphate, 100 nM okadaic acid and a cOmplete protease inhibitor cocktail tablet (Roche)) added. The cells suspended in the lysis buffer were then sonicated for 10s intervals on ice at an amplitude of 11 microns using a 3 mm exponential microprobe attached to a MSE Soniprep 150 plus motor unit. After sonication, the samples were centrifuged at 4°C for 30 min at 5525 *x* g to pellet unwanted cellular debris and a 200 µl supernatant sample was collected and stored at -20°C. The soluble cell lysate was purified by IMAC (described below)

NOK: A single colony in BL21(DE3)pLysS *E. coli* strain was picked using a sterile tip and used to inoculate 3 ml liquid LB supplemented with Kanamycin (50 µg/ml). After the OD reached 0.8 a sample was frozen and IPTG added to the remaining culture. After incubation with IPTG for the appropriate time, the cells were pelleted and whole cell lysates generated by the addition of 2 x SDS PAGE loading buffer, which were sonicated and the proteins resolved by SDS-PAGE, along with the uninduced fractions.

2.17 Lysis of Sf9 cell pellets

Cell pellets (~$2x10^9$ cells) (supplied by Dr Edward Mackenzie, University of Manchester) expressing His tagged NOK catalytic domain (98-422) or His tagged full length Trib2 (1-343) were lysed in cell lysis buffer (50 mM Tris pH 7.4, 300 mM NaCl, 1 mM DTT, 10 mM imidazole, 0.1 mM Na-vanadate, 0.1 mM NaF, 10 mM β-

glycerophosphate pH 7.4, 100 nM okadaic acid, 0.1% Triton X-100, 1 x cOmplete protease inhibitor tablet) and sonicated 6 times for 20 seconds followed by three 20 second pauses on ice. The lysate was cleared of insoluble matter by centrifugation and was then incubated with TALON resin (described below).

2.18 Immobilised Metal Affinity Chromatography (IMAC) of recombinant His tagged proteins

Following lysis of the bacterial cell pellet, which contains the endogenous and exogenous recombinant proteins, the cleared lysate was either applied to a 5 ml Ni Sepharose His Trap HP column (GE Healthcare) or TALON metal affinity resin (Clontech). The cleared lysate which contained either expressed His tagged Trib2, Trib3 SgK495, STRADα, Aurora A or GST-His CASK was applied to the Ni Sepharose resin that had been equilibrated in 5 column volumes of filtered, degassed wash buffer (50 mM Tris-HCl pH 7.4, 500 mM NaCl, 20 mM imidazole, 1mM DTT) using an Äkta FPLC system (GE Healthcare) as the pump and sample collector. Following injection of the lysate on to the resin, the column was washed with 5 column volumes of wash buffer and then 3 column volumes of elution buffer (50 mM Tris-HCl pH 7.4, 300 mM NaCl, 300 mM imidazole, 1 mM DTT, 10% glycerol). Throughout the washing and elution process 500 μl fractions were collected by a Frac-920 (GE Healthcare), prior to the washing step 1.5 ml fractions of the flowthrough were collected. All fractions were immediately transferred to ice. The fractions that corresponded to the peak on the elution profile (monitored by the absorbance at A_{280nm}) were analysed by SDS-PAGE.

Bacterial NOK expressing cell lysates and Sf9 lysates containing expressed Trib2 or NOK proteins were applied to wash buffer-equilibrated TALON (cobalt conjugated) metal affinity resin. The columns containing the resin and lysate were incubated for 2 hours at 4°C on a see-saw rocker. The lysate was then drained into a collection tube and the resin washed with a total of 40 column volumes of wash buffer (50 mM Tris-HCl pH 7.4, 500 mM NaCl, 20 mM imidazole, 1mM DTT), which was collected and then six column volumes of elution buffer (50 mM Tris-HCl pH 7.4, 300 mM NaCl, 300 mM imidazole, 1 mM DTT, 10% glycerol) was added and this was collected in 0.5 ml fractions, all performed on ice. The presence of eluted protein was checked by observing a colour change by adding 5 μl to 495 μl

Coomassie Plus Protein Assay Reagent (Thermo Scientific Pierce) and all eluted fractions were resolved by SDS-PAGE.

Unless the proteins were purified further by gel filtration, the fractions that contained the eluted tagged recombinant protein were pooled and dialysed into (described in Chapter 3, buffer A) 50 mM Tris pH 7.4, 150 mM NaCl, 1 mM DTT 10% glycerol or (buffer B) 20 mM bicine pH 9.0, 100 mM NaCl, 1 mM DTT, 10% glycerol, the buffer was replaced after the initial 30 minutes and aliquots were snap frozen in liquid nitrogen then stored at -80°C. Unless stated, all Trib2 preparations were dialysed into buffer B.

The Trib2 protein yield obtained by purification from TALON resin and Ni Sepharose was comparable and therefore Ni Sepharose in combination with the Äkta FPLC was routinely used for rapid purification of Trib2 recombinant protein by IMAC.

2.19 Purification of GST-C/EBPα

Following cell lysis of bacterial cells expressing GST-C/EBPα (as described above), the cleared lysate was slowly re-circulated through the 1ml GSTrap column (equilibrated in wash buffer prior to lysate addition) (GE Healthcare) packed with Glutathione Sepharose High Performance resin for 2 hours at 4°C. The column was then washed with 30 column volumes of wash buffer (described above) and GST-C/EBPα was eluted by the addition of 10 mM reduced glutathione in 50 mM Tris pH 8.0, 5 mM DTT. Fractions (500 μl) were collected and proteins detected by SDS PAGE. Fractions that contained GST-C/EBPα were pooled and dialysed into 20 mM bicine (pH 9.0), 100 mM NaCl, 1mM DTT and 10% (v/v) glycerol.

2.20 Molecular Weight Gel Filtration Standard curve

2 mg/ml Blue Dextran, 10 mg/ml albumin, 5 mg/ml alcohol dehydrogenase, 4 mg/ml β-amylase, 3 mg/ml carbonic anhydrase and 2 mg/ml cytochrome c protein standards were dissolved in 500 μl IMAC elution buffer and analysed on a Superdex200 10/300 gel filtration column (GE Healthcare). The proteins were eluted from the gel filtration column in 20 mM bicine pH 9.0, 100 mM NaCl, 10% glycerol, 1 mM DTT. The column elution volumes (Ve) were measured from the centre of the peaks and the Ve/Vo value derived, where Vo is the void volume (2 mg/ml Blue Dextran). The MW for each protein were plotted on a semi-log (Linear X-axis, log-

scale Y-axis) graph as a function of the Ve/Vo values and the line of best fit plotted. This allowed estimation of the molecular mass of proteins that eluted in a known volume, and is discussed further in Chapter 3.

2.21 Size exclusion chromatography of Trib2 for buffer exchange and purification

IMAC-purified Trib2 at a concentration of 2 mg/ml or higher (no more than a 1 ml volume was applied at any one time to prevent the peaks broadening and reducing the separation between constituent proteins), was applied to an equilibrated (20 mM bicine pH 9.0, 100 mM NaCl, 1 mM DTT, 10% glycerol) Superdex 200 10/300 GL gel filtration column (GE Healthcare) attached to an Äkta FPLC. The protein was loaded on to the column and eluted in the buffer used for equilibration at a flow rate of 0.5 ml/min or lower depending upon the detected pressure. If the pressure reached 1.5 MPa, then the flow rate was reduced. The molecular weight of the eluted proteins could be estimated by comparing their elution volume with reference to the Molecular Weight standards (Chapter 3). The fractions were subjected to SDS PAGE analysis. To prevent aggregation on the column, monomeric Trib2 can only be obtained by including 10% glycerol in the buffer. Size exclusion not only facilitates a buffer exchange but also permits the isolation of purified soluble proteins in native complexes.

2.22 Mass Spectrometry analysis for Trib2 MW determination

Electrospray ionisation mass spectrometry (ESI-MS) was performed using a Waters Q-TOF Global and a nano-electro spray, on gel filtered Trib2 that eluted in the volume of the monomeric species. BSA was used as a standard and the data deconvoluted using MAXENT1 software (Waters) by Dr. Claire Eyers (University of Liverpool).

2.23 Bradford Assay

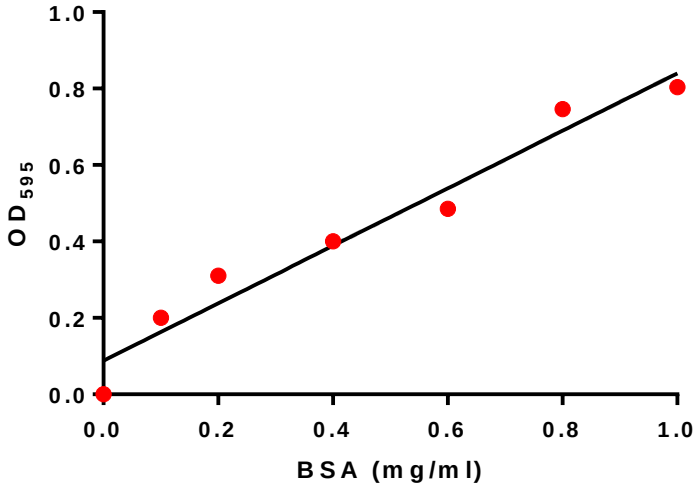

Figure 2.1 Bradford Assay Standard Curve for determination of protein concentration. At 595 nm the optical density of BSA concentrations incubated with the Coomassie based reagent were determined and a standard curve generated. A linear increase in absorbance at concentrations up to 1.0 mg/ml was determined

An Albumin protein standard (2mg/ml) (Thermo Scientific) was diluted to various concentrations (ranging from 0 – 1 mg/ml) in Coomassie Plus Protein Assay Reagent (Thermo Scientific), using the method of Bradford (Bradford, 1976). The A_{595nm} absorbance levels of samples were measured relative to the blank (no BSA) and a standard curve plotted to allow estimation of the protein concentration for any unknown sample.

To determine sample protein concentrations, 5 µl of sample was added to 495 µl of Coomassie Plus Protein Assay Reagent and the A_{595nm} value was recorded after shaking for 5 seconds. The concentration of protein was then calculated by comparison with the standard curve.

An alternative (non-Coomassie based) method that can be used to measure Trib2 concentration is to measure the absorbance at 280 nm by using a Nanodrop device and the equation Concentration (M) = Absorbance at A_{280nm} / Molar Extinction coefficient (His tagged Trib2 Molar extinction coefficient assuming all disulphide bonds are reduced is 0.629). This technique was used to estimate Trib2 concentration for NMR analysis alongside a very basic calculation that A_{280nm} of 1.0 ≈ 1 mg/ml soluble protein.

2.24 SDS PAGE.

Following protein concentration determination, equal (or unknown) amounts of proteins were denatured in 5x SDS sample buffer to a final concentration of 2% SDS and boiled for 5 minutes before being resolved using SDS Polyacrylamide Gel Electrophoresis. Each sample was run on 12% (or 15% if proteins below 20 kDa were analysed) polyacrylamide gels for 65 minutes (or until the dye front had exited the base of the gel) in an electric field strength of 20 Vcm^{-1} in running buffer (25mM Tris, 190mM glycine, 0.1% SDS). Known amounts of BSA standard were run alongside the samples in polyacrylamide gels. After electrophoresis was complete, the resolving gel was placed into Coomassie stain (0.2% Brilliant blue R-250, 7.5% acetic acid, 50% methanol) and left for up to 1 h on a See-Saw Rocker for the gel to become fully stained. The non-specific Coomassie stained regions were then removed, leaving visible bands of protein by washing the gel for 12 hours in multiple changes of destain buffer (7.5% acetic acid, 50% methanol).

2.25 Western Blotting

Samples were resolved by SDS-PAGE electrophoresis but upon completion instead of placing the gel into Coomassie strain it was placed into a cassette along with nitrocellulose membrane (Whatman Protran) to transfer the protein from the gel to a solid membrane support. A gel was run as described for SDS-PAGE. The cassettes containing the membranes were then placed into a tank containing transfer buffer (25mM Tris, 190mM glycine, 0.1% SDS, 20% methanol) and the voltages set for protein transference at either 80V for 2 hours (at 4°C) or at 20 V for 10 hours. The membranes were then placed in block (5% non-fat milk (Marvel) in TBS-T) for 30 minutes and incubated for 12 hours at 4°C with primary antibody at various dilutions in 5% non-fat milk in TBS-T or 5% BSA in TBS-T depending upon which primary antibody was employed (see Table 2.1). The membranes were washed 3 times in TBS-T and the secondary antibody, also diluted to a specific concentration (usually 1/5000 dilution in 5% non-fat milk TBS-T) and added for one hour at room temperature. The membranes were then washed a further 3 times in TBS-T and placed into a developing cassette. ECL (Amersham) developing agent was added to the membranes in accordance with the manufacturer's protocol and films were exposed and developed.

The BSA standards used for Coomassie stained gels were replaced by positive controls that could be detected with the desired antibody.

2.26 Preparation of working stocks of γ^{32}P-ATP

ATP (adenosine 5'-triphosphate, tetra(triethylammonium) salt in 10mM Tricine (pH 7.6)) that was γ^{32}P-labelled, was supplied by Perkin Elmer in volumes of 35 μl (5 mCi), and had an activity equivalent to ~140 μCi/ml at the 'activity' date. For pseudokinase assays, generally 995 μl of 10 mM ATP was added to 5 μl of ^{32}P-ATP radionucleotide giving a 10 x working stock solution at ~700 μCi/ml. In most experiments, a final concentration of ATP of 1 mM was used per assay, and the final volume of each assay was 30 μl, meaning that 3 μl of the radiolabelled 10x working stock of ATP was added; this equates to ~2.3 μCi γ^{32}P ATP per assay. Prior to addition of the radionucleotide, the 10 mM stock of ATP was adjusted to pH 9.0. Note, the half-life of ^{32}P is ~14.3 days, and so the ratio of ^{32}P ATP was adjusted as the stock solution decayed.

2.27 *In vitro* kinase assays

Either 250 pmoles of bacterially expressed pseudokinase, or 250 pmoles Trib2 WT (Sf9) in 20 mM bicine pH 9.0, 100 mM NaCl, 1 mM DTT, 10% glycerol was incubated with 1 mM ATP (2.2 μCi γ^{32}P ATP), 10 mM of the appropriate divalent cation or 2 mM EDTA (as required) and various concentrations of protein substrates (as required) in a total volume of 30 μl. Each condition was performed in duplicate. For each assay the following concentration of substrates were tested: α-Caesin 1 mg/ml, MBP 0.5 mg/ml, Histones (H1, H2A, H2B, H3 and H4) 1mg/ml, GST-C/EBPα.

For NOK (Sf9) assays, the required volume of lysate to equal 1 μg protein was incubated with either 10 mM Mg^{2+}, 10 mM Mn^{2+} or no cation and 1 mM ATP, both unlabelled and labeled (as described above for the Trib2 assays). When assayed with unlabelled ATP, the protein was transferred by western blotting to membrane for phosphotyrosine analysis.

The ATP was added immediately prior to the start of the assays which were staggered to allow for termination at the stipulated timepoint. The assays were

performed at 30°C whilst on a temperature-controlled Eppendorf shaking platform. The reactions were terminated by the addition of 5x SDS loading buffer and heated at 95°C for 5 minutes. A sample of each terminated assay (25 μl) was loaded into 12% SDS PAGE gels (a 15% gel was employed if low molecular weight kinase substrates were assayed) and the proteins resolved for 65 minutes at 20 Vcm^{-1}. Subsequently, proteins were visualized by staining with Coomassie Blue and following destaining of the gels, were dried onto blotting paper using a slab gel drier (SCIE-PLAS) for 2 hours at 80°C (or < 3 hours for 15% gels, it is worth noting that these times are extended if multiple gels are dried at the same time). The gels were then placed into a cassette that contained a reflector screen and were taken to the dark room where, under red light, an X-ray film was placed on top for analysis by autoradiography. The cassette was transferred to the -80°C freezer and left for a minimum of 48 hours, during which time the film becomes blackened as a function of ^{32}P decay. The films were subsequently developed and fixed following standard procedures. For phosphorimage analysis, a phosphorscreen was placed over the top of the gels for ~12 hours, and ^{32}P decay detected by photo-stimulated luminescence on a Fuji FLA-3000 phosphorimager. Data was analysed with ImageReader Software. The values obtained following phosphorimage analysis were averaged and plotted graphically using GraphPad Prism6 software.

2.28 Differential Scanning Fluorimetry analysis of Trib2

To determine the extent of folding of recombinant Trib2 after expression in *E. coli*, 5 μM of purified Trib2 was mixed, or boiled for 5 minutes and then mixed, with Sypro Orange dye of unknown final concentration. Prior to addition, the dye (supplied as a '5000 x' solution by Invitrogen) was diluted 1:40 in 20 mM bicine (pH 9.0), 100 mM NaCl, 1 mM DTT to create a 10 x working stock solution (as used to analyse kinases previously (Eathiraj *et al.*, 2011)). The total volume of each reaction was made up to 25 μl in buffer B (see IMAC purification) and for each reaction, master mixes sufficient for assays to be performed in triplicate were made. The solutions were thoroughly mixed and 25 μl dispensed into individual wells of a 96 well plate along with a buffer-dye solution that did not contain protein for a blank. The plates were sealed by optical adhesive covers to prevent sample evaporation and centrifuged for 15 seconds at room temperature. They were then placed into a real time PCR machine (Applied Biosystems StepOne Plus) for thermal

analysis. The temperature range was set between 25°C and 90°C and the temperature increased at a rate of 0.3°C/minute. The data was collected by the StepOne Software v2.1 and using a combination of Microsoft Excel and GraphPad Prism 6, the detected fluorescence readings for each temperature increment were averaged and thermal denaturation curves generated.

To analyse ATP binding to proteins, 5 μM Trib2 or Aurora A was incubated with increasing concentrations of ATP (pH 9.0) from 10x working stock solutions and mixed with Sypro Orange dye as described previously. From the generated thermal denaturation curves, the Tm was determined by the fitting of the Boltzmann equation (Y=Bottom+(Top-Bottom)/(1+exp((V50-X)/Slope)) with the V50 value equating to the Tm of the unfolding protein GraphPad Prism). Ligand binding was determined when the ΔT_m was >2°C higher than protein in the absence of ligand

Following the identification of Trib2 divalent cation sensitivity in the *in vitro* kinase assays, either magnesium ions or EDTA were added to reaction mixtures of 5 μM Trib2 and 1 mM ATP at final concentrations of 10 mM and 2 mM respectively and DSF performed as previously described.

A range of concentrations of the ATP-competitive kinase ligand DAP (N′2′-(4-aminomethyl-phenyl)-5-fluoro-N′4′-phenyl-pyrimidine-2,4-diamine, dianilinopyrimidine), obtained from SYNKINASE, (Murphy *et al.*, 2014b) which had been reconstituted in 100% DMSO to a concentration of 20 mM, was further diluted to create 10x working stock solutions. The 10x DAP (in 20% DMSO) solutions were added to 5 μM Trib2 or Aurora A and Sypro Orange Dye (final DMSO concentration 2%) and Tm values were compared to protein plus a 2% DMSO control.

Either 5 μM Trib2, Trib2 F130A, F130G in 20 mM bicine pH 9.0, 100 mM NaCl, 1 mM DTT, 10 % glycerol were incubated with 250 μM bulky PP1 analogues (unless otherwise stated for a titration experiment) that were supplied as a 10 mM stock solutions dissolved in 100% DMSO (kind gift of Professor Kevan Shokat, UCSF). The final concentration of DMSO was 2.5% and the T_m values were compared to the T_m of the proteins without inhibitor but containing 2.5% DMSO as solvent.

2.29 Measuring the intrinsic fluorescence and static light scattering of Trib2 during a thermal ramp

To determine the T_m of Trib2 by detecting the intrinsic fluorescence, or the T_{agg} by analysis of the static light scattering, 1 μg (~2.5 μM) Trib2, Trib2 mutants, or Aurora A were either mixed with ATP ± 2 mM EDTA/10 mM Mg^{2+}or incubated with a series of compounds, including CZ 30 and HxJ 42, which were aliquoted into glass microcuvette arrays in triplicate (9μl volume). The samples were placed into the Optim2 device and excited with both 266 nm and 473 nm lasers for 1000 ms (1s) during a thermal ramp which increased by 0.3°C increments, from 15°C (starting) to 95°C (ending) on an Optim2 system (Avacta Analyticals). The 266 nm laser was used to measure the thermal stability (reported as T_m) of the proteins whilst concurrent measurements of protein aggregation (reported as T_{agg}) by static light scattering were performed by analysis of data captured by the 473 nm laser. The first derivative was fitted to the detected intrinsic fluorescence curves (266 nm) and the T_m was identified. The T_{agg} (Aggregation Onset Temperature) was identified following static light scattering analysis and was determined at the temperature that gave 10% of the maximum detected signal detected by the 473 nm laser. Average T_m and T_{agg} values were calculated and ΔTm measurements (for ligands) for each protein were plotted using GraphPad Prism6.

2.30 Purification and initial crystallization trials with recombinant Trib2

Full length His tagged Trib2 was purified from two litres of *E. coli* as previously described through a two step procedure, Ni-IMAC purification followed by gel filtration chromatography. Trib2 was eluted from the Superdex200 column 10/300 in 20 mM bicine (pH 9.0), 100 mM NaCl, 1 mM DTT, 10% glycerol. The fractions that contained protein were resolved by SDS PAGE and the fractions that contained Trib2 and eluted in the volume predicted for monomeric Trib2 were concentrated to 10 mg/ml by centrifugation using a Vivaspin 2 (10 kDa MWCO) concentrator column (GE Healthcare). The concentration was determined using Coomassie based methods and confirmed by the absorbance at 280 nm. Using a Screenmaker 96+8 liquid handling system, 100 nl of protein was transferred to each sitting drop crystallography well and mixed with 100 nl of the reservoir buffer dispensed into that well. Seven, 96 well plates were set up for crystallography trials.

After dispensing the protein, buffer and reservoir, the trays were heat sealed with an adhesive optical cover and centrifuged for 20 seconds and then placed on a dark shelf away from any vibrations at room temperature. The plates were checked on days 3 and 5 post trial initiation and then at least once every two weeks to identify crystal formations. The seven buffer screens used were Wizard 1 and 2 (Emerald Biosystems), 'Pact premier' (moleculardimensions.com), JCSG-plus (moleculardimensions.com), Morpheus (moleculardimensions.com), PEGRx1 and 2 (Hampton Research), Crystal Screen 1 and 2 (Hampton Research) and Cryo 1 and 2 (Emerald Biosystems).

2.31 Generation of ^{15}N-labeled Trib2 for NMR analysis

Trib2 expression was induced by the addition of IPTG for 18 hours at 18°C, when two litres of media inoculated with pET30 EK/LIC Trib2 transformed *E. coli* (full length) had reached an A_{600nm} of 0.8. The Trib2 had been grown in M9 minimal media. Flasks containing 14.6 g Na_2PO_4 (anhydrous), 5.4 g KH_2PO_4 (anhydrous), 1g ^{15}N labeled NH_4Cl and H_2O (RO) made up to 1 litre were autoclaved for 15 minutes at 121°C and following this, to each 1 litre flask 2 g glucose was added along with 20 ml of 0.1 M $MgSO_4$, 2.5 mM $CaCl_2$, 0.75 mM $MnCl_2$, 0.25 mM $FeSO_4$ that had been filter sterilized.

After incubation at 18°C for 18 hours, the cells were pelleted and harvested as previously described. Trib2 was purified by Ni-IMAC, which was followed by gel filtration through a Superdex200 10/300 GL column and then anion exchange chromatography through a MonoQ 5/50 (GE Healthcare) column.

Coomassie staining of gel filtered ^{15}N Trib2 revealed the presence of contaminants in the sample. To remove these minor contaminants, and therefore provide a homogenous Trib2 sample for ^{15}N-HQSC NMR, gel filtered Trib2 was applied to a MonoQ 5/50 GL (GE Healthcare) column equilibrated in 20 mM bicine pH 9.0, 100 mM NaCl, 1 mM DTT 10% glycerol. Following loading of protein on to the column, the concentration of NaCl was increased linearly to a final volume of 10 ml up to a concentration of 1000 mM. The location of the eluted Trib2 was observed by referring to the elution profile and SDS-PAGE, and the concentration of NaCl that eluted Trib2 from the MonoQ column was deduced by referring to the gradient. Trib2 was transferred to a suitable NMR buffer (20 mM Tris pH 7.4, 50 mM NaCl, 1

mM DTT) by buffer exchange through a NAP-10 column, and was then analysed by ^{15}N-HSQC NMR on a Bruker 800 MHz solution state NMR for 12 hours after being supplemented with 10% D_2O.

2.32 Maintenance and growth of Adherent Human Cell Lines

Flp-In T-REx-HeLa cells (Invitrogen) or Flp-In T-REx-293 human embryonic kidney cells (Invitrogen) were grown in Dulbecco's Modified Eagle's medium (DMEM) that contained 10% Foetal Calf Serum (FCS) that had been filter sterilized to prevent contamination and 50,000U Penicillin and 50,000 μg Streptomycin (Gibco) added, along with the following selective, sterile-filtered antibiotics: Pre-transfected (parental) Hela Flp-In T-REx cells: Blasticidin (Melford) 4 μg/ml, Zeocin 50 μg/ml (Invitrogen). After transfection: HeLa Flp-In T-REx cells were maintained in: Blasticidin 4 μg/ml, Hygromycin B (Invitrogen) 200 μg/ml, final concentrations.

Flp-In T-REx 293 cells were cultured in similar conditions to the Flp-In T-REx HeLa cells described above, however, the selective antibiotics used were as follows: Pre-transfected (parental) cells: Zeocin 100 μg/ml, Blasticidin 15 μg/ml. After transfection: Blasticidin 15 μg/ml, Hygromycin B 150 μg/ml.

The cells were cultured at 37°C in a 5% CO_2 atmosphere and were passaged approximately every 3 days in a lamina flow hood after trypsinolysis in trypsin/EDTA (versine) and cell counting.

Zeocin selects for the pFRT/*lac*Zeo vector that contains an integrated FRT (Flp recombination Target) site. Following cotransfection of a Flp recombinase (pOG44) and pcDNA5/FRT/TO vector containing Trib2/NOK, the pOG44 expresses the Flp Recombinase and homologously recombines the FRT sites in pFRT/*lac*Zeo and pcDNA5/FRT/TO. The cells, which were previously resistant to Zeocin are sensitised, but become resistant to Hygromycin B (the resistance gene in pcDNA5/FRT/TO). The pcDNA6/TR, which encodes the Tet repressor gene, is selected for and maintained by the constant presence of Blasticidin.

2.33 Growth of suspension human cell lines

THP-1 (a suspension monocytic cell line) was cultured in RPMI, supplemented with Penecillin and Streptomycin, 10% low endotoxin FCS, 1% L-glutamine and 0.2 mM β-mercaptoethanol. Cells were maintained at 37°C and 5%

CO_2 and to maintain exponential growth, the cells were passaged when the concentration was ~ 8 x10^5 cells/ml.

2.34 Human Cell Transfection with double stranded DNA plasmids

HeLa Flp-In T-REx parental cells were cultured to 80-90% confluency, washed 3 times with Phoshate Buffered Saline (PBS) and standard transfection protocols were followed. Briefly, for stable cell lines, 1 μg pcDNA5/FRT/TO-Trib2/NOK and 9 μg pOG44 (this 1:9 was suggested in the suppliers manual and pOG44 Flp recombinase expression vector is required for stable integration of transfectants), were combined in a sterile microcentrifuge tube and a volume of Lipofectamine appropriate for the size of flask or dish used was added (as described in the Lipofectamine 2000 manual). After 5 minutes, 50 μl of serum-free DMEM was added to this mixture and was left for 30 minutes in the lamina-flow hood. The parental cells for transfection were washed three times with PBS and had 2ml serum-free DMEM dispensed onto them. The contents of the microcentrifuge tubes were added to the plate/flask containing the cells for transfection and these were incubated for 3-5h at 37°C in 5% CO_2. Then 10 ml of serum containing DMEM was added to the transfections. Selective media was added 24h later. Expression of the Flp recombinase mediates ligation of the plasmid sequence into a pre-defined site of the genome. Tetracycline (sterile-filtered stock solution was 1mg/ml in 70% EtOH) was added at a final concentration of 1 μg/ml to induce the expression of the recombinant protein in the stably transfected cells, and this was confirmed by western blotting.

2.35 Human Cell Lysis

Mammalian cell lysis buffer (1% Triton x-100 or 0.1% Triton x-100, 100 mM NaCl, 10 mM Tris pH 7.4, 10 mM β-glycerophosphate pH 7.5, 1 mM EDTA pH 8, 1 mM EGTA pH 8, 1 x protease inhibitor tablet, 100 nM okadaic acid, 10 mM NaF, 0.5 mM Na orthovanadate, the latter three are protein phosphatase inhibitors) was added to cells after they had been trypsinised and the trypsin neutralized by the addition of growth media containing 10% FCS. To prevent re-attachment, the cells were immediately pelleted by gentle microcentifugation at 1000 *x g* 18°C, to prevent premature cell lysis. The media was discarded and the pellet gently washed in PBS and pelleted 3 times in succession. The pellet was then resuspended in ice cold cell lysis buffer and left for 20 min on ice with occasional agitiation. The solution was

then centrifuged at 20,000 *x g* in a refrigerated centrifuge at 4°C for 20 min. The supernatant fraction (soluble after Triton x-100 extraction) was left on ice or stored at -20°C whilst the pellet was resuspended in 2 x SDS Lysis buffer and then boiled for 10 min prior to SDS-PAGE.

2.36 Generation of antibody raised against recombinant Trib2

To detect endogenous, untagged NOK as well as exogenous and recombinant Trib2, a new antibody was raised in rats using recombinant His-tagged human Trib2 as immunogen, in collaboration with SI Biologics. Samples of sera were tested from each rat to test for an immune response directed against Trib2 (assessed by ELISA). Following successful reactivity, the sera was collected and purified. CnBr-activated Sepharose (GE Healthcare) was first coupled to recombinant His-tagged Trib2 by swelling the 1g resin (swells to ~ 3.5 ml) in 200 ml 1 mM HCl for 1 hour. The resin was then washed using a vacuum pump and 0.22 μm nitrocellulose membrane with a further 200 ml 1 mM HCl followed by 200 ml Coupling Buffer (100 mM $NaHCO_3$ pH8.3, 500 mM NaCl) and 5 mg lyophilized recombinant full length His- Trib2 was dissolved in 5 ml Coupling Buffer. The resin was centrifuged and resuspended in the Coupling Buffer dissolved 5 ml His- Trib2 and incubated for 2 hours on a see-saw rocker. The resin was then gently washed with 5 gel volumes Coupling buffer and then incubated in 20 ml Blocking buffer (100 mM Tris-HCl pH 8.0) for 2 hours. Following a further wash with 20 ml Coupling buffer, 4 rounds of alternating 10 ml of Cycle buffer 1 (100 mM acetic acid pH 4.0, 500 mM NaCl) and Cycle buffer 2 (100 mM Tris-HCl pH 8.0, 500 mM NaCl) commenced and then washed with 20 ml PBS and stored in a 1:1 ratio with PBS. Two milliliters of the antiserum was then added to 1 ml of the Trib2 conjugated Sepharose slurry (bead volume 500 μl) packed into a BioRad Econo-Pac chromatography column and incubated for 1 hour. The flow through was then collected and the resin washed with 100 ml PBS. The Trib2 reactive antibodies were eluted by the addition of 4 ml Elution Buffer (100 mM glycine pH 2.5), and ~500 μl was collected in each microfuge collection tube that contained 100 μl Neutralisation buffer (1M Tris-HCl pH 8.0) and fractions tested by western blotting for Trib2 immunoreactivity. Antibodies were stored at either 4°C or -20°C prior to analysis.

2.37 Immunoprecipitation (IP) of endogenous Trib2 from THP-1 cells

Approximately $30x10^6$ THP-1 cells were washed and pelleted by centrifugation and then lysed in 1 ml lysis buffer as described above. Twenty microlitres was saved and snap frozen. The remaining lysate was split into two aliquots, one of which was incubated with 10 μl (~2 μg antibody) of the rat anti-human Trib2 antibody and rotated end-over-end for 3 hours at 4°C. 10 μl G-Sepharose beads (equilibrated in cell lysis buffer) were added to both aliquots of cell lysate (+/- antibody) and left rotating overnight at 4°C. The Sepharose resin was pelleted by gentle centrifugation (~1000 *x g*) for 2 minutes at 4°C and the supernatant extracted (using a gel loading pipette tip to minimize disruption to the pellet), which was snap frozen stored at -20°C. The pellet was then washed 3 times with cell lysis buffer. The first wash was in cell lysis buffer that had an increased NaCl concentration of 500 mM. Following the final washing step, the pellet was resuspended in 50μl 2x SDS loading buffer and boiled. Samples of the input, supernatant and IP (+/- antibody) were resolved by SDS PAGE and western blotted using the same Trib2 antibody to identify the presence of Trib2 in the IP.

2.38 Immunoprecipitation of overexpressed FLAG-tagged Trib2 from Flp-In T-REx-293 cells for mass spectrometric analysis

Twenty, 15 cm dishes were seeded with Flp-In T-REx-293 cells. Upon reaching 80-90% confluency, half of the plates were treated with tetracycline to induce FLAG tagged Trib2 protein expression. Twenty four hours later both control and Tet-induced plates were trypsinised, washed in PBS three times following trypsin neutralisation, pelleted and then lysed in 1 ml (total) lysis buffer (on ice) with regular agitation to ensure complete cell lysis. Following removal of insoluble matter by centrifugation, the lysates were incubated with 50μl FLAG M2 conjugated agarose beads (Sigma) that had been equilibrated in cell lysis buffer in 2 ml (round bottomed) Eppendorf tubes, which were rotated overnight at 4°C. The beads were pelleted and washed 3 times in 15 ml cell lysis buffer. Following this, 10 μl 5mg/ml 3xFLAG peptide (Sigma) was diluted in 150 μl ice cold PBS and added to each pellet to elute the FLAG-tagged Trib2. This was kept on ice for 30 minutes with regular agitation. Both immunoprecipitations (+/- tetracycline) were centrifuged and the eluate saved. Samples from each step (input, elution and supernatant) were

immunoblotted and the remaining immunoprecipitations were analysed by LC-MS/MS mass spectrometry (Synapt HDMS quadrupole-time-of-flight Mass Spectrometer, Waters) by Ms. Alice Wadkin at the University of Manchester. The samples were desalted and applied to a nano-ESI source with a PicoTip emitter (New Objective, Woburn, MA,USA) at 300 nl/min. The data was acquired by both MS^E and DDA experiments, which was analysed and putative interacting Trib2 partners were identified by the online software MASCOT (Matrix Science) matching peptide ion fragments with the Swissprot database. The proteins that were identified in both of the methods are described in Chapter 4.

2.39 siRNA transfection of NOK Flp-In T-REx-HeLa cells

Cells were grown to ~70% confluency and transfected as described in the transfection reagent protocol with either 200 pmoles of a NOK targeted pool consisting of equimolar amounts of 4 NOK targeting siRNA oligonucleotides or 200 pmoles of a non-coding siRNA pool (On target Plus, Thermo scientific (Dharmacon)) dissolved in RNase free sterile H_2O using Lipofectamine 2000 as the transfection reagent. The siRNA treated and control cells were lysed 48 hours post transfection. Lysates were generated as previously described and Trib2 protein levels determined by western blotting.

The NOK target sequences of each constituent of the siRNA pool are:

siRNA1: CCCAGUAGCUGCACACAUA

siRNA2: GGUGGUACCUGAACUGUAU

siRNA3: GAUUAGGCCUGGCUUAUGA

siRNA4: GAAAAGCUGCCACUCUAUA

2.40 Immunofluorescence of Fixed Human Cells

Stably transfected Flp-In T-REx cells (1 x 10^5 cells) were seeded into wells of a 6 well plate that contained sterile glass coverslips. Protein expression was induced by the addition of tetracycline (1μg/ml) for 18 hours once the cells had reached ~80 % confluency. The cells on the coverslips were fixed in 2.5 ml 3.7% PFA (paraformaldehyde) for 20 minutes and then washed 3 times in PBS and placed in a blocking solution of 0.1 M glycine (pH 8.5) for 5 min. Cells were washed again

then permeablised in 0.1% Triton X-100 in PBS for 4 min, and a further 2 washes performed. The appropriate primary antibody, at the optimal concentration (antibody diluted in PBS, Table 2.1) was added and incubated for 60 minutes. The cells were then washed 3 times in PBS and 15 μl of FITC- or Cy-3- conjugated secondary antibodies diluted 1/20 in PBS were added and left in the dark for 30 min. The cells were again washed 3 times in PBS before 1 μg/ml DAPI (4',6-diamidino-2-phenylindole) solution in PBS was added and left for 5 min in the dark. The cells were washed 3 times and placed face down upon a droplet of Vectashield Mounting Medium that rested on a microscope slide and the edges were sealed with nail varnish. Images were captured on a Nikon Eclipse T200 inverted microscope (Melville). A 200 metal arc lamp (Prior Scientific) and a Hamamatsu Orca ER camera were used to obtain images through a 60x oil immersion objective lens. Volocity software version 6.1.1 (Improvision) was used to overlay the captured images.

2.41 Nocodazole exposure (cell arrest at metaphase/anaphase boundary)

HeLa cell lines transfected with Myc-tagged full length NOK in the pcDNA5/FRT/TO vector were split into 4 T-75 flasks, and two of these were supplemented with tetracycline (1 μg/ml). All 4 flasks were grown until >90% confluent. Once the cells had reached >90% confluency, nocodazole, (0.2 μg/ml) was added to each ± Tet T-75 flask. The cells were then incubated for 12 hours at 37°C in a 5% CO_2 atmosphere before harvesting, including the floating cells. The cells were washed 3 times in 10ml of PBS, but not discarded. One millilitre trypsin was then added to the flasks and left for 5 min at 37°C in a 5% CO_2 atmosphere. This was then added to the post-wash PBS and spun to pellet the cells. The supernatant was discarded. The cell pellet was washed and resuspended in PBS and re-pelleted. This was repeated twice more. After the final wash step the cell pellet was resuspended in Cell Lysis Buffer containing 1% Triton X-100, and left for 20 min on ice. The microcentrifuge tubes were then spun for a further 20 min at 4°C in a refrigerated centrifuge. Protein concentration was quantified by Bradford Assay, whilst the Triton X-100 insoluble pellet was resuspended in 100 μl 1x SDS Buffer and boiled for 10 min. Equal amounts of supernatant (typically 30 μl) were analysed by 15% SDS-PAGE, after boiling in 1/5 volume of 5X SDS loading buffer,

alongside the resuspended pellets, and including a ladder of pre-stained protein markers. The gel was transferred for 10 h at 18V onto Nitrocellulose membrane. The membrane was cut at 25 kDa, the membrane containing proteins of size <25 kDa was probed for phospho-Histone H3 Ser 10, whilst the >25 kDa proteins were probed for Myc-tagged NOK for 18 hours. Subsequently, the membranes were then washed 3 times in TBS-T and exposed to secondary antibodies diluted in 5% milk-TBS-T for 1h at RT. The membranes were then exposed to ECL reagents as described in the western blotting section (above).

CHAPTER 3. Biochemical analysis of recombinant human Trib2

Human Tribbles 2 (Trib2), a human homologue of the *Drosophila* Tribbles protein, is a pseudokinase linked to a multitude of human diseases, and is consistently overexpressed in a variety of cancers. Trib2 is also termed Hs.155418, GS3955, TRIB2 and TRB2, but will be referred to as Trib2 throughout this thesis. As demonstrated by Keeshan and colleagues, an intact catalytic domain and a COP1-binding DQLVP motif (part of the C-terminal 18 amino acids) in Trib2 are required for oncogenic transformation in *vitro*, and the degradation of C/EBPα requires the recruitment of both Trib2 and a specific Ubiquitin E3 ligase, either COP1 in blood malignancies or TRIM21 in solid lung tumors (Keeshan *et al.*, 2010, Grandinetti *et al.*, 2011). The mechanism by which Trib2 specifically controls C/EBPα degradation has yet to be elucidated, and whether Trib2 binds ATP and/or is a catalytically-active pseudokinase remains unknown.

The deduced protein sequence of Trib2 suggests that the polypeptide contains a eukaryotic protein kinase (ePK) domain located between amino acids 64-308. The kinase domain of Trib2, is however, non-canonical because several invariant amino acid residues that are usually involved in the alignment of metals and ATP and that catalyze phosphoryl transfer in classical kinases (Hanks and Hunter, 1995) are absent (Chapter 1). Specifically, the metal-binding DFG and Asn motifs are missing in all vertebrate Trib2 homologues (Figure 1.1). This observation originally led to the classification of the human Tribbles-related proteins Trib1, Trib2, Trib3 and SgK495 as pseudokinases (Manning *et al.*, 2002).

Recently, pseudokinases including the tyrosine kinase HER3 (Jura *et al.*, 2009a, Shi *et al.*, 2010), the pseudokinase-containing JH2 domain of JAK2 (Ungureanu *et al.*, 2011), and the CAMK family member CASK (Mukherjee *et al.*, 2008) have demonstrated the ability to both bind and hydrolyse ATP, albeit with reduced specific activity compared to typical protein kinases. In contrast, the pseudokinase VRK3 is unable to bind to ATP and is thus unable to transfer phosphate groups to substrates (Scheeff *et al.*, 2009). In between these extremes lies STRADα, a pseudokinase that can bind, but is unable to hydrolyse, ATP *in vitro* (Zeqiraj *et al.*, 2009b).

To determine whether Trib2 can hydrolyse ATP and phosphorylate a substrate, obtaining a yield of pure Trib2 sufficient for biochemical assays is a prerequisite. One benefit of using *E. coli* as a source of recombinant human Trib2 is that all kinases present in the bacterium are prokaryotic, and only a few members of the bacterial kinome are known to autophosphorylate or to phosphorylate non-specific substrates. Examples include DnaK, the nucleotide diphosphate kinase and Era, a GTPase (Macek *et al.*, 2008). However, in order to determine whether Trib2 can bind ATP and/or phosphorylate substrate proteins, a general control for background kinase contamination was generated, in which lysine 90 in the β3 sheet of the kinase N-lobe was mutated to an uncharged residue. The corresponding mutation in many kinases reduces, and usually abolishes, detectable catalytic activity (Iyer *et al.*, 2005b) and therefore the experiments detailed in this chapter are performed alongside a series of Trib2 'β3 lysine' point mutants, including K90M.

Results

3.1 Affinity purification of recombinant human Trib2 from *E. coli*

Flasks inoculated with the *E. coli* strain BL21(DE3)pLysS that had been transformed with Trib2 containing IPTG-inducible pET-30 Ek/LIC were incubated at 37°C (1 *x g*) until the A_{600nm} reached 0.8 (mid-log phase) as described in Chapter 2. To identify conditions for optimal Trib2 expression, induction with (0.5 mM) IPTG was performed at 37°C or 18°C, for 3 and 18 h respectively. Following induction, His-tagged Trib2 in the cleared bacterial lysate was captured on immobilized Ni-Sepharose resin (5 ml HisTrapHP), washed, and then eluted with a buffer containing 300 mM imidazole. The eluted proteins were distinguished on chromatograms by their absorbance at a wavelength 280 nm (left panels of 3.1 A and B). To visualize proteins by SDS-PAGE, they were resolved and the fractions that contained the highest levels of Trib2, which ran as a single band ~45 kDa (judged by Coomassie staining and immunoblotting) were pooled. Of the conditions tested, maximum Trib2 expression was observed following induction at 18°C for 18 h, as judged by SDS-PAGE. As such all *E. coli* derived human Trib2 proteins, unless otherwise stated, were expressed under these conditions. Final yields of purified WT and mutant Trib2 protein are listed in Table 3.1.

Of interest, two additional high molecular weight proteins migrating at a size different to Trib2 were observed following IMAC of recombinant proteins from bacterial sources (Figure 3.1, arrowed). The ratio of these bacterial proteins to the over-expressed tagged protein varies between one purification and another, despite an attempt to follow identical protocols and by using the same glycerol stocks. To identify these proteins, they were separated by SDS-PAGE and excised after staining and destaining. Mass spectrometry (performed by Alice Wadkin, University of Manchester) identified the proteins as GroEL (57 kDa CH60_ECO24) and DnaK (69 kDa, DNAK_ECOH5) which are two common contaminants of IMAC-purified proteins from *E. coli* (Bolanos-Garcia and Davies, 2006). Since these are unlikely to be physiological Trib2-binding proteins, perhaps interacting with partially folded Trib2, or interacting directly with the resin, they were later successfully removed by further rounds of purification.

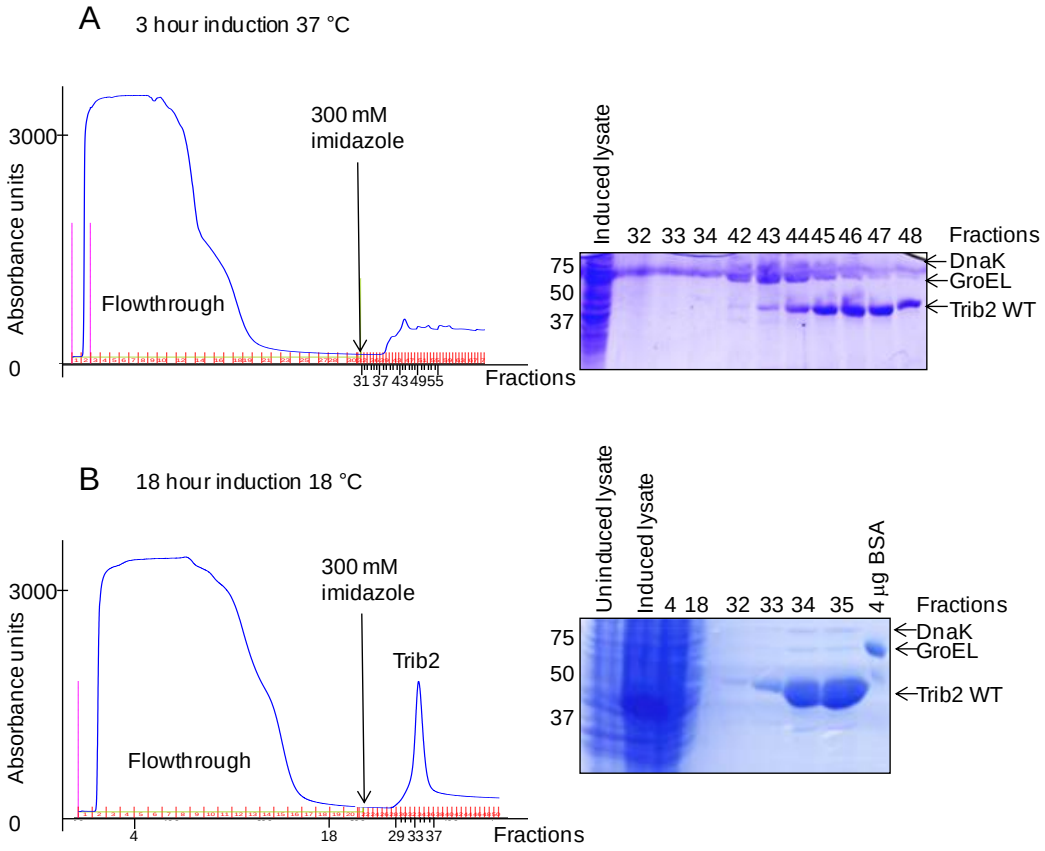

Figure 3.1 A comparison of experimental conditions assessed for recombinant His-tagged Trib2 expression in BL21(DE3)pLysS competent *E. coli*. Protein expression was induced for either (A) 3 hours at 37°C or (B) 18 hours at 18°C and purified by nickel ion affinity chromatography. Left panel: The elution of Trib2 was observed by absorbance changes on the chromatogram (blue line). The position where the imidazole concentration was raised to 300 mM has been labelled as have the fractions that correspond to the gels on the right. Right hand panel: SDS-PAGE of the fractions eluted from the Ni-Sepharose resin along with samples from the uninduced and induced total cell lysates and 4 µg BSA protein standard. The protein was stained with coomassie stain. Trib2 and the contaminating proteins are labelled and the fraction numbers correspond to the fraction numbers on the chromatogram.

Protein	Soluble Trib2 yield (mg Trib 2 / litre of LB)
Trib2 WT	2
Trib2 K90M	1.3
Trib2 K90A	1.0
Trib2 K90R	1.5
Trib2 DFG K180N	1.0
Trib2 F130A	2.5
Trib2 F130G	2.5

Table 3.1 Yields of His-tagged Trib2 obtained following elution from Ni-Sepharose and dialysis. The average yield of Trib2 WT and mutants purified from 1 litre of LB induced at 18°C for 18 hours and dialysed into 20 mM bicine pH 9.0, 100 mM NaCl, 1 mM DTT, 10% (v/v) glycerol are listed.

3.2 Purified recombinant WT Trib2 transitions to an unfolded state when heated

Biochemical analysis of Trib2 function requires the purified recombinant human protein to be appropriately folded, which is often challenging in prokaryotic organisms that lack the fine-tuning pathways normally associated with eukaryotic protein expression. One method to determine if Trib2 is folded is to subject it to Differential Scanning Fluorimetry (DSF). This technique involves incubating a protein with a hydrophobic fluorescent dye such as Sypro Orange. In an aqueous environment the dye is strongly quenched, but over the course of a 'DSF assay' the temperature is raised incrementally, causing the protein to gradually unfold and denature, thus exposing buried hydrophobic residues. Binding of these hydrophobic surfaces by Sypro Orange results in an increase of fluorescence emission and when the detected fluorescence is plotted as a function of temperature, thermal denaturation curves can be produced that describe the behavior of the protein as it unfolds (Niesen *et al.*, 2007).

To evaluate whether Trib2 was appropriately folded after expression in bacteria, DSF was performed in duplicate, on affinity purified Trib2 or on Trib2 that had been denatured by heating for 5 minutes at 95°C. The fluorescence emitted at each temperature interval was recorded, averaged and used to generate thermal denaturation curves (Figure 3.2). The blue line (non-denatured Trib2) had a melting curve consistent with the profile of a folded protein unlike the red line (denatured Trib2) which resembled an unfolded protein (Uniewicz *et al.*, 2012). This demonstrated that bacterially expressed Trib2 was in a folded conformation following IMAC purification.

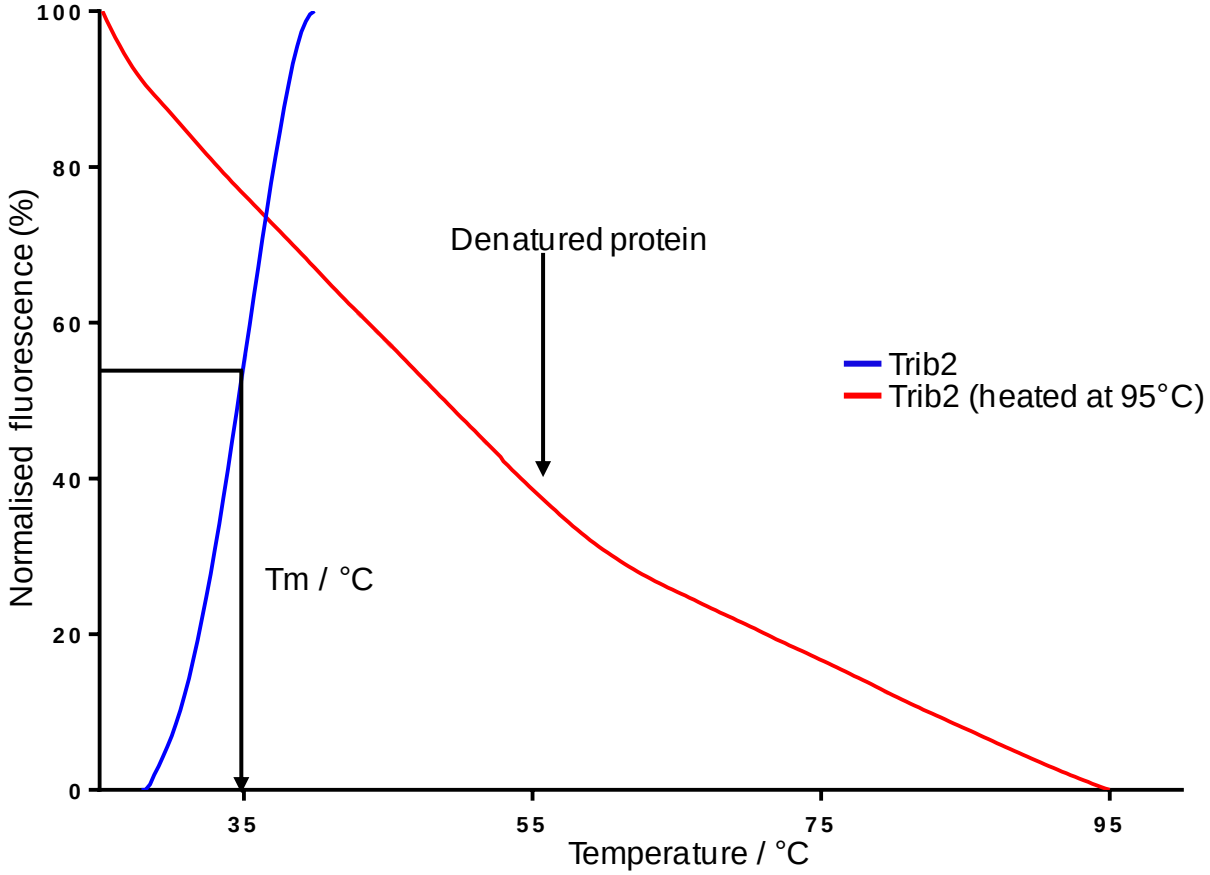

Figure 3.2 His-tagged Trib2 exhibits a thermal denaturation profile typical of a folded protein. DSF was performed on 5 μM Trib2, either denatured by heating for 5 minutes at 95°C (red line), or without heating (blue line). For each condition, the average fluorescence intensities from the triplicate assays were normalised and plotted as a function of temperature. The Tm value of the average thermal denaturation profile has been annotated.

3.3 Trib2 solubility can be improved following buffer optimisation

Trib2 exhibited signs of aggregation and precipitation following IMAC purification, which is in agreement with Vedadi et al., (2006) who previously observed Trib2 instability in solution. However, this study identified 20 mM bicine, 100 mM NaCl, 1mM DTT and 10% glycerol as a buffer that greatly improved the stability of the purified recombinant Trib2 catalytic domain. We therefore investigated whether the same buffer conditions could stabilize full length human Trib2 purified from bacteria.

Affinity purified Trib2 was either dialysed into a buffer used routinely in our lab for IMAC purification of kinases (buffer A, 50 mM Tris pH 7.4, 150 mM NaCl, 1 mM DTT, 10% glycerol) or into the buffer optimized by Vedadi and colleagues (buffer B, 20 mM bicine pH 9.0, 100 mM NaCl, 1 mM DTT, 10% glycerol).

Following dialysis, white insoluble protein aggregation was observed in the dialysis tubing that contained Trib2 equilibrated in buffer A, whilst no aggregation was detected in the buffer B dialysed sample. To investigate the yield of soluble protein, insoluble protein aggregates were removed by rapid centrifugation and the soluble protein concentration was determined by Bradford Assay. The findings are summarized in Table 3.2A, along with SDS-PAGE analysis (Figure 3.3A). When Trib2 was concentrated by centrifugation using a Vivaspin 2 (10 kDa MWCO) centrifugal concentrator, Trib2 in buffer A only reached 6 mg/ml, whilst Trib2 in buffer B could be concentrated in excess of 10 mg/ml without protein aggregation.

A mutation to the conserved lysine located within the β3 sheet of the kinase N-lobe (K72 in the model Ser/Thr kinase PKA) reduces the catalytic activity of most kinases (Iyer *et al.*, 2005b), and a mutation was also generated for Trib2. Trib2 K90M was also soluble in buffer B, and following dialysis no white insoluble aggregation was observed. After centrifugation, the concentration of Trib2 and Trib2 K90M dialysed into buffer B at pH 9.0 or pH 8.0 was determined (Table 3.2 B) and the samples resolved by SDS-PAGE (Figure 3.3 B). Consistently, a lower yield of Trib2 K90M was obtained compared to WT from *E. coli*. The concentrations of both Trib2 K90M and Trib2 remain higher following dialysis into buffer B at pH 9.0 compared to pH 8.0 (Table 3.2B), suggesting increased stability at a higher pH. To confirm that this was the case, Trib2 was dialysed into buffer B at pH 7.4 and pH 9.0, which resulted in more soluble protein at the higher pH (Table 3.2C).

Furthermore, following a single freeze thaw cycle, approximately half the protein at pH 7.4 was lost compared to Trib2 at pH 9.0 which still contained ~85% of soluble Trib2. Unless otherwise stated, buffer B was employed for all future Trib2 purification procedures from *E. coli*.

A

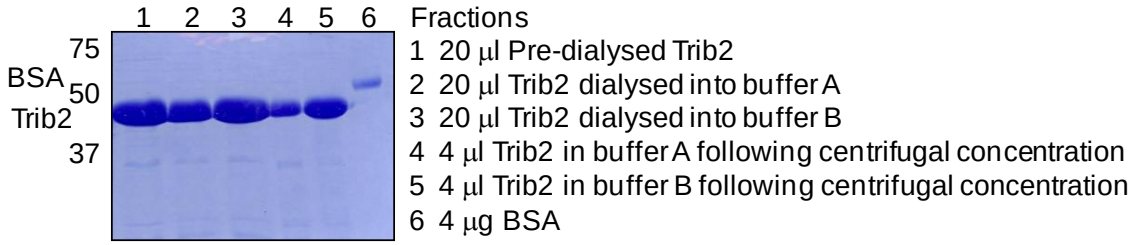

B

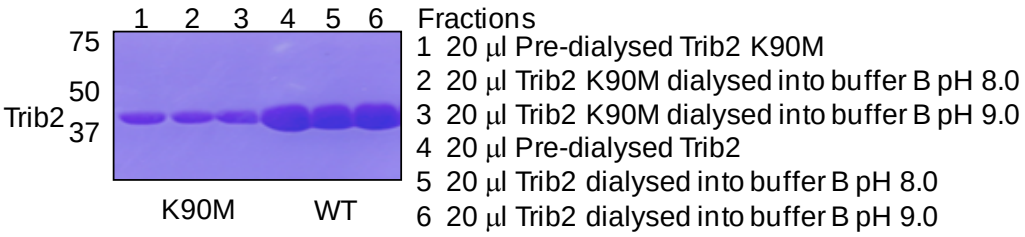

Figure 3.3 Optimising experimental conditions for maximising Trib2 solubility. A) Trib2 was purified by IMAC and the peak fractions containing the eluted Trib2 were pooled then samples of the pool were dialysed in either buffer A (50 mM Tris pH 7.4, 150 mM NaCl, 1 mM DTT, 10% glycerol) or buffer B (20 mM bicine pH 9.0, 100 mM NaCl, 1 mM DTT 10% glycerol) and subjected to SDS-PAGE where 20 μl of the predialysed sample (lane 1) was resolved alongside the same volume of Trib2 dialysed in to buffer A or buffer B (lanes 2 and 3 respectively). The remaining dialysed Trib2 samples were concentrated by centrifugation in a Vivaspin2 column and resolved by SDS-PAGE (lane 4 = buffer A, lane 5 = buffer B). Lane 6 contained 4 μg of a BSA standard. The protein was observed by coomassie staining. B) Trib2 K90M (lanes 1-3) and Trib2 WT (lanes 4-6) were purified concurrently under identical conditions and dialysed into either buffer B at pH 8, or buffer B pH 9 and 20 μl samples subjected to SDS-PAGE. The concentrations of the purified proteins are noted in Tables 3.2 A and B.

A

	Following IMAC	Following dialysis into buffer A	Following dialysis into buffer B	Buffer A dialysed Trib2 after centrifugal concentration	Buffer B dialysed Trib2 after centrifugal concentration
Trib2 concentration µg/µl	6.4	2.1	6.2	6.0	13.2

B

	Trib2 K90M			Trib2 WT		
	Following IMAC	Following dialysis into buffer B (pH 8.0)	Following dialysis into buffer B (pH 9.0)	Following IMAC	Following dialysis into buffer B (pH 8.0)	Following dialysis into buffer B (pH 9.0)
Trib2 concentration µg/µl	0.8	0.65	0.72	2.2	1.8	2.2

C

	Trib2 WT				
	Following IMAC	Following dialysis into buffer B (pH 7.4)	Following dialysis into buffer B (pH 9.0)	Frozen and thawed Trib2 (buffer at pH 7.4)	Frozen and thawed Trib2 (buffer at pH 9.0)
Trib2 concentration µg/µl	2.6	1.3	2.4	1.15	2.2

Table 3.2 Summary tables for Trib2 solubility optimisation. Concentrations of the dialysed proteins in Figure 3.3 were determined by Bradford analysis at 595 nm. A) The concentrations of Trib2 dialysed into buffer A and buffer B are noted. The concentration of each sample of Trib2 in either buffer A or buffer B is also recored following centrifugal concentration using a Vivaspin 2 column, until the protein concentration remained constant. B) The concentrations of Trib2 K90M and Trib2 WT purified by IMAC are listed and the concentrations following dialysis into buffer B, either at pH 8.0 or pH 9.0. C) Trib2 WT was purified using IMAC and the pooled fractions were dialysed into buffer B at either pH 7.4 or pH 9.0. The concentration before dialysis and after dialysis was noted and and the fractions were snap-frozen in liquid nitrogen. Following one freeze thaw cycle, the concentrations of the proteins were also measured, to assess the effects of storage at -80°C.

3.4 Affinity purified Trib2 is catalytically active

The ability of the Trib2 pseudokinase domain to transfer the γ–phosphate from ATP to a protein substrate has yet to be demonstrated, and many pseudokinases are known to be catalytically inactive when analysed *in vitro* towards exogenous substrates, meaning that other approaches are needed to analyse their biochemical functions (Murphy *et al.*, 2014b) (Riterer et al., 2014 (TCB In press)). To analyse Trib2 catalytic potential, the fractions that contained Trib2 that eluted from the Ni-Sepharose column (see chromatogram in Figure 3.4 A) were assayed for autophosphorylation in the presence of 1 mM ATP (2.25 μCi γ ^{32}P ATP) (Figure 3.4 B and Figure 3.4 C) to identify whether any detectable activity was associated with Trib2. Trib2, like the pseudokinase CASK, whose kinase activity was inhibited by divalent cations (Mukherjee *et al.*, 2008), does not have a divalent cation-binding asparagine residue located in the catalytic motif, nor a magnesium ion binding 'DFG' motif in kinase subdomain VII (Trib2 has SLE instead), and so magnesium ions were not added to the reaction mixture.

As shown in Figure 3.4 B, 250 pmoles of affinity purified Trib2 from each of the fractions that corresponded to the protein peak on the chromatogram (Figure 3.4 A) were assayed in duplicate for 30 minutes in the absence of any divalent cation. Another preparation of Trib2 was affinity purified and the protein in the peak fractions were assayed alongside the fractions that eluted either side of the peak (Figure 3.4 C).

In both of these assays it was interesting to observe that the pseudokinase Trib2 had become autophosphorylated, meaning ^{32}P was incorporated directly into Trib2. Trib2 that eluted in the fractions that corresponded to the centre of the peak autophosphorylated to a greater extent than Trib2 towards the peak shoulders, perhaps indicating that the protein in the shoulders of the peaks was more aggregated.

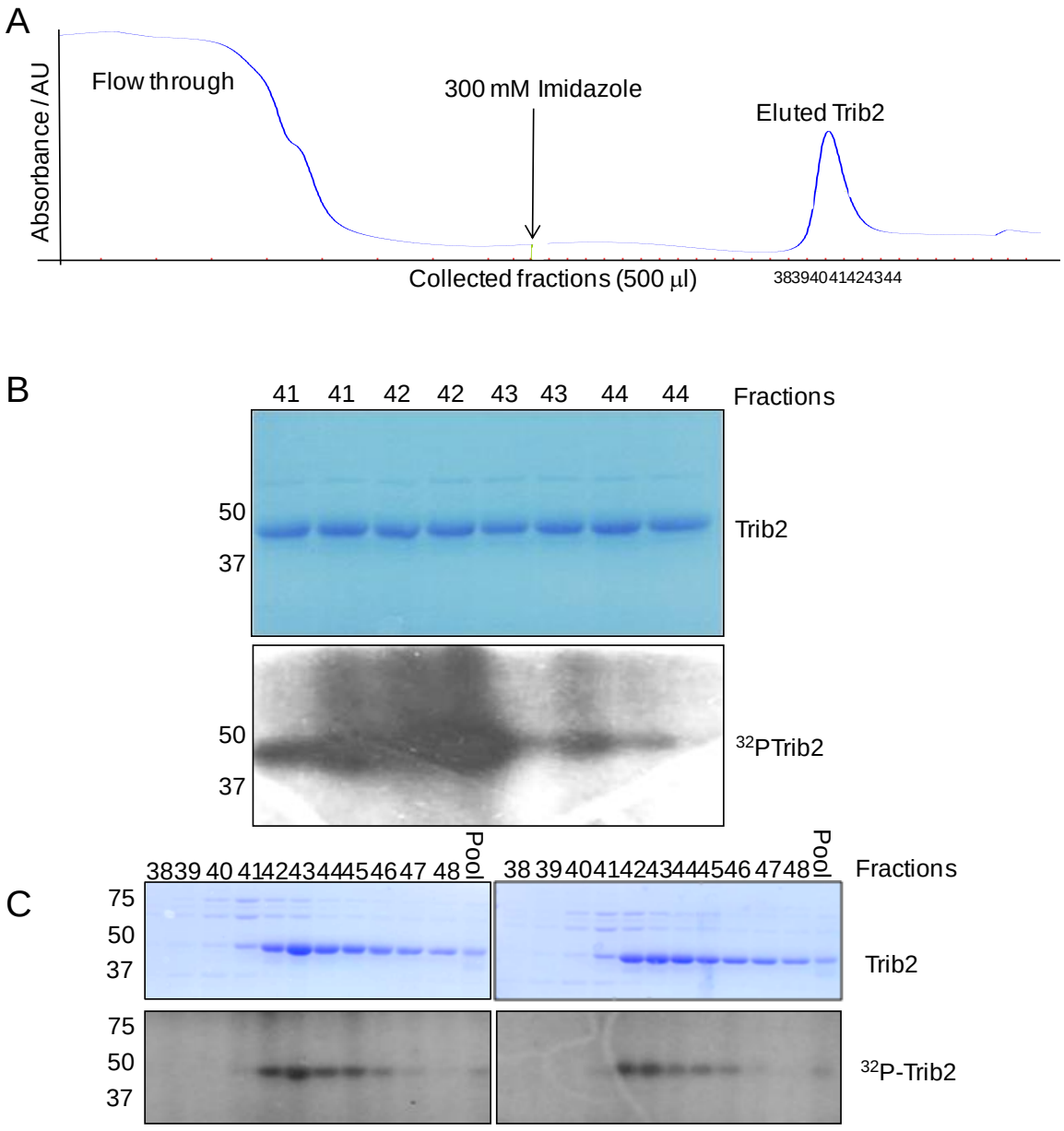

Figure 3.4 Isolating the catalytically active fractions of Trib2 following Ni IMAC A) The absorbance peak observed on the chromatogram indicated the fractions that contained protein following IMAC chromatography. B) Trib2 (250 pmoles, ~11.75 µg) from fractions 41-44 were assayed in duplicate for 30 minutes at 30°C on a shaking platform with 2 mM EDTA and 1 mM ATP (2.2 µCi γ-^{32}P ATP). The reactions were stopped by the addition of 5 x SDS loading buffer and 25 µl of each assay were resolved by SDS-PAGE. The protein was stained with coomassie stain and the gels were dried and treated to autoradiography. C) In duplicate, 250 pmoles of fractions 38-48 were assayed on a shaking platform for 30 minutes. The individual fractions were assayed alongside 100 pmoles Trib2 WT (Pool) that had been purified previously and dialysed into buffer B, 25 µl of the reaction mixtures were subjected to SDS-PAGE and subjected to autoradiography.

3.5 Isolation of Monomeric Trib2

As discussed in Section 3.3, affinity purified Trib2 is very prone to aggregation. Importantly, gel filtration (often termed size-exclusion) chromatography can be employed to separate aggregated Trib2 away from appropriately folded Trib2, which interacts with the column and elutes in a native complex. Gel filtration separates the proteins by molecular weight, in non-denaturing conditions (Stellwagen, 1990) and permits further Trib2 purification.

Prior to gel filtration of Trib2 using a Superdex 200 10/300 column (GE Healthcare), purified protein standards of varying molecular weights were dissolved in standard IMAC elution buffer, and then applied to the column, permitting a standard curve to be generated (Figure 3.6B) (as described in Chapter 2). The elution volumes of each standard are determined by direct reference to this chromatogram (Figure 3.5 and summarised in Table 3.3 A). Following gel filtration, the Ve values of the chromatograph peaks (Figure 3.6 A) were divided by the Vo of Blue Dextran. The apparent molecular weight was estimated by applying these values (summarised in Table 3.3B) to the molecular weight standard curve (Figure 3.6 B). The predicted molecular weight of monomeric Trib2 with a 6His tag is 43524 Da (ExPASy ProtParam). The Ve of peak 3 predicts a protein of ~45 kDa, (Figure 3.6A and Table 3.3 B), which indicates the presence of monomeric Trib2 in these fractions. The protein was confirmed by SDS-PAGE (Figure 3.6 C) and western blotting as Trib2. The fractions labelled in red (Fig 3.6 C) were snap frozen in liquid nitrogen and stored at -80°C prior to analysis. Trib2 that eluted in a lower Ve (higher MW in non-denaturing conditions) such as detected in peak 2 (Figure 3.6), could potentially be aggregated or disulphide bonded oligomers. To determine whether Trib2 remained monomeric following freeze-thaw procedures, purified Trib2 was applied to a gel filtration column as described above. The elution profile (Figure 3.7 A) confirmed that several fractions contained a protein that eluted in the Ve (14.7 ml) that was expected for monomeric Trib2, and SDS PAGE confirmed that Trib2 was present in these fractions (Figure 3.7 B). Higher MW contaminants were separated from the protein that eluted in a volume predicted for monomeric Trib2. These Trib2-containing fractions were pooled, freeze-thawed, and the protein was again applied to the gel filtration column. Analysis of the chromatogram (Figure 3.8 C) shows that after gel filtration the Trib2 conformational equilibrium mainly favored monomeric

Trib2, rather than a transition to the higher MW forms of the protein observed following affinity chromatography.

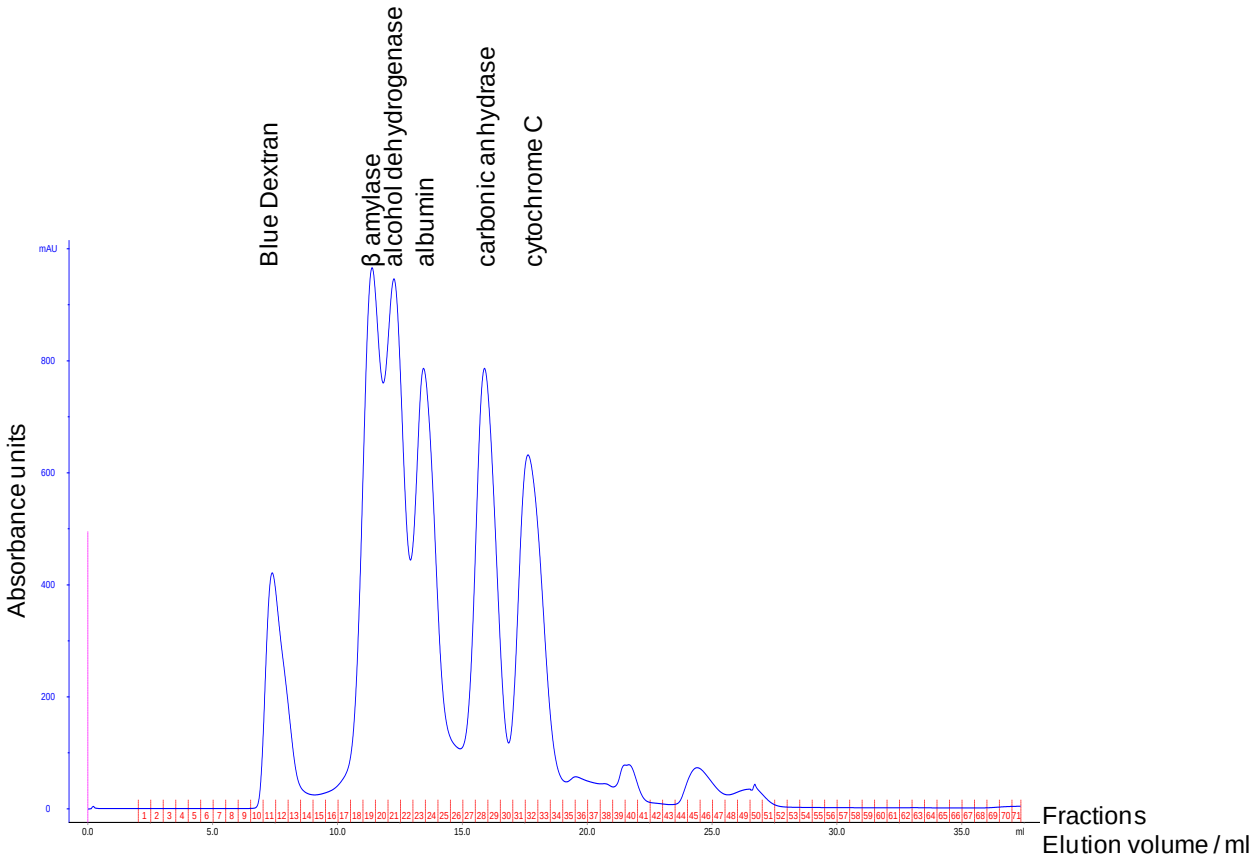

Figure 3.5 Gel filtration of Molecular Weight protein standards. Albumin 10 mg/ml, 5 mg/ml alcohol dehydrogenase, 4 mg/ml β-amylase, 3 mg/ml carbonic anhydrase, 2 mg/ml cytochrome c protein standards were dissolved in 500 µl elution buffer (containing 300 mM imidazole, see Materials and Methods) and subjected to gel filtration in 20 mM bicine pH 9.0, 100 mM NaCl, 10% glycerol, 1 mM DTT. The elution volumes (Ve) were measured from the centre of the peaks (recorded in Table 3.3A) and the Ve/Vo value derived, where Vo is the void volume (2 mg/ml Blue dextran). These values were used to generate a standard 'curve' for this Superdex 200 10/300 gel filtration column (Figure 3.6B).

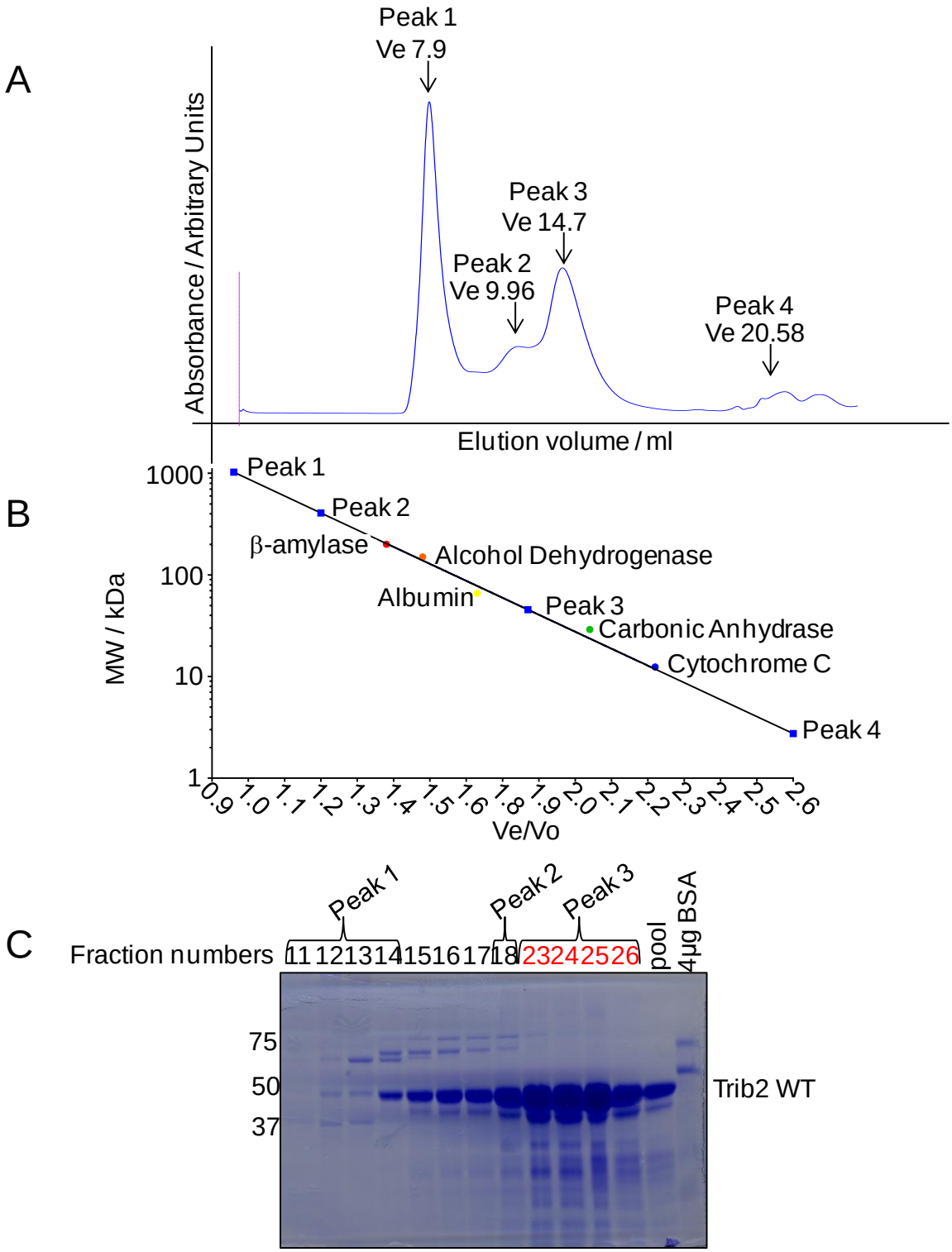

Figure 3.6 A population of Trib2 elutes from a gel filtration column in a volume that corresponds to the Ve predicted for monomeric Trib2 A) Trib2 (1 mg) that had been purified by IMAC chromatography was applied to a Superdex 200 10/300 gel filtration column and the elution volumes of each peak were recorded. B) The Ve/Vo ratio was determined for each peak by dividing the Ve values with the Vo from Blue Dextran. The MW of the proteins in each absorbance peak were inferred by refering to the MW protein standard curve. C) SDS-PAGE was used to resolve 20 µl of the collected fractions along with 4 µg of a BSA standard. The fractions that eluted in the predicted Ve for monomeric Trib2 (peak 3 fractions 23-26 Ve = 14.7ml) were pooled (red font). Predicted MWs for each peak are summarised in Table 3.3B.

A

	MW kDa	Vo ml	Ve ml	Ve/Vo
Blue Dextran	2000	8.25		
β Amylase	200		11.39	1.38
Alcohol Dehydrogenase	150		12.27	1.48
Albumin	66		13.43	1.63
Carbonic Anhydrase	29		15.86	1.94
Cytochrome c	12.4		17.63	2.12

B

	Vo ml	Ve ml	Ve/Vo	Interpolated MW from standard curve kDa
Blue dextran	8.25			
Absorbance peaks		**Ve ml**	**Ve/Vo**	
1		7.9	0.96	1024
2		9.96	1.2	407
3		14.68	1.77	45
4		20.58	2.5	2

Table 3.3 Summary of Ve values interpolated MW of following gel filtration of protein standards and Trib2 A) The MW of each standard (10 mg/ml abumin, 5 mg/ml alcohol dehydrogenase, 4 mg/ml β-amylase, 3 mg/ml carbonic anhydrase, 2 mg/ml cytochrome c) dissolved in 500 μl IMAC elution buffer is listed along with the elution volume (Ve) of each protein measured from the middle of the corresponding protein peak following elution from the Superdex 200 10/300 gel filtration column and the elution volume of Blue Dextran (Vo). B) 1 mg Trib2 was applied to the gel filtration column and the Ve/Vo for each of the peaks determined. The MW of protein eluted in these peaks was estimated from the standard curve (Figure 3.6 B)

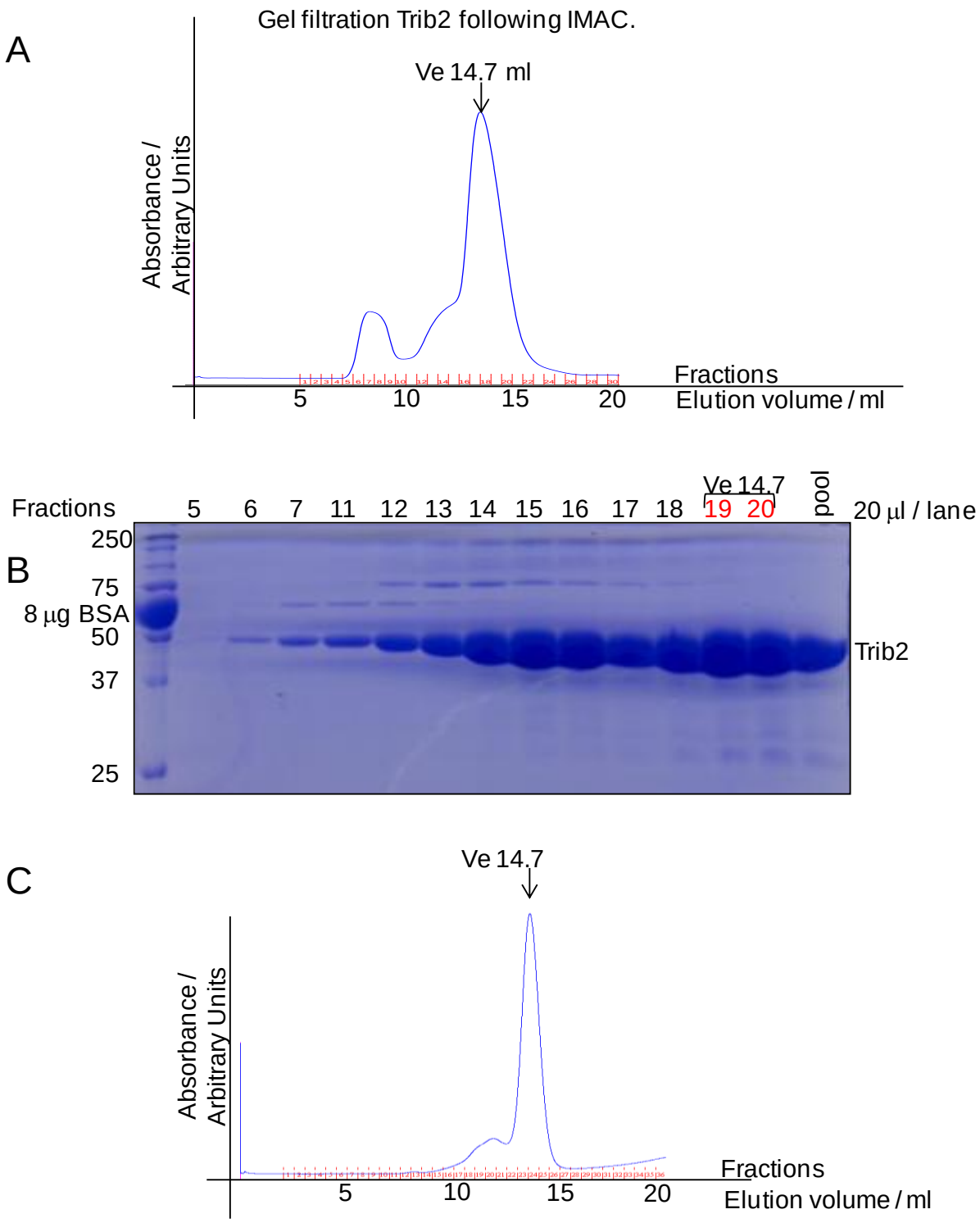

Figure 3.7 The majority of Trib2 retains a monomeric elution profile with further gel filtration A) IMAC purified Trib2 was applied to the Superdex 200 10/300 gel filtration column and the protein eluted in buffer B (500 µl). The elution volume of the main peak was determined and 20 µl fractions were resolved by SDS-PAGE (B). The protein was stained with coomassie stain and lanes 19 and 20 (red font) corresponded to the fractions that had a Ve representative of monomeric Trib2 (Ve 14.7). These were pooled together and 20 µl resolved alongside (Pool). The pooled protein (fractions 19 and 20) was snap frozen in liquid nitrogen then thawed and C) gel filtered again. Interestingly, the majority of the protein eluted again as a sharp peak of Ve ~14.7 ml.

To confirm that the purified protein was Trib2, and further investigate its native sequence, Mass Spectrometry analysis (ESI-MS) of gel filtered Trib2 (Figure 3.8) was employed. This revealed that Trib2 had an intact average mass of 43,582 Da, compared to a predicted MW of 43,524 Da (ProtParam) and an estimated molecular mass after gel filtration interpolated from the standard curve of ~45,500 Da (Figure 3.6 B). Together, these data confirm the predominance of monomeric, non-covalently modified Trib2 in these preparations.

3.6 Trib2 purified by gel filtration still autophosphorylates *in vitro*

Gel filtered Trib2 was subjected to an *in vitro* kinase assay to determine whether it could still autophosphorylate (Figure 3.9A) as previously demonstrated for IMAC-purified Trib2 (Figure 3.4). Fractions of Trib2 that were predicted to be monomeric (fractions 19 and 20, Ve 14.6 ml) were subjected to an *in vitro* kinase assay in the presence of 1 mM ATP (2.25 μCi γ^{32}P ATP per assay) in the absence of divalent cations. As shown in Figure 3.9B, Trib2 was still able to autophosphorylate after separation from the higher molecular weight contaminants that were present after affinity purification. Autophosphorylation was visualised by autoradiography, which detected the presence of the radiolabelled phosphate that had been incorporated by Trib2 during the *in vitro* kinase assay. The active kinase Aurora A (tagged with the same N-terminal His tag and isolated in an identical fashion from *E. coli*) was also assayed as a positive control in the presence of Mg^{2+}, and affinity purified Trib2 autophosphorylated in the absence of magnesium ions as previously demonstrated (Figure 3.4). The fractions that contained monomeric Trib2 were pooled and assayed (Figure 3.9 C). The time-dependent increase of the signal intensity was indicative of autophosphorylation and confirmed that Trib2 hydrolysed ATP and incorporated the released γ-phosphate rather than non-specifically binding to it in the gel.

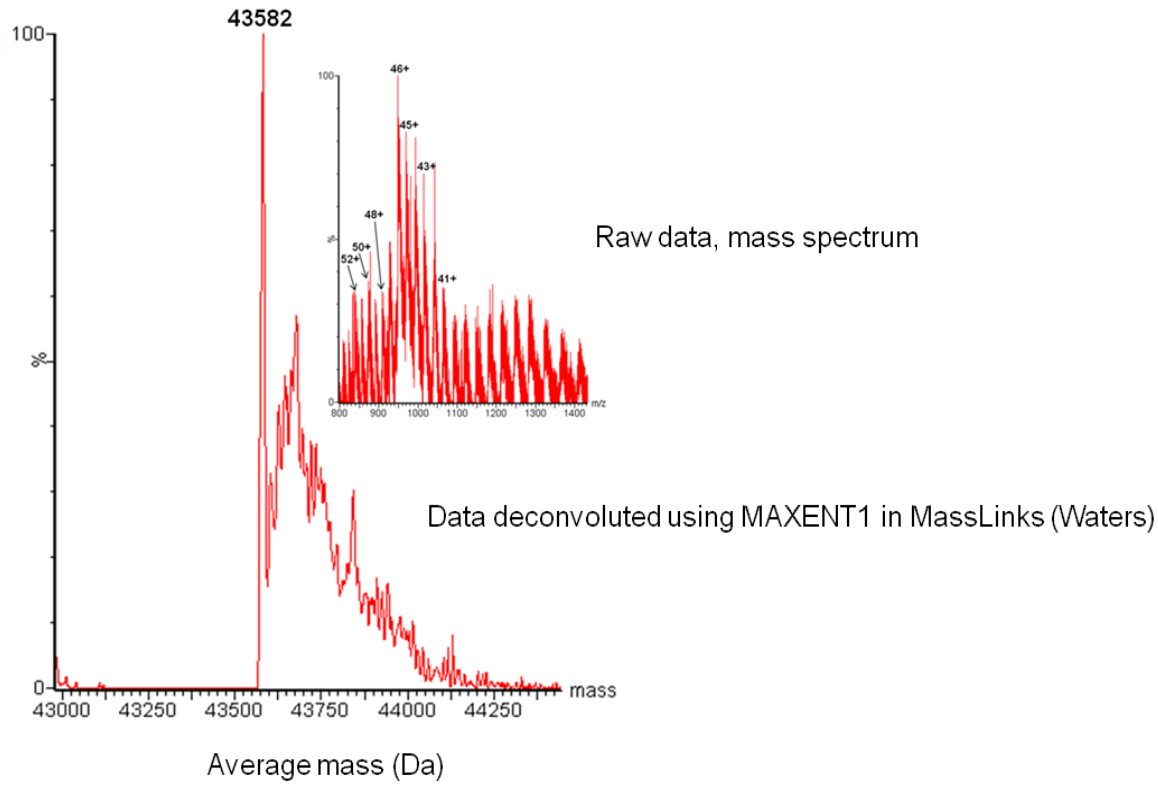

Figure 3.8 Exact MW of gel filtered Trib2 was determined by Mass Spectrometry. An intact average mass of Trib2 was calculated using a Waters Qtof Global by nanoES. A MW of 43582 Da compared to the predicted 43524 Da was obtained by ESI-MS analysis, using BSA (average mass 66432.96 Da) as a standard (performed by Dr Claire Eyers, University of Liverpool).

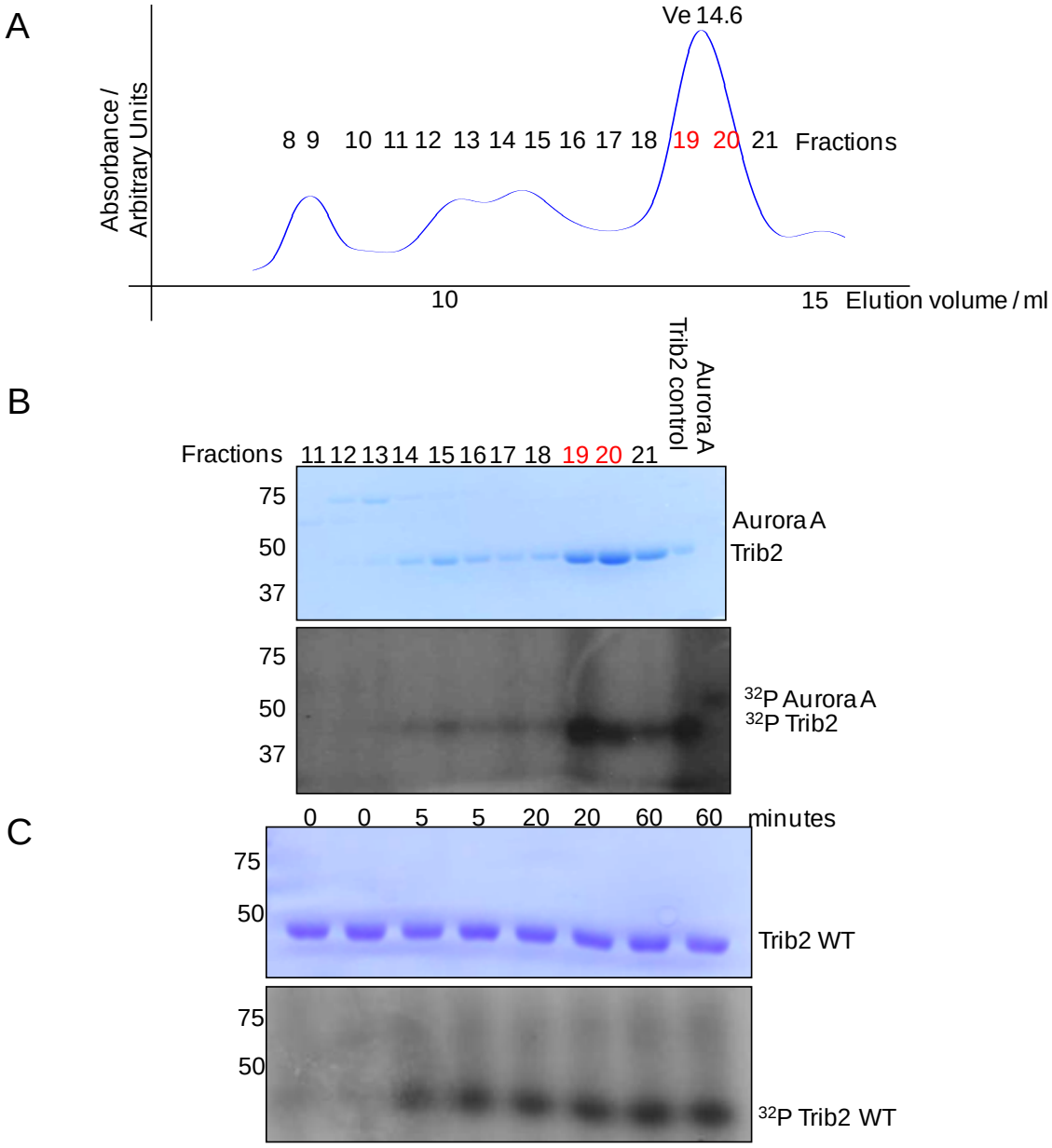

Figure 3.9 Trib2 autophosphorylated after gel filtration A) Gel filtration chromatogram of IMAC purified Trib2 eluted into buffer B. The fractions collected are numbered and the fractions that eluted in 14.6 ml buffer, the predicted elution volume of monomeric Trib2 are highlighted in red font (fractions 19 and 20) B) The gel filtered Trib2 (from A) was subjected to an *in vitro* kinase assay and resolved by SDS-PAGE. Fractions 19 and 20, highlighted in red, were the fractions that eluted from the gel filtration column (panel A) in a volume (14.6 ml) that was expected for monomeric Trib2. Alongside the assays of the fractions, 250 pmoles of a Trib2 control (purified previously by IMAC) and 25 pmoles Aurora A were also assayed and resolved by SDS-PAGE. The protein was stained by coomassie stain (top panel) and autorads show the presence of incorporated radiolabelled phosphate in the protein (bottom panel). C) The fractions 19 and 20 (eluted in a volume predicted for monomeric Trib2) were pooled together and 250 pmoles were assayed in the same manner as in Figure 3.9 B. The assays were terminated at the stated time by the addition of 5 x SDS PAGE loading buffer and heating. They were then treated to SDS-PAGE analysis and the protein stained with coomassie stain (top panel). The gels were dried and subjected to autoradiography (bottom panel shows the autorads and the signals correspond to protein containing radiolabelled phosphate).

3.7 Trib2 autophosphorylation is decreased by mutation of classical invariant kinase residues in the Trib2 catalytic domain.

With the discovery that the Trib2 has an intrinsic ability to autophosphorylate, its mechanistic biochemistry was investigated further. It is standard practice in the field (Carrera *et al.*, 1993, Iyer *et al.*, 2005a), for the conserved lysine in the β3 motif of classical kinases (PKA K72, corresponding to Trib2 K90) to be mutated in an attempt to create a kinase domain with a reduced level of catalytic activity. To verify whether the Trib2 pseudokinase domain is catalytically active through a conventional mechanism that involves amino acids in stereotypical positions in the kinase, affinity purified Trib2, and the Trib2 mutants K90M and K177A were incubated with radiolabelled γ^{32}P ATP. Trib2 K90M contained a mutation to the lysine that is conserved throughout the β3 motifs of 'classical' human kinases. This coordinates the α- and β- phosphates of ATP in the kinase active site, facilitating the catalytic hydrolysis of the γ-phosphate. Trib2 K177A is a mutation to a lysine located within the catalytic motif. Previous studies identified that following a mutation to K177, the stability in cells and oncogenic transforming capability of cells expressing K177A and levels of C/EBPα degradation were reduced, compared to WT Trib2-expressing cells (Keeshan *et al.*, 2010). As shown in Figure 3.10 A, 250 pmoles Trib2 autophosphorylated in a readily detectable manner but this was markedly reduced when Trib2 K90M (Figure 3.10 B) or Trib2 K177A (Figure 3.10 C) were assayed alongside. The positive control for these experiments was 25 pmoles of the active kinase Aurora A (Figure 3.10 D) and 250 pmoles of the point mutant Aurora A D274N (Figure 3.10 E), which is a mutation to the magnesium ion binding Asp in the DFG motif that prevents metal binding, were assayed for 60 minutes. This experiment demonstrated that the D274N mutation in the catalytic domain of Aurora A kinase reduced catalytic activity (assessed by autophosphorylation) to a level lower than that present in Trib2. However, 10-fold less active WT Aurora A was assayed alongside Trib2, yet despite this, Aurora A autophosphorylated to a greater extent than Trib2 (determined by visual analysis of the autorad intensities), which indicated that Trib2 catalytic activity is rather low when compared directly to an active kinase.

To quantify the difference in catalytic activities of Trib2 and mutant Trib2 proteins, an *in vitro* kinase assay was performed (Figure 3.11). The gels were subjected to autoradiography (Figure 3.11 A) and radioactivity was quantified by

normalizing the density of each signal to the coomassie stained protein using the ImageJ software. A representative gel is shown in Figure 3.11 A, with the normalized, averaged values plotted in Figure 3.11 B, which clearly displays the increased ability of WT Trib2 to incorporate the radiolabelled phosphate compared to the pseudokinase domain-mutated proteins.

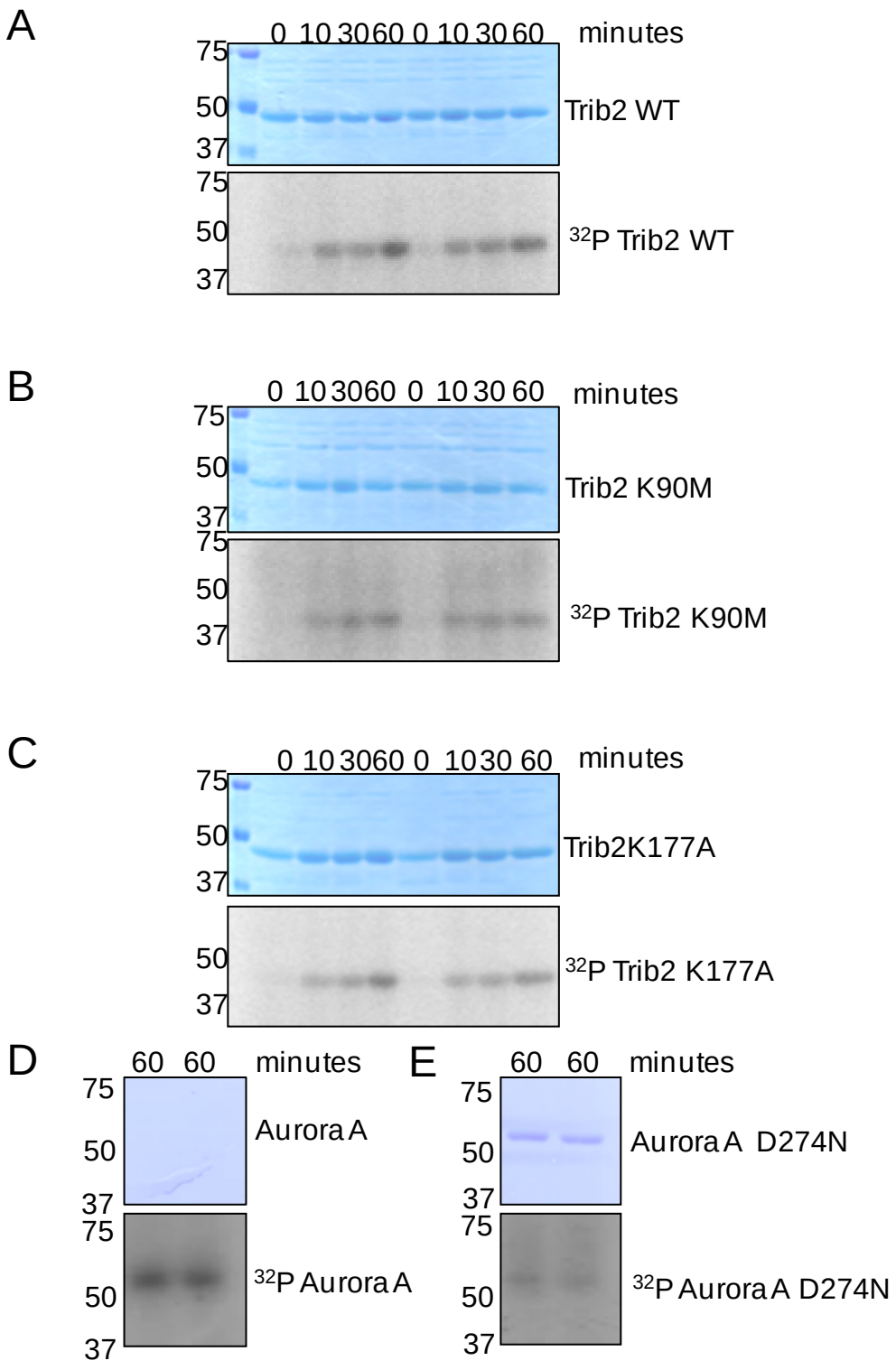

Figure 3.10 Catalytic domain mutations reduce Trib2 autophosphorylation. A, B, C) Trib2 WT, K90M and K177A (250 pmoles, 11.75 μg) were incubated with 2 mM EDTA and 1 mM ATP (2.25 μCi γ-^{32}P ATP) for the stated time in duplicate. The assays were stopped by the addition of 5 x SDS loading buffer, boiled for 5 minutes and samples run on 12% polyacrylamide gels. The protein was stained with coomassie stain and dried (top panels). The gels were subjected to autoradiography (bottom panels). D) 25 pmoles Aurora A WT and E) 250 pmoles Aurora A D274N were incubated with 10 mM Mg^{2+} and 1 mM ATP for 60 minutes. At which point the assays were terminated as in A-C.

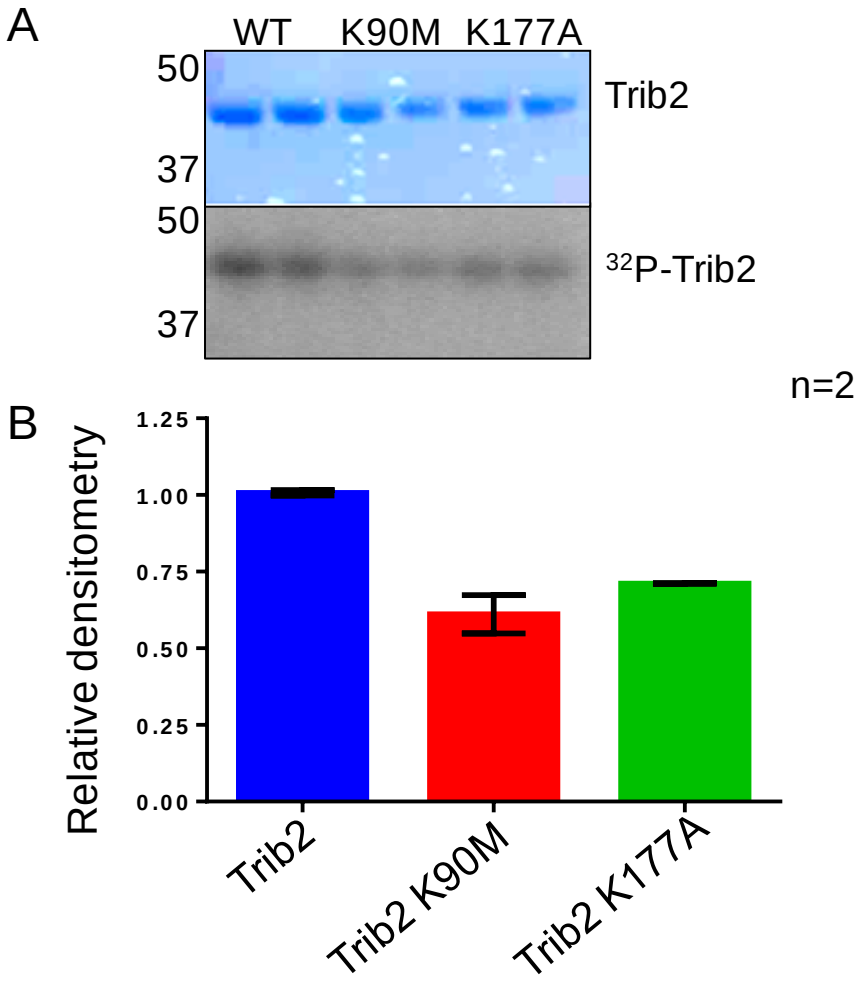

Figure 3.11 Trib2 K90M and K177A autophosphorylate to a lesser extent than WT Trib2. A) In duplicate, 250 pmoles Trib2 WT, K90M and K177A were assayed *in vitro* for 30 minutes. The gel containing the stained protein (top panel) was subjected to autoradiography (bottom panel). B) The stained protein from A and signals in the autoradiograms were quantified by densitometry using imageJ software. The ^{32}P signals were normalised to the protein (approximated by densitometry of the coomassie stained protein in the gels). The averaged signals for the two experiments that were performed with different preparations of protein (in duplicate) were plotted in the bar chart along with the standard deviation.

3.8 Analysis of K90 Trib2 mutants

K90M Trib2 demonstrated a reduced ability to autophosphorylate when compared to WT Trib2 (Figure 3.12). The autoradiograms demonstrate that WT Trib2 incorporated the hydrolysed radiolabelled phosphate to a greater extent than K90M over the course of the assay and this was quantified by phosphorimage analysis. Two other K90 mutants, Trib2 K90A and Trib2 K90R, were therefore assayed in the same manner, to see whether the effect was true for a variety of K90 mutants or was specific to K90M.

Trib2 (Figure 3.13 A), K90A Trib2 (Figure 3.13 B) or K90R Trib2 (Figure 3.13 C) were assayed as above (250 pmoles), in the presence of 1 mM ATP (2.25 μCi γ^{32}P ATP) and the reactions were stopped in SDS sample buffer at the indicated time points. Trib2 autophosphorylation increased in a time-dependent manner. However, mutating K90 to Ala (Trib2 K90A) where the charged lysine is mutated to an uncharged Ala, led to the abrogation of autophosphorylation. Conversely, K90R Trib2, in which Lys was mutated to a similarly positively charged Arg residue, remained catalytically active and was able to autophosphorylate to a similar degree as WT Trib2

3.9 Trib2 cannot phosphorylate common exogenous kinase substrates

Most kinases autophosphorylate weakly due to dimerisation, especially at high protein concentrations, but nearly all function to phosphorylate specific substrate proteins to trigger downstream signaling pathways, examples being members of the MAPK cascade. Analysing substrate phosphorylation would be advantageous for elucidating the biochemical activity of Trib2 because it would allow for the possibility of examining phosphorylation using techniques other than autoradiography of radiolabelled proteins after SDS-PAGE, which can be a very slow procedure (up to a week) when analyzing pseudokinases that have low levels of catalytic activity, such as Trib2. One technique that could be adopted for Trib2 assays requires discovery of a substrate that has a net positive charge. When such substrates are phosphorylated and applied to negatively charged P81 phosphocellulose paper (Glass *et al.*, 1978) the rate of phosphorylation can be quantified using a liquid scintillation counter. 3 types of classical protein substrates, two of which are amenable to the p81 phosphocellulose procedure,

were therefore tested for phosphorylation by Trib2. These are a range of Histone proteins (H1, H2A, H2B, H3 and H4), Myelin Basic Protein (MBP) and alpha casein (Figure 3.14). However, despite being phosphorylated by the active kinase Aurora A, there was no observable phosphorylation of any of these substrates by Trib2. A high background signal was detected for the histone proteins even in the absence of Trib2, which indicated that the high concentration and specific activity of the ATP used had caused a false-positive signal.

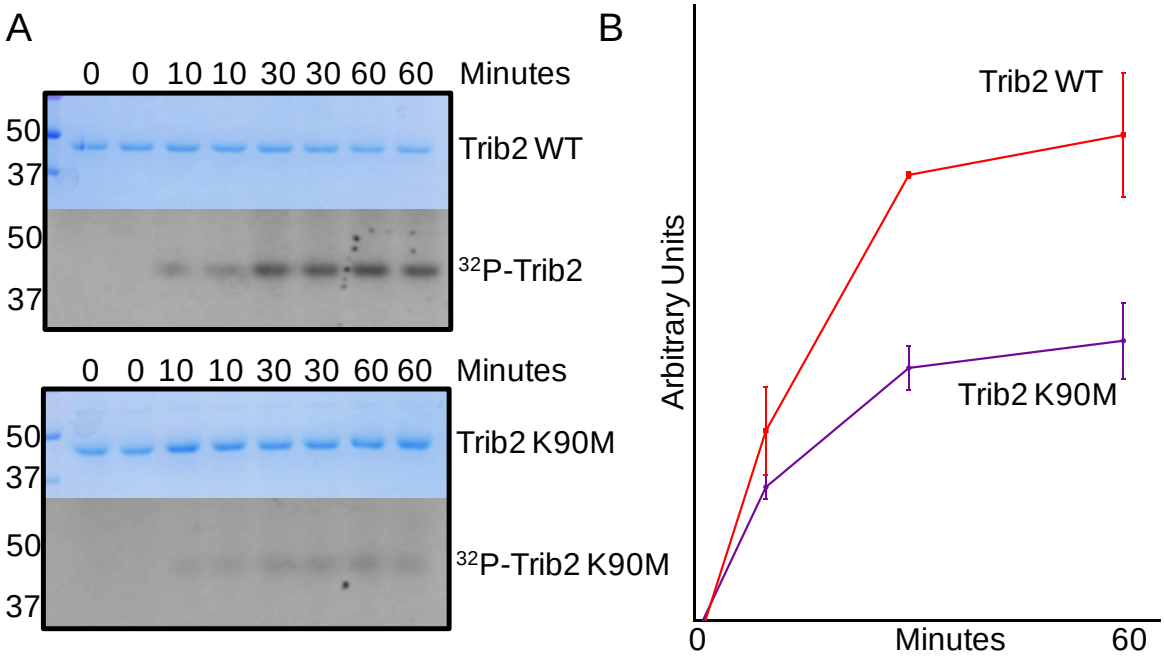

Figure 3.12 Trib2 autophosphorylates to a greater extent than the β3 Lysine mutant K90M A) Trib2 and Trib2 K90M were assayed in the presence of 1 mM radiolabelled ATP and 20 mM EDTA, The assays (in duplicate) were stopped by the addition of 5 x SDS loading buffer at the stated timepoints, boiled for 5 minutes and samples run on 12% polyacrylamide gels. The protein was stained with coomassie stain and autophosphorylation observed on X-ray film. B) The autophosphorylation was quantified using a phosphorimager. The values corresponding to each timepoint were averaged and plotted in GraphPad Prism 6, along with the standard deviation values.

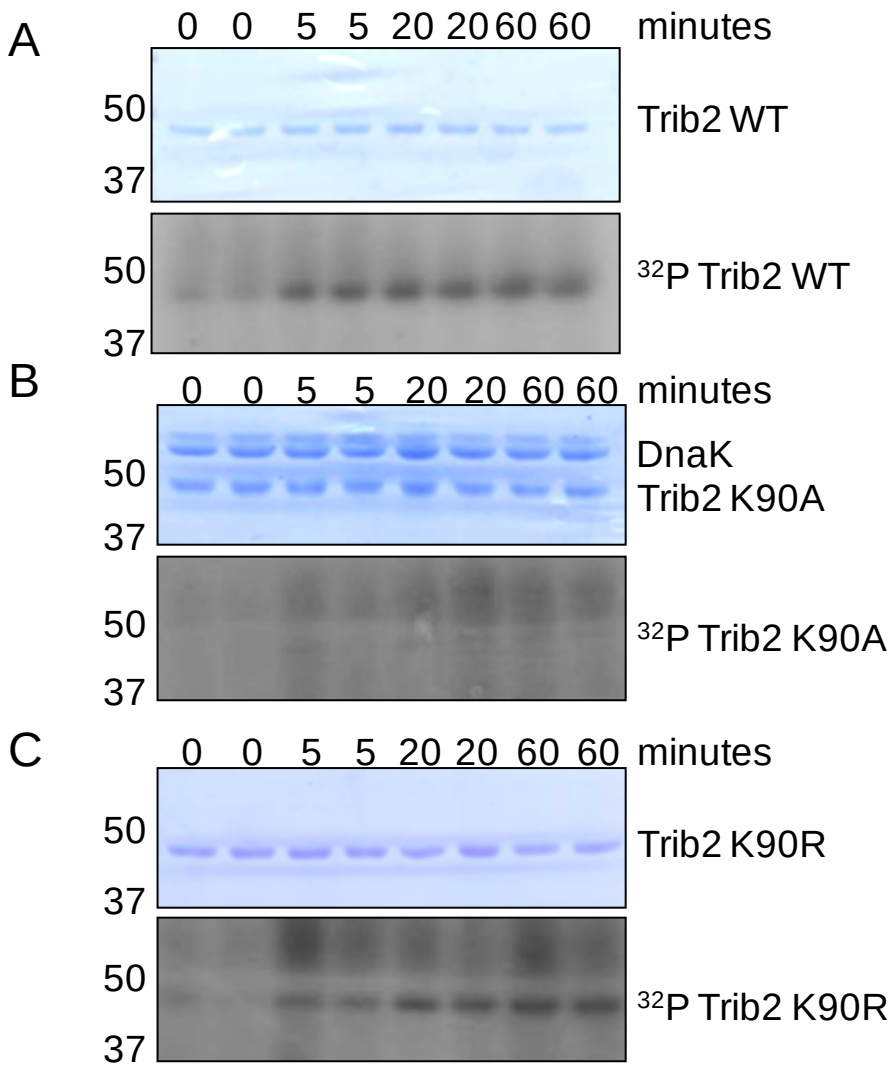

Figure 3.13 Trib2 K90R retains residual catalytic activity unlike Trib2 K90A. A) Trib2 WT, B) Trib2 K90A and C) Trib2 K90R (250 pmoles), were incubated at 30 °C on a shaking platform for the given time in the presence of 2 mM EDTA and 1 mM ATP (2.25 µCi γ-^{32}P ATP). The assays were terminated and the protein in the assays resolved by SDS-PAGE. The protein was stained (top panels of A, B and C) and gels were dried and treated to autoradiography, where the film was exposed to the stained and dried SDS-PAGE gels containing the radioactive samples for 48 hours (lower panels).

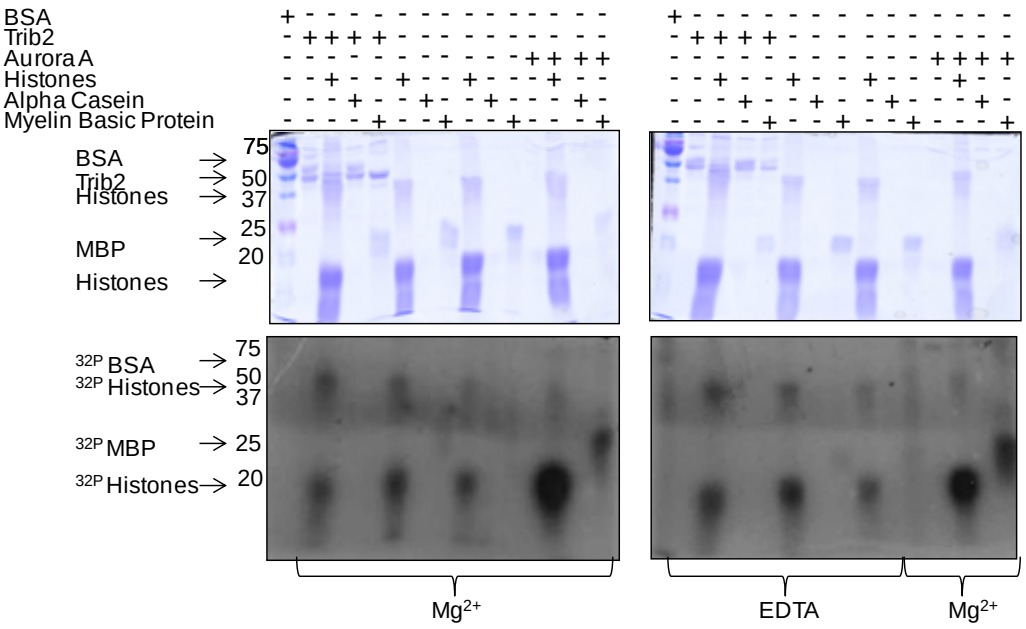

Figure 3.14 Trib2 WT does not phosphorylate 3 commonly used kinase exogenous substrates. Trib2 (250 pmoles) or 25 pmoles Aurora A were assayed in the presence of either mixed histones, alpha-casein or Myelin Basic Protein, and with 1 mM ATP (2.2 μCi γ^{32}P ATP) and 'cofactor' (either 2 mM EDTA or 10 mM Mg^{2+}) . The substrates were also incubated with ATP but without any additional kinase present. 250 pmoles BSA was assayed alongside. The assay duration was 30 minutes. The assays were terminated by the addition of loading buffer containing SDS and then heated for 5 minutes. The protein was observed by coomassie staining of the SDS-PAGE resolved assays (top panel) and the incorporated phosphate was observed on the corresponding autorads (lower panel). BSA (250 pmoles), was used as a negative control and assayed in the same manner as Trib2 and Aurora A.

3.10 Trib2 does not phosphorylate GST-C/EBPα in *in vitro* kinase assays

No evidence of Trib2 catalytic activity directed towards several exogenous substrates was observed *in vitro*, although Trib2 can autophosphorylate in these assays. In cellular systems Trib2 interacts with the E3 Ubiquitin ligases COP1 and TRIM21 and this then targets the transcription factor C/EBPα for degradation, although other proteins such as acetyl CoA carboxylase are also substrates in HeLa cells (Dedhia *et al.*, 2010). All members of this complex are required to actively target C/EBPα for degradation (Keeshan *et al.*, 2010). To identify whether C/EBPα is a substrate for Trib2 phosphorylation in the absence of COP1, recombinant GST-C/EBPα (a kind gift from Dr. Karen Keeshan, University of Glasgow) was expressed in BL21(DE3)pLysS and purified as described in Chapter 2 (Figure 3.15 A). To assay for substrate phosphorylation, GST-C/EBPα was incubated at a 1:1 molar ratio with 250 pmoles of Trib2 in the presence of 1 mM ATP (2.25 μCi γ^{32}P ATP) for 30 minutes. Under these assay conditions, Trib2 did not phosphorylate GST-C/EBPα, whereas GST-C/EBPα, which contains two potential (weak) Aurora A phosphorylation consensus sequences (RxS) (Ferrari *et al.*, 2005), was phosphorylated detectably in the presence of Aurora A and magnesium ions (Figure 3.15B). Interestingly, Trib2 autophosphorylation was partially reduced in the presence of GST-C/EBPα compared to when C/EBPα is absent, but this was not investigated further. These findings suggest that GST-C/EBPα is not a direct substrate for Trib2-mediated phosphorylation.

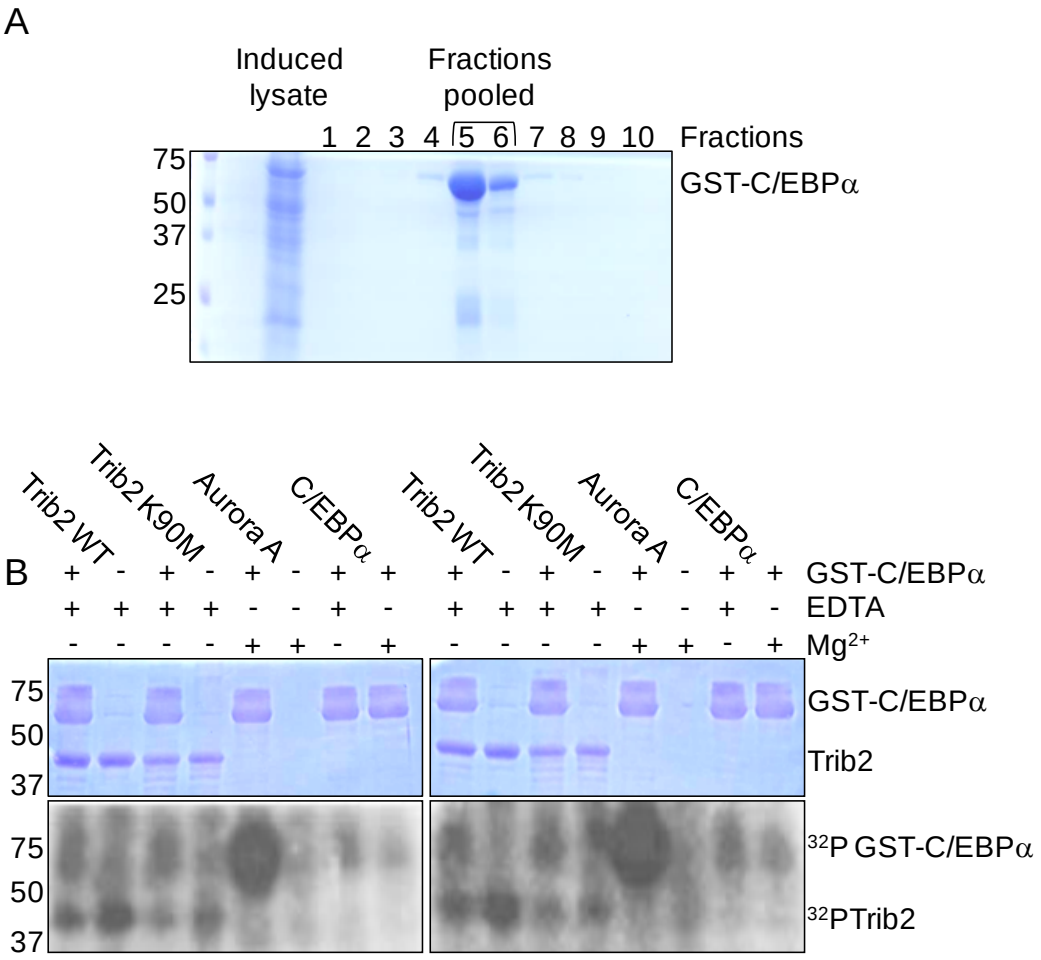

Figure 3.15 Trib2 does not phosphorylate GST-C/EBPα A) Twenty microlitres of the fractions collected following IMAC purification of GST-C/EBPα were resolved on 12% SDS-PAGE gels alongsdide 10 μl induced lysate. The protein was stained with coomassie stain and fractions 5 and 6 were pooled together. B) Trib2 WT or K90M (250 pmoles), or 25 pmoles Aurora A WT, were incubated with/without 250 pmoles of GST-C/EBPα and radiolabeled ATP (2.2 μCi γ^{32}P ATP) at 30 °C on a shaking platform for 30 minutes. The assays were stopped by the addition of loading buffer, boiled, subjected to SDS-PAGE (15% SDS-PAGE gels) and the protein stained with coomassie stain (top panel of B). The gels were dried and an X-ray film placed over the film. The incorporated radiolabelled phosphate was then observed on the film (lower panel of B).

3.11 Trib2 autophosphorylation is inhibited by divalent cations *in vitro*

In data described so far, Trib2 has demonstrated the unusual ability of autophosphorylation in the absence of Mg^{2+} ions, which were not added to the reaction mixture because, Trib2 does not possess the metal ion-binding residues that are observed in active kinases. Most of these kinases require the presence of divalent metal ions to phosphorylate substrates. However, one recent study with the pseudokinase CASK is a notable exception (Mukherjee *et al.*, 2010). Similar to CASK, Trib2 can autophosphorylate in the absence of Mg^{2+} ions (Figure 3.16). Remarkably, autophosphorylation is actually inhibited in the presence of 10 mM Mg^{2+} and Mn^{2+} ions, as judged by the reduced intensities of the autophosphorylated proteins on an autoradiogram (Fig 3.16 A) Trib2 K90M residual activity is also sensitive to divalent cation addition (Figure 3.16 B). Trib2 was inhibited by Mg^{2+} ions in a concentration-dependent manner with inhibition observed at as low as 5 mM Mg^{2+} (Fig 3.16 C). It is difficult to judge whether Trib2 autophosphorylation is inhibited to an even greater extent by the Mg^{2+} concentration exceeding 10 mM, because when *in vitro* assays were performed in the presence of 50 mM Mg^{2+}, the solubility and/or stability of Trib2 decreased markedly, as observed by SDS-PAGE (Figure 3.16 C)

Intriguingly, the level of Trib2 autophosphorylation was affected to varying degrees by different divalent cations (Figure 3.17). Ni^{2+} and Zn^{2+} ($ZnAc_2$), inhibited Trib2 autophosphorylation to a similar extent as Mg^{2+}. Whilst the addition of several other divalent cations, including Cd^{2+}, Cu^{2+}, Co^{2+}, Ca^{2+} and Zn^{2+} ($ZnCl_2$), also appeared to reduce Trib2 autophosphorylation, this may well have been the result of decreased Trib2 solubility in the assay, as judged by the reduced amount of Coomassie-stained Trib2 present.

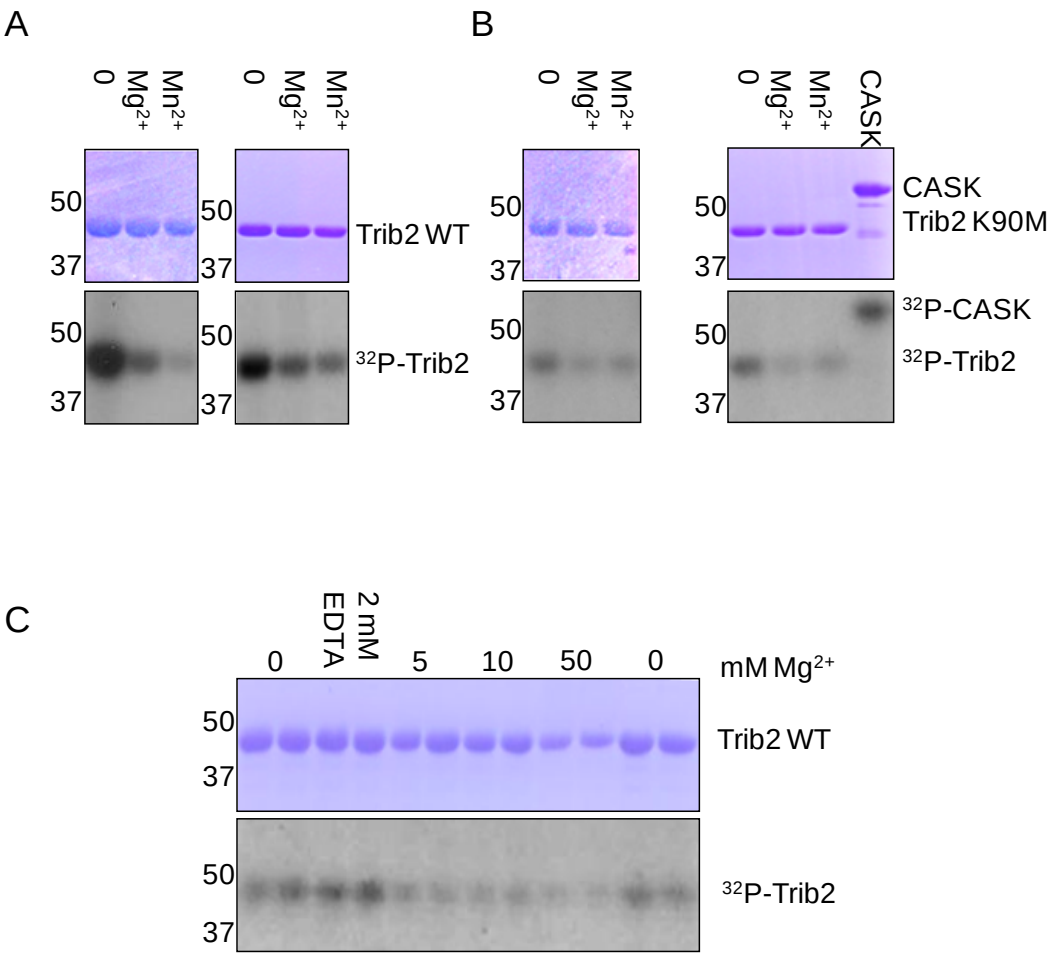

Figure 3.16 Trib2 autophosphorylation is inhibited by Mg^{2+} and Mn^{2+} ions. A) Trib2 WT and B) Trib2 K90M (250 pmoles) were assayed in the presence of 1 mM ATP at 30°C for 30 minutes with either no additional ions (0) or 10 mM Mg^{2+} or Mn^{2+} as indicated above the respective lanes of the SDS-PAGE gels. The protein was stained by coomassie stain (top panels) and the Trib2 incorporation of $\gamma^{32}P$ was detected by autoradiography after termination of the assay and SDS PAGE (bottom panels). CASK (250 pmoles) was assayed as a positive control with no additional divalent cations added. C) Twenty minute radiometric assays of 250 pmoles Trib2 WT in the absence of (0), or presence of the indicated concentrations of Mg^{2+} or 2 mM EDTA. The protein was resolved by SDS-PAGE, and stained using coomassie (top panel). The gels were dried and subjected to autoradiography (bottom panel) to observe the incorporated radiolabelled phosphate.

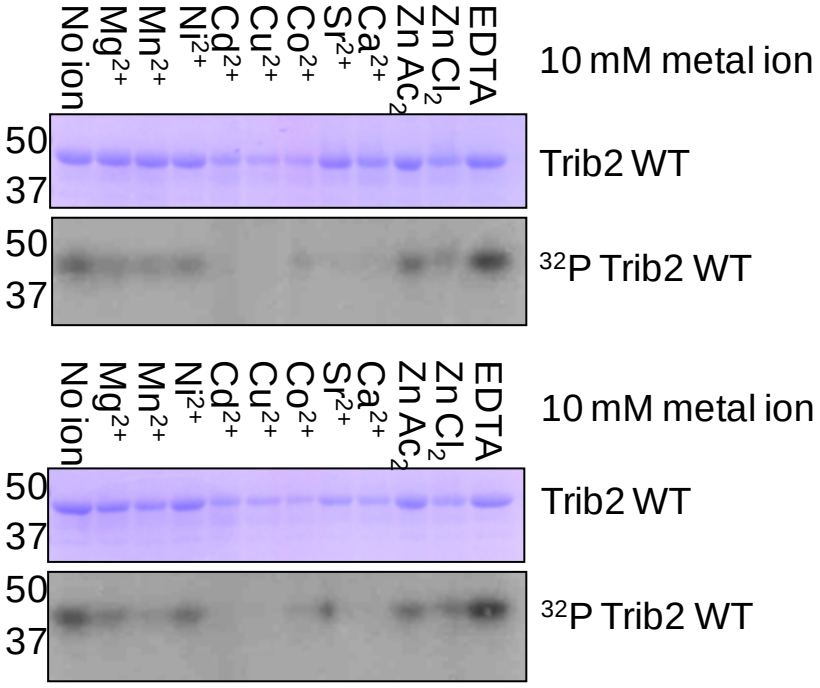

Figure 3.17 Trib2 is differentially sensitive to distinct divalent cations. Trib2 WT (250 pmoles) was assayed either in the absence or presence of the 10 mM divalent cation listed, or 2 mM EDTA for 30 minutes in duplicate. Added to the reaction mixture was 1 mM γ^{32}P ATP (2.2 μCi ATP). The reactions were terminated upon addition of SDS loading buffer and the samples were boiled for 5 minutes. The samples were then subjected to SDS-PAGE and upon completion, the duplicate gels were coomassie stained to visualise the protein (top segment of each of the duplicate experiments). After gel drying, γ^{32}P incorporation was detected by autoradiography on X-ray film (lower segments).

3.12 CASK autophosphorylates under assay conditions adapted for Trib2 autophosphorylation

CASK is a catalytically active pseudokinase that is inhibited by divalent cations (Mukherjee *et al.*, 2008). As demonstrated in Figure 3.18A, Trib2 and GST-His CASK that were purified using identical procedures and dialysed into identical 20 mM bicine pH 9.0, 100 mM NaCl, 1 mM DTT 10% glycerol buffers, were assayed in the absence of divalent cations. Trib2 autophosphorylation increased during the assay in a similar fashion to GST-His CASK, as reported previously (Mukherjee *et al.*, 2008) (Figure 3.18A). This clearly shows that under the assay conditions used for Trib2 autophosphorylation, a pseudokinase with reported catalytic activity can also autophosphorylate. Of note, no signal was detected on the autoradiogram when a non-pseudokinase control (250 pmoles BSA) was assayed, confirming an enzymatic role of the pseudokinases.

3.13 Can Trib2 biochemical function be changed by mutagenesis?

In an attempt to subvert the catalytic behaviour of Trib2 from a very low activity, metal-inhibited pseudokinase to one that more closely resembles a typical active kinase, Trib2 residues K180 and S195, L196 and E197 were mutated to the equivalent canonical Mg^{2+} binding residues find in classical kinases (PKA DFG motif; D184, F185, G186) (Trib2 S195D, L196F, E197G and K180N). As previously observed, Trib2 WT demonstrated optimal activity in the absence of divalent cations. Trib2 K180N, and Trib2 'DFG', a Trib2 triple mutant (S195D L196F E197G), were still able to weakly autophosphorylate in the absence of divalent cations, but their activity was not augmented by Mg^{2+}, or Mn^{2+}. Simultaneous insertion of both of these motifs to produce a Trib2 DFG K180N quadruple mutant resulted in no detectible autophosphorylation (Figure 3.18B), showing that mutagenesis had not successfully activated Trib2 under these conditions. Consistently, no signal was observed for BSA, a non-kinase secreted protein that was employed as a negative control.

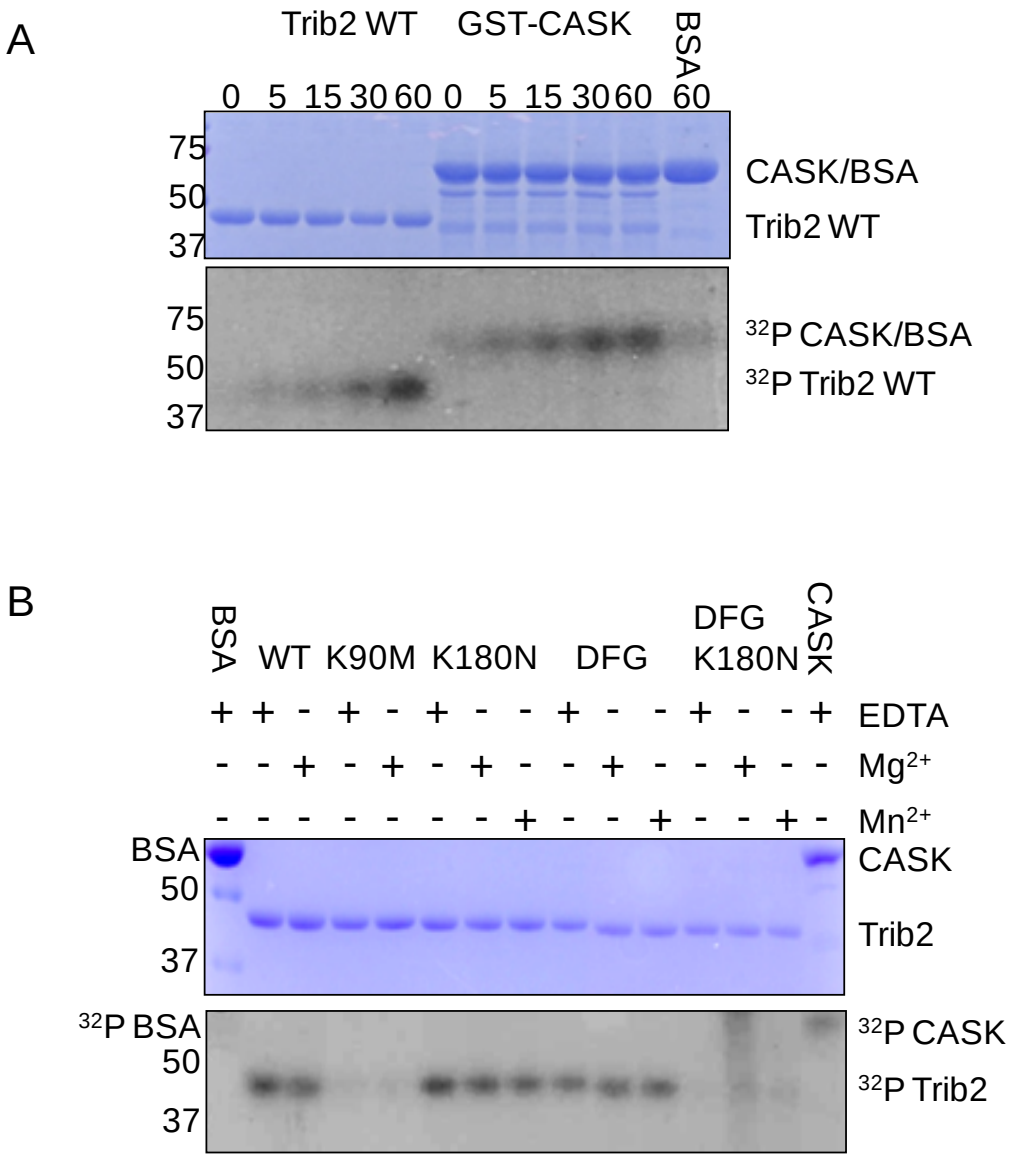

Figure 3.18 Trib2 divalent metal inhibition cannot be removed by mutating the metal binding residues to canonical kinase residues. A) Trib2 (250 pmoles) were radiometrically assayed for the allocated time, alongside 250 pmoles GST-CASK and 250 pmoles BSA (60 minutes) in the absence of Mg^{2+} ions. B) Mutant Trib2 proteins containing the classical kinase Mg^{2+} binding residues were generated (DFG and DFGK180N) and 250 pmoles were subjected to radiometric kinase assay for 30 minutes in the presence of either 2 mM EDTA or 10 mM of the divalent cations as listed. GST-tagged CASK and BSA (250 pmoles) were used as autophosphorylation controls. The assays were terminated and the protein resolved by SDS-PAGE. The stained protein (top panels of A and B) were subjected to autoradiography and the incorporated ^{32}P visualised on X-ray film (bottom panels).

3.14 Purification of recombinant human Trib2 from eukaryotic cells

Some human protein kinases are inactive, or less active, when isolated from *E. coli*. For example, a study performed by (Zhang *et al.*, 2004) identified lower levels of activity for the Cγ subunit of PKA when purified from *E. coli* compared to a eukaryotic source (Sf9 cells). This suggests that eukaryotic factors may be required for the production of a fully functional enzyme. Furthermore, it is well-known that human kinases purified in prokaryotic expression systems will lack the upstream regulators that often activate them, an example being the members of the MAPK family, which are sequentially phosphorylated and activated as part of kinase cascades (Khokhlatchev *et al.*, 1997).

To analyse the catalytic behavior of Trib2 expressed in a eukaryotic cell type, Sf9 cells, derived from the pupal ovarian tissue of *Spodoptera frugiperda*, were transfected with Trib2-pBAC2cp plasmid, and transformants selected. Expression levels of recombinant 6His- Trib2 WT, K90M or DFGK180N mutants present in Sf9 cell lysates are shown in Figure 3.19. Note that the expression levels of Trib2 WT and DFGK180N are much higher than the expression of the K90M mutant. In order to assay Trib2, Trib2 WT was partially purified from the lysate of ~$2x10^9$ Sf9 cells using TALON metal affinity resin (described in Chapter 2). Eluted fractions that contained Trib2 (2, 3 and 4, Fig 3.20A) were pooled. Five microlitres of each of the fractions, and 5 μl of pooled fractions were subjected to an *in vitro* kinase assay for 30 minutes (Figure 3.20 B), in the presence of either 10 mM Mg^{2+} or 2 mM EDTA.

In the presence of Mg^{2+}, there were multiple signals observed on the gel autoradiogram (Figure 3.20 B) at both the molecular weight previously established for Trib2 autophosphorylation and at much higher molecular weights. In the absence of Mg^{2+} ions, a much fainter signal was detected at the size of monomeric Sf9-derived human Trib2, and the higher molecular weight signals were no longer visible. This indicated that many of these bands were the phosphorylation products of classical, magnesium-dependent, kinases. The recombinant Trib2 derived from Sf9 cells was dialysed into either buffer A or buffer B (described in Chapter 2) in case the buffer affected the solubility of the protein as observed previously for recombinant Trib2, which is stabilized in buffer B, and 250 pmoles of the pooled fractions of Sf9-derived human Trib2 were assayed either in the presence or absence of Mg^{2+} ions (Figure 3.20 C). In the absence of magnesium, weak

autophosphorylation of Trib2 from Sf9 cells was observed, consistent with findings with bacterially-expressed Trib2. In the presence of magnesium ions, there were a number of higher molecular weight phosphorylation contaminants and also an intense signal detected at the appropriate size of Trib2. However, this band is likely to be caused by the Sf9 contaminant kinases phosphorylating Trib2, and these contaminants have been the cause of a variety of pseudokinases being attributed catalytic activity when none exists, an example being the inactive pseudokinase Titin (Bogomolovas *et al.*, 2014). Aside from the bacterial (*E. coli*) and eukaryotic (Sf9) protein sources described above, recombinant or endogenous Trib2 could be obtained from mammalian cell lines by immunoprecipitation. One advantage of using mammalian cell lines for protein production instead of insect lines is their ability to perform more complex protein glycosylation, which could be required for correct protein trafficking, folding or substrate interactions (Kost *et al.*, 2005). As with the other cell types, when assays are performed, the correct controls, including a 'kinase-inert' mutant must be used because pseudokinases such as BUBR1, when immunoprecipitated and assayed, initially appeared to be catalytically active. However, mutation to the catalytic residues did not alter the substrate phosphorylation and so it was concluded that the originally observed phosphorylation originated from co-purifying proteins rather than BUBR1 itself (Suijkerbuijk *et al.*, 2012). To ensure the observed autophosphorylation of Sf9 derived JAK2 was not caused by a contaminating kinase, assays were performed using *in vitro* translated JH2 (cell-free system), which supported the intrinsic catalytic activity of the insect JH2 protein and demonstrated that it was not caused by copurified kinase(s) (Ungureanu *et al.*, 2011).

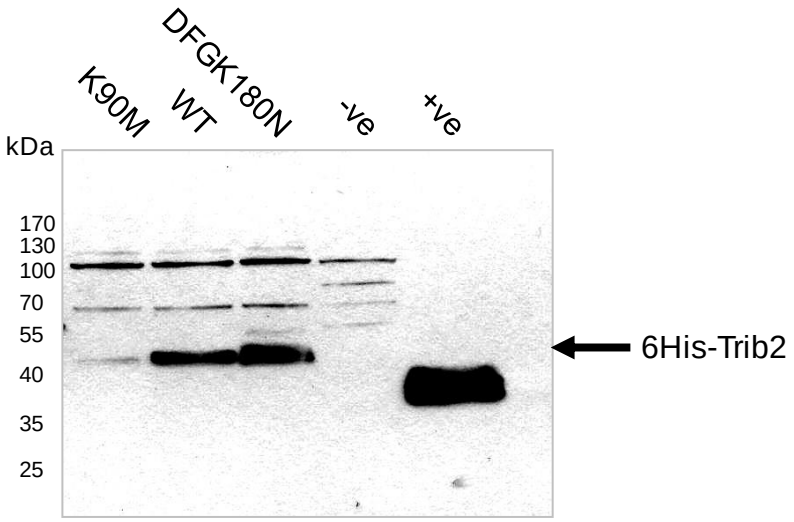

Figure 3.19 Expression of Trib2 WT and mutants in Sf9 cells. Trib2 K90M, Trib2 WT, and Trib2 DFGK180N expressing Sf9 cells were lysed and protein was immunoblotted with an anti-His antibody (Sigma, mouse monoclonal) along with an untransfected cell lysate and a 6His tagged control lysate. Eddie Mackenzie, University of Manchester.

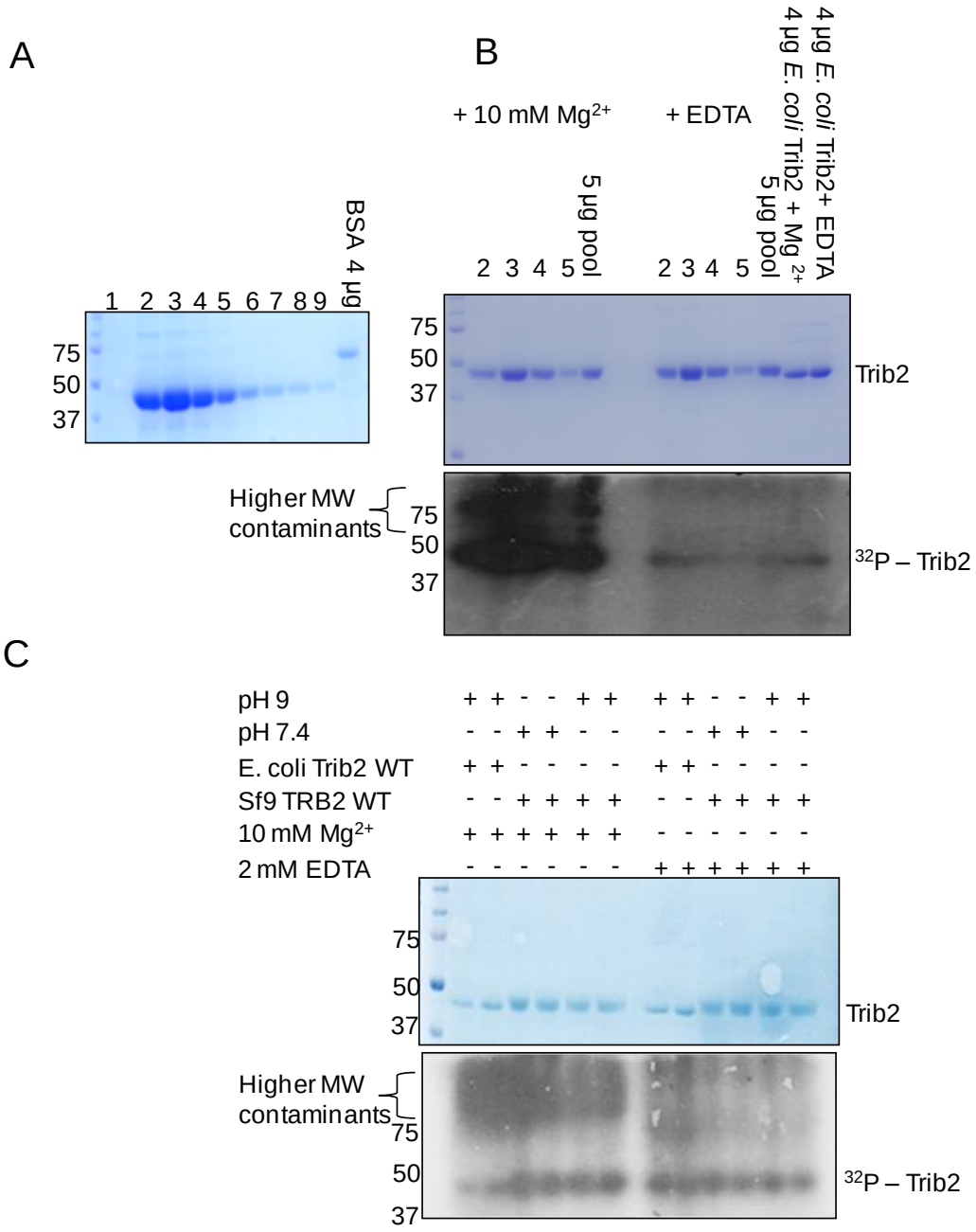

Figure 3.20 Purification of Trib2 from Sf9 cells. A) Fractions (1-9) eluted from TALON resin and 4 µg BSA were resolved by SDS-PAGE and the protein stained with coomassie stain. B) Protein from each individual fraction (2-5 from panel A), or the pool of fractions 2-5 (5 µg) were assayed with either 10 mM Mg^{2+} or 2 mM EDTA. The protein was observed after SDS-PAGE by coomassie staining (top panel). The incorporated labelled phosphate was observed by autoradiography (bottom panel). Signals detected >75 kDa are annotated 'Higher MW contaminants.' C) Following dialysis in to either 20 mM bicine pH9.0, 100 mM NaCl, 1 mM DTT, 10% glycerol (pH9) or 50 mM Tris, 150 mM NaCl, 1 mM DTT 10% glycerol (pH 7.4), 250 pmoles Trib2 derived from *E. coli* or Sf9 cells were assayed in the presence or absence of metal ions and 1 mM ATP (2.2 µCi γ ^{32}P ATP) and the SDS-PAGE resolved and coomassie stained protein (top panel) was subjected to autoradiography. Signals observed on the autorads at MWs that are higher than expected for Trib2 have been labelled 'Higher MW contaminants.'

To isolate a homogenous population of monomeric recombinant Trib2 derived from Sf9 cells, affinity purified Sf9 Trib2 was applied to a Superdex 200 10/300 gel filtration column. The absorbance peaks (Figure 3.21 A) identified a series of proteins with different Ve values. Elution fractions 17-19 contained Trib2, as judged by SDS-PAGE and by immunoblotting with antibodies directed against the 6His tag (Figure 3.21 B and C) and had elution volumes indicative of the monomeric species (as discussed in Section 3.5).

Trib2 containing fractions were pooled and 250 pmoles were assayed without divalent cations to observe any Trib2 catalytic activity that was not caused by contaminating kinases, alongside Trib2 WT purified from *E. coli*. As shown, Trib2 autophosphorylation increased over time. This indicated that Trib2 from both Sf9 cells and *E. coli* cells are able to hydrolyse ATP in the absence of divalent cations, albeit the signal for *E. coli* derived human Trib2 is more intense than that from Sf9 (Figure 3.22). This means that in the assay conditions used, the incorporation of radiolabelled phosphate by bacterial Trib2 was higher than the incorporation by Sf9 Trib2.

As mentioned previously, these experiments are likely to contain contaminating eukaryotic kinases and their substrates, which contribute to the strong signal seen when ATP and cations are added. To control for this, the assays should be performed in tandem with a Trib2 K90M mutant purified from Sf9 cells. However, the soluble protein yield of this mutant was far too low for accurate biochemical assays to be performed and therefore the intense signal seen at ~45kDa in Figure 3.20 in the presence of 10 mM magnesium ions, cannot be classed as Trib2 autophosphorylation unless this signal reduces in assays that contain protein has been purified further and the assays are controlled by a 'kinase-dead' control (K90M). This signal is therefore more than likely a by-product of eukaryotic kinase contamination. With regards to the faint time-dependent phosphorylation observed in Figure 3.22, this is much more likely to be *bona fide* Trib2 autophosphorylating activity because divalent cations are absent in this assay, however until the issue of kinase contamination has been fully explored and controlled for, using Sf9 cells as a source of Trib2 for biochemical analysis cannot be recommended.

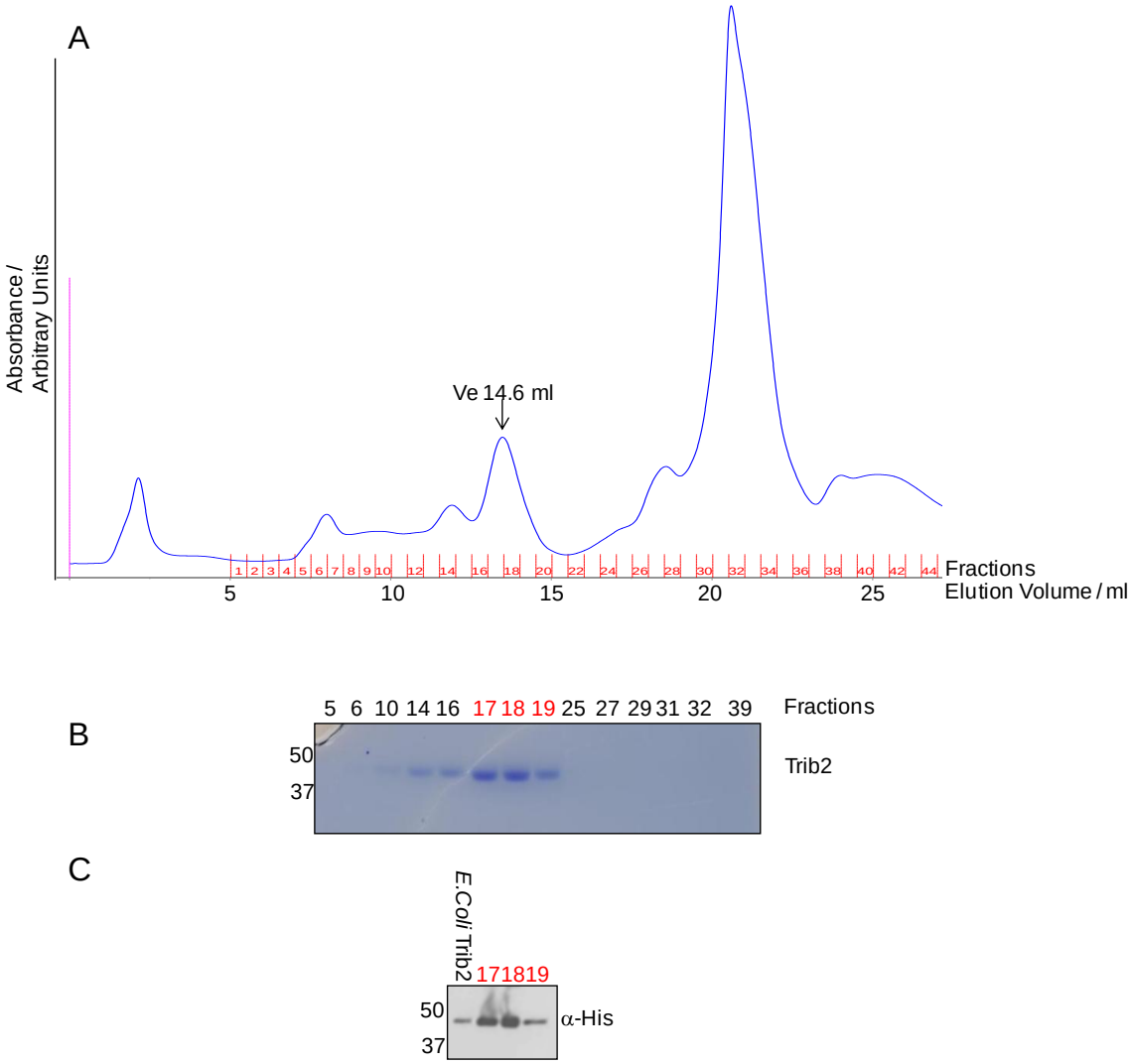

Figure 3.21 Gel filtration of Sf9 Trib2 reveals a fraction that elutes at the predicted volume expected for monomeric Trib2 A) IMAC eluate containing Sf9 derived Trib2 was gel filtered into buffer B (20 mM bicine, 100 mM NaCl, 1mM DTT, 10% glycerol). The elution volumes of the peaks were determined and the peak fractions (17-19) that correspond to the predicted MW of monomeric Trib2 were isolated (Ve 14.6 ml). B) Twenty microlitres of select fractions were subjected to SDS-PAGE and the protein stained with coomassie stain. The fraction numbers in red (17-19) correspond to the peak with a predicted MW of monomeric Trib2. C) One hundred nanograms of Trib2 WT purified from *E. coli* was resolved by electrophoresis in a polyacrylamide gel alongside 2 μl fractions 17, 18 and 19. The protein was transferred to nitrocellulose membrane by western blotting and the membrane probed with α-His HRP conjugated antibody.

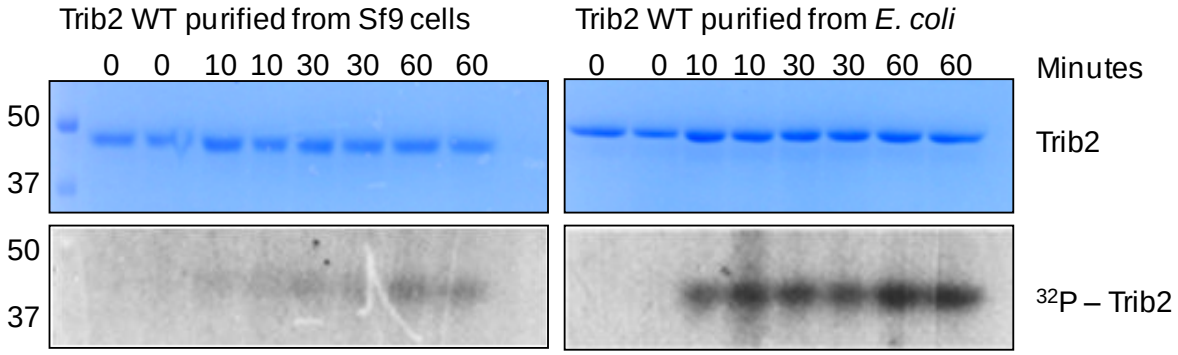

Figure 3.22 Sf9 Trib2 demonstrates very low levels of autophosphorylation. Gel filtered Sf9 or *E. coli* derived Trib2 (250 pmoles) were assayed in the presence of 2 mM EDTA and 1 mM ATP (2.25 µCi γ^{32}P ATP). The assays were stopped by the addition of 5 x SDS loading buffer at the stated timepoint, heated for 5 minutes at 95°C and samples run on 12% polyacrylamide gels. The protein was stained with coomassie stain and the gels subjected to autoradiography, and the ^{32}P incorporated visualised on the X-ray film.

3.15 Trib3, a closely related protein to Trib2, also autophosphorylates in the absence of magnesium ions

Trib2 is one of the four human Tribbles related proteins, which are pseudokinases that lack the magnesium ion binding residues present in canonical kinases. To determine whether Trib3 can also autophosphorylate in the absence of magnesium ions after isolation from *E. coli*, full-length Trib3 and a β3 lysine mutant K97M (corresponding to Trib2 K90M) were expressed in *E. coli* and purified in an identical fashion to Trib2 and Trib2 K90M. Trib2 WT and K90M, and Trib3 WT and K97M were assayed in duplicate for 30 minutes in the absence of divalent cations. As shown in Figure 3.23, both Trib2 and Trib3 exhibited the ability to autophosphorylate *in vitro*, in contrast to the K90M (Trib2) or K97M (Trib3) β3 lysine mutant controls.

3.16 The Trib-related protein SgK495 does not autophosphorylate under the experimental conditions validated for Trib2/3.

The Trib related protein SgK495, has a highly degraded kinase-fold, with amino acid alignment showing that it does not have a typical glycine-rich loop in the pseudokinase domain, lacks a lysine residue in the β3 sheet of classical kinases, and lacks the 'DFG' metal ion binding motif. However, the catalytic aspartate located within the catalytic loop of kinases is present in SgK495, along with an asparagine, which is the terminal residue of this motif and, in classical kinases, interacts with a Mg^{2+} ion. SgK495, unlike Trib 1, 2 and 3, has a canonical glycine-rich loop located N terminal to the pseudokinase domain. Whether this is involved in binding ATP has yet to be determined because no crystal structures or biochemical analyses of SgK495 have been published. STRADα, was also assayed here, and is a pseudokinase that has demonstrated the ability to bind to ATP but not hydrolyse nor incorporate the γ phosphate (Zeqiraj *et al.*, 2009b). His-tagged Trib2, Trib2 K90A, Trib2 K90R, SgK495 and STRADα were purified from BL21(DE3)pLysS competent *E. coli* by IMAC. Following dialysis, Trib2 (Figure 3.24 A), Trib2 K90A (Figure 3.24 B), Trib2 K90R (Figure 3.24 C), SgK495 (Figure 3.24 D) and STRADα (Figure 3.24 E) were assayed in duplicate. The upper panels in Figures 3.24 A-E show the Coomassie-stained protein and the lower panels are the corresponding autoradiography films. The average signals from each duplicate timepoint were quantified by phosphorimaging and plotted in GraphPad Prism6 (Figure 3.24 F). As

previously observed, Trib2 WT and Trib2 K90R autophosphorylation increased during the assay (Figure 3.24 A and C respectively), whereas very low autophosphorylation was observed for Trib2 K90A (Figure 3.24 B). Neither SgK495, nor STRADα exhibited detectable autophosphorylation.

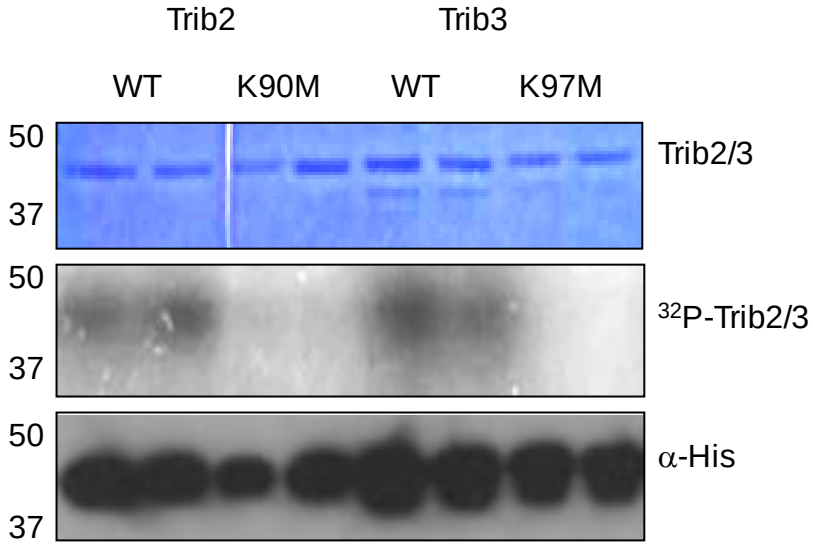

Figure 3.23 Trib3 autophosphorylates in the absence of Mg^{2+} ions. Trib2 WT and K90M, and Trib3 WT and K97M (250 pmoles) were assayed in the presence of 2 mM EDTA and 1 mM ATP (2.25 µCi γ-^{32}P ATP) for 30 minutes. The reactions were stopped by the addition of 5 x SDS loading buffer and samples were resolved by SDS-PAGE. The protein was coomassie stained (top panel) and phosphate incorporation was observed by autoradiography (middle panel). Loading was determined by the coomassie stained gel and immunoblotting 5 µl of each assay using an αHis antibody (bottom panel).

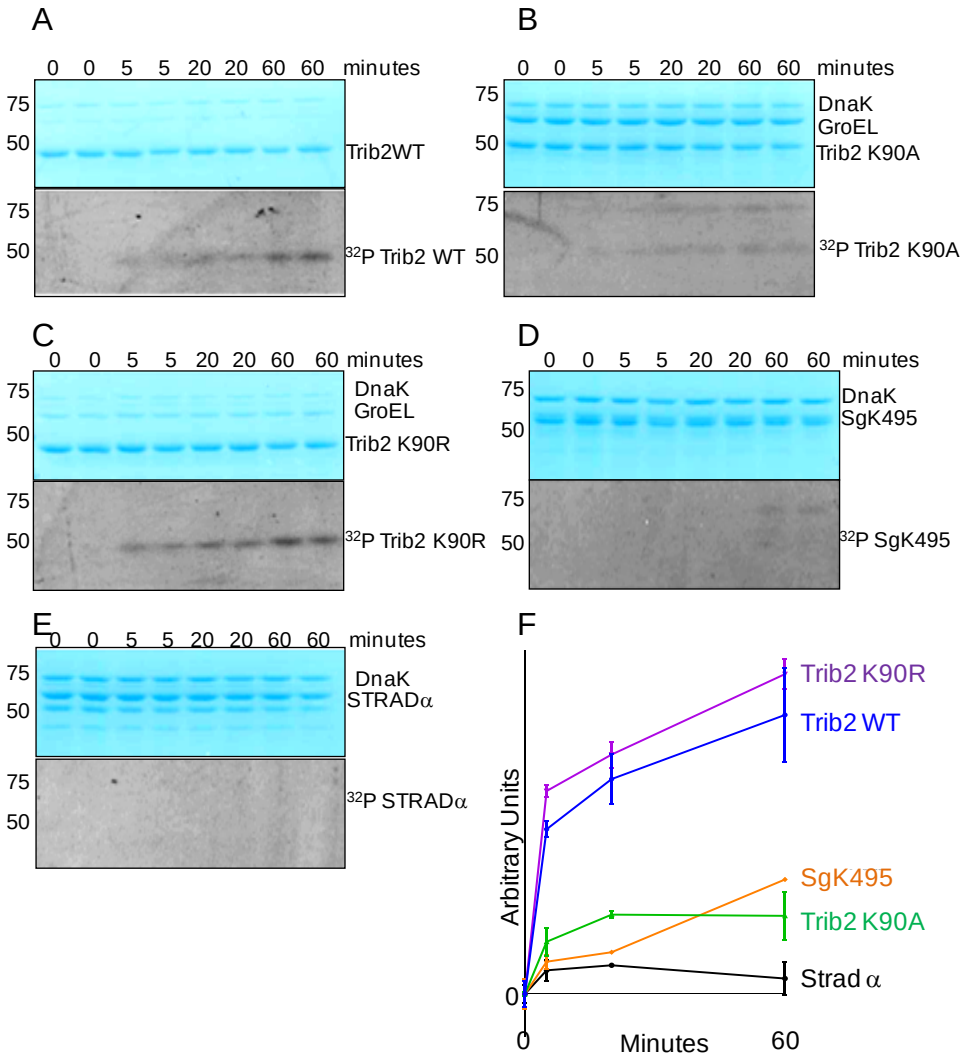

Figure 3.24 SgK495, a Trib-related protein does not demonstrate autocatalytic activity. Radiometric kinase assays of 250 pmoles A) Trib2 WT, B) K90A Trib2, C) K90R Trib2, D) SgK495 and the inactive pseudokinase E) GST-STRADα were carried out in duplicate over a time period of 60 minutes, with assays terminated at intermittent time periods. Samples were subjected to SDS-PAGE (top panels) and autoradiography (lower panels). F) The signals were then quantified by phosphorimager and average values plotted in GraphPad Prism 6 along with the standard deviation for each point.

3.17 Purification of Trib2 for X-Ray Crystallographic analysis

There are currently no available structural co-ordinates for any of the Trib related proteins (www.sgc.ox.ac.uk and www.pdb.ed.ac.uk). A crystal structure of Trib2 will be vital to observe the accessibility of the ATP binding site and identify how ATP and ligand binding sites might be manipulated for development of Trib2-specific inhibitors.

This lab recently used pET30 Ek/LIC to express and purify, then solve the structure of the canonical kinase Mps1 (Chu *et al.*, 2008). To purify high-quality, high concentration protein for this purpose, Trib2 was affinity purified and the Trib2-containing fractions were pooled and applied to the Superdex 200 10/300 gel filtration column and eluted in 20 mM bicine pH 9.0, 10 mM NaCl, 1 mM DTT, 10% glycerol. The protein in the fractions that correspond to the peaks on the chromatogram (Figure 3.25 A) were resolved by SDS-PAGE (Figure 3.25 B) and fractions that eluted in the volume predicted for monomeric Trib2 (Ve 14.6 ml), 22-25, were pooled and concentrated by centrifugation using a Vivaspin 2 (10 kDa MWCO) concentrator to 10 mg/ml. Ten micrograms was resolved by SDS-PAGE and the presence of a single coomassie stained band highlights the purity of the sample, alongside 8 μg BSA standard (Figure 3.25 C).

Trib2 (100 nl per well) was mechanically transferred (described in Chapter 2) to 7, 96 well sitting drop crystallography trays, into which 100 nl of the buffers from the crystal screens listed in Chapter 2, were added. The trays were sealed and left at room temperature to facilitate crystal formation. The buffers added were from the crystal screening buffer libraries listed in Chapter 2. The trays were sealed and left at room temperature to facilitate crystal formation and observed regularly. Trib2 formed aggregates in many of the conditions but did not form any crystals (Figure 3.26 A-D).

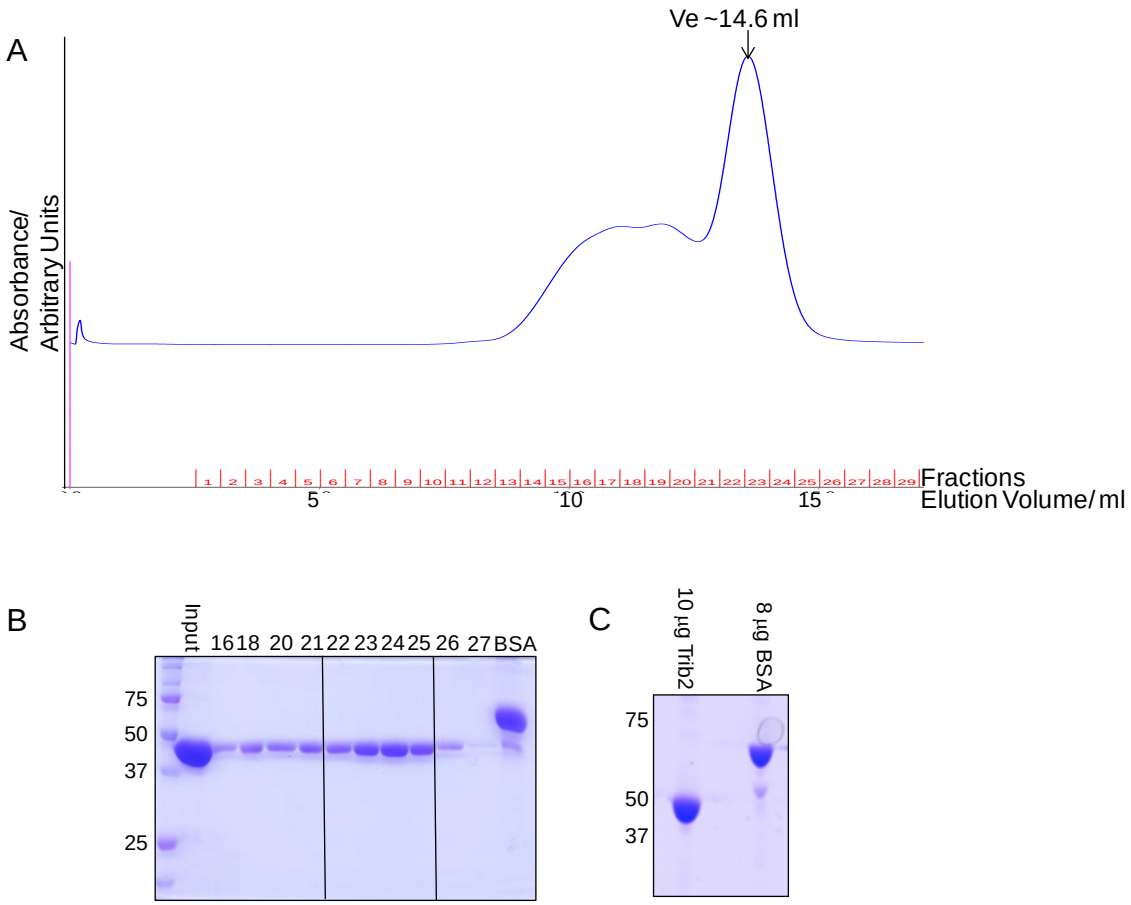

Figure 3.25 Purification of Trib2 for X-Ray crystallography trials. A) Affinity purified Trib2 was gel filtered into 20 mM bicine, 100 mM NaCl, 1 mM DTT and 10% glycerol and the fractions collected. Peaks in the absorbance spectrum (blue line) were used to identify the fractions in which protein was eluted. The peak that contains protein which eluted in 14.6 ml buffer (expected volume for elution of Trib2 monomer) B) Twenty microlitres of the fractions (16-27) were resolved by SDS-PAGE and the protein was observed by coomassie stain. The fractions that eluted in the Ve that corresponded to the predicted MW of monomeric Trib2 (22-25) were pooled together and the protein was concentrated to 10 mg/ml using a Vivaspin2 centrifugal column. C) One microlitre of Trib2 was resolved by SDS-PAGE and coomassie stained alongside 8 µg BSA standard.

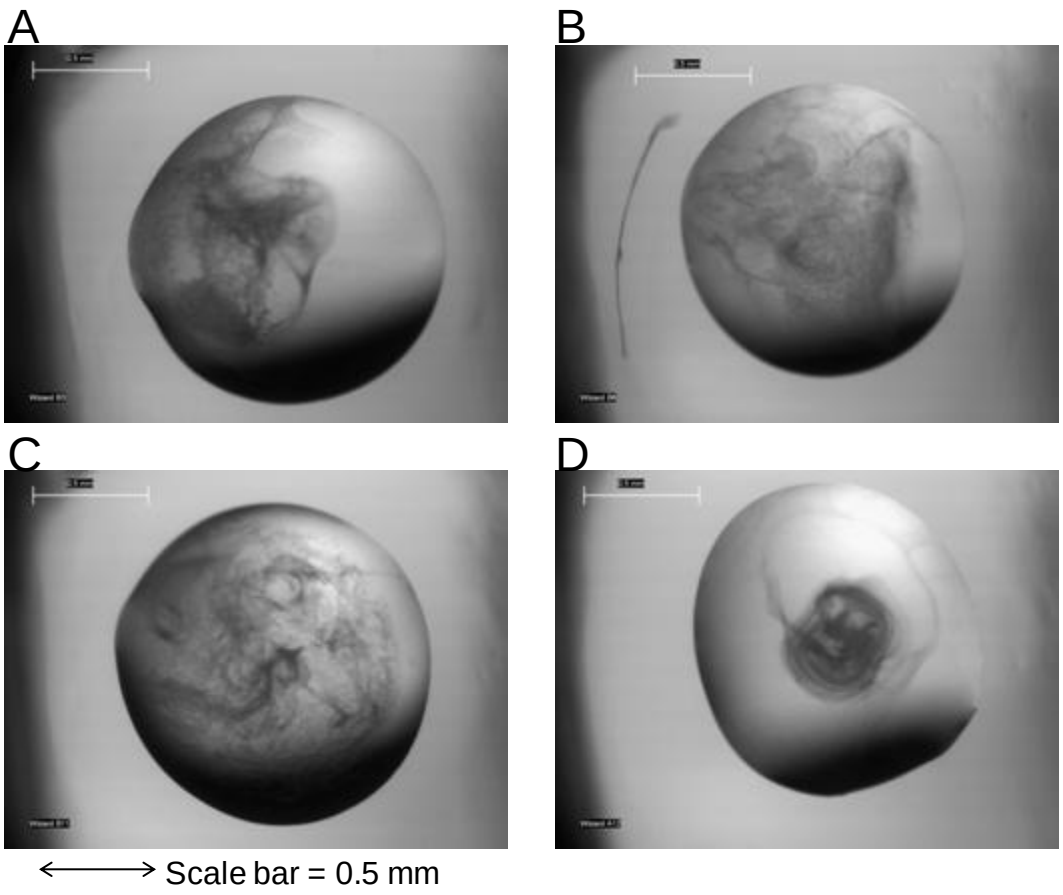

Figure 3.26 Trib2 aggregation was observed in crystal trials. Images demonstrating the high levels of protein aggregation observed in the sitting drop crystal trials. One hundred nanolitres of TRB2 (10 mg/ml) was added to 100 nl A) 10% (w/v) PEG-3000, 0.1 M imidazole pH 8.0, Li_2SO_4, .B) 1.0 M K/Na tartrate, 0.1 M imidazole, pH 8.0, 0.1 M NaCl, C) 15% (v/v) ethanol, 0.1 M imidazole pH 8.0, 0.1 M $MgCl_2$. Images were captured on a Leica M795 microscope using a KL1500 LCD lightsource with a 60 x objective.

3.18 Purification of ^{15}N-labelled Trib2 for 2D NMR

Another method that could determine Trib2 structural features is 2D ^{15}N-HSQC NMR. NMR can be used to determine the structure of macromolecules, with the number of protein structures deposited into the online RCSB Protein Data Bank structural database at this present time that have been solved using solution NMR being in excess of 10,000, some 10-fold less than for X-ray crystallography, for which 100,000 structures have now been deposited in the PDB resource. For successful NMR spectroscopy, the backbone amine groups require labeling with ^{15}N, whose nucleus contains an odd mass number, and integral spin value of 1/2. In the ^{15}N-HSQC spectra, a signal for each ^{1}H-^{15}N covalent bond is detected. This process occurs in solution and is non-denaturing. By comparing the peaks before and after the addition of a ligand, the spectra can be used to identify whether binding occurred. To incorporate radiolabeled ^{15}N atoms into the Trib2 backbone, the protein has to be expressed in *E. coli* that has been grown in minimal media supplemented with ^{15}N ammonium sulphate. Prior to expression in labeled media, it needed to be determined whether Trib2 was expressed in *E. coli* grown in 1 L minimal media (M9). Once an A_{600nm} 0.8 was reached, Trib2 expression was induced with 0.5mM IPTG at 18°C for 18 h. The cells were harvested and Trib2 purified by elution from a 5 ml HisTrap. The fractions were resolved by SDS-PAGE, which confirmed the presence of Trib2 (Figure 3.27 A).

Following successful Trib2 expression in minimal media, Trib2 was expressed (as above) in 2 L of minimal media supplemented with radiolabeled ^{15}N ammonium sulphate (Figure 3.27 B and C). Monomeric Trib2 was isolated as previously described (Figure 3.27 D). When analysed by coomassie stain (Figure 3.27 E), the fractions that contained monomeric Trib2 also had protein contaminants present and to ensure the sample was homogenous for NMR analysis, anion exchange chromatography using a MonoQ 5/50 column was performed and Trib2 eluted in 20 mM bicine pH 9.0, 460 mM NaCl, 1 mM DTT, 10% glycerol (Figure 3.27F), SDS-PAGE confirmed the presence of purified Trib2 (Figure 3.27 G) The Trib2 containing fractions were then pooled (fractions numbered in red) and subjected to buffer exchange in a NAP-10 column to transfer Trib2 into an NMR-suitable buffer (20 mM Tris pH 7.4, 50 mM NaCl, 1 mM DTT) and analysed by ^{15}N-HSQC by Dr. I. Barsukov, University of Liverpool, on a 800 MHz Bruker solution state NMR machine.

3.19 ^{15}N-HSQC spectrum indicates that recombinant human Trib2 generates a spectrum consistent with a folded protein in solution

The spectrum obtained following ^{15}N-HSQC of recombinant Trib2 showed a broad distribution of non-uniform signals. Each signal corresponded to a covalently bonded ^{15}N atom and ^{1}H atom and was plotted on the spectrum, determined by their respective chemical shift values. When proteins are folded, the chemical environment that each covalently bonded ^{15}N amide-Hydrogen pair occupies is different. This means that each amide-proton pair exhibits a different chemical shift than other amide-protons throughout the protein, providing a broad spectrum of signals as observed in Figure 3.28. If, on the other hand, the protein was unfolded, then the chemical environment that each amide proton occupies and by association, the chemical shift of each proton, will be similar to one another because they all are exposed to buffer. This is indicated by a narrow ^{15}N-HSQC spectrum (Kwan *et al.*, 2011). The concentration of Trib2 used in this experiment (~1mg/ml) was too low to determine any other features other than protein 'foldedness.' Ideally, with a higher concentration of Trib2, NMR will be a very useful tool for not only determining structural components of Trib2 but for observing ligand and inhibitor interactions.

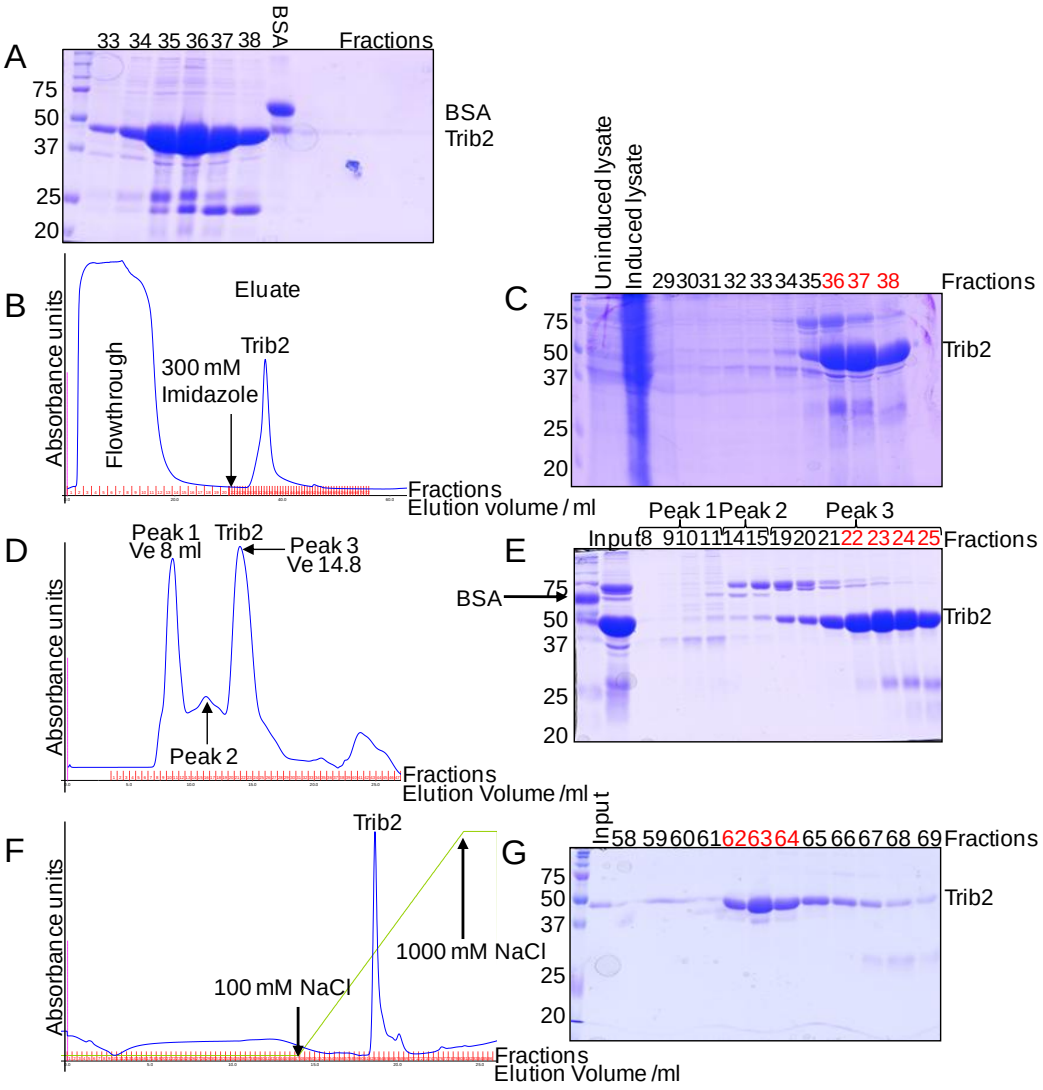

Figure 3.27 Purification of ^{15}N-labelled Trib2 for NMR analysis To determine whether Trib2 could be expressed using 'minimal media', lysate from *E. coli* that expressed Trib2 in A) One litre minimal (unlabelled) media was subjected to IMAC and the eluted fractions treated to SDS-PAGE analysis alongside 8 μg BSA. The protein was visualised by coomassie stain. Trib2 is located between 37 kDa and 50 kDa. B) The fractions containing eluted IMAC purified ^{15}N labelled Trib2 after application of a 300 mM imidazole containing elution buffer, could be identified by analysis of the absorbance profile. C) Fractions (20 μl) from the elution of ^{15}N labelled Trib2 B (29-38), were resolved in a 12% SDS-PAGE gel along with 5 μl of the uninduced lysate and induced lysate. D) Following IMAC, the pooled ^{15}N labelled Trib2 (red fractions in C, 35-38) was gel filtered and the elution volumes were determined by analysis of the absorbance spectrum. The peak Ve values are labelled. E) The peak fractions from D were treated to SDS-PAGE and protein visualised by coomassie stain. The fractions that corresponded to monomeric ^{15}N labelled Trib2 were pooled (Ve 14.8, fractions 22-25) and passed through a F) MonoQ Anion exchange column, where ^{15}N labelled Trib2 eluted in 460 mM NaCl. G) The eluted protein was resolved by gel electrophoresis and the fractions that contained the highest concentration of ^{15}N labelled Trib2 were pooled (62-64).

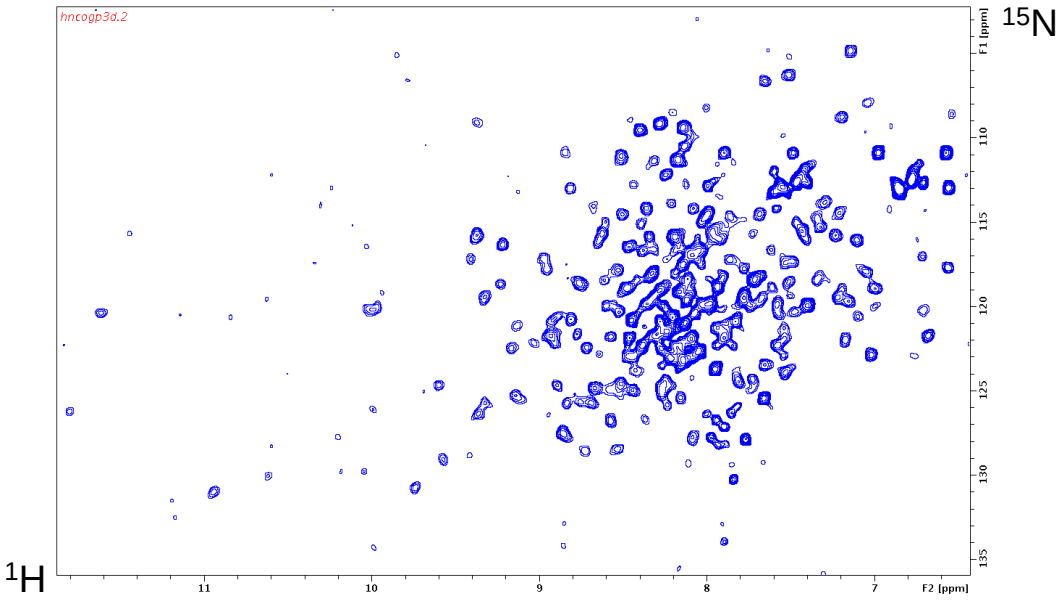

Figure 3.28 ^{15}N-HSQC Spectra of Recombinant Trib2. Purified ^{15}N labelled Trib2 (Figure 3.27G) was supplemented with 10% D_2O and was loaded into a Bruker 800 MHz solution state NMR machine for 12 hours. Each point on the spectra corresponded to a ^{15}N atom that is covalently bonded to a ^{1}H atom and the location of the points are ascertained by the chemical shift values for each of the constituent atoms. The chemical shift values for ^{1}H atoms are determined by referring to the X-axis, and the Y-axis corresponds to the ^{15}N chemical shift values.

3.20 Discussion

The work presented in this chapter describes a robust protocol for the purification of *E. coli* derived full length recombinant human Trib2 in sufficient yields to perform careful biochemical analyses using monomeric, soluble protein. Trib2 was most stable in a slightly alkaline pH buffer, specifically 20 mM bicine pH 9.0, 100 mM NaCl, 1 mM DTT and 10% glycerol, allowing protein concentrations in excess of 10 mg/ml to be obtained without evidence of protein precipitation. Recombinant aggregation of Trib2 catalytic domain was previously evaluated by Vedadi et al., (2006), who reported that the catalytic domain of Trib2 was most stable in a buffer containing 20 mM bicine at pH 9.0 (Vedadi *et al.*, 2006). Monomeric preparations of Trib2 were successfully separated from higher molecular weight Trib2 aggregates and contaminant proteins by a combination of gel filtration and anion exchange chromatography. The presence of folded and monomeric Trib2 was then confirmed by a combination of DSF, MS and NMR.

Excitingly, when recombinant Trib2 was assayed in the presence of radiolabelled ATP, it autophosphorylated, although this was weak when compared to the active kinase Aurora A. Trib2 autophosphorylation, observed by autoradiography and quantified by phosphorimage analysis, was consistently higher than the β3 lysine mutants K90M and K90A. Reduced catalytic activity by mutation of the β3 conserved lysine in classical kinases has been observed previously for PKA (PKA 72) (Iyer *et al.*, 2005a) and it is known that this Lys interacts not only with the α- and β- phosphates of ATP assisting with the correct orientation of ATP in the binding site but it can also form a salt bridge with the conserved Glu residue in the αC helix (Glu91 PKA), helping to maintain the kinase domain in an active conformation (Scheeff and Bourne, 2005). Intriguingly, it is difficult to identify a conserved Glu residue in the Trib2 sequence, which has a short predicted αC helix (Chapter 1). Interestingly, the Trib2 mutant K90R was able to autophosphorylate to a similar level as Trib2 WT despite the mutation and so, it could be possible that in Trib2 this mutation is tolerated more than in PKA, where K72R has a markedly reduced catalytic activity (Iyer *et al.*, 2005a). However, K90R equivalent mutations have been shown to lead to preservation of activity in other active kinases, such as Aurora A, where ~10% of WT activity is maintained by mutation of the equivalent lysine and mutation of the DFG motif to AFG is necessary to abolish activity completely (Haydon *et al.*, 2003). To confirm that the detected signals are caused by

Trib2 autophosphorylation, the assayed proteins could be treated with a phosphatase (e.g. lambda phosphatases) to demonstrate that the labelled phosphate can be removed enzymatically. Assays should also be performed with the Trib2 catalytic Asp (D175) mutants D175N or D175A. The expectation is that the autophosphorylation levels would be reduced compared to WT, albeit there is a possibility the activity may not be completely abrogated, because HER3 and JAK2 are catalytically active pseudokinases that possess an Asn residue in this position, and mutation of this Asp in EGFR to Asn still facilitates (low-efficiency) phosphotransfer (Shi *et al.*, 2010, Ungureanu *et al.*, 2011). The mutation of the catalytic Asp in CASK (D141A) did not reduce the level of autophosphorylation (Mukherjee *et al.*, 2008, Supplementary Figure 5), as mentioned below.

The presence of K177 in the catalytic loop helps place the Trib2 pseudokinase domain into the Ser/Thr (rather than Tyr) kinase sub-family (Hanks and Hunter, 1995). Mutation of K177 to an Arg residue results in depleted C/EBPα degradation in cells that also become unable to form colonies in an assay measuring cell transformation, compared to WT (Keeshan *et al.*, 2010). When Trib2 K177 was mutated to Ala, to abolish a positive charge at this position, it displayed reduced autophosphorylation compared to Trib2 WT, possibly because the mutation has altered the ability of Trib2 to recognize the substrate recognition/dimerisation sequence, or because it affects the ability of Trib2 to either bind to ATP or autophosphorylate. This could suggest that Trib2 catalytic activity may be linked to the oncogenic progression of Trib2 driven cancers and highlights the catalytic domain of Trib2 as a new potential target for small molecule inhibition.

Interestingly, no other phosphorylated Trib2 substrates (should they exist) have been reported in the literature. Neither standard exogenous protein kinase substrates such as Histones nor the known Trib2-regulated protein GST-C/EBPα were phosphorylated by Trib2 under the conditions adopted for *in vitro* kinase assays. One simple possibility is that Trib2 does not need to phosphorylate proteins for biological function. Furthermore, Trib2 might not only be a protein pseudokinase, but also phosphorylate non-protein molecular substrates. For example, the pseudokinase SgK196, has recently been shown to phosphorylate the 6-position of O-mannose (Yoshida-Moriguchi *et al.*, 2013).

Autophosphorylation of Trib2 occurred in the absence of divalent cations including Mg^{2+}, which classical kinases appear to require for catalytic activity (Waas *et al.*, 2004), and intriguingly bacterially-expressed Trib2 autophosphorylation was inhibited in the presence of divalent cations, although this was less marked for Sf9-expressed Trib2 preparations, which may also be contaminated with other kinases that co-purify with Trib2. Magnesium ion independent autophosphorylation has only been identified for one other member of the human kinome, the pseudokinase CASK, which like Trib2, does not have canonical magnesium ion binding residues. However, mutation of classical inactivating residues (β3 Lys K41A or the Catalytic Asp D141A) did not alter CASK's ability to autophosphorylate, but a CASK double mutation; S24D V26L selected following structural analysis of the ATP-binding pocket, did reduce autophosphorylation and phosphorylation of neurexin-1. (Mukherjee *et al.*, 2008). CASK can be converted to a kinase that behaves similarly to a classical Mg^{2+} ion stimulated kinase, by mutation of 4 residues in the ATP binding pocket; 2 of which align with the classical kinase magnesium binding residues and 2 of which are conserved throughout CaM-Kinases but are not found in CASK (Mukherjee *et al.*, 2010). However, mutating the residues in Trib2 that align to the canonical Mg^{2+} binding residues of classical kinases, did not confer on Trib2 increased Mg^{2+} dependent autophosphorylation, suggesting that other (unknown) residues are present in Trib2 that prevent metal-dependent ATP hydrolysis. Furthermore, abrogation of WT-levels of autophosphorylation for the Trib2 DFG K180N tetra-point mutation was observed, which was likely to be a result of protein denaturation (See Chapter 4 for further details). It has been postulated that CASK, which phosphorylates neurexin-1 and is a pseudokinase that is also inhibited by divalent cations, could be regulated by surges of divalent cations caused by synaptic activity in neurons, with levels of CASK activity highest during the development of neurons and then decreasing following neuronal maturity and the activation of signaling to the synapses (Mukherjee *et al.*, 2008). Whether anything similar occurs with Trib2 will be investigated in the future in human cell models, as will the potential regulatory functions of other metal cations, some of which appear to stimulate or inhibit Trib2 *in vitro* (Figure 3.17).

Sf9-expressed human Trib2 was also purified to identify whether a eukaryotic expression system was required for higher levels of Trib2 activity to be revealed. There was a large amount of kinase background 'noise' present in the

assays of partially purified Trib2 from Sf9 cells assayed in the presence of Mg^{2+}, and I speculate that non-specific kinases could be the cause of the phosphorylation detected at the size of Trib2 on the radiolabelled gels. Sf9 Trib2 appeared to autophosphorylate in the absence of Mg^{2+} ions (canonical protein kinases should be almost completely inactive in these conditions) however, the detected signals were weaker than for the same amount of Trib2 derived from *E. coli*. This could mean that Trib2 derived from Sf9 cells is catalytically inert and the faint signal is residual activity from other kinases, or it is not folded correctly and autophosphorylates at a lower level or favors substrate phosphorylation rather than favoring autophosphorylation. Whatever the cause may be, until the assays are performed in tandem with Trib2 K90M protein expressed in eukaryotic cells, it is impossible to determine whether the signal detected for Trib2 WT derived from Sf9 cells is truly autophosphorylation. However, the expression of the K90M mutant was considerably lower than the WT protein (Figure 3.19). It could be that the ability of Trib2 to bind ATP or autophosphorylate stabilizes the nascent protein. Because of the difficulty obtaining Sf9 expressed Trib2 K90M there was insufficient protein available for comparable kinase assays, and the data showing hyperactivity of Trib2 from Sf9 cells in the presence of Mg^{2+} ions be judged preliminary.

The Trib2 related pseudokinase, Trib3, also demonstrated autophosphorylation in the absence of Mg^{2+} ions. To confirm that this was intrinsic to the Trib3 pseudokinase, I showed that autophosphorylation occurred to a greater extent in Trib3 when compared to the β3 lysine mutant (Trib3 K97M). This indicated that a conserved magnesium-independent mechanism is likely to exist throughout this family, which perhaps enables Tribbles proteins to bind ATP and transfer the gamma phosphate to itself as part of a regulatory mechanism. However, this finding suggests that the inability of Trib3 to drive AML in animal models, or to degrade C/EBPα (but not ACC) *in vitro*, is unlikely to be due to an inability to bind ATP or to weakly autophosphorylate (Dedhia *et al.*, 2010).

SgK495, a more distantly related Tribbles pseudokinase, did not autophosphorylate under the assay conditions tested, but the SgK495 pseudokinase domain is much more degraded than Trib1-3, although intriguingly it does have at least one canonical glycine-rich loop located very close to the N-terminus of the pseudokinase domain. Assayed alongside SgK495 was the pseudokinase

STRADα which did not autophosphorylate under any conditions, consistent with previous work by other groups showing that STRADα cannot autophosphorylate, despite binding to ATP with relatively high affinity (Zeqiraj *et al.*, 2009b).

Trib2 autophosphorylation has yet to be examined in cell lines and no direct phosphorylation substrates other than Trib2 itself have been identified. Magnesium independent autophosphorylation is an interesting observation for recombinant Trib2 *in vitro*, because magnesium is present in cells with a concentration flux of 5 – 30 mM (Waas *et al.*, 2004) and as demonstrated in this Chapter, Trib2 was inhibited in the presence of 5 mM Mg^{2+}, and so the ability of Trib2 to bind to ATP *in vivo* needs to be determined along with a structure of Trib2 bound to ATP for a full understanding of the mechanism and function of Trib2 autophosphorylation. However, due to the aggregation-prone nature of Trib2 at high concentrations, our attempts to produce crystals for X-Ray analysis have thus far been unsuccessful. Screening Trib2 in a variety of buffer conditions has so far failed to yield any protein crystals for X-ray analysis, with aggregation being the main constituent of the majority of wells.

Another method used to investigate the structural properties of Trib2 was ^{15}N-HSQC NMR, which demonstrated that purified Trib2 was in a folded conformation. Future analysis of Trib2 using this technique will focus upon identifying the residues on the spectra which would not only facilitate the generation of a Trib2 structure, but because NMR allows the protein to remain in solution, it permits the observation of structural dynamics that could enable the identification of residues that undergo a conformational change when a ligand binds or residues that are in close proximity to the ligand i.e. the ligand binding surfaces or pockets.

3.21 Conclusion

Human Trib2 expressed in *E. coli* demonstrates the ability to hydrolyse ATP and auto-incorporate the released phosphate in a metal ion-sensitive manner. This poses some very interesting questions about Trib2. If Trib2 can bind to ATP using a different mechanism than utilized by classical kinases, which require the presence of Mg^{2+} ions and ATP binding, and given its documented importance for the transformation of cells and progression of the oncogenic phenotype, then this might make the pseudokinase domain of Trib2 an exciting and novel drug target, with the

unique catalytic domain providing an opportunity to develop a specific Trib2 targeting therapeutic molecule.

Chapter 4 describes the development of some specific tools required to investigate interaction of Trib2 with ATP *in vitro* and in a cellular environment. These will be essential to determine whether the pseudokinase domain of Trib2 can be specifically targeted by small molecules.

CHAPTER 4. Biophysical and cellular analysis of Trib2

4.1 Introduction

In Chapter 3, I demonstrated that recombinant Trib2 was capable of *in vitro* autophosphorylation, despite lacking the metal ion binding residues conserved in nearly all canonical protein kinases. This autophosphorylation event was inhibited by several different divalent cations, an effect currently described for only 3 members of the human kinome; CASK (Mukherjee *et al.*, 2008), Trib2 and Trib3 (Chapter 3). It has been reported that an intact ATP binding site is essential for Trib2-mediated C/EBPα degradation and Trib2-driven oncogenesis (Keeshan *et al.*, 2010, Liang *et al.*, 2013, Lohan and Keeshan, 2013). If ATP binding by Trib2 mediates the observed phenotypes of Trib2-overexpressing cells (Lohan and Keeshan, 2013, Grandinetti *et al.*, 2011), then this would make the ATP binding site of this pseudokinase a novel therapeutic target, especially if overexpression of Trib2, which is linked to ubiquitination and transcription factor turnover, could be blocked by compounds binding in the ATP site. To investigate the impact of Trib2-mediated ATP binding both *in vitro* and in intact cells, several new strategies must be developed. These include new methodologies and tools to develop screens to identify small molecules that directly target Trib2, the identification of its cellular interacting partners and the generation of Trib2 overexpressing cell-lines.

Results

4.2 DSF can be exploited to identify ATP binding to a purified pseudokinase domain

To permit transfer of the gamma phosphate group from ATP to an amino acid on a substrate, protein kinases must first bind to ATP, usually in the presence of a divalent cation. The cellular concentration of ATP lies in the low (1-5 mM) range (Huang *et al.*, 2003, Traut, 1994). However, different kinases have different affinities for ATP in the presence of different substrates, for instance in the presence of artificial *in vitro* peptide substrates, Chk1 has a K_m[ATP] of 1.4 μM, but the K_m[ATP] for MuSK (Muscle-specific kinase) is much higher at 380 μM (Knight and Shokat, 2005) while cellular kinases interact with metals and nucleotides with K_m

values ranging from low micromolar to low millimolar, representing some three orders of mangnitude of affinities (Becher *et al.*, 2013). Since Trib2 is capable of weak autophosphorylation, it must also bind to ATP, although the affinity is presumably relatively low since incubation of recombinant Trib2 with sub-millimolar (~0.2 mM) concentrations of ATP does not elicit marked thermal stabilization, although fluctuations above control levels are evident (Murphy *et al.*, 2014b). Several non-enzymatic methods for detecting ATP binding have been described, including direct and indirect approaches for measuring changes in fluorescence. For example, ligand binding to a protein can be detected by observing an increase of protein thermal stability (folding vs. unfolding), and, by association, a Tm (melting temperature) can be calculated (Celej *et al.*, 2003). DSF (Differential Scanning Fluorimetry) is a technique that determines the Tm of a protein by measuring the increased fluorescence intensity emitted by an exogenous dye that is added to the reaction mixture. The fluorescence intensity, when plotted as a function of temperature, generates a thermal denaturation curve that can be used to determine the Tm of essentially any folded protein. The Tm of a protein can increase markedly when a ligand is bound and so the protein is said to be 'thermally stabilized'. This is observed experimentally by the melting curve shifting to the right (increased temperature) when plotted on the graphical X axis. In general, the higher the change in melting temperature (ΔTm), the stronger the binding affinity for the ligand (Bullock *et al.*, 2005), although cut-offs are relatively arbitrary for minimum and maximum detectable ΔTm's, and some ligands may produce less effect than others. In terms of nucleotide, metal and ligand binding to single domain kinases, pseudokinases or bromodomains (which interact with acetylated lysine residues), several *in vitro* experimental procedures have recently been published that take advantage of DSF to evaluate ligand binding (Scheeff *et al.*, 2009, Murphy *et al.*, 2013, Krishna *et al.*, 2013, Filippakopoulos *et al.*, 2010).

To uncover if the binding of ATP to Trib2 can be detected using this assay format, and to extend a previous independent analysis employing Trib2 in a DSF-based assay performed in a collaboration that used a rather low ATP concentration (200 μM) that is not representative of the intracellular environment (Murphy *et al.*, 2014b), I analysed the ability of Trib2 to interact with several ligands.

A previous analysis of Trib2 formed part of a screen that established the binding abilities of a range of pseudokinases for ATP, GTP and divalent cations (Murphy *et al.*, 2014b). Analysis of this data led to pseudokinases being classified into four groups, which depended upon their ability to bind ligands, as detected by DSF (Chapter 1). Briefly, class 1 pseudokinases demonstrated no detectable nucleotide or cation binding, class 2 pseudokinases demonstrated the ability to bind to a nucleotide in the absence of cations, whilst class 3 solely bound metal cations. Pseudokinases that bound nucleotides and cations were grouped together in class 4. Trib2 and CASK were both grouped into class 1 because neither had ΔTm values that exceeded the threshold for any of the ligands tested, which was ±3°C in this analysis (Murphy *et al.*, 2014b).

Sypro-orange based DSF was employed to analyse the pseudokinases Trib2 and CASK, by comparing them to Aurora A, a kinase that is known to bind ATP with high affinity. As shown in Figure 4.1 A and 4.1 B, I was unable to detect a marked ΔTm for either of these pseudokinases in the presence of ATP, despite *in vitro* kinase assays and fluorescent ATP analogue studies demonstrating that CASK binds ATP with a measured K_m[ATP] of 563 μM (Mukherjee *et al.*, 2008) and that both Trib2 and CASK can autophosphorylate *in vitro* (Chapter 3). In marked contrast, SgK495 (Figure 4.1 C), a highly degraded pseudokinase that was also grouped with the class 1 pseudokinases (Murphy *et al.*, 2014b), exhibited concentration-dependent ATP binding. When the concentration of ATP increased, the thermal stability of SgK495 also increased, which, if confirmed, might place SgK495 into the pseudokinase class 2 (binds nucleotide but not metals). Importantly, as a positive control, DSF analysis was performed under identical conditions with the canonical kinase Aurora A, which has a known K_m for ATP of ~10 μM (Sloane *et al.*, 2010), clearly showed that it is stabilized by >5°C in the presence of ATP and metal co-factor (Figure 4.1 D).

4.3 A modified assay procedure permits Trib2 ATP binding to be detected by DSF

In Chapter 3, my *in vitro* kinase assays demonstrated conclusively that Trib2 catalytic activity was inhibited by Mg^{2+} ions. The consensus ΔTm increase that validates ligand binding throughout the biological literature is ±2-3°C. For example, ligands that potently inhibit the ATP binding site of MAP2K4 only impart a

detectable ΔTm value of 2°C or higher (Krishna *et al.*, 2013). This same threshold was reported as the temperature increase that occured when ligands bind to a protein with μM affinity, which might be expected for some, but not all, physiological ligands (Vedadi *et al.*, 2006). Indeed, a ΔTm increase of ~2°C is observed for the classical kinases VRK1 and VRK2 when incubated with ATP and magnesium ions and analysed by DSF. As a control, the VRK3 pseudokinase (which cannot bind a nucleotide due to amino acid blockade of the ATP site) was assayed alongside and was actually less stable in the presence of a nucleotide (Scheeff *et al.*, 2009).

Following addition of EDTA (a magnesium chelator) to the DSF reaction, ATP binding to Trib2 now became detectable (Figure 4.2 A), and the Trib2 Tm increased by ~ 2°C compared to the Tm of Trib2 with EDTA alone. Importantly, the ΔTm was >6°C when compared to Trib2 alone (no EDTA). The melting temperature of Trib2 also increased in the presence of both ATP and magnesium together (but it was not stabilised as highly as Trib2 following ATP and EDTA addition) although the ΔTm was only 2.93°C compared to Trib2 in the absence of any additions. The melting curves for three mutations designed to reduce ATP binding, namely Trib2 K90M (Figure 4.2 B), Trib2 K90A (Figure 4.2 C) and Trib2 K90R (Figure 4.2 D) did not show marked thermal stabilisation following addition of ATP, and are clearly different to WT Trib2, with decreases of essentially 100% binding for K90M, K90M and K90R calculated. Finally, the denaturation profile of Trib2 DFGK180N quadruple mutant resembled that of an unfolded protein (Figure 4.2 E), in marked comparison to all other Trib2 proteins assayed (Uniewicz *et al.*, 2012). Consistently, this mutant did not autophosphorylate *in vitro* (Figure 3.18 B). In contrast, the control kinase Aurora A was stabilized in the presence of both ATP and Mg^{2+} (Figure 4.2 F), consistent with its functioning as a canonical protein kinase.

4.4 Trib2 does not bind detectably to the kinase inhibitor DAP

Following the detection of ATP binding to Trib2 by DSF, which was expected given the ability of this pseudokinase to autophosphorylate weakly but reproducibly (Chapter 3), Trib2 and Aurora A ligand binding was investigated by incubation with the generic ATP competitive kinase inhibitor DAP (Figure 4.3), which has been shown to bind to 6 out of 32 (19%) of the pseudokinases towards which it has been tested, consistent with it being a general ATP-site ligand suitable for DSF analysis (Murphy *et al.*, 2014b, Bantscheff *et al.*, 2007). However, Trib2 did

not bind to DAP (Figure 4.3A) in agreement with the previous analysis by Murphy, although DAP binds to Aurora A in a concentration-dependent manner (Figure 4.3 B).

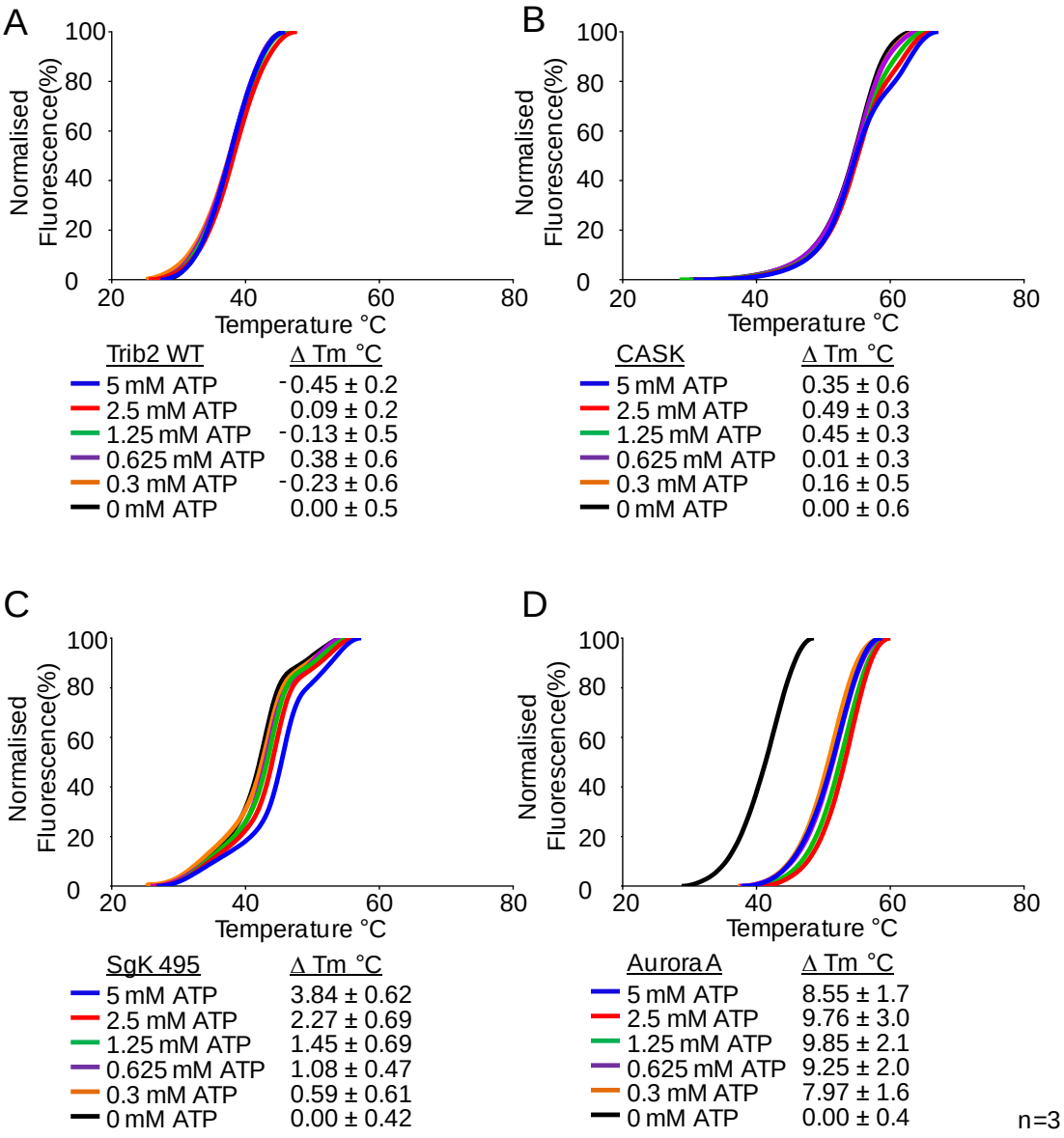

Figure 4.1 Sgk 495, a Trib family member is thermally stabilised by the presence of ATP A) Trib2 WT, B) CASK, C) SgK 495 or D) Aurora A (5 μM) were incubated with increasing concentrations of ATP (0-5 mM). In the presence of Sypro Orange, thermal denaturation profiles were generated by detecting the emitted fluorescence and melting temperatures were determined by applying the sigmoidal Boltzmann equation to the normalized denaturation curves. The ΔTm values were determined by subtracting the Tm for protein alone from the TM values in the presence of either ATP and/or cofactor. This was repeated 2 further times in triplicate and the average ΔTm values are listed ± the standard deviation for the 3 constituent experiments, alongside typical thermal denaturation curves.

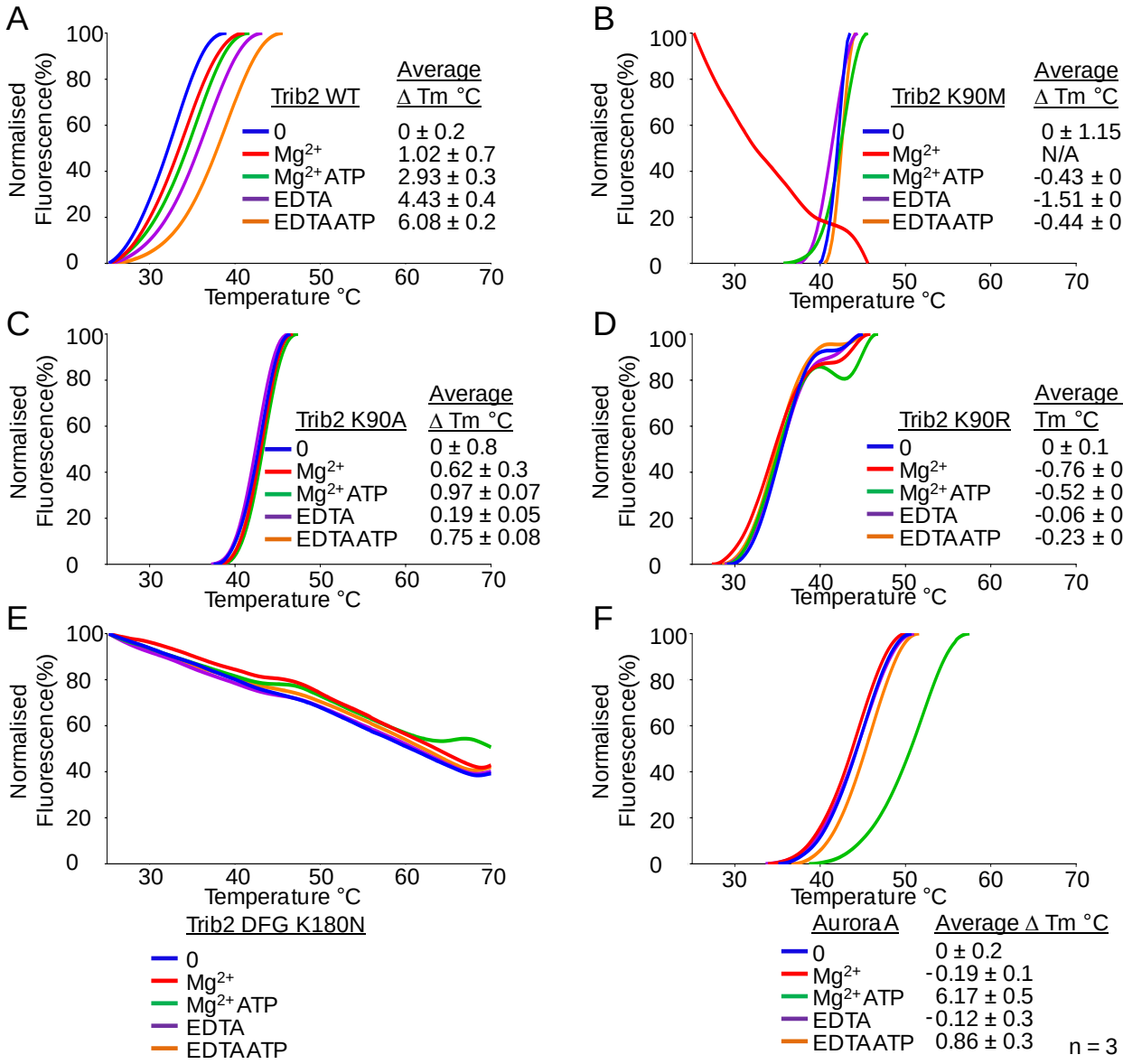

Figure 4.2 ATP demonstrates a small protective effect on Trib2 in the presence of EDTA. Representative normalised denaturation curves and average ΔTm values with the standard deviation are listed for three independent experiments each performed in triplicate. A) Trib2 WT, B) K90M, C) K90A, D) K90R, E) DFGK180N or F) Aurora A (5 μM) were incubated with either 10 mM $MgCl_2$ (green or red) or 2 mM EDTA (purple or orange), with samples supplemented with 1 mM ATP (green and orange) and Sypro Orange dye added to all.

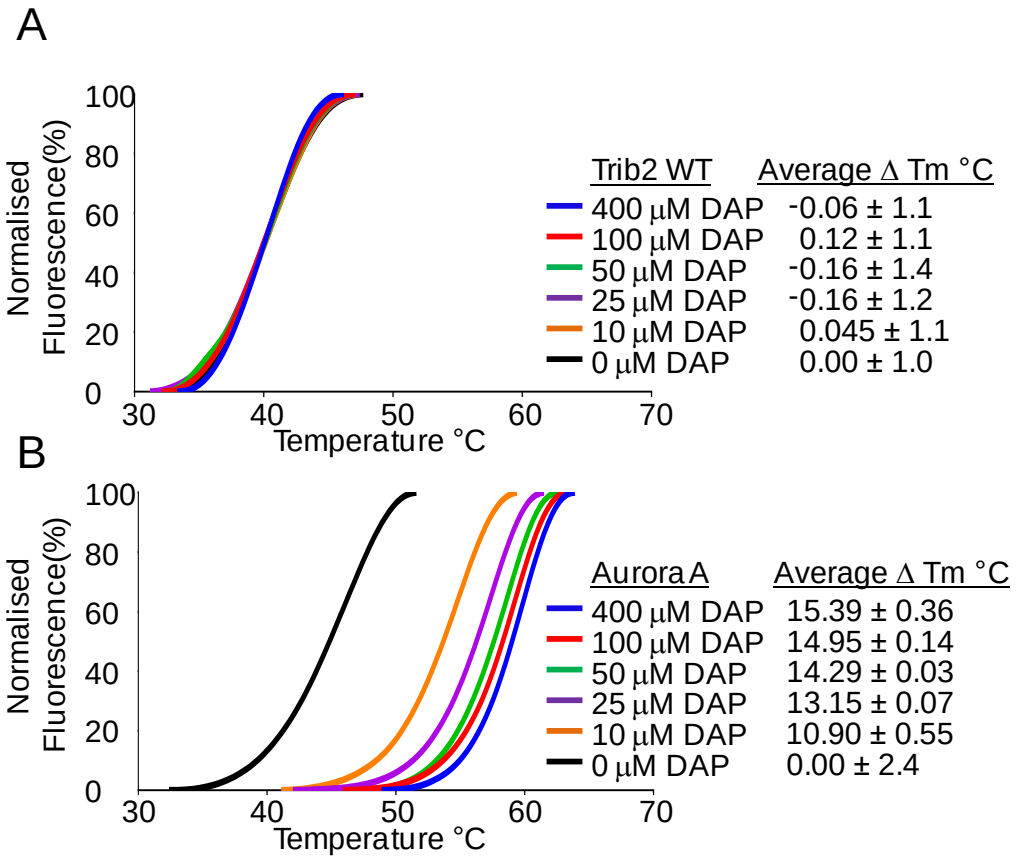

n = 2

Figure 4.3 Trib2 does not bind the kinase inhibitor DAP. DSF was performed on 5 μM A) Trib2 and B) Aurora A with increasing concentrations of DAP. The average ΔTm values including the standard deviation values from 2 repeat experiments (performed in triplicate) are shown alongside the normalised denaturation curves representative of the experiments.

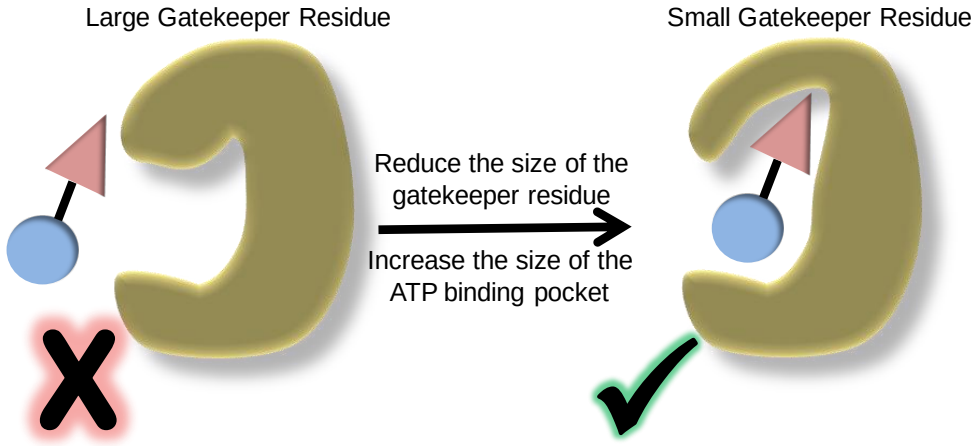

Figure 4.4 Mutating the 'gatekeeper' residue of a protein kinase or a pseudokinase can increase the accessibility of the ATP binding site. A cartoon that depicts how a bulky inhibitor (*e.g.* an analogue of the kinase inhibitor PP1) cannot access the ATP binding site of a WT kinase but can enter the ATP-binding site of an enlarged (analogue-sensitive) kinase.

4.5 Trib2 gatekeeper mutants specifically bind small molecule inhibitors

A chemical genetic approach that might help elucidate the function of Trib2 is to block the ATP binding site by employing cell permeable small molecule inhibitors and characterizing any phenotypic changes. Targeting a specific protein kinase in a cell is, however, inherently difficult because of the high degree of conservation shared between all kinase domains in the human kinome, and the promiscuity of small molecules developed to target them (Bantscheff *et al.*, 2007, Davis *et al.*, 2011). Within the human kinome, a conserved amino acid termed the 'gatekeeper' residue occludes the binding of bulky kinase inhibitor analogues (e.g. PP1 analogues), since they cannot access a hydrophobic cavity located within the ATP binding pocket. Most clinically approved kinase inhibitors target kinases with a small (Thr) gatekeeper residue, although only ~20% of the human kinome have evolved a Ser or Thr amino acid in this position. Interestingly, mutation of Thr to a more 'bulky' amino acid can cause drug resistance (e.g. The BCR-Abl T315I kinase is resistant to Imatinib and EGFR T790M is resistant to Erlotinib) (Alaimo *et al.*, 2005).

No human kinase possesses the smallest amino acid side-chains (Gly or Ala) at this position (Liu *et al.*, 1998, Alaimo *et al.*, 2005) and following mutation to either of these residues, the enlarged ATP binding pockets of such 'analogue-sensitive' gatekeeper kinases now possess the ability to specifically interact with bulky kinase inhibitor analogues (e.g. PP1 analogues such as Na-PP1 and NM-PP1), which have the enormous advantage of being unable to target the vast majority (but not all) WT kinase ATP binding sites (Figure 4.4) (Liu *et al.*, 1998, Hengeveld *et al.*, 2012, Bain *et al.*, 2007).

The majority of the 'CMGC' family of kinases contain a phenylalanine gatekeeper residue (Huang *et al.*, 2010), including all Tribbles family members, which are located between the CMCG family and CAMK divisons on the phylogenetic kinome 'tree' (Chapter 1). CDK2 is an example of a kinase that has a phenylalanine gatekeeper residue at this position, and following mutation of the CDK2 gatekeeper residue to Ala or Gly, the kinase domain can be specifically targeted by an ATP analogue, whilst maintaining its substrate and phosphorylation site specificity along with K_m and V_{max} values that are comparable to WT CDK2 (Elphick *et al.*, 2009). In addition, the gatekeeper residue of the pseudokinase KSR2

(T739) can be mutated to a small Gly residue, which permits it to bind to the bulky ATP analogue benzyl ATP and identify it as a direct activator of MEK (Brennan *et al.*, 2011). However, this approach clearly does not work for all kinases, since the gatekeeper residue is involved in stabilizing the active kinase conformation (Garske *et al.*, 2011) To build upon my initial work with Trib2, I therefore decided to test whether this pseudokinase was amenable to chemical genetics by generating 'analogue-sensitive' gatekeeper Trib2 mutants.

4.6 Purification of recombinant mutant Trib2 proteins (F130A or F130G)

Trib2 gatekeeper mutants were expressed in *E. coli* and purified by IMAC (see Chapter 2). The column fractions that corresponded to Trib2, Trib2 F130A, Trib2 F130G (Figure 4.5 A, C and E) from a Ni-Sepharose column were analysed by SDS-PAGE on 12% polyacrylamide gels (Figure 4.5 B, D, F) to identify those that contained Trib2 and Trib2 point mutants; these were then pooled and dialysed into buffer B (Chapters 2 and 3).

Since two phenylalanines (F129/F130) lie adjacent to each other in the ATP binding site of Trib2, and there is no crystal structure available to confirm if F129 or F130 are directly or functionally equivalent to the canonical gatekeeper residue, two 'gatekeeper -1 mutants' (F129A/G) were also created for analysis. If F130 was the gatekeeper residue then the F130A/G mutants might be predicted to bind specifically to bulky ATP-dependent kinase inhibitor analogues, whereas the F129A/G proteins would likely remain unaffected, since this amino acid equivalent does not interact with the region guarding the pocket in model kinases. However, although Trib2 F129A and F129G mutants were synthesised at high levels in *E. coli* and could be observed following Coomassie staining, they were both completely insoluble after bacterial lysis, and were not observed in the Coomassie-stained gels following SDS-PAGE, unlike Trib2, Trib2 F130A and Trib2 F130G, which were readily detected after purification from a soluble *E. coli* extract.

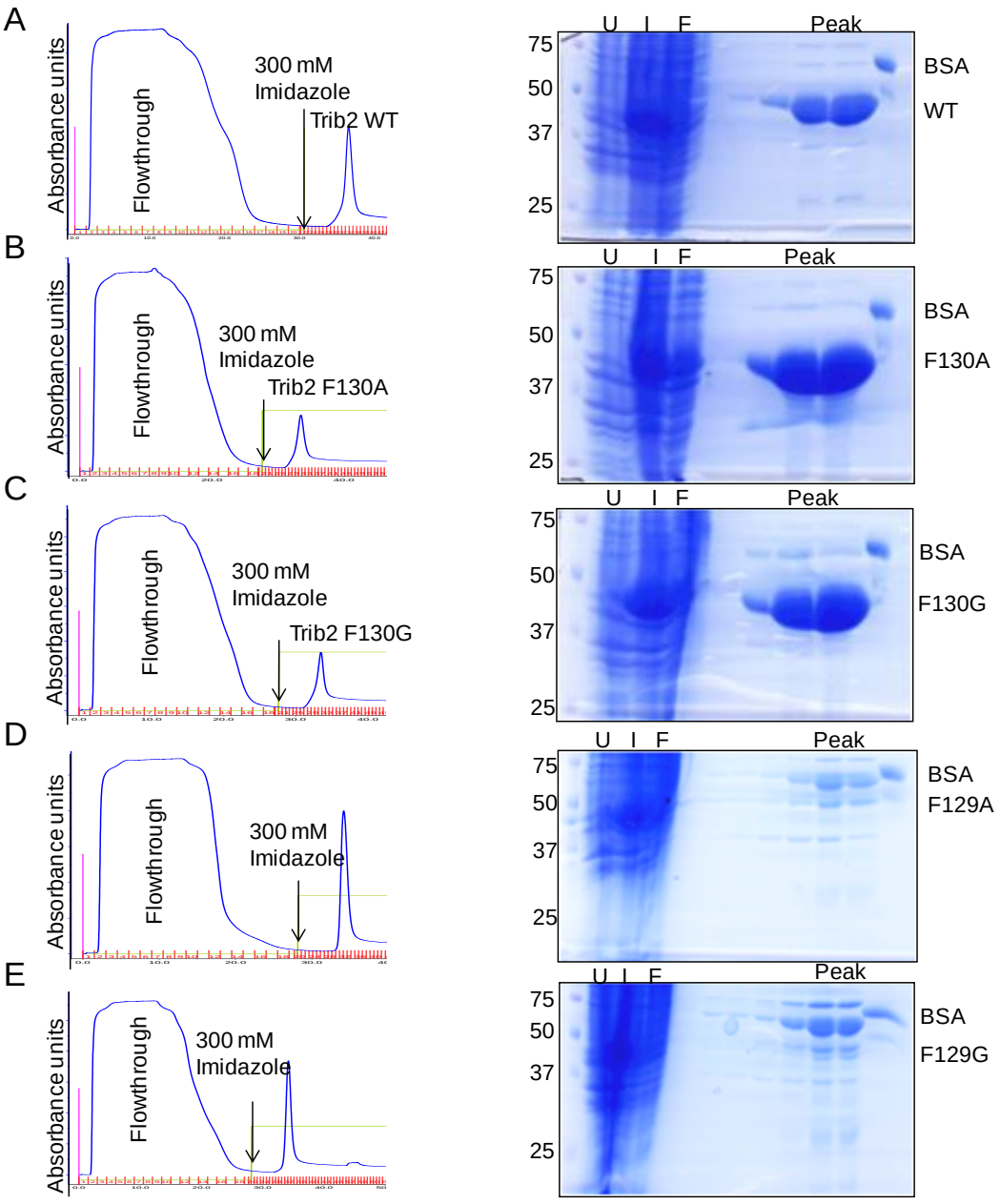

Figure 4.5 Trib2 F129A and F129G mutants are synthesised but present in the insoluble fraction. A-E) Left panel: The elution profile of recombinant Trib2 proteins WT, K90M, F130A, F130G, F129A and F129G were eluted from nickel Sepharose after the application of 300 mM imidazole elution buffer. Right panel: Protein resolved by SDS PAGE and stained with coomassie stain. U = Uninduced total cell lysate, I = Induced total cell lysate, following IPTG induction, F = Unbound protein in the flowthrough, Peak= Fractions corresponding to the peak observed on the elution profiles in the left hand panels. BSA (4 μg) was resolved by SDS PAGE alongside the fractions eluted during affinity chromatography.

4.7 Identifying ligands that interact with Trib2 gatekeeper mutants

In order to maximize the chances of discovering a Trib2 ligand, a panel of 30 synthetic PP1-derived bulky inhibitors (kindly supplied by Professor Kevan Shokat, UCSF) were screened to look for candidates that could access the enlarged ATP binding site of the Trib2 analogue sensitive gatekeeper mutants. As shown in Figure 4.6D, DSF identified two of these bulky PP1 analogues, which are termed CZ 30 and HxJ 42. CZ 30 markedly increased the thermal stability of Trib2 F130A and Trib2 F130G by 20.53°C and 19.74°C respectively, whereas in the presence of HxJ 42 the ΔTm of F130A and F130G was 11.99°C and 9.39°C. Importantly, however the ΔTm of WT Trib2 was unaffected by the addition of either CZ 30 or HxJ 42 (Figure 4.6). This was consistent with the inhibitors binding to the ATP binding site of the analogue-sensitive Trib2 mutants with high specificity. In my initial screen, I measured the Tm for 5 μM Trib2, F130A and F130G mutants in the presence of 250 μM of each inhibitor. As discussed above, I used a threshold ΔTm of >2°C to indicate an interaction. Along with CZ 30 and HxJ 42, Trib2 F130G (Figure 4.6 C) was also stabilized by ~ 7°C in the presence of CZ 24 (7.26°C), 3MB PP1 (7.95°C), CZ 89 (7.83°C), ZFZ 19 (7.59°C), and ZFZ 11 (7.96°C). However, only HxJ 42 and CZ 30, increased the Tm of both Trib2 F130A (11.99°C and 20.53°C respectively) (Figure 4.6 B) and F130G (9.39°C and 19.74°C respectively) (Figure 4.6 C) when compared to WT Trib2 (Figure 4.6 A), and these ligands were therefore employed for further analysis.

Trib2 (Figure 4.7 A), Trib2 F130A and Trib2 F130G (Figure 4.7 B and C) were incubated with 250 μM HxJ 42 in a further 3 separate experiments, each performed in duplicate. The melting curves of both Trib2 F130A and Trib2 F130G consistently shifted dramatically to the right in the presence of HxJ 42 compared to the DMSO vehicle control and the Tm increased on average by 15.18°C ± 3.7 for Trib2 F130A and 12.91°C ± 3.5 for Trib2 F130G. In contrast, CZ 24 does not increase the Tm of F130A, unlike the Tm of F130G, which is 5.3°C ± 3.4 higher than F130G in the presence of DMSO. Trib2 F130G is stabilized by more of the bulky inhibitors tested in this panel than F130A, potentially because the Gly facilitated increased accessibility to the active site than Ala.

Trib2 (Figure 4.8A), Trib2 F130A (Figure 4.8B) and Trib2 F130G (Figure 4.8 C) were also incubated with CZ 30 in three separate experiments. The averaged ΔTm values for Trib2 in the presence of CZ 30 was 1.8°C ± 2.2 compared to Trib2 F130A and F130G, where the respective ΔTm compared to the DMSO controls were 16.7°C ± 5.3 and 20.1°C ± 5.1. CZ 24, again increased the Tm of F130G but not F130A nor Trib2.

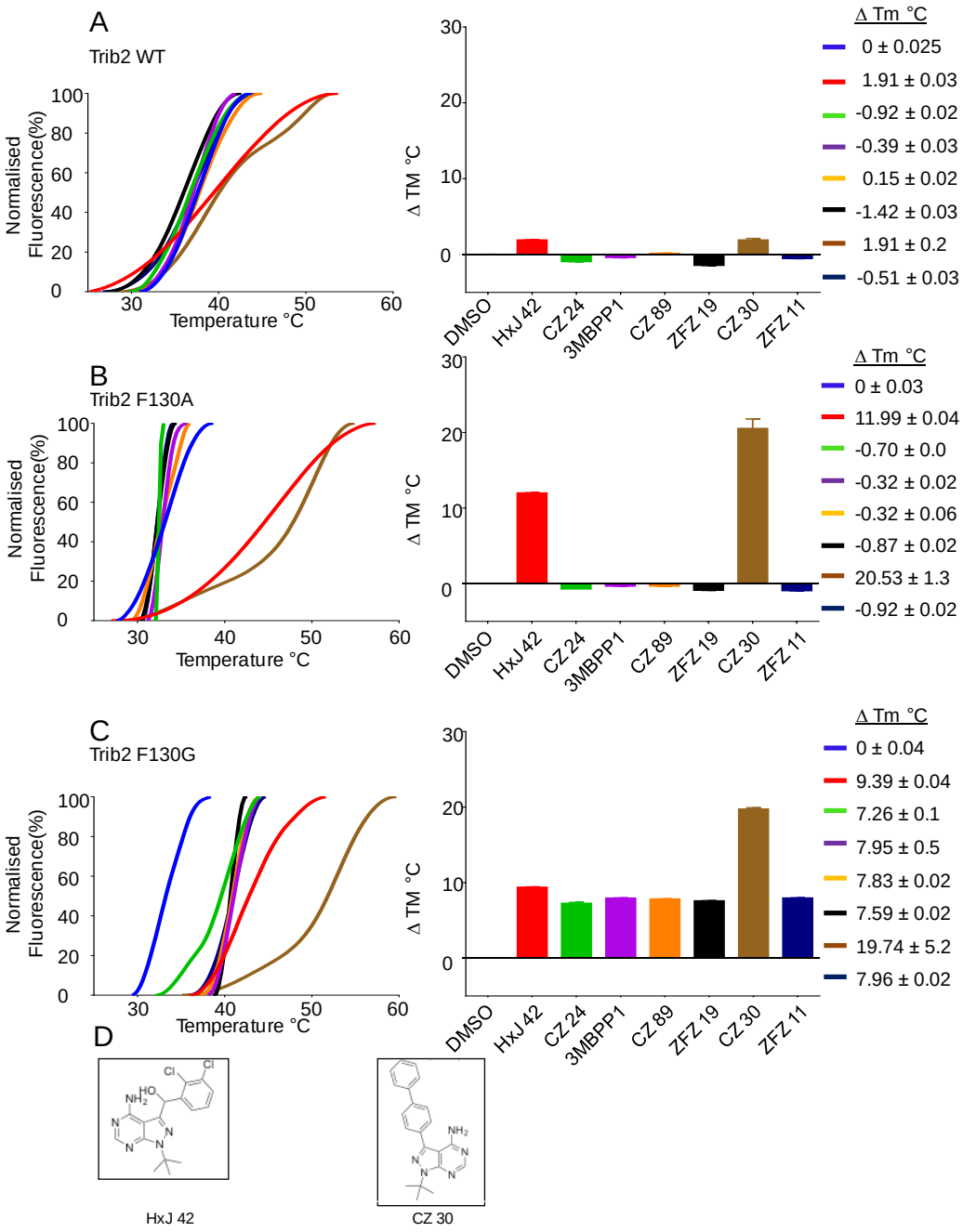

Figure 4.6 Trib2 gatekeeper mutant kinase domains can be targeted by bulky PP1 derivatives. A) Trib2 WT, B) Trib2 F130A or C) Trib2 F130G were incubated with 250 μM bumped PP1 kinase inhibitor analogues in triplicate. The fluorescence signals were normalised which generated the thermal denaturation profiles (left) and from these the average melting temperatures determined by application of the Boltzmann sigmoidal equation. The average ΔTm values were plotted in the bar charts on the right along with the standard deviation. D) Chemical structures of the PP1-related compounds HxJ 42 and CZ 30 were drawn using ChemBioDraw.

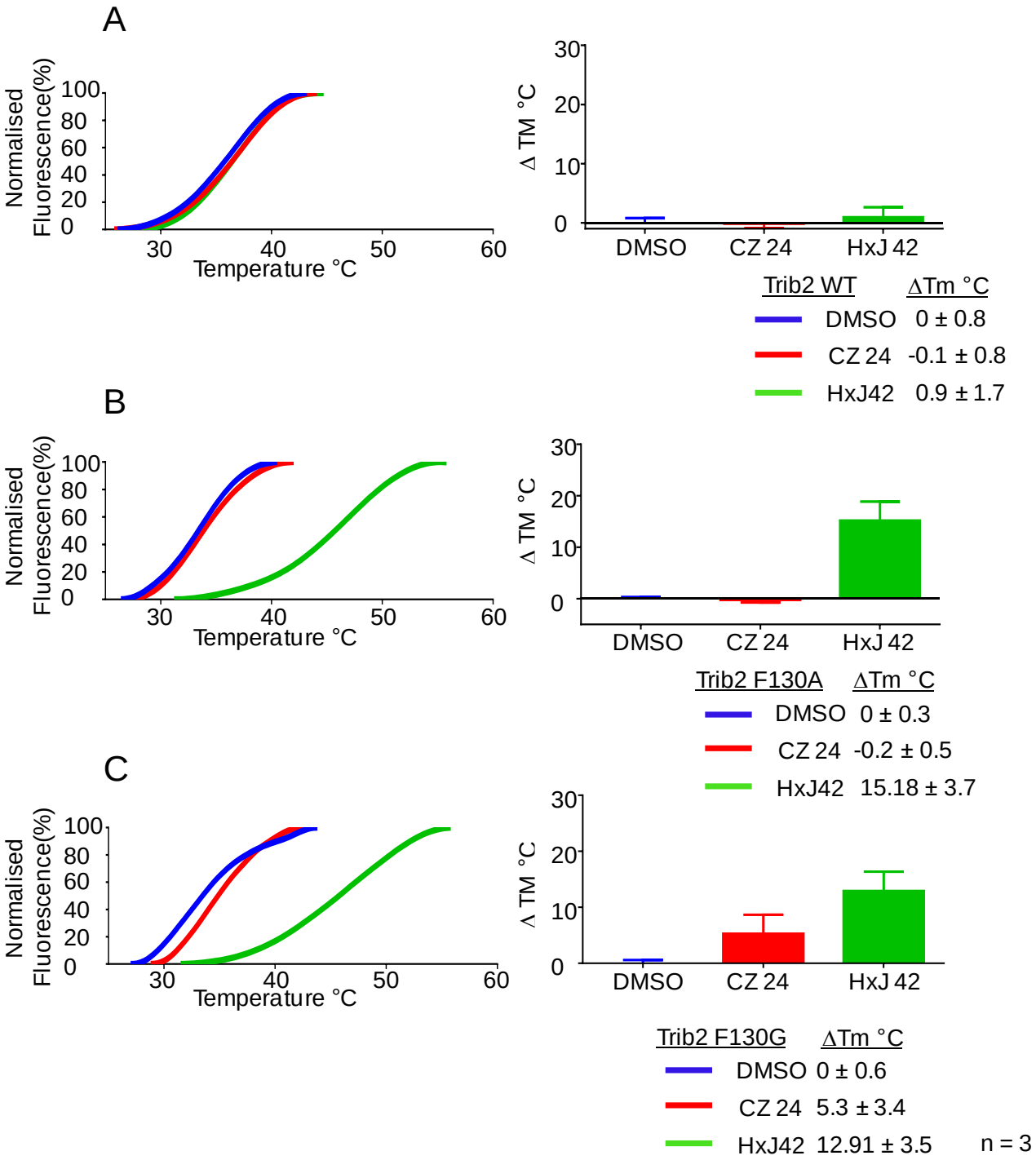

Figure 4.7 Trib2 F130 gatekeeper mutants can bind to the inhibitor HxJ 42, whilst WT Trib2 is unaffected. Three separate DSF experiments were performed in duplicate on either A) Trib2 WT B) Trib2 F130A or C) Trib2 F130G that were incubated with either DMSO, 250 μM of the bulky PP1 kinase inhibitor HxJ 42 or CZ 24. Fluorescent denaturation curves were normalised and plotted (representative curves shown on the left). From these curves the ΔTm values were determined and averaged (right, ± SD shown alongside).

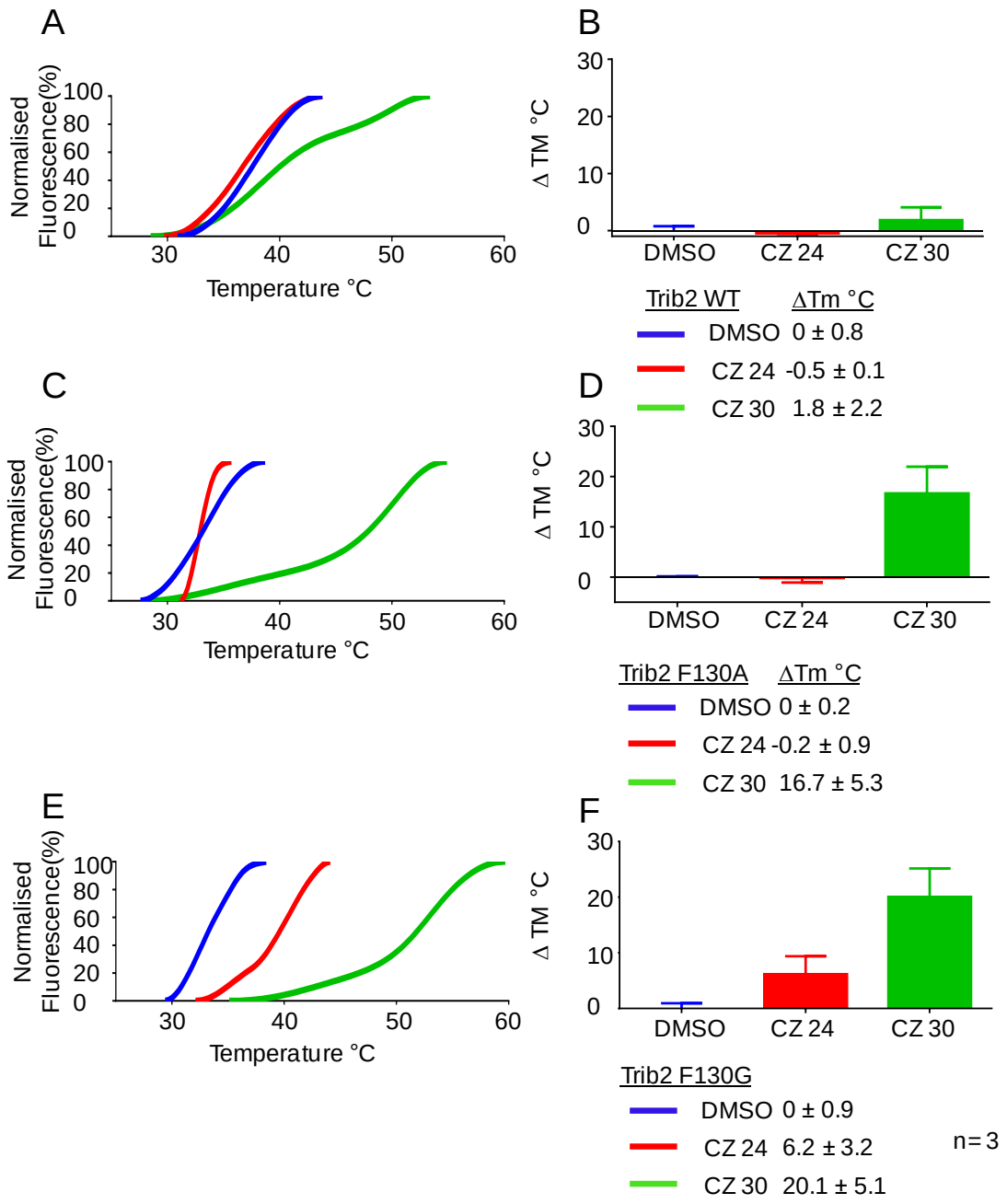

Figure 4.8 Trib2 F130A and F130G mutants bind to the PP1-related inhibitor CZ 30 In the presence of either DMSO, CZ 24 or CZ 30, A) Trib2 WT, B) Trib2 F130A and C) Trib2 F130G were thermally denatured and the detected fluorescence was averaged and normalised, which generated thermal denaturation curves. The curves observed in the left panels are representative of the three separate experiments. The Tm values from each curve were determined by applying the Bolztmann equation and then averaged. The average ΔTm values (± SD) are shown on the right.

WT Trib2 does not bind to CZ 30, and this was confirmed by findings shown in Figure 4.9, where the ΔTm of Trib2 was not markedly increased in the presence of CZ 30. Conversely, Trib2 F130G (Figure 4.9 B) exhibited a ΔTm of 27.7°C ± 1.6 in the presence of CZ 30 whereas the classical kinase Aurora A ΔTm was 8.7°C ± 0.04 (Figure 4.9 C), which is ~20°C lower than the ΔTm of Trib2 F130G. In contrast, the ΔTm for SgK495 is 4.3°C ± 0.08 (Figure 4.9 D), although this represents a much lower binding affinity than Trib2 F130G.

The CZ 30-related inhibitors CZ 28 and CZ 29 were incubated with Trib2 and the Trib2 analog-sensitive mutant Trib2 F130A. As expected, Trib2 did not detectably bind to either CZ 30, CZ 28 or CZ 29 with the respective ΔTm values being below the 2°C threshold that I have adopted for these experiments (Figure 4.10 A). The ΔTm Trib2 F130A increased by 19.41°C (Figure 4.10 B) when incubated with 250 μM CZ 30, but this effect was not observed following the addition of 250 μM CZ 29 or CZ 28, and the ΔTm values were consistently below 2°C, ΔTM 1.11 and -0.96°C respectively. The melting profile of Trib2 F130A in the presence of CZ 30 appeared to be biphasic, which can be observed when there are populations of both ligand-bound and apo-protein in the solution (Vivoli *et al.*, 2014).

The binding of CZ 30 to Trib2 F130A was not observed to be concentration dependent, because when assayed in the presence of 125 μM or 25 μM CZ 30, the ΔTm were not above the binding threshold.

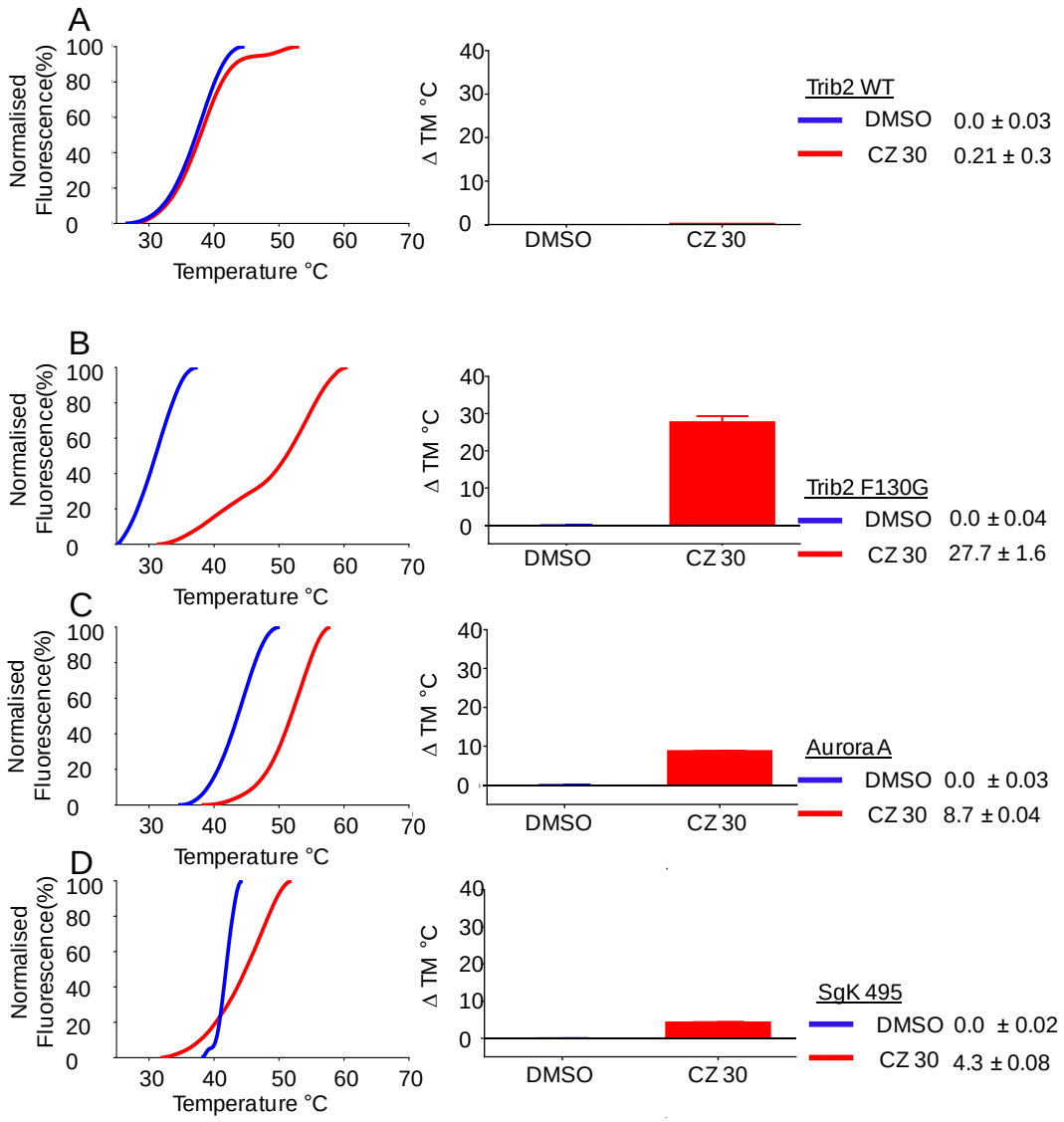

Figure 4.9 CZ 30 increases the thermal stability of the Trib2 F130G more than the classical kinase, Aurora A, or the Trib related protein SgK495. In triplicate A) Trib2 WT, the analogue sensitive B) Trib2 F130G, C) Aurora A and D) SgK495 were incubated with either DMSO or 250 μM of the bulky PP1 kinase inhibitor CZ 30. Thermal denaturation profiles were generated by normalising the detected fluorescence signal. These curves were used to determine the Tm by the Boltzmann equation. The average Tm values of proteins in the presence of DMSO were subtracted from the Tm values of proteins in the presence of CZ30. The averaged ΔTm values are plotted in the right panels.

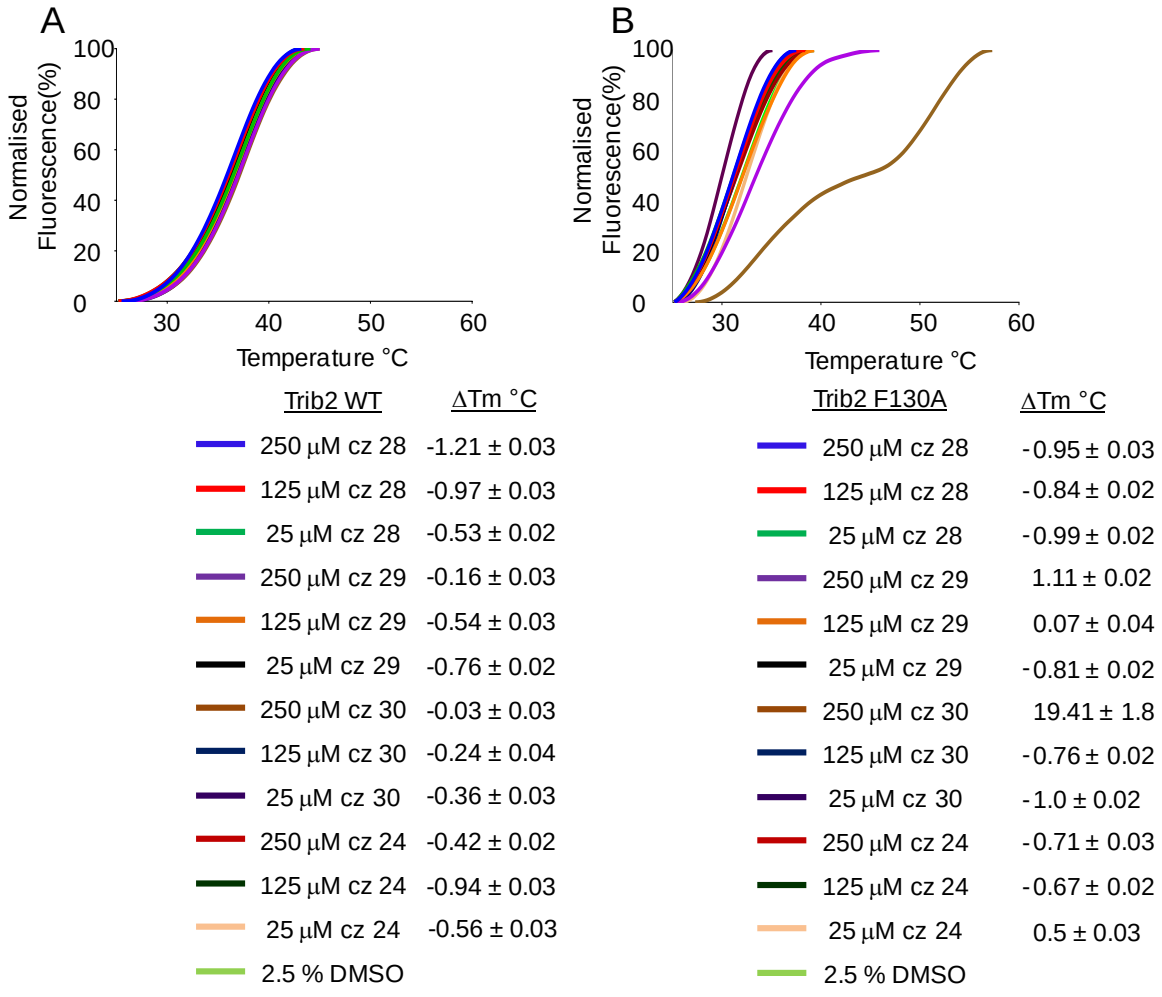

Figure 4.10 Compounds related to CZ 30 do not demonstrate similar binding interactions to F130A Trib2 WT and B) Trib2 F130A (5 μM) were incubated with either 250 μM, 125 μM or 25 μM of the bulky PP1 kinase inhibitors CZ 28, CZ 29, CZ 30 and CZ 24, or DMSO and following DSF, thermal denaturation profiles were generated by normalising the detected fluorescence. The Boltzmann equation fitted to the curves provided the melting temperatures, and from these profiles the ΔTm values could be calculated and are listed below the denaturation curves.

4.8 Intrinsic fluorescence measurements readily detect Trib2 ligand binding

Not all proteins can be analysed using Sypro Orange dye (Niesen *et al.*, 2007), and it is possible that pseudokinases such as Trib2, which is rather unstable and prone to denaturation (Chapter 2) are not ideally suited to this dye-based approach. Indeed, a quarter of soluble proteins subjected to DSF in a case study reported in the literature are not amenable to DSF because of the high fluorescence background caused by the dye binding to solvent-exposed hydrophobic pockets (Vedadi *et al.*, 2010). To help negate the addition of an extrinsic fluoroprobe, the changing intensity of *intrinsic* fluorescence of a protein as it unfolds can also be measured, and changes in Tm invoked to infer ligand binding (Gaudet *et al.*, 2010).

As a protein melts, the hydrophobic, fluorescent Trp and (less-so) Phe residues residing in the protein interior gradually become more exposed to solvent. Therefore, the emitted fluorescence associated with the indole and phenyl moieties changes (usually increases) as a function of temperature. To evaluate the effects of ligands on Trib2 thermal stability, intrinsic fluorescence was measured using an Avacta Optim2 system. Typical fluorescence curves generated during each experiment are shown in Figure 4.11 A-D. The experiments in the right panels were supplemented with 1 mM ATP. The first derivative fitted to the curve (thin red line) from which the Tm was determined. The average Tm values from two separate experiments, with each condition being assayed in triplicate were used to ascertain ΔTm values, which are plotted on the chart showing the mean ± SD (Figure 4.11 E).

Interestingly, the average Trib2 Tm in the presence of ATP was 3.6°C higher than Trib2 in the absence of ATP, suggesting that ATP binding to Trib2 can be detected using 1 mM nucleotide in the absence of metal ions. The thermal stability of Trib2 K90M and K90A mutants were also assessed alongside WT Trib2 and although the ΔTm for Trib2 K90M (ΔTm 1.6°C, 56% decrease) and K90A (ΔTm 0.23°C 94% decrease) were detectable, neither was stabilized in the presence of ATP to the same extent as WT Trib2. As a control, the kinase Aurora A was stabilized in the presence of ATP with a ΔTm of 3°C, as assessed by this intrinsic fluorescence approach. The identification that the Trib2 WT ATP binding site is accessible to ATP will facilitate future development of inhibitors to this site that could prevent ATP from binding and therefore, potentially, block WT activity.

As shown in Figure 4.12, intrinsic fluorescence could also be used to detect an interaction between the Trib2 F130A and F130G point mutants and the bulky PP1 analogues HxJ 42 and CZ 30, in agreement with my DSF analysis using Sypro orange dye. Consistently, HxJ 42 (Figure 4.12 A) increased the melting temperature of both F130A and F130G (ΔTm 2.7°C and ΔTm 3°C respectively) but destabilized WT Trib2 (ΔTm -0.32°C). Intriguingly, CZ 30 markedly increased the Tm of Trib2 by 10.8°C (Figure 4.12 B), but this was 20°C lower than the ΔTm values for Trib2 F130A (ΔTm 33.8°C) and F130G (ΔTm 38.6°C). Note that Trib2 F130A/G and WT were assayed on 2 independent experiments in duplicate, and the average ΔTm values are recorded here

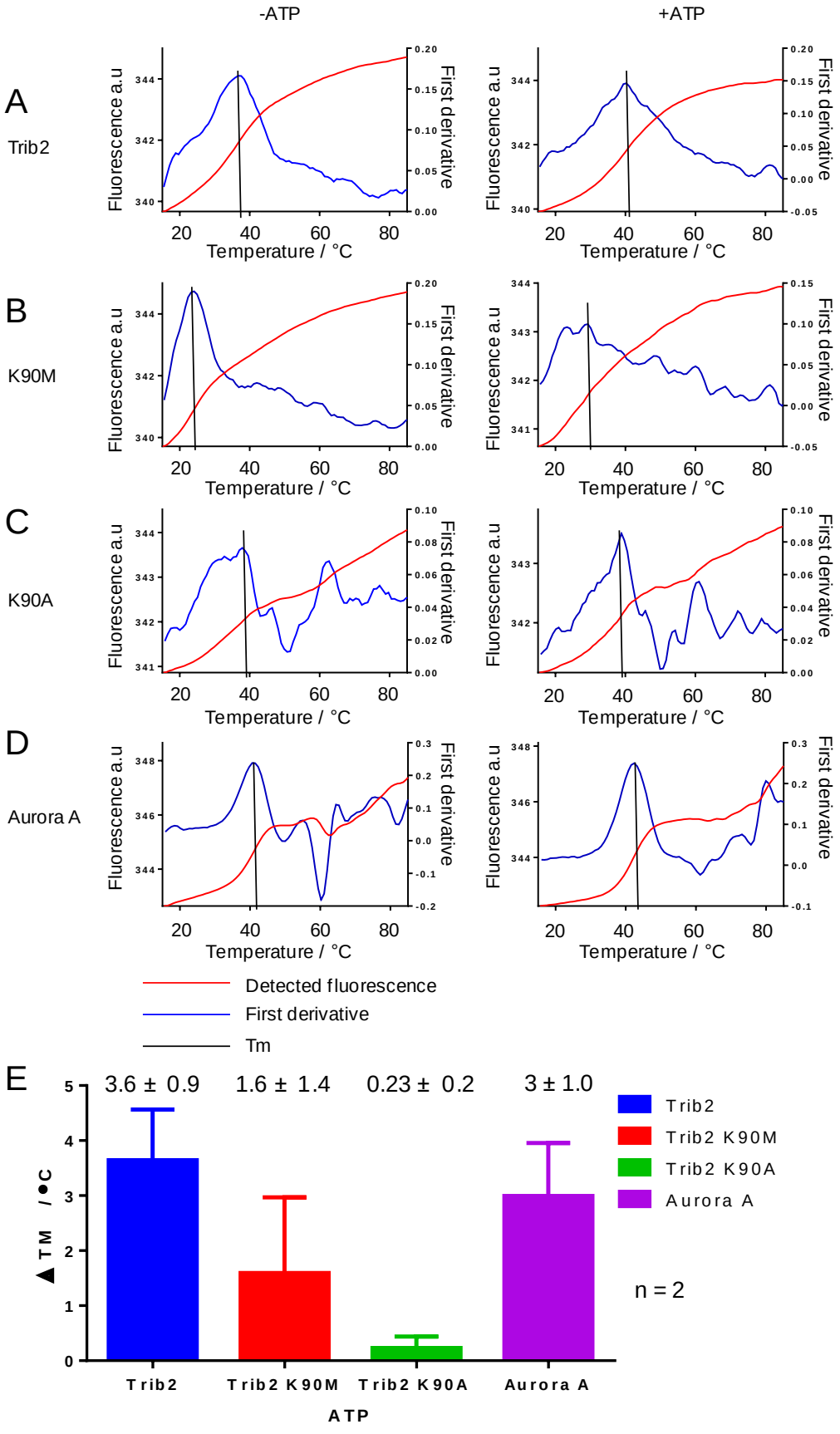

Figure 4.11 ATP has a thermally protective effect on Trib2 WT when analysed using intrinsic protein fluorescence as a read-out. Representative figures of detected intrinsic fluorescence as Trib2 WT (A), K90M (B), K90A (C) and Aurora A (D), unfold ±1 mM ATP. Each condition was tested in triplicate. The red line is the detected fluorescence, whilst the blue line is the fitting of the first derivative. The centre of the first derivative peak corresponded to the Tm for the protein (black line). The average Tm for each protein in each condition (+/- ATP) was determined and the average ΔTM (°C) was plotted using the software GraphPad Prism6 (E).

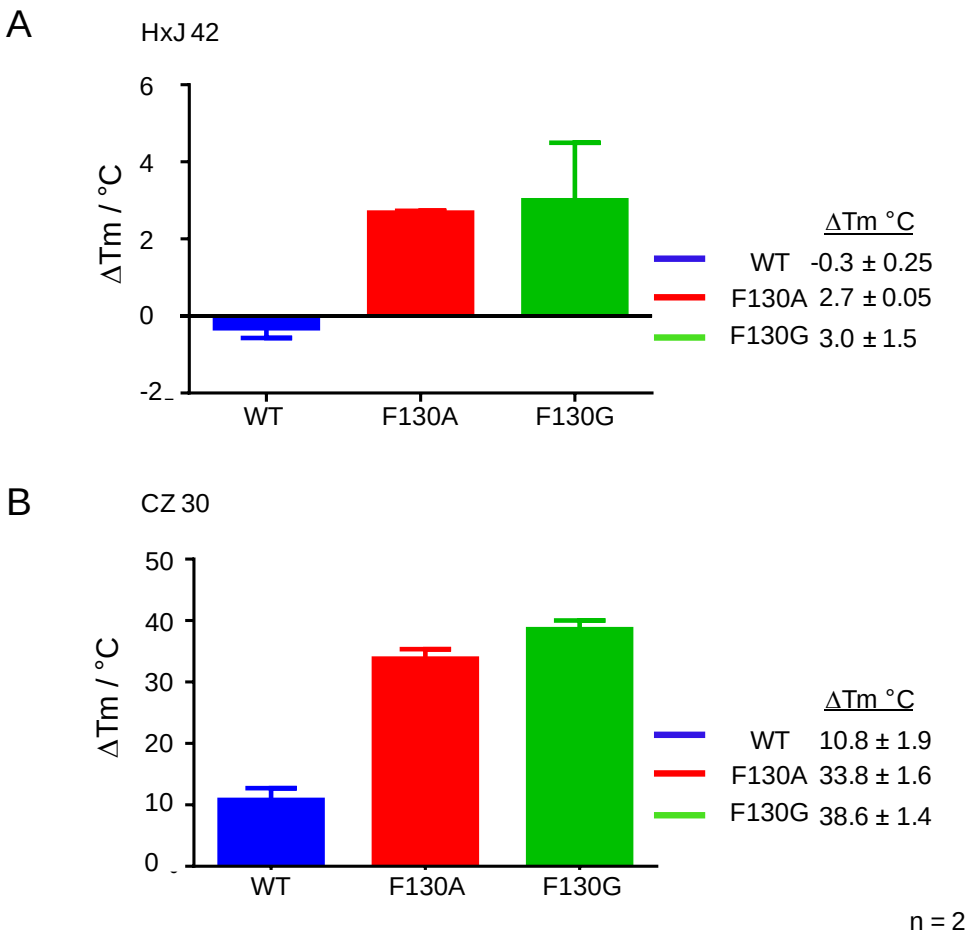

Figure 4.12 Measuring the intrinsic fluorescence of Trib2 as it unfolds also demonstrated the pseudokinase domain is targetable by bulky PP1 analogues In duplicate, the average Tm for each protein in each condition A) +/- HxJ 42 or B) +/- CZ 30 was determined detecting the intrinsic fluorescence and fitting the first derivative to the obtained curve. The average ΔTM (°C) values were determined from the two experiments along with the standard deviation and plotted in the tables (blue = Trib2 WT, red = F130A, green = F130G).

4.9 The Trib2 Gatekeeper mutants F130A and F130G autophosphorylate weakly

DSF assays revealed two bulky PP1 analogues (CZ 30 and HxJ 42) that markedly increased the melting temperatures of both the F130A and F130G Trib2 mutants, but not WT Trib2. This suggested that they bound specifically to the ATP binding site of the analogue- sensitive mutants and will be useful for probing the function of appropriately mutated Trib2. However, it is well known that gatekeeper mutations can sometimes lead to a loss of intrinsic kinase activity in protein kinases (Oh *et al.*, 2007, Hengeveld *et al.*, 2012). To examine if this was also the case for Trib2, the rate of autophosphorylation for each mutant was analysed *in vitro*. Trib2 (Figure 4.13 A), Trib2 K90M (Figure 4.13 B), Trib2 F130A (Figure 4.13 C) and Trib2 F130G (Figure 4.13 D) were subjected to an *in vitro* kinase assay to determine whether the mutant proteins could hydrolyse ATP as efficiently as the WT pseudokinase *in vitro*. As presented in Figure 4.13A and B, WT Trib2 autophosphorylation was readily detected, in contrast to Trib2 K90M, which exhibits much lower levels of autophosphorylation. Interestingly, Trib2 F130A (Figure 4.13 C) and F130G (Figure 4.13 D) mutants also exhibited very low levels of autophosphorylation, which were similar to K90M Trib2, indicating a defect in the ability to bind or hydrolyse ATP. To quantify the incorporation of the hydrolysed phosphate, SDS-PAGE gels that contained immobilized, assayed Trib2 were analysed by phosphorimager (top panels in Figure 4.13 A-D). The duplicate signals were averaged (Figure 4.14 A), and plotted using GraphPad Prism6 software, which confirmed that both F130A and F130G Trib2 can only autophosphorylate weakly *in vitro* in the presence of 1 mM ATP. To evaluate whether this marked decrease in autophosphorylation by F130A and F130G Trib2 was mirrored by a change in ATP affinity, intrinsic fluorescence during thermal unfolding in the presence and absence of ATP was measured. This confirmed that although F130A and F130G Trib2 gatekeeper mutant Tm values increased when ATP was added (ΔTm ~1°C), this was below the 2°C threshold that suggests strong ligand binding, a marked decrease from WT Trib2 (ΔTm ~4°C) yet a measurable increase from Trib2 K90M (ΔTm 0.1°C, Figure 4.14 B).

4.10 Evaluation of Trib2 aggregation as a function of temperature

An additional advantage of using the Avacta system to measure the intrinsic fluorescence of an unfolding protein is that protein aggregation can be monitored

simultaneously during the process of denaturation. Protein aggregation is detected by static light scattering at a wavelength of 266 nm. The temperature at which the scattered light signal was 10% of the final maximum is termed the Tagg, or Aggregation Onset Temperature. The Tagg of WT Trib2 is 42.5°C (Figure 4.15A), whereas the Tagg for Trib2 K90M was 32.2°C (Figure 4.15 B), suggesting partial destabilization of this mutant *in vitro*. Interestingly, the aggregation of both Trib2 F130A and F130G initiated at 29.8°C and 29.5°C respectively (Figure 4.15 C and D), suggesting that mutant Trib2 proteins are much more unstable and more prone to aggregation than either WT or K90M Trib2, which are themselves relatively unstable. In contrast, the average Tagg of Aurora A kinase is similar to Trib2 WT, at approximately 40°C (37.8°C).

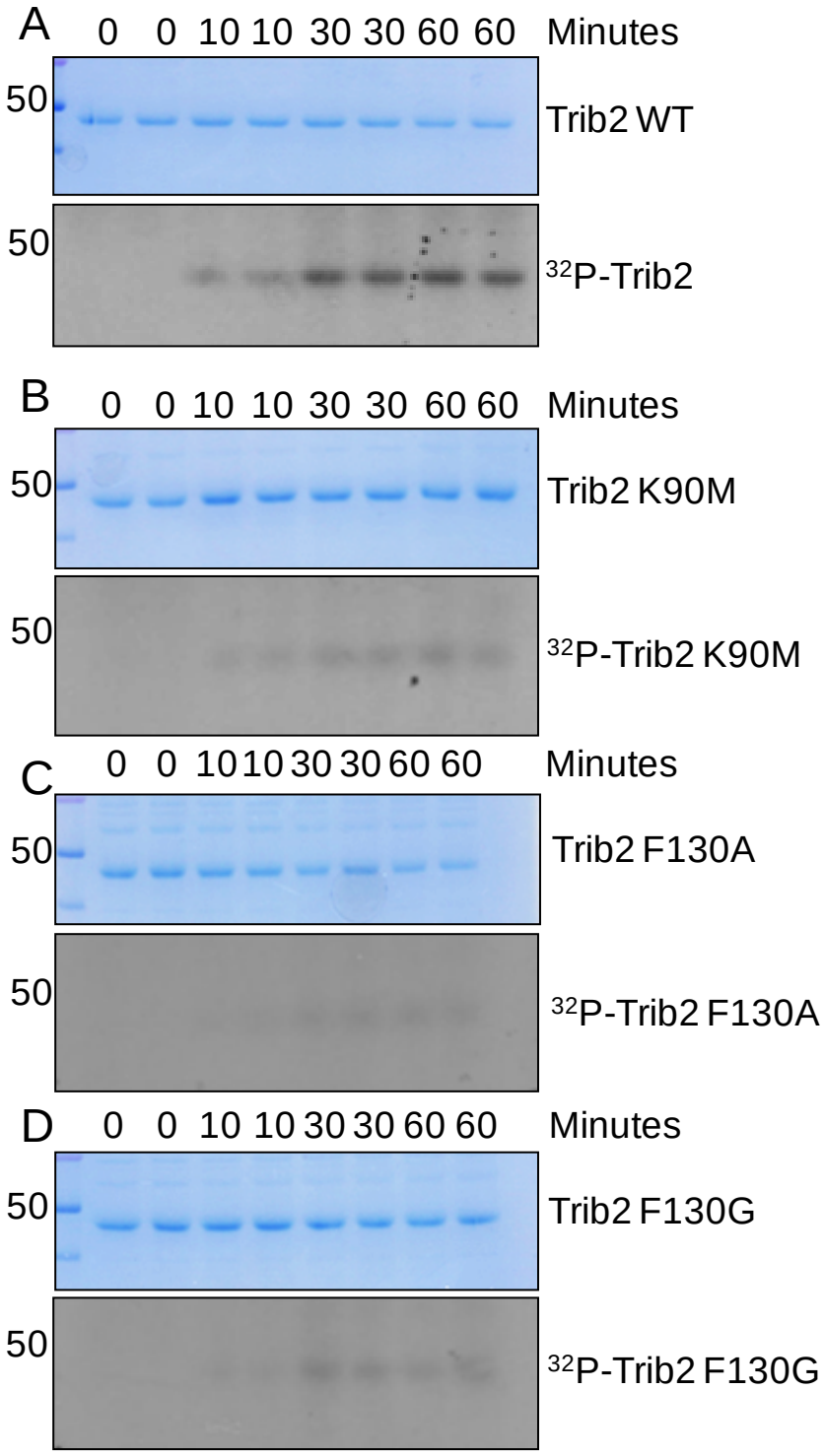

Figure 4.13 Trib2 catalytic activity is abrogated by mutating the gatekeeper residue. Two millimolar EDTA and 1 mM ATP (2.25 µCi γ-^{32}P ATP) were added to A) Trib2 WT, B) K90 M and the gatekeeper mutants C) F130A and D) F130G. The assays were stopped by the addition of 5 x SDS loading buffer after the stated timepoint, boiled for 5 minutes and samples resolved on 12% polyacrylamide gels. The protein was stained with coomassie stain (top panels) and subjected to autoradiography (bottom panels).

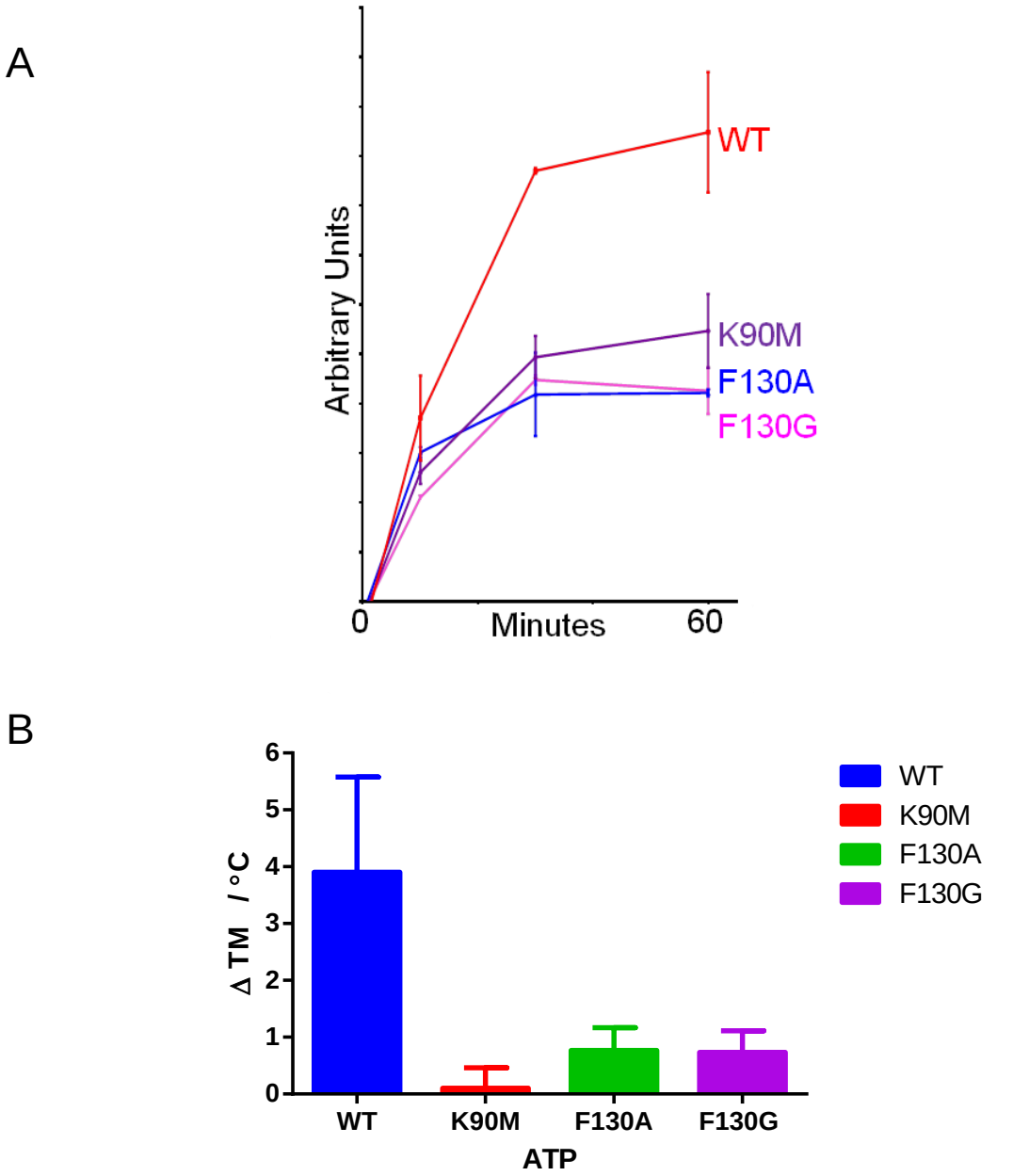

Figure 4.14 Trib2 gatekeeper mutants autophosphorylate less than WT Trib2, but bind to ATP more so than Trib2 K90M. A) The gels in Figure 4.13 were placed into a cassette with a phosphorimage screen for 24 hours. The detected signals for each timepoint were quantified and averaged with standard deviation error bars. B) Average ΔTm values were determined following the thermal unfolding and detection of intrinsic fluorescence of Trib2 (blue), Trib2 K90M (red), Trib2 F130A (green) and Trib2 F130G (purple) in the presence of and absence of 1 mM ATP in triplicate. The Tm values were determined by the fitting of the first derivative to the detected intrinsic fluorescence curves and the Tm values from the 3 assays were averaged. The ΔTm was determined by subtracting the average Tm values for the protein that was not supplemented with ATP from the average Tm values of Trib2 in the presence of ATP. The ΔTm values were plotted in B using GraphPad Prism software.

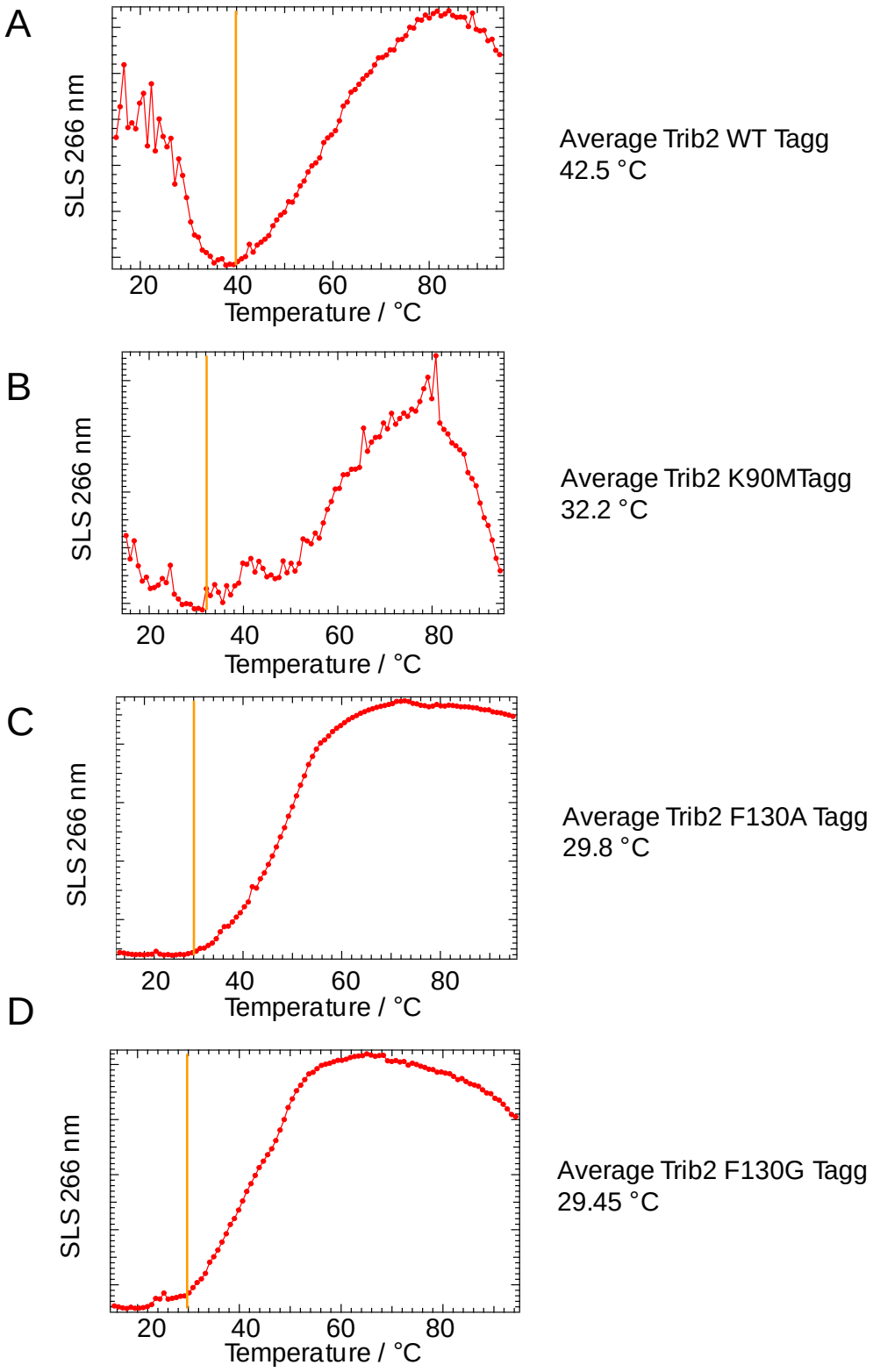

Figure 4.15 Trib2 F130A and F130G aggregate at temperatures lower than the temperature used for *in vitro* kinase assays. The aggregation of A) Trib2 WT, B) K90M, C) F130A and D) F130G was measured on an Optim2 (Avacta) by detecting static light scattering (266 nm) as the temperature increased by 0.3°C/min. The Average Tagg was determined for each protein. Each experiment was performed in duplicate, and aggregation curves representative of each experiment shown. WT and K90M n=3, F130A and F130G n =2.

4.11 Generation of Isogenic Tet-inducible lines for cellular Trib2 analysis

The identification of two bulky inhibitors that bind to Trib2 F130A and F130G (but not WT Trib2) *in vitro*, raises the possibility that these compounds could be used to determine cellular phenotypes that are driven by Trib2 binding to ATP in cells, which might be important for signaling processes downstream of this pseudokinase. To make this approach a reality, human stable cell lines overexpressing either WT, F130A or F130G Trib2 were generated. This chemical biology approach was originally validated by employing matched pairs of v-Src or v-Src I338G (gatekeeper mutant)-expressing NIH3T3 fibroblasts. Both lines displayed the attributes of Src-transformed cells; that is they had a rounded morphology with reduced contact inhibition of growth and could phosphorylate the v-Src substrate protein p36. However, following treatment with a bulky PP1-like inhibitor, the v-Src expressing cells maintained the transformed appearance and the ability to phosphorylate p36, but the morphology of v-Src I338G expressing cells reverted to an untransformed phenotype and phosphorylation of p36 was abrogated, which indicated that the bulky inhibitor specifically inhibited the v-Src I338G protein but not WT Src, or other kinases relevant to cell transformation present in these cell lines (Bishop *et al.*, 1998).

As introduced above, by following a similar approach, inhibition of the ATP binding site of Trib2 F130A and F130G gatekeeper mutants might permit the elucidation of phenotypes that are dependent upon the ATP binding site of Trib2. For instance, it has been demonstrated that cells expressing Trib2 with a mutated catalytic motif display reduced levels of C/EBPα degradation and transformation ability despite still being able to bind COP-1, which indicated the integrity of the ATP binding motif (and potentially the ability to bind ATP directly) is important for Trib2 phenotypic effects (Keeshan *et al.*, 2010). Therefore, by comparing changes in cellular behavior of Trib2 F130A/G cell lines and WT Trib2 cell lines in the presence of a bulky inhibitor, we might be able to validate if ATP binding by Trib2 is required for its oncogenicity, therefore opening up the ATP binding site of Trib2 as a therapeutically important drug target in AML and other cancers where it is overexpressed. In addition, such cell lines might be useful for validation of other ATP-dependent/independent functions of Trib2, which might include its own stability, and/or that of multiple downstream targets.

To this end, Flp-In T-REx HeLa cell lines were generated in which FLAG-tagged full length Trib2, K90M, F130A or F130G Trib2 were expressed after the inducing agent Tetracycline (Tet) was added to the media. As shown in Figure 4.16, FLAG-tagged Trib2 proteins were detected following immunoblotting of soluble cell lysates that had been treated with Tet. No signal was observed in Tet-negative lanes, which suggested that the cell lines were truly inducible. Interestingly, the signal intensity detected for FLAG tagged Trib2 K90M (even when adjusted for the total amount of protein in the cells) was much lower than that WT Trib2, despite loading similar levels of alpha tubulin, which was employed as a loading control (Figure 4.16, bottom panel). The expression levels of F130A and F130G were intermediate when compared to K90M and WT Trib2. As detailed above, both of the analogue-sensitive Trib2 mutants were stabilized by ATP less than WT but more so than K90M Trib2 *in vitro*, which suggests that the ability of Trib2 to bind ATP correlates with the ATP turnover of Trib2 *in vitro* and mutant stability upon expression in human cells.

4.12 Generation of a Trib2 antibody for analysis of Trib2 expression

In order to analyse the concentration of Trib2 in human cells, an anti- Trib2 antibody was generated to compare endogenous levels of Trib2 with exogenous Trib2 in stable cell lines. To this end, an antibody was raised in rats against recombinant full length human Trib2 purified from *E. coli*. The Trib2 reactive antibody was purified from the rat sera using CnBr activated resin conjugated to recombinant Trib2 (Chapter 2). After Trib2 antibody isolation, cell lysates from inducible HeLa cells and 293 cells that overexpressed FLAG tagged Trib2 were resolved by SDS PAGE and transferred to nitrocellulose. This was then immunoblotted with the purified anti- Trib2 antibody, and overexpressed Trib2 was readily detected in the Tet-positive lanes at the apparent size as the FLAG-tagged Trib2 (compare Figure 4.16 and Figure 4.17). However, endogenous Trib2 could not be detected in either of these cell lines using this antibody, which demonstrated that the background levels of Trib2 were very low, and suggested that the levels of induced Trib2 are either much above the endogenous, or that Trib2 is not expressed in these cells. Endogenous Trib2 has previously been reported in lysates isolated from the human monocytic leukaemia cell line THP-1 (Eder *et al.*, 2008). To determine if this rat Trib2 antibody also recognized endogenous Trib2 in these cells,

Trib2 was first concentrated by immunoprecipitation (IP) from the lysate, and subsequently identified by western blotting using the same antibody (Figure 4.18). No equivalent signal was observed in the lane corresponding to the control IP, which was performed alongside the endogenous Trib2 IP, however the lysate was not incubated with purified Trib2 antibody prior to addition of G-Sepharose beads and so the Trib2 was isolated by the antibody and not by a non-specific interaction with the G-Sepharose beads.

4.13 Trib2 expression in a variety of model cancer cell lines

To evaluate the levels of Trib2 expression in a panel of cell lines with this new antibody, 13 different cancer cell extracts were probed with the anti- Trib2 antibody. A densitometric approach, using ImageJ software, allowed an approximate comparison between the levels of Trib2 in each cell line, normalized to the alpha tubulin to identify cell lines that could be used for future analysis of endogenous Trib2 (Figure 4.19). The cell line in which the highest level of Trib2 was detected when normalized to alpha tubulin was the fetal lung fibroblast derived MRC5-VA line, followed by HCT116 (colorectal carcinoma). Interestingly, despite a lack of endogenous Trib2 observed in commercial Flp-In T-REx 293 cell lines (Figure 4.17), the HEK293 (human embryonic kidney, non cancer) lines obtained from the commercial supplier ATCC, expressed detectable levels of Trib2. Endogenous Trib2 was also detected in the MDH2774 (ovarian cancer), RT112 and U2OS cell lines. In the SKOV3 (ovarian cancer), urothelial, RT4 (bladder cancer) and HeLa cell lines however, much lower levels of Trib2 were detected. The relative level of Trib2 in the MRC5-VA, HEK293 and HCT116 cell lines compared to the others, could make these lines particularly useful in future endogenous cell line analysis. Unfortunately, the current NCI-60 cell line proteome database lacks data concerning Trib2 protein expression (Moghaddas Gholami *et al.*, 2013). However, using the BioGPS online database (www.biogps.org) (Wu *et al.*, 2009), the mRNA expression of the NCI-60 cell lines is available and can be mined for data concerning Trib2 (dataset NCI60 on U133A) and this showed that the expression of Trib2 in HEK293 cells is higher than HeLa, SKOV3, DLD-1 and U2OS, which was a similar pattern to the protein expression observed in my analysis (MRC5-VA was not present in this dataset). Interestingly, the neuroblastoma cell line SH-SY5Y (retinoic acid treated) had the highest Trib2 mRNA expression out of all the cell lines in this data set and it would be interesting to test the Trib2 antibody on this cell line in the future. Initially, the

inability to detect endogenous Trib2 in the Flp-In T-REX 293 system using the Trib2 antibody was intriguing, considering the high level observed in HEK293 cells. Further mining of this dataset highlighted that the Trib2 mRNA expression in the Flp-In T-REX 293 cells was considerably lower than in parental HEK293 cells, supporting the differences observed at the protein level (Wu *et al.*, 2009).

4.14 Trib2 expression in primary cancer samples

Trib2 overexpression has been reported as a driver of lung cancers (Grandinetti *et al.*, 2011), blood malignancies (Keeshan *et al.*, 2010) and melanomas (Zanella *et al.*, 2010). Analysis of the Oncomine database (www.oncomine.org) confirms that Trib2 is also overexpressed in a multitude of brain tumour samples, including pilocytic Astrocytomas, where the Trib2 expression was increased by >7-fold, and in glioblastomas where the fold increase was ~5 when compared to normal tissue (Table 4.1). Other cancers located in the head region also exhibited overexpression of Trib2 when compared to normal tissue. In addition, Trib2 mRNA expression in both the salivary gland adenoid cystic carcinoma and the oral cavity carcinoma samples had a fold increase of > 3. Follicular Lymphoma, a cancer of the lymphatic system, exhibited a 6-fold difference in mRNA expression compared to control. Trib2 overexpression has been implicated in another lymphatic cancer, T-ALL (Hannon *et al.*, 2012), and Trib2 overexpression in T-ALL was some 2.6-fold above control levels.

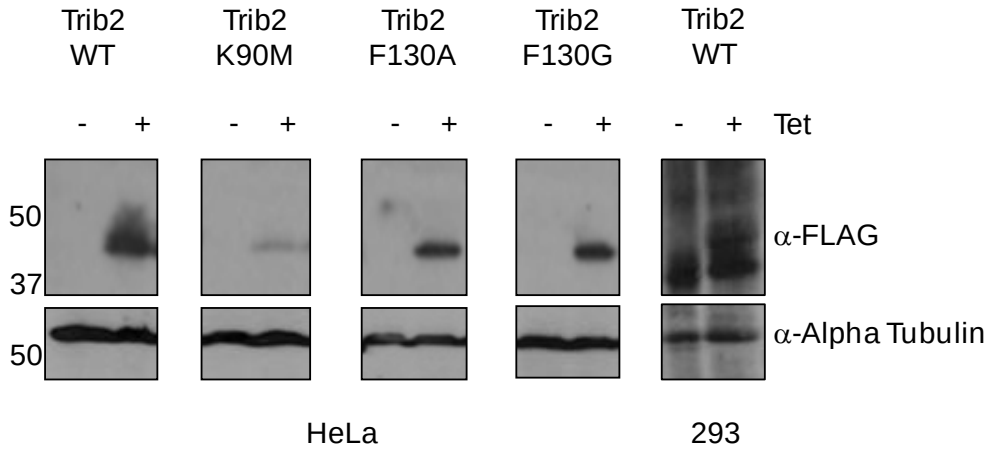

Figure 4.16 Isogenic Trib2 over-expression in a Tet-inducible system. Stable Trib2 WT and mutant overexpressing Flp-In T-Rex (HeLa and 293) cells were cultured in DMEM containing 10% FCS, PenStrep and selective antibiotics. Tetracycline was added to induce Trib2 expression. Fifty micrograms of cell lysates were transferred to nitrocellulose membrane which was immunoblotted with a FLAG specific antibody to detect induced FLAG-Trib2 and the loading was determined by using an alpha tubulin antibody

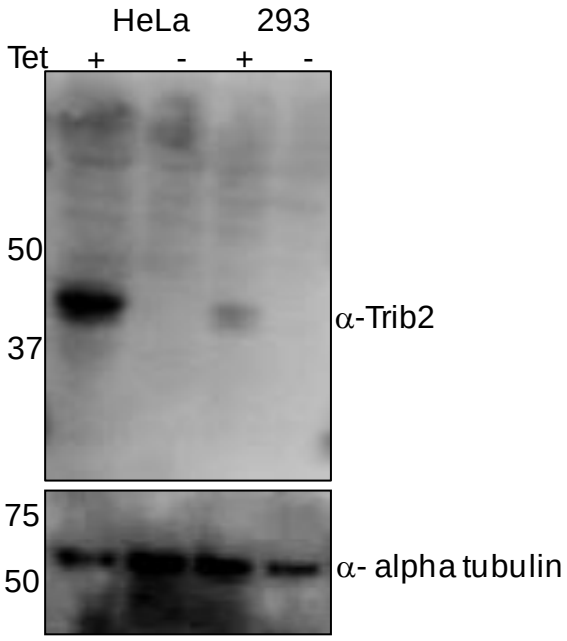

Figure 4.17 Purified Trib2 antibody detects recombinant Trib2 purified from *E. coli* and exogenous Trib2 expressed in induced human cell lysates. Lysates from Flp-In T-Rex HeLa and 293 Flp-In T-REx cell lines that overexpressed FLAG tagged Trib2 were immunoblotted using a Trib2 polyclonal antibody generated in rats, which had been raised against recombinant full length human TRB2. An α- alpha tubulin antibody was used to establish similar loading in each lane

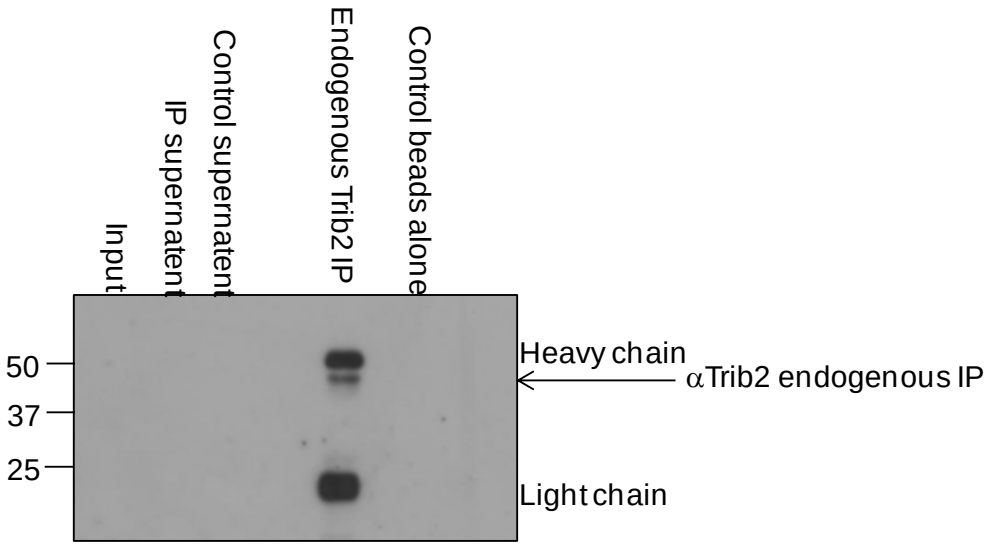

Figure 4.18 Endogenous Trib2 isolated from THP-1 cells by immunoprecipitation. Endogenous human Trib2 was immunoprecipitated from an acute monocytic leukaemia cell line, THP-1. Twenty microlitres of lysate was resolved in the input lane of the SDS PAGE gel alongside the αTrib2 IP and the control IP and samples of the supernatents (unbound fractions). These were immuno-blotted with α-Trib2. The detected heavy and light chains of the antibody are labelled

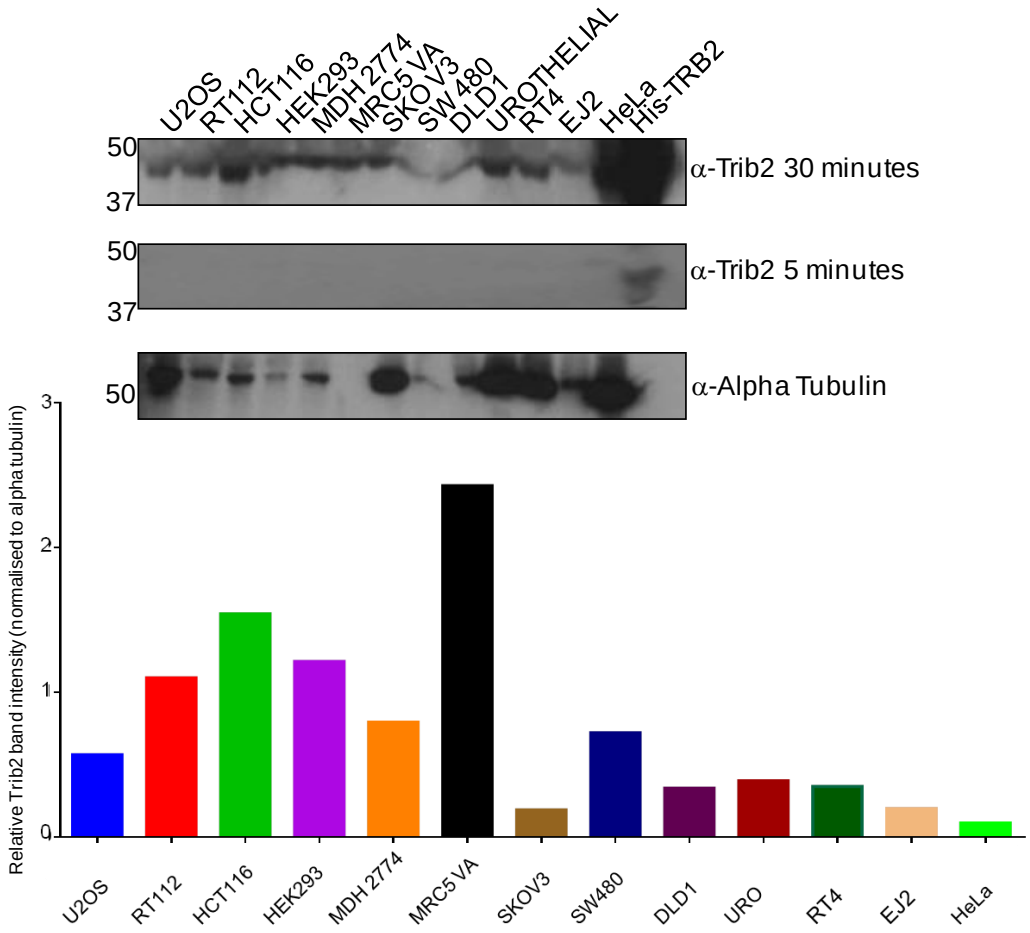

Figure 4.19 Endogenous Trib2 expression in a variety of cancer cell lines was examined. Thirteens cell lysates from a variety of cancers were immunoblotted with purified Trib2 antibody, alongside 500 ng His tagged Trib2 isolated from *E. coli*. To allow for an estimation of the relative total protein loaded in each cell line, alpha tubulin was also immunoblotted, which revealed very uneven protein loading. Densitometric analysis was performed using imageJ software, which following normalisation of the Trib2 bands to the corresponding alpha tubulin allowed approximate comparison of Trib2 protein levels in the different cell lines.

Cancer	Fold change	Oncomine Dataset	Reference to Primary Study
Cutaneous Melanoma	10.506	Talantov Melanoma	(Talantov *et al.*, 2005)
Pancreatic Ductal Adenocarcinoma Epithelia	7.623	Grutzmann Pancreas	(Grutzmann *et al.*, 2004)
Pilocytic Astrocytoma	7.027	Gutmann Brain	(Gutmann *et al.*, 2002)
Follicular Lymphoma	6.120	Rosenwald Multicancer	(Rosenwald *et al.*, 2001)
Follicular Lymphoma	5.812	Alizadeh Lymphoma	(Alizadeh *et al.*, 2000)
Glioblastoma	4.646	Shai Brain	(Shai *et al.*, 2003)
Melanoma	4.581	Haqq Melanoma	(Haqq *et al.*, 2005)
Fibrosarcoma	4.383	Detwiller Sarcoma	(Detwiller *et al.*, 2005)
Cutaneous Melanoma	4.305	Riker Melanoma	(Riker *et al.*, 2008)
Desmoplastic Medulloblastoma	3.931	Pomeroy Brain	(Pomeroy *et al.*, 2002)
Pancreatic Ductal Adenocarcinoma	3.749	Badea Pancreas	(Badea *et al.*, 2008)
Salivary gland Adenoid Cystic Carcinoma	3.499	FriersonHF Salivary-gland	(Frierson *et al.*, 2002)
Pancreatic Adenocarcinoma	3.323	Logsdon Pancreas	(Logsdon *et al.*, 2003)
Pancreatic Carcinoma	3.279	Segara Pancreas	(Segara *et al.*, 2005)
Oral cavity Carcinoma	3.266	Pyeon Multi-cancer	(Pyeon *et al.*, 2007)
Esophageal Adenocarcinoma	3.088	Hao Esophagus	(Hao *et al.*, 2006)
Anaplastic Oligodendroglioma	3.010	French Brain	(French *et al.*, 2005)
Angioimmunoblastic T-cell Lymphoma	2.603	Piccaluga Lymphoma	(Piccaluga *et al.*, 2007)

Table 4.1 Trib2 mRNA expression levels reported in the Oncomine database. Analysing Trib2 expression differences between normal and oncogenic tissues using the Oncomine database highlighted cancer samples that markedly overexpress Trib2. Cancerous tissues that expressed Trib2 at a higher level than compared to normal (p value= 0.05) are listed above, along with the names of the datasets which reported the data and the citations of the primary studies.

4.15 Trib2-interacting proteins identified by Mass Spectrometry

To gain a better understanding of the functions of Trib2 in its natural cellular environment and to identify potential Trib2 substrate phosphorylation (including autophosphorylation) or ATP-binding dependent substrates, it is crucial to determine the function of Trib2 in cellular signaling pathways and how it interacts with other constituent members. For instance, it was previously determined that Trib2 inhibited TLR5-dependent NF-κB activation, but it was only after MS/MS mass spectrometry was performed that the transcription factor NF-κB was identified as a putative binding partner of Trib2 and from this it was possible to identify the binding site, which is reported to be located within the catalytic loop of Trib2 (Wei *et al.*, 2012). To identify Trib2 interacting-proteins in a human cell line that is well-characterised and suitable for proteomics, FLAG-tagged Trib2 was immunoprecipitated from Flp-In T-REx-293 Tet-inducible cells, with uninduced cells used as a negative control for background interaction. Following incubation of the lysates with M2 FLAG antibody conjugated beads FLAG-tagged Trib2 was competitively eluted following the addition of FLAG peptide. Samples of the IP and control were resolved by SDS-PAGE and immunoblotted, which showed that FLAG- Trib2 had been successfully specifically purified from the induced lysate (Figure 4.20 A). All the proteins present in the Trib2 and control IPs were resolved by SDS PAGE and analysed by coomassie staining using a known amount of BSA as a control (Figure 4.20 B). The proteins in both the IP lane and control lane were subjected to in-gel digestion by the addition of trypsin and LC-MS/MS mass spectrometry (performed by Ms. Alice Wadkin, University of Manchester). The data was then analysed using MASCOT software. Proteins that interacted with Trib2 and were present only in the +Tet IP have been summarised in Table 4.2. The bands on the gel that were analysed are numbered 1-11 (highlighted in the gel in Figure 4.20) and in Table 4.2 the number of the band where the peptides were identified are noted along with both the SwissProt identifier and the full name. The protein score is the sum of all the peptide ion scores and takes into account the size of the protein, number of peptides detected and the peptide score. The observed Mr is the molecular weight of the ion detected in the MS/MS spectra (these values include doubly charged ions, for instance). The molecular weight expected for the neutral compound, in its natural form (Mr(expt)) and the isotopic masses of the peptides (Mr(calc)) are also reported in the table. The peptide score is derived from the size of the peptide and how likely it is to fragment as

expected and is a score of how confident the peptide matches the predicted protein. A peptide score (above or equal to 20) indicates a detected peptide is likely to be a 'real' match. The expected values are the number of matches with equal or better scores than the threshold in the database. The lower the expectation value, the more confidence there is that the protein has been detected in the sample. It is also worth noting how many peptide fragments for each protein have been detected; the more observed, the more likely the protein is to be present (Mascot database www.matrixscience.com).

Amongst the proteins that coimmunoprecipitated with Trib2 was a canonical protein kinase STK38 (NDR1), which has constituent peptides that have scores greatly above 20, low expectation values and there are 7 matched peptides which is highly suggestive that it is a protein that interacts with Trib2 and it would be very interesting to perform the reciprocal immunoprecipitation to confirm this interaction. Another kinase that was detected was the metabolic regulator Creatine kinase (both kinases are highlighted in yellow in Table 4.2). In contrast to NDR1, it had only one peptide hit in the analysis, but this exhibited a relatively high peptide score. More than one peptide for each of the proteins calmodulin-regulated spectrin associated protein, protein arginine N-methyltransferase 5, nicotinamide phosphoribosyltransferase 5 were identified in the analysis. Only one, however, was identified for each of the 60s Ribosomal proteins L8 and L19, and Shroom 3, which were also recovered with FLAG-tagged Trib2 in Flp-In T-REx 293 cells.

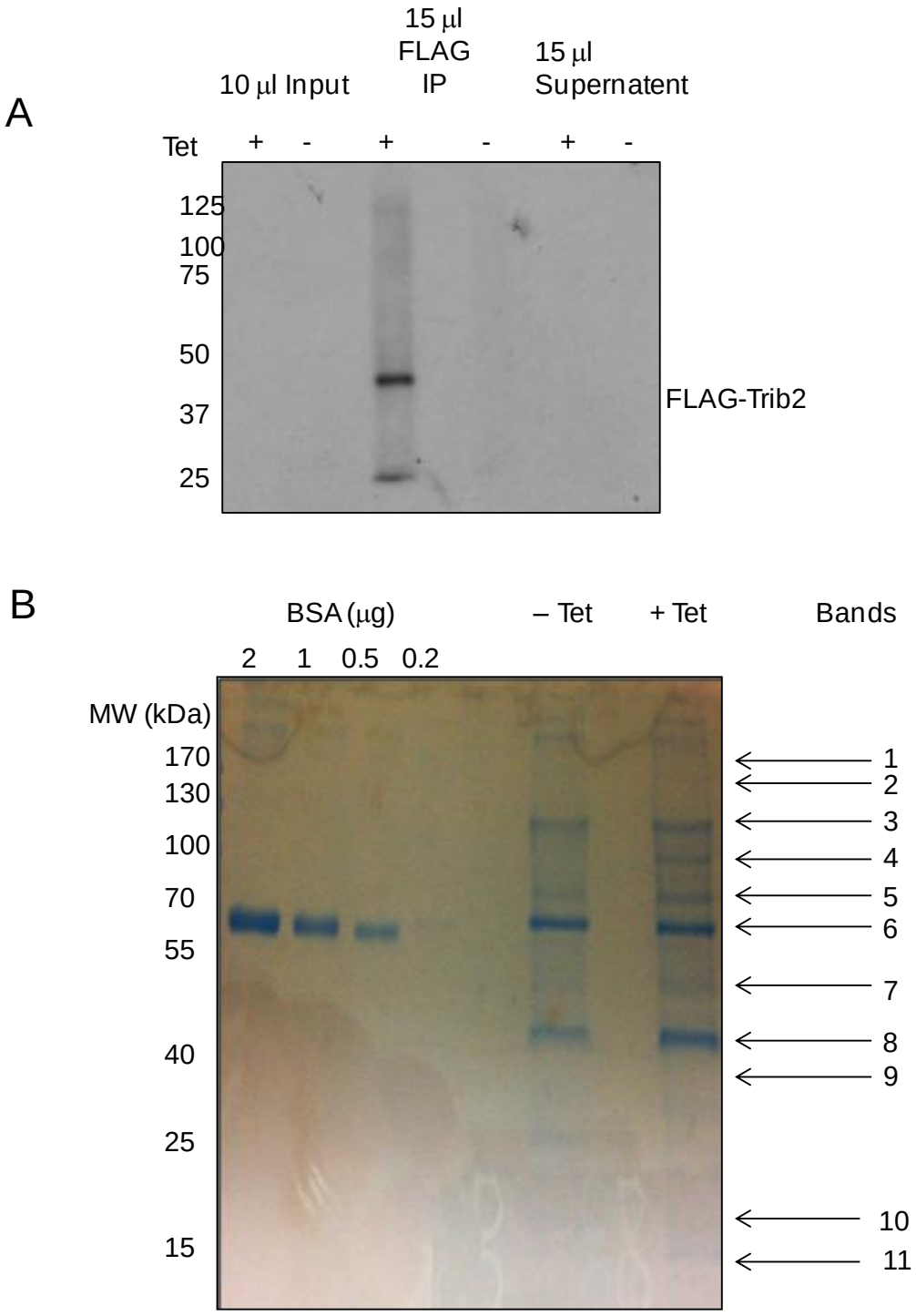

Figure 4.20 Trib2 isolated by α-FLAG immunoprecipitation Following FLAG immunoprecipitation of FLAG-Trib2 from inducible Flp-In T-Rex 293 cells (+/- Tet), A) the input, IP and supernatents were immunoblotted using an anti-FLAG antibody B) Forty microlitres of the eluted immunoprecipitation were resolved in an SDS-PAGE gel along with known amounts of BSA and stained with coomassie stain. The numbers refer to the bands in which the proteins in Table 4.2 were identified.

Band	Protein	Protein Name	MW	Protein Score	Peptides	Observed	Mr (expt)	Mr (calc)	Peptide Score	Expect
3	CAMP3 HUMAN	Calmodulin regulated spectrin associated protein	135464	41	LSAALSSLQR	523.3734	1044.7322	1044.5927	8	7.9
					SAFLQVQPR	523.383	1044.7514	1044.5716	41	0.0027
					LSAALSSLQR + Deamidated (NQ)	523.8688	1045.723	1045.5767	9	8.3
8	STK38 HUMAN	Serine/threonine protein kinase	54498	40	KETEFLR	922.5009	921.4936	921.492	12	5.3
					IGAPGVEEIK	1012.57	1011.5627	1011.56	15	2.7
					LGLEDFESLK	1150.6058	1149.5985	1149.5917	40	0.0091
					ERPAAISIEIK	1226.7126	1225.7053	1225.703	21	0.63
					DIKPDNLLLDSK	1370.7524	1369.7451	1369.7453	31	0.067
					SNSFFEGVDWEHIR	1722.7955	1721.7882	1721.7798	2	58
					VTLENFYSNLIAQHEER	2063.0266	2062.0193	2062.0119	12	5.5
8	ANM5 HUMAN	Protein Arginine N-Methyltransferase 5	73322	72	GPLVNASLR	463.8442	925.6738	925.5345	47	6.50E-04
					YSQYQQAIYK	646.4155	1290.8164	1290.6244	46	0.0014
8	NAMPT HUMAN	Nicotinamide Phosphoribosyltransferase 5	55772	54	VLEILGK	386.3092	770.6038	770.4902	39	0.0061
					AVPEGFVIPR	542.8906	1083.7666	1083.6077	39	0.0043
9	KCRB HUMAN	Creatine Kinase B-Type	42902	40	VLTPELYAELR	652.4621	1302.9096	1302.7183	40	1.30E-03
10	RL8 HUMAN	60s Ribosomal Protein L8	28235	53	AVVGVVAGGGR	471.3479	940.6812	940.5454	53	0.00018
11	RL19 HUMAN	60s Ribosomal Protein L19	23565	75	LASSVLR	373.2847	744.5548	744.4494	36	0.036
					LLADQAEAR	493.8366	985.6586	985.5192	72	4.80E-06
11	SHRM3 HUMAN	Protein Shroom3	218321	36	SSPATADKR	466.822	931.6294	931.4723	36	2.40E-02

Table 4.2. A list of proteins that interact with FLAG-Trib2. The proteins listed were detected in the IP from lysate that had been exposed to Tetracycline aside from Trib2. The column titled 'Band' corresponds to the numbered bands highlighted in Figure 4.20. The proteins in this table were only observed in the IP from cells in which FLAG-Trib2 was overexpressed. The peptides identified are listed along with the Swiss-Prot and full protein name, observed weight, expected mass and calculated mass. The peptide scores and expected values are also listed (mass spectrometry peformed by Ms. Alice Wadkin). Two kinases identified by this analysis are highlighted in yellow.

4.16 Discussion

My prior biochemical analysis of recombinant Trib2 in Chapter 3 demonstrated that Trib2 is a very low activity pseudokinase, similar to the pseudokinase CASK, which functions in neurons to regulate the substrate neurexin-1 (Mukherjee *et al.*, 2008). The finding that Trib2-mediated ATP hydrolysis can be abrogated by mutating known catalytic residues in the pseudokinase domain *in vitro*, along with evidence that an intact catalytic domain is required for Trib2 oncogenic transformation and C/EBPα degradation (Keeshan *et al.*, 2010) suggests that ATP binding to Trib2 could be a potential driver of the oncogenic behavior displayed by Trib2 overexpressing cells, including those highlighted in NSCLC (Grandinetti *et al.*, 2011) and AML (Rishi *et al.*, 2014).

The aim of the work presented in this chapter was to develop an ATP-binding assay for Trib2, and to determine whether the Trib2 ATP binding site was targetable by small molecule inhibitors. In addition, I have begun to develop tools such as inducible Trib2 overexpressing cell lines that will help identify the roles of Trib2 ATP-binding, autophosphorylation, overexpression, stability and Trib2 proteomics in cells.

Recombinant Trib2 binds to ATP

Data presented in this chapter prove unequivocally that Trib2 binds to ATP (Figures 4.2 and 4.11). One advantage of using DSF as a technique to identify ATP/ligand binding by a pseudokinase is that the thermal denaturation curves are only influenced by the main protein constituent of the reaction mixture and the results are not affected by the presence of low amounts of contaminating proteins (Murphy *et al.*, 2014b), which have historically been problematic for *in vitro* kinase assays performed on pseudokinases. BUBR1 is an example of a pseudokinase that was initially deemed to be catalytically active following *in vitro* kinase assay analysis (Taylor *et al.*, 1998), however the activity was later attributed to active kinases that had contaminated the BUBR1 sample when the pseudokinase was isolated by immunoprecipitation (Suijkerbuijk *et al.*, 2012). A similar case is true for ILK, which demonstrated catalytic activity and could phosphorylate MBP as well as cellular substrates (Hannigan *et al.*, 1996) and when key residues in the catalytic domain were mutated, the observed phosphorylation was reduced (Persad *et al.*, 2001). However, it was later shown that ILK is not catalytically active, but that the

mutations reduced the interactions with ILK binding partners including α-parvin and β-parvin (Attwell *et al.*, 2003, Yamaji *et al.*, 2001, Lange *et al.*, 2009) and a crystal structure confirmed instead that ILK is a catalytically inactive pseudokinase that binds to ATP with high affinity (Fukuda *et al.*, 2009).

In addition, other advantages of DSF to determine ATP/ligand binding include the requirement of only 2-5 μM of purified pseudokinase (Lucet *et al.*, 2013) in a volume of 25 μl, and the use of a relatively basic thermocycler for thermal control and signal detection, allowing analysis in 96-well plates, which facilitates the analysis of multiple ligands and conditions at any one time and a rapid turnover of results. Indeed, DSF data-set could be obtained 90 minutes after the initiation of the assay, in marked contrast to ^{32}P-based experiments, with a time-to-analysis of almost a week in some cases, due to the very low levels of ATP hydrolysis and limits to the amount of ^{32}P ATP that can be utilised.

Published thermal shift assays previously performed on His-tagged Trib2 isolated using our pET30-based Trib2 plasmid and purification procedures (Murphy *et al.*, 2014b) demonstrated that there was no interaction between Trib2 and 200 μM ATP, or any other potential ligands tested. The same results were obtained for CASK at 200 μM ATP, consistent with previous biochemical and structural work highlighting CASK's ability to bind to ATP in the very high μM range (Mukherjee *et al.*, 2008). This led to both proteins being classified as 'Group 1 pseudokinases: Devoid of detectable nucleotide and cation binding.' These results were reproduced and are shown in Figure 4.1. Surprisingly, I found that SgK495 was also able to bind to ATP in our assay, despite having an ATP binding site with low sequence conservation compared to canonical kinases. Interestingly, there is no observable canonical Gly-rich loop in the predicted pseudokinase domain of SgK495, however there is a canonical GXGXXG motif located N-terminal to the typical start of the catalytic domain, and it will be interesting to assess if this is involved in ATP binding. There is also no typical lysine residue in the β3 motif when the sequence is aligned with Trib2 and PKA (Chapter 1) but SgK495 does have an intact catalytic motif, HRDLKLGN, with the magnesium chelating Asn present, although it also lacks the magnesium-binding Asp in the DFG motif (NFC) similar to Trib1, Trib2 and Trib3. Murphy and colleagues recently classified SgK495 as a group 1 pseudokinase that did not bind to nucleotides or divalent cations (Murphy et al.,

2014). However, the only concentration of ATP assessed in this screen was 200 μM, and in Figure 4.1, a ΔTm of >1°C only occurs when SgK495 is incubated with an ATP concentration in excess of 625 μM. This demonstrated that to accurately determine whether a pseudokinase has the biochemical ability to bind to ATP, DSF should be employed using multiple concentrations of ATP, and by combining the data with site-directed mutagenesis of the ATP-binding site. *In vitro* kinase assays (Figure 3.25 D) have thus far provided no evidence that SgK495 is catalytically capable of hydrolysing ATP, but in this thesis, I provide some evidence that it can bind to ATP *in vitro*. There is still the potential that a substrate for SgK495 phosphorylation has yet to be discovered, but until one is found, SgK495 demonstrates the properties attributed to Class 2 pseudokinases that are defined by Murphy et al., 2014 as being able bind to ATP in the absence of cations. In the future, it will be important to test whether mutations in potential SgK495 ATP binding residues, such as either of the Gly-rich sequences (GAGETS (9-14) or GSGISG (21-25)) in the SgK495 N-terminus or amino acids in the canonical catalytic loop (H195-N202), decrease binding of this pseudokinase to ATP. A 3D structure is ideally required to decipher how SgK495 folds and and whether it adopts a classical kinase fold and if so, how it binds to ATP. For example, it has recently been demonstrated that SgK495 complexed to RCN2 is able to activate the ERK/MAPK pathway required for maturation of murine lung tissues (Yu *et al.*, 2013), but whether ATP binding by SgK495 is required for this process has yet to be determined. Another member of the class 2 group of pseudokinases is the well studied pseudokinase STRADα, which modulates the activity of the classical kinase LKB1 through ATP binding but not hydrolysis (Zeqiraj *et al.*, 2009a), and it is possible that SgK495 has a similar kinase-activating function in human cells.

DSF analysis of Trib2 and other pseudokinases

Interestingly, when DSF reactions were supplemented with 2 mM EDTA (Figure 4.2), replicating the conditions used in the *in vitro* kinase assays described in Chapter 3, Trib2 was stabilized by ATP, unlike any of the K90 Trib2 point mutants. Interestingly, when analysed by DSF, K90R behaved much more like K90M and K90A, and its thermal stability did not increase under these conditions, despite demonstrating the ability to autophosphorylate efficiently in Chapter 3. The presence of 10 mM Mg^{2+} ions and ATP increased the Tm of Trib2 (Figure 4.2 A), but not as

markedly as EDTA and ATP, again supporting the *in vitro* kinase data presented in Chapter 3, which showed Trib2 autophosphorylation occurred in the presence of divalent cations, but that this level of autophosphorylation was less than in their absence. DSF has indicated that the reason for this reduction is that Trib2 in the presence of magnesium and ATP has a lower ΔTm than for Trib2 in the presence of EDTA and ATP; therefore on the basis that there is a positive correlation between the ΔTm and the affinity of a protein for a ligand (Bullock *et al.*, 2005), Trib2 has a lower affinity for ATP when Mg^{2+} is present. The thermal protective effect that ATP imparted upon Trib2, was indicative of ligand binding. I therefore suggest that Trib2 should be moved from characterization as a class 1 pseudokinase (Murphy *et al.*, 2014b), where members did not demonstrate nucleotide or cation binding, and securely placed into class 2. Although when Trib2 was assayed by Murphy et al., it was not thermally stabilized by ATP, its Tm was lower than 40°C and this is also observed in the data presented in this thesis. Murphy et al., also noted that the majority of kinases that had a low melting temperature were Class 4 proteins that bind ATP, compared to Class 1 proteins whose Tm were generally >40°C and they suggest this low melting temperature indicates that there is a higher degree of flexibility between the N and C lobe because in the absence of a ligand, the ATP binding site is more open and that it could be the binding of ATP by Class 2 or 4 pseudokinases that increases the rigidity of the kinase domain and provides the structural integrity required to perform its function, such as acting as a protein scaffold for instance (Murphy *et al.*, 2014b).

DSF was also useful for explaining why Trib2 DFGK180N did not autophosphorylate *in vitro* (Chapter 3). Analysis of this quadruple point mutant by DSF (Figure 4.2 E) revealed that it was already unfolded prior to the thermal ramping step (Uniewicz *et al.*, 2012) and this is entirely consistent with the inability of the mutant protein to autophosphorylate in the presence or absence of metal ions (Chapter 3). In the future, it will be important to try and generate a constitutive active 'back' mutation of Trib2 to evaluate what its potential biological role might be when unhindered by a low affinity for ATP. In addition, it is important to note that at the low millimolar ATP concentrations found in the cell, which might fluctuate in subcellular regions, Trib2 is likely to interact with ATP, meaning that a nucleotide-binding function is theoretically possible, and biologically quite likely.

An additional technique, which used a similar principle to DSF, determined the Tm of a protein by measuring changes of intrinsic fluorescence as it unfolded, which negated the need for an extrinsic fluorescent dye. Analysis of Trib2 melting temperatures derived from intrinsic fluorescence thermal denaturation curves identified that the thermal stability of Trib2 increased markedly in the presence of 1 mM ATP (Figure 4.11 E). The ΔTm for Trib2 is 2°C higher than for Trib2 K90M and > 3°C higher than Trib2 K90A. Neither of these Trib2 β3 motif lysine mutants autophosphorylated to the same extent as Trib2 (Chapter 3). The lower ΔTm values for the Trib2 K90 mutants compared to WT in the presence of ATP indicated that mutating this residue in Trib2 affected the affinity of Trib2 for ATP (Bullock *et al.*, 2005), and supported the decreased catalytic activity observed following *in vitro* kinase assays (Chapter 3). Had time permitted, bacterially-expressed Trib2 K177A and Trib3 alongside K97M Trib3 would also have been assayed by DSF to uncover their ATP binding properties. It will be very interesting to ascertain whether K177A could bind to ATP, because it would indicate whether the reduced autophosphorylation (Chapter 3) was caused by a reduced affinity for ATP or direct inhibition of the catalytic phosphotransfer mechanism, and a mutation at this position (K177R) has demonstrated a reduced ability to degrade C/EBPα in conjunction with COP1, and then initiate Trib2 mediated AML in mouse models (Keeshan *et al.*, 2010). Further evaluation of the Trib3 ATP binding site by DSF would further validate the Mg^{2+} independent autophosphorylation observed for Trib3 (Chapter 3) and help drive the initiation of Trib3 ligand binding studies to identify whether ATP-binding is critical for the degradation of COP-1 mediated degradation of substrates such as Acetyl CoA Carboxylase (Dedhia *et al.*, 2010).

DSF was also used to investigate the accessibility of the Trib2 ATP binding site to kinase inhibitors. DAP (N′2′-(4-aminomethyl-phenyl)-5-fluoro-N′4′-phenyl-pyrimidine-2,4-diamine), a generic kinase inhibitor did not bind to Trib2 in thermal shift assays when used at a concentration of 40 μM when previously tested (Murphy *et al.*, 2014b). In Figure 4.3, Trib2 was incubated with a variety of DAP concentrations, ranging up to 400 μM, and even at this high concentration, no thermal protective effect was conferred onto Trib2. The highly active kinase Aurora A was, however, stabilized by DAP in a concentration-dependent manner. Despite the discovery that Trib2 could bind to and hydrolyse ATP, and that the pseudokinase

domain of Trib2 was required for Trib2-mediated oncogenesis (Keeshan *et al.*, 2010), it is still unclear whether ATP binding by Trib2 is essential for C/EBPα degradation and the transformation of cells. To investigate this, small molecule inhibitors that target the ATP binding site of Trib2 might now be employed, although it would also be most useful to construct cell lines of the immune lineage in which to test this where there is a confirmed phenotype for Trib2 over-expressing cells.

Increasing the size of the ATP binding pocket, by reducing the size of the gatekeeper residue, enables access of bulky small molecules that previously could not have entered because of size constraints. These have previously been used to elucidate the activities of dozens of canonical kinases beginning with Src (Liu *et al.*, 1998) and extending to CDK2 (Elphick *et al.*, 2009), and have also recently been employed to identify direct substrates of pseudokinase phosphorylation. An example of this was the discovery that MEK1 is directly phosphorylated by KSR2, in an *in vitro* kinase assay. The bulky ATP analogue N6-phenethyl ATPγS was incubated with both WT KSR2 and KSR2 T739G, which contains a mutated gatekeeper residue, creating a kinase domain with an enlarged ATP binding pocket. Phosphorylation of MEK1 was only observed in the assays containing the T739G mutated KSR2 and not WT KSR2 (Brennan *et al.*, 2011). Another advantage of using this chemical genetic technique in the drug discovery process was that the manipulation of the gatekeeper residue can also be used in cell-based and *in vivo* model systems because the small molecule inhibitors are cell permeable and have low toxicity in mice (Shokat and Velleca, 2002).

Analysis of Trib2 gatekeeper mutants as tools for examining Trib2 biology

Trib2 gatekeeper mutants F130A and F130G were purified from *E. coli* and facilitated the identification of bulky small molecules that targeted the (predicted) enlarged ATP binding sites of the mutants. DSF enabled a fast and relatively economical method of identifying ligands that interacted with the mutant Trib2 kinase domains. If the addition of an inhibitor from the panel of 30 that were tested caused Trib2, Trib2 F130A or F130G aggregation, then the inhibitor was not included in Figure 4.6. From the remaining 7 ligands, two increased the Tm of both the gatekeeper mutants but did not affect the Tm of Trib2. Further analysis by DSF and detection of intrinsic fluorescence showed that these two inhibitors (HxJ 42 and

CZ 30) stabilized Trib2 F130A and F130G but did not affect Trib2, nor was the stability of Aurora A or SgK495 increased to the same extent. Closely related analogs of the biphenyl-PP1 analogue CZ 30; CZ 28 and CZ 29, did not stabilize the gatekeeper mutants, and the reason for this is not currently known.

Following the discovery of two bulky analogues that specifically interacted with recombinant F130A and F130G, isogenic inducible stable human cell lines, expressed FLAG tagged Trib2, K90M, F130A and F130G were generated that could facilitate the future identification of cellular phenotypes that change following application of inhibitors that interacted with the ATP binding sites of gatekeeper mutants and could help determine whether specifically targeting the ATP binding site of Trib2 would be therapeutically advantageous. The HeLa Flp-In T-REx and 293 Flp-In T-REx inducible cell lines express low levels of endogenous Trib2 that are not detectable with the purified Trib2 antibody. However, endogenous Trib2 was detected in a variety of oncogenic cell lines, including in the human colon adenocarcinoma cell line HCT116, which when the levels of total protein loaded were taken into account, had the highest amount of Trib2 detected by western blot (Figure 4.19). HCT116 cells overexpress the oncogenic protein YAP which is a downstream target of the Hippo signaling pathway (Wang *et al.*, 2013d) and in hepatocarcinoma cells (HCCs), Trib2 stabilises YAP by interacting with βTrCP, an E3 ligase, and the presence of Trib2 is crucial for the cells transformative phenotype (Wang *et al.*, 2013b). To identify whether Trib2 is an oncogenic driver in the HCT116 cell line, as in the HCCs, the cells could be treated with Trib2 siRNA and the levels of apoptosis and colony formation analysed. Endogenous Trib2 can also be detected in HeLa and HEK293 cells, unlike the Flp-In T-REx variants, which indicates that the Flp-In T-REx cell lines would be a good model to study overexpressed Trib2 WT and mutants without significant background endogenous Trib2 contamination, but if required, the 'normal' well-characterised HeLa or HEK293 cells can be utilized to study Trib2 endogenously.

Trib2 expression in patient samples was investigated by analysis of the Oncomine database, which looked at the fold changes between tumor samples and normal tissue from published studies. I focused on presenting Trib2-overexpressing samples because of the previous studies that reported the significance of Trib2 overexpression in cancers (Grandinetti *et al.*, 2011, Zanella *et al.*, 2010, Rishi *et al.*,

2014). The tissue sample that had the largest Trib2 expression change was in a melanoma sample, and it has been reported previously that Trib2 is overexpressed in melanoma, where it represses the tumor suppressor FOXO, and knockdown of Trib2 in melanoma cells reduces the cell proliferation by reinstating contact-inhibition growth and also reduces the ability of cells to form colonies (Zanella *et al.*, 2010). Noticeably, Oncomine highlighted a variety of tumors that overexpressed Trib2, were isolated from brain tissue. Interestingly, the level of 'free' ATP (ATP that is not complexed to Mg^{2+}) is high in brain compared to other tissues. In normal brain tissue it was revealed that ~24% ATP was not complexed with magnesium, in contrast to muscle tissue where only ~4% of ATP was free (Taylor *et al.*, 1991), and as shown in the *in vitro* kinase assays presented in Chapter 3, Trib2 catalytic activity is inhibited by magnesium ions and so, the brain could be a potential *in vivo* site where Trib2 catalytic ATP binding is particularly important, and might well be oncogenically relevant.

Interestingly, the amount of induced recombinant Trib2 K90M expressed in HeLa cells is much lower compared to WT Trib2, suggesting that it is more rapidly turned over, and this could be investigated further by employing proteasome inhibitors such as MG132 (Dedhia *et al.*, 2010). A similar destabilisation has also been observed following expression of Trib2 K90M in *E. coli* and Sf9 cells, which potentially indicates that the ability of Trib2 to bind ATP affects the rate of Trib2 turnover and stability. The amount of expressed FLAG-tagged Trib2, is also higher than Trib2 F130A and F130G. Consistently, ATP did provide a marginal thermo-protective effect on F130A and F130G with an average ΔTm ~1°C (performed in triplicate), which despite not being above the 2°C threshold indicative of ligand binding, was higher than the ΔTm increase observed for Trib2 K90M, in the presence of ATP (ΔTm 0.1°C) but was lower than Trib2 (ΔTm 4°C). Despite these results hinting at a link between Trib2 stability and the ability to bind ATP, further work will be required before any biological relevance can be attached to this observation.

Despite DSF indicating that Trib2 F130A and F130G were very slightly stabilized by the presence of ATP, when they were assayed *in vitro*, there was no evidence of autophosphorylation, perhaps because they were much less stable and didn't interact as strongly. Static light scattering analysis that was performed

concurrently with the detection of intrinsic fluorescence whilst Trib2 and the gatekeeper mutants were incubated with ATP, showed that at 30°C (the temperature of the *in vitro* kinase assays) Trib2 F130A and F130G were aggregating. In both cases, the Tagg (onset of aggregation temperature) was ~29°C, whereas Trib2 K90M aggregated at a temperature above 30°C, so aggregation was not the likely reason for the lower activity observed by the K90M mutant. To categorically determine whether the Trib2, Trib2 F130A and Trib2 F130G mutants expressed in cell lines can bind to ATP, they could be FLAG-immunoprecipitated and subjected to an *in vitro* kinase assay alongside Trib2 K90M as a control, using autophosphorylation or phosphorylation of Trib2 K90M as a substrate.

Reduced catalytic activity of the gatekeeper mutants is not unique to Trib2 but has been observed for ~30% of the kinases that have been tested so far (Hengeveld *et al.*, 2012). It has been suggested that mutating the gatekeeper residue could disrupt the hydrophobic spine of the kinase fold and reduce its stability (Garske *et al.*, 2011). Aurora B is an example of such a kinase where a Gly or Ala mutation to the gatekeeper Leu residue (L154G/A) abrogates catalytic activity. However, a second site mutation (H250Y) reinstates WT-like phosphorylation to gatekeeper mutated proteins (Hengeveld *et al.*, 2012). The Syk tyrosine kinase is also unable to tolerate a gatekeeper mutation and Syk mutants have reduced catalytic activity. By aligning Syk with Src, which remained catalytically active following mutation of the gatekeeper residue, it was noticed that residues in close contact with the Src gatekeeper residue (T338) are Gln and Leu whereas in Syk, the corresponding residues are Arg425 and Met426 (Syk gatekeeper residue M442). The catalytic activity of the R425Q M426L M442A Syk mutant increased compared to M442A alone. However, these secondary mutations did not increase the catalytic activity of Syk M442G (Oh *et al.*, 2007).

A strategy to identify second site mutations that reinstate the catalytic activity of gatekeeper mutant kinases has been identified and concluded that mutating a residue located within the 3 middle β sheets of the N-lobe of the kinase to a branched amino acid, did not reduce the space opened up in the ATP binding domain brought about by the mutated gatekeeper residue but restabilized the N lobe of the kinase domain and increased the catalytic activity of the analog sensitive mutants, and these could still bind to the bulky analogues (Zhang *et al.*, 2005a). Structural and

sequence analysis of tolerant gatekeeper mutant kinases identified that a valine was often present (c-Src V284), and alignment of Cdc5, which is intolerant to mutation of the gatekeeper, has a Cys residue at this position. In budding yeast, when Cdc5 is doubly mutated, with C96V and either L158A or L158G, the yeast are viable, unlike when the gatekeeper is the sole mutation (Zhang *et al.*, 2005a). Alignment of Trib2 with c-Src has indicated that the aligned residue is also a valine (V75 Trib2), so this is not the position to locate a 'second-site' mutation in Trib2 and further analysis of the sequence, and ideally a structure (when available) is required to help predict where a mutation should be placed to increase tolerance of a gatekeeper mutation.

Irreversible kinase inhibitors:

Another method that creates an analogue-sensitive gatekeeper mutant kinase without increasing the size of the ATP binding pocket (and potentially prevents catalytic spine disruption) is the mutation of the gatekeeper residue to a cysteine, which can then be targeted by electrophilic small molecules, which covalently bind to the protein. Initial work was performed on Src, and although no second site mutations in the N lobe were required to maintain catalytic activity, screens to identify new reactive compounds needed to be performed (Garske *et al.*, 2011). If F130C Trib2 displays similar stability, ligand binding and catalytic activity as WT Trib2, then DSF could be used to identify electrophilic inhibitors that bind to F130C Trib2, but not WT Trib2. Additionally, Cys residues are present in over 200 ATP-binding sites in the kinome (Zhang *et al.*, 2009, Liu *et al.*, 2013) and these could be exploited, or Cys residues introduced, into Trib2 so that ligands specifically targeting a Cys residue can be developed.

Recent analysis of the catalytically active pseudokinase HER3 (Shi *et al.*, 2010), a member of the EGFR family, has revealed that upon binding to the ATP-competitive inhibitor Bosutinib, the binding affinity of HER3 for EGFR, which it activates allosterically, increases. This therefore predicts, and was recently validated *in vitro*, that Bosutinib 'inhibition' actually increases HER3-mediated downstream signaling rather than reducing it. A similar property has been observed for the kinase BRAF. The MAPK pathways in cells expressing an oncogenic form of BRAF (BRAF V600E), were blocked following the addition of ATP-competitive RAF

inhibitors. However, in B-RAF WT cells, the 'inhibitors' trigger MEK/ERK phosphorylation (Hatzivassiliou *et al.*, 2010, Claus *et al.*, 2013). This means that following inhibitor treatment of Trib2 (or any kinase domain) the downstream signaling pathways must be fully evaluated to ensure the catalytic activity of the targeted protein, or allosterically-regulated binding partners are not inadvertently activated when the goal was inhibition (as might be the case in Trib2-driven cancers).

The Trib2 interactome:

Although I did not confirm the interaction between Trib2 and a number of binding partners, it is interesting to speculate what the role of these interactions might be if confirmed. An interesting protein that coimmunoprecipitated with Trib2 was STK38, more commonly known as NDR1, which is a key kinase in the Hippo pathway and controls cell size and proliferation through the transcription factor YAP. Interestingly, Trib2 has recently been shown to interact with the E3 ligase βTrCP, and this interaction increases the stability of YAP in liver cells. Moreover, YAP transcriptional activity is inhibited by CEBP/α in liver cancer cells, and Trib2 relieves this repression by targeting CEBP/α for degradation (Wang *et al.*, 2013b). Interestingly, NDR1 (STK38) can phosphorylate YAP *in vitro*, although there is, so far, no evidence of YAP phosphorylation by NDR1 in cell lines (Hao *et al.*, 2008). The consensus sequence of NDR1 phosphorylation identified by Hao et al., is also conserved throughout the AGC kinase family, of which p70S6K is a member. Intriguingly, p70S6K decreased Trib2 stability via phosphorylation of serine 83 (Wang *et al.*, 2013c). The NDR1 phosphorylation consensus sequence observed in YAP, H V R A H S^{127} (H x H/R/K x x S /T) (Hao *et al.*, 2008) is partially conserved surrounding Ser 83 in Trib2: A V H L H S^{83}, with the only deviation being the initial Ala residue. To determine whether Trib2 S83 is phosphorylated by NDR1, the stability of Trib2 could be assessed following transfection of NDR1 siRNA or mutation of Trib2 S83. It would also be interesting to examine whether the activity of NDR1 or the transcriptional activity of YAP was altered in Trib2 K90M overexpressing cells compared to WT because this could indicate whether the binding of ATP by Trib2 influences Trib2 phosphorylation by NDR1, and if so this could potentially be disrupted by the exposure of either HxJ 42 or CZ 30 to F130A or F130G Trib2 overexpressing cell lines. Interestingly, Shroom3, another putative

binding partner of Trib2 identified in Table 4.1, recruits Rho kinases to apical cell junctions (Nishimura and Takeichi, 2008) and Rho kinases are also constituents of the AGC kinase family (Pearce *et al.*, 2010). Creatine Kinase also coimmunoprecipitated with Trib2. It catalyses the reversible phospho transfer from ATP to creatine (Dzeja and Terzic, 2003), and has been predicted to interact with C/EBPβ (Hu *et al.*, 2011b), which has previously been immunoprecipitated with Trib2 from HEK293 cells (Naiki *et al.*, 2007). The relevance of this link is worthy of further investigation. Finally, Protein Arginine N-Methyltransferase 5 (ANM5/PRMT5) was also identified by Mass Spectrometry following FLAG immunoprecipitation of Trib2. ANM5 interacts with other protein kinases and modulates their behaviour, including the activity of EGFR, where it methylates Arg1175, which stimulates the transautophosphorylation of Tyr1173 (Hsu *et al.*, 2011). JAK2 (Pollack *et al.*, 1999) and JAK1, also interact with ANM5 which methylates and activates STAT6 (Igarashi *et al.*, 2009).

Several techniques described in this Chapter have allowed me to demonstrate unequivocally that Trib2 binds ATP, and that the ATP binding domain of engineered Trib2 mutants are targetable by small molecule inhibitors. Throughout the human kinome a large range of K_m values for ATP and ligands have been reported (Knight and Shokat, 2005, Davis *et al.*, 2011, Becher *et al.*, 2013) and the catalytically active pseudokinase CASK has a reported 'low' affinity for ATP with a K_m value 563 μM (Mukherjee *et al.*, 2008). The generation of Trib2 overexpressing cell lines, will allow specific targeting of the ATP binding domain by the identified bulky inhibitors, which could potentially isolate ATP dependent Trib2 driven phenotypes. One very interesting phenotype to be investigated in the future is the turnover of C/EBPα, which has been associated with the progression of AML. When Trib2 was overexpressed, the turnover of C/EBPα increased and the protein level reduced. This caused increased cell transformation and reduced differentiation, which are characteristics of cancerous cells. The proteasomal turnover of C/EBPα is dependent upon the integrity of the Trib2 catalytic motif, with cells that expressed the mutated Trib2 K177R protein displaying phenotypes that were less oncogenic (Keeshan *et al.*, 2010). Recombinant Trib2 K177A produced in *E. coli* displayed a reduced ability to autophosphorylate (Chapter 3), however the ability for Trib2 K177A to bind ATP was not determined by DSF and ideally should be performed in the future.

These findings suggest that if direct ATP binding is required for Trib2-mediated oncogenesis, chemical genetic approaches that use analogue sensitive Trib2 mutants along with DSF, can be used to discover Trib2 ligands that might also be inhibitors, and therefore drug targets.

In this Chapter, I have used different techniques to show that Trib2 *does* bind ATP and that the ATP binding site of Trib2 mutants can be targeted by small molecule analogues. This has demonstrated that the Trib2 ATP binding site is 'druggable', and, to my knowledge, is the first identification of any small molecule ligand that can bind to Trib2. Trib2 is not the only Tribbles pseudokinase that is implicated in disease progression, Trib3 is associated with a variety of diseases, including breast cancer (Wennemers *et al.*, 2011b). In Chapter 3, Trib3 also demonstrated the ability to autophosphorylate and it would be very interesting to see whether DSF can identify ATP binding to Trib3, as it does for Trib2 and SgK495, which would indicate that this member of the Tribbles family also has an ATP binding pocket that could be targeted by ATP analogues. Further work is still required to fully validate the implication of ATP binding by Trib2 upon the oncogenicity of Trib2 overexpressing cells and to determine whether current 'gatekeeper' mutants are active in a cellular environment, or whether further N lobe mutations or generating Trib2 F130C are required to reinstate ATP binding and catalytic activity. What can be appreciated by this work is that by combining techniques such as DSF and chemical genetics, the function of pseudokinases can begin to be elucidated along with the identification of druggable ATP binding sites and the discovery of new pseudokinase-targeted ligands.

4.17 Conclusion

Analysis of Trib2 by DSF enabled the first detection of ATP binding by Trib2 in an assay that is amenable for establishment of large scale Trib2 ligand and inhibitor screens. DSF is a particularly valuable technique for pseudokinase functional analysis, especially when used in tandem with *in vitro* kinase assays as performed here for Trib2. The advantages of following up *in vitro* kinase assays with DSF was observed following disappointing results with a Trib2 DFGK180N mutant, which was designed to 're-activate' this kinase, making it a highly active, Mg^{2+}-dependent kinase. However, Trib2 DFGK180N did not autophosphorylate in the presence of ATP, but after analysis by DSF, it was apparent that the lack of

autophosphorylation was caused, at least in part, because the protein was unfolded prior to the assay. Using DSF as a technique to probe the accessibility of the Trib2 ATP binding site has facilitated the initiation of inhibitor binding trials. Two bulky PP1 analogues that specifically bind to Trib2 F130A and F130G (but not Trib2) have so far been identified. In the future, cell lines overexpressing Trib2, Trib2 F130A or F130G can be exposed to the bulky inhibitors to determine whether inhibiting the ATP binding site causes perturbations to the downstream signalling pathways it has been implicated in regulating, including the analysis of changes to C/EBPα stability, NF-κB signalling, YAP/TEAD transcriptional activation, AKT activation and the MAPK pathway.

By developing the tools and cell lines described in this chapter I have confirmed that Trib2 binds ATP *in vitro*, and facilitated the transition from recombinant *in vitro* functional assessment of Trib2 to identifying that the Trib2 ATP binding site is potentially targetable by small molecule inhibitors in cells. This work might lead to the identification of whether inhibiting ATP binding, or placing a ligand in the unusual Trib2 'nucleotide-binding site' can alter the oncogenic behaviour displayed by Trib2-overexpressing cells in diseases such as AML, ALL, NSCLC and hepatic cancers. This will help determine whether the Trib2 ATP binding site would make a novel drug target, and because the Trib2 pseudokinase domain differs from the majority of the human kinome (does not have the Mg^{2+} binding residues), the therapeutics developed have the potential to be highly specific.

CHAPTER 5. Analysis of NOK, a novel Receptor Protein Tyrosine Pseudokinase

5.1 Introduction

In Chapters 3 and 4 of this thesis, I demonstrated that like the pseudokinase CASK (Mukherjee *et al.*, 2008), Trib2 and Trib3 could also weakly bind to ATP and autophosphorylate in the absence of divalent cations. Both CASK and Trib2 were originally defined as pseudokinases because they lack the Asp residue in the 'DFG' motif of the kinase domain. Consistently, CASK and Trib2 (but not Trib2 containing point mutations in the ATP-binding site) can still interact (weakly) with ATP when assayed using thermal stability assays, which suggests a potential reliance on nucleotide binding for cellular function. In the human kinome, seven other human pseudokinases do not contain a canonical DFG motif, but still retain other conserved residues that clearly define them as protein kinase domains. These residues are defined as the Asp residue in the catalytic loop and a conserved lysine in the β3 sheet of the N lobe kinase, which interacts with the α- and β- phosphates of ATP to facilitate nucleotide positioning and binding (Boudeau *et al.*, 2006). The pseudokinases that contain a magnesium ion binding loop that deviate greatly from the canonical DFG motif are CCK4 (PTK7) (Figure 5.1C), SgK223, SgK269, NOK, Trib1, Trib2 (Figure 5.1 C), Trib3 and SgK495 (Eyers and Murphy, 2013). Interestingly, the pseudokinase Titin, which has a more conservative change in the canonical DFG motif (to EFG), has very recently been reported to be catalytically inactive (Bogomolovas *et al.*, 2014). However, both Trib2 and Trib3 have demonstrated the ability to autophosphorylate *in vitro*, but only in the absence of divalent cations (Chapter 3), while SgK495, although unable to autophosphorylate under the conditions tested, appears to bind to ATP when analysed by DSF (Chapter 4).

A particularly interesting pseudokinase in which the DFG motif is mutated is NOK (Novel Oncogenic Kinase), which has also been termed STYK1 (Serine/Threonine/Tyrosine Kinase 1) and SuRTK106 (Sugen Receptor Tyrosine Kinase 106). Analysis of the human, mouse and *Xenopus tropicalis* NOK amino acid sequences reveals a predicted transmembrane domain located between residues 26-

49 in the N-terminus of NOK (human numbering, Figure 5.1A,B). Along with this putative hydrophobic transmembrane domain, the NOK gene also encodes a pseudokinase domain, and residing in this domain is a catalytic motif that closely resembles those observed in the tyrosine kinase sub-family, namely HxDxAARN (Figure 5.1C) (Kannan *et al.*, 2007, Lemmon and Schlessinger, 2010, Mendrola *et al.*, 2013). Specifically, NOK has also retained the canonical His, catalytic Asp, two Ala residues, an Arg and an Mg^{2+}-coordinating Asn, all of which are typically found in the catalytic motif of tyrosine kinases. However, the magnesium-ion binding motif in the 'DFG' motif (which is also highlighted in Figure 5.1C), is highly atypical compared to those observed in canonical tyrosine kinases, because NOK has evolved a GLG sequence. As discussed previously, both the Asp and Phe residues in this motif are important for kinase activity, and NOK shares between 20-30% overall amino acid identity with the Platelet-Derived Growth Factor (PDGF) and Fibroblast Growth Factor Receptor Protein Tyrosine Kinase family members (Liu *et al.*, 2004). Interestingly, however, NOK lacks a prominent extracellular domain, in marked contrast to other growth factor receptors linked to tyrosine kinases and no extracellular or intracellular ligand binding domains are predicted when the protein sequence is interrogated by bioinformatic or biochemical evaluation.

A

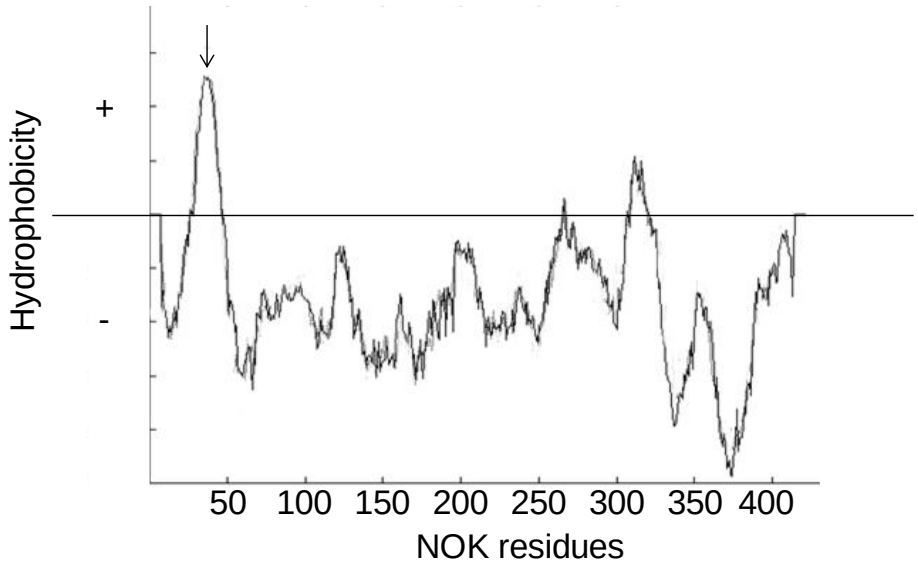
Hydrophobicity
+
-
50 100 150 200 250 300 350 400
NOK residues

B

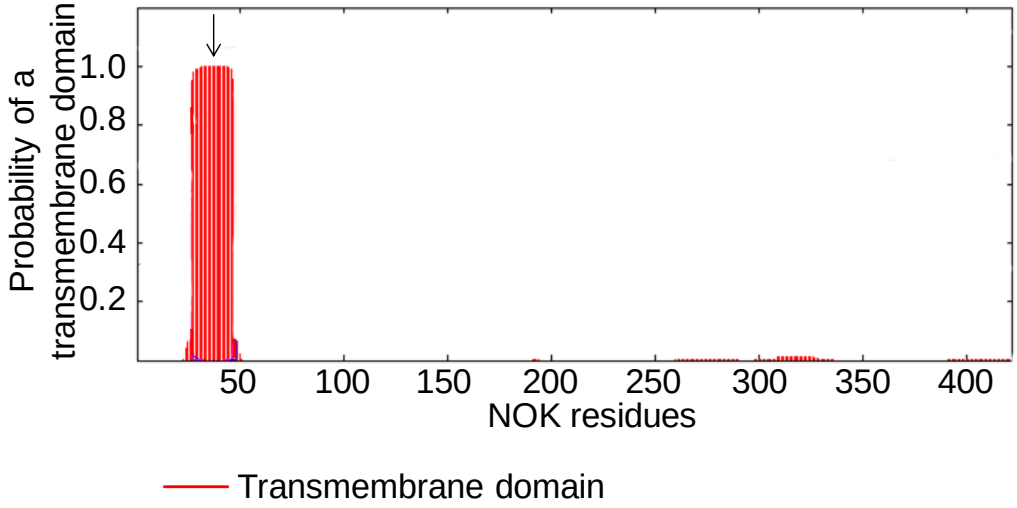
Probability of a transmembrane domain
1.0
0.8
0.6
0.4
0.2
50 100 150 200 250 300 350 400
NOK residues
Transmembrane domain

C

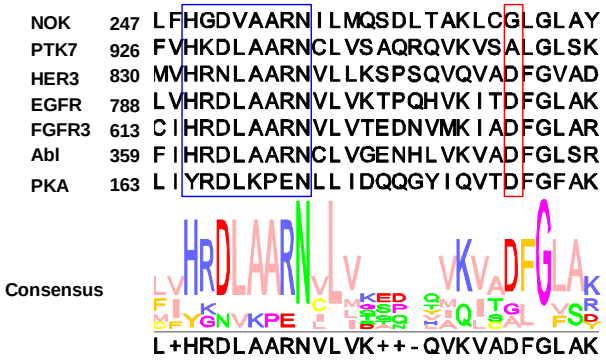
NOK 247 LFHGDVAARNILMQSDLTAKLCGLGLAY
PTK7 926 FVHKDLAARNCLVSAQRQVKVSALGLSK
HER3 830 MVHRNLAARNVLLKSPSQVQVADFGVAD
EGFR 788 LVHRDLAARNVLVKTPQHVKITDFGLAK
FGFR3 613 CIHRDLAARNVLVTEDNVMKIADFGLAR
Abl 359 FIHRDLAARNCLVGENHLVKVADFGLSR
PKA 163 LIYRDLKPENLLIDQQGYIQVTDFGFAK
Consensus
L+HRDLAARNVLVK++-QVKVADFGLAK

Figure 5.1 Bioinformatic analysis of NOK predicts a single pass transmembrane domain and an intracellular tyrosine kinase like-pseudokinase domain. A) TMPred output following analysis of all NOK residues (1-422) highlights the presence of a predicted single pass transmembrane domain, which lies between residues 26 and 49. Positive Y-axis values on the hydropathy plot represent predicted hydrophobic regions, whilst negative values are hydrophilic, and therefore are not predicted to form a transmembrane region. The X-axis represents the NOK residue number. B) TMHMM software predicts, as the TMPred software did in A, that the residues between 26-49 form a membrane-spanning helix. Predicted transmembane regions are denoted with an arrow in A and B. C) The catalytic loops and DFG motifs of the pseudokinases NOK and PTK7, which both have a non-DFG metal ion binding Asp (red box) were aligned using MUSCLE software, using HER3 pseudokinase (which lacks the catalytic Asp) and the canonical active RPTKs EGFR, and FGFR3 for comparison. Abelson kinase (Abl) is a cytoplasmic TK, and also forms part of this analysis as does the Ser/Thr kinase PKA for comparative purposes. The consensus motifs emerging from the alignment is displayed underneath using Weblogo, a graphical representation of the amino acid multiple sequence alignment where the height of the amino acid is proportional to its relative conservation in a motif.

NOK research remains in its infancy, with the majority of the literature focusing on the finding that NOK mRNA is commonly overexpressed in human tumors, including acute leukemia (Kondoh *et al.*, 2009), ovarian (Jackson *et al.*, 2009), castration-resistant prostate (Chung *et al.*, 2009), and breast cancers (Kimbro *et al.*, 2008). NOK has also been implicated in the metastatic progression of cancer cells (Liu *et al.*, 2004). Interestingly, a fusion between the extracellular domain of mouse erythropoietin receptor (EPOR) and the NOK-transmembrane-and-intracellular domain, termed EPOR/NOK has been suggested to be 'constitutively active' leading to EPOR/NOK dimerisation and autophosphorylation of NOK (Liu *et al.*, 2004). In a separate study by the same group, immunoprecipitated EPOR/NOK was assayed using an *in vitro* kinase assay, which demonstrated autophosphorylation of the fusion protein (Chen *et al.*, 2005b). However, contamination by other kinases was neither controlled for, nor ruled out, although the fusion protein might well alter the conformation or behavior of NOK. If NOK can bind to ATP, and if ATP binding is important for NOK-driven oncogenesis, then the ATP binding site of NOK might become a novel drug target in the future should cancer cells exhibit specific sensitivity to NOK ligands/inhibitors. Other RPTK ATP binding domains that have been successfully targeted in clinical trials include EGFR (Berardi *et al.*, 2013), BCR-Abl (Zhang *et al.*, 2010), c-Kit (Ashman and Griffith, 2013), SRC (Creedon and Brunton, 2012) and PDGFR (Michael *et al.*, 2010), and because NOK overexpression has been implicated in a number of blood-borne and solid cancers, it is important to determine whether it too, can, be targeted with kinase ligands that might function as inhibitors in cells. As discussed in Chapters 3 and 4, approaches that combine elucidation of the cellular biology and biochemistry of pseudokinase are important to determine both function and potential 'druggability.' The results described in this Chapter represent some of the preliminary findings from my evaluation of human NOK.

To identify cell lines that expressed detectable levels of NOK, a panel of 13 cell lines (described in Chapter 4) were immunoblotted using a commercial NOK antibody (Figure 5.2). However, apart from the positive control lane, which contained recombinant GST-His NOK that had been expressed in *E. coli* and purified by IMAC, no NOK signal was detected following either a 10 minute or 60 minute exposure, and this limited my ability to analyse endogenous NOK cellular behavior. To counter this potential problem, inducible cell lines that expressed

recombinant epitope-tagged NOK were therefore generated (Figure 5.3). In addition, a differential analysis of NOK expression in cancer samples compared to normal samples was undertaken using the Oncomine database (summarized in Table 5.1), which showed that NOK expression in cancer cell lines varied markedly. For example, superficial bladder cancer showed a 10-fold increase in NOK expression, while NOK expression in pancreatic, testicular, skin and ovarian carcinomas was ~5-6 fold greater than normal tissues, whilst lung carcinoma NOK expression was four times higher than controls. NOK overexpression was also detected in renal cell carcinomas, at levels some 3 times higher than in normal kidney tissue. Elevated NOK mRNA expression has previously been reported in 92.3% (12/13) of lung tumor tissues analysed from a small cohort of patients and compared to samples from healthy patients. Moreover, in lung cancer tissues, NOK mRNA was detected in 97.6% (40/41) of the samples compared to normal tissue, where only 38% (5/13) of the samples stained positive for NOK mRNA (Amachika *et al.*, 2007). Currently, and to my knowledge, there have been no reported associations between elevated NOK expression in either bladder or pancreatic carcinomas, and the four epithelial bladder cell lines analysed in this work did not reveal any detectable expression of NOK using a commercial antibody (Figure 5.2). NOK mRNA was, however, undetectable by Northern blot analysis of normal pancreatic samples (Liu *et al.*, 2004), and this same group detected high levels of NOK mRNA expression in human 293T cells. However, when I probed HEK293 cell extracts with a NOK antibody, no immunoreactive band was detected by western blotting (Figure 5.2). Furthermore, NOK mRNA was reported by RT-PCR in a panel of ovarian cancer cell lines (including SkOv3), which expressed different forms of the Oestrogen receptor, and in a small sample study, malignant ovarian tissues stained strongly for NOK, whereas benign tissues were only weakly immunoreactive and no immune-staining was observed in normal ovarian tissues (Jackson *et al.*, 2009). All of these findings suggest that high levels of NOK mRNA, (but not necessarily NOK protein), are associated with cancer and that the cellular function of NOK requires further investigation.

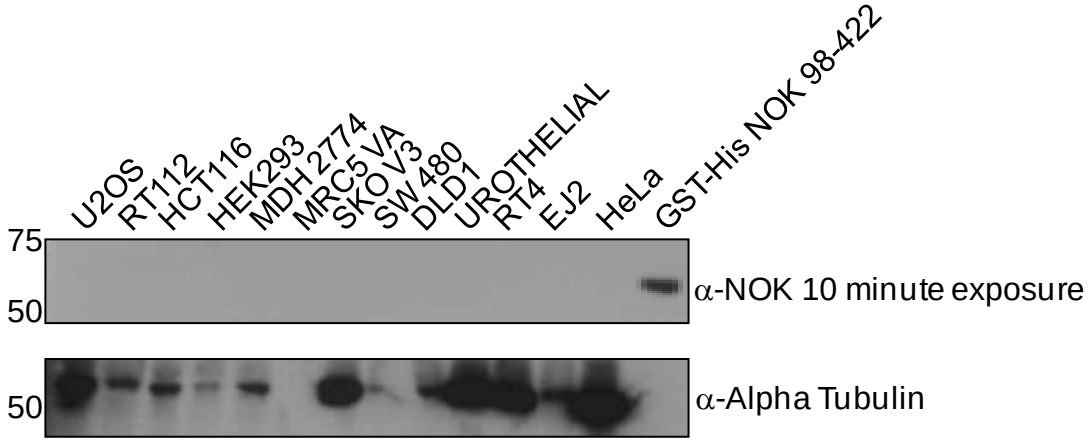

Figure 5.2 Endogenous NOK was not detected in any of the cell lines tested. Thirteen cancer cell lines were lysed in 1% Triton X-100, and soluble lysates were immunoblotted with a NOK antibody. Five hundred nanograms GST-His tagged NOK was included as an antibody control and the relative loading was determined by a comparison of the levels of detected alpha-tubulin (same experiment as Figure 4.19).

Cancer	Fold change	Oncomine Dataset	Reference to Primary Study
Superficial Bladder Cancer	10.814	Sanchez-Carbeyo Bladder 2	(Sanchez-Carbayo *et al.*, 2006)
Pancreatic Carcinoma	5.92	Pei Pancreas	(Pei *et al.*, 2009)
Testicular Embryonal Carcinoma	5.146	Skotheim Testis	(Skotheim *et al.*, 2005)
Actinic (Solar) Keratosis	4.782	Nindl Skin	(Nindl *et al.*, 2006)
Ovarian Serous Adenocarcinoma	4.631	Yoshihara Ovarian	(Yoshihara *et al.*, 2009)
Lung Adenocarcinoma	3.936	Su Lung	(Su *et al.*, 2007)
Lung Adenocarcinoma	3.658	Okayama Lung	(Okayama *et al.*, 2012)
Chromophobe Renal Cell Carcinoma	3.014	Jones Renal	(Jones *et al.*, 2005)

Table 5.1 A summary of NOK overexpression reported in the Oncomine database. NOK overexpression was examined by performing a 'Cancer versus Normal' analysis. The tissues that had the highest fold change compared to normal (p=0.05) are listed using an arbitrary 3-fold change cut-off. The names of the datasets and primary study citations are listed.

5.2 Overexpression of epitope-tagged NOK in human cells

To facilitate an analysis of NOK signaling in the model HeLa ovarian human cancer cell line, HeLa Flp-In T-REx parental cells were transfected with full-length human NOK cDNA cloned in the pcDNA5 FRT/TO vector that was individually tagged at either the C terminus with a FLAG epitope (predicted intracellular epitope tag) or at the N terminus with a Myc epitope (predicted extracellular epitope tag). The pseudokinase domain is located between amino acids 114 and 384, C-terminal to the putative transmembrane domain. After addition of Tetracycline (Tet), epitope tagged NOK protein expression was evaluated by western blotting and immunofluorescence. To test the expression and solubility of NOK after cell lysis, cell extracts were made by employing cell lysis buffer that contained either 0.1% Triton X-100 or 1% Triton X-100, which will vary the amount of membrane-bound proteins solubilised. Proteins were resolved by SDS-PAGE and transferred to nitrocellulose membrane. The membrane was then probed with commercial antibodies corresponding to each specific epitope tags.

As shown in Figure 5.3 A, immunoblotting with anti-Myc antibody confirmed that Myc-tagged NOK and alpha tubulin (detected by an alpha tubulin reactive antibody used as a loading control) were both present in the ‘soluble’ (0.1% Triton) and ‘insoluble’ (0.1% Triton pellet resuspended in SDS) fractions. The inducibility of the system was confirmed because Myc-NOK was observed only in the lysates that had been prepared from cells treated with Tetracycline (Figure 5.3 A).

The proportion of full length NOK present in the soluble lysates was increased by lysing the Myc-tagged full length NOK expressing cells (Figure 5.3 B) and FLAG tagged full length NOK (Figure 5.3 C) expressing cells in a cell lysis buffer that consisted of 1% Triton X-100. The lysates and insoluble pellets were resolved by SDS-PAGE. The resulting signals observed following immunoblotting of the epitope tags, confirmed that by increasing the Triton X-100 concentration, the proportion of soluble NOK (and also alpha tubulin) increased.

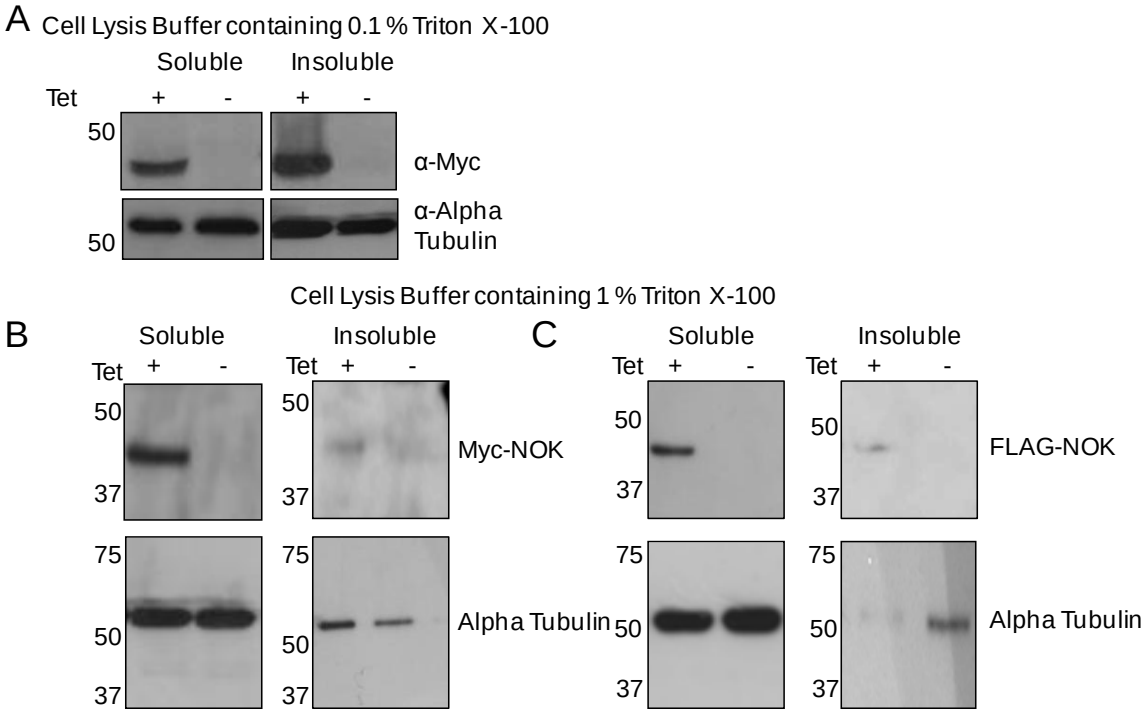

Figure 5.3 Expression of epitope-tagged NOK in stably transfected HeLa Flp-In T-REx cells. Myc tagged NOK expressing HeLa Flp-In T-REx cells were lysed in cell lysis buffer that contained either A) 0.1% Triton X-100 or B) 1% Triton X-100. The soluble and insoluble fractions were resolved by SDS PAGE and western blotted with an α-Myc antibody and the loading determined by analysis of alpha tubulin levels C) FLAG tagged full length NOK expressing cells were lysed in the 1% Triton X-100 containing lysis buffer and following western blotting, the inducibilty of the cells was determined by probing the membrane with a FLAG antibody. Alpha tubulin was used to analyse the loading. Epitope tagged NOK expression was induced by Tetracycline (Tet).

5.3 Epitope-tagged NOK co-localises adjacent to mitotic chromatin

Following the generation of human cell lines expressing tagged-NOK, it was important to try to identify its cellular localization, and try to help correlate this with its function. Amino acid analysis suggested that NOK has a putative transmembrane domain between amino acids 26 and 48 (Figure 5.1). However the reported localization of NOK differs throughout the literature, with EGFP-tagged NOK reported to be found in the cytosol (Liu *et al.*, 2004), whilst HA-tagged NOK localizes to endosomal compartments (Ding *et al.*, 2012). HeLa Flp-In T-REx cells that expressed Myc-tagged full length NOK were therefore stained with DAPI, a fluorescent stain that binds to DNA and highlights the nucleus, allowing the visual differentiation of mitotic cells from cells in interphase by virtue of the chromosomal condensation that occurs in mitotic cells. Myc- tagged NOK was fluorescently stained with an anti-Myc epitope antibody and visualized with a corresponding secondary antibody conjugated to a fluorophore. As shown in Figure 5.4A, intense fluorescence was observed surrounding the mitotic chromatin of Tet-treated cells, whereas no signal was observed for Tet-negative cells. A similar pattern of staining was observed for cells probed with an anti-Lamin B1 antibody (Figure 5.4B). Lamin B1 usually lines the inner nuclear envelope, but in mitotic cells Lamin B1 is cleaved (Chandler *et al.*, 1997), which facilitates mitotic progression by dissolution of the nuclear envelope and allowing the mitotic spindle to access the condensed chromatin (Burke, 2001).

5.4 Myc tagged NOK expression increases in mitosis

To evaluate if there was any change to the levels of expressed tagged NOK during mitosis, HeLa Flp-In T-REx cells were treated with Nocodazole, which arrested the cell cycle during mitosis due to its ability to depolymerise the mitotic spindle and activate the spindle assembly checkpoint (SAC) (Jordan *et al.*, 1992). Nocodazole-treated and control cells were harvested (adherent and non-adherent mitotic cells) in both Tet positive and untreated populations, resolved by SDS-PAGE on a 15% gel and then immobilized on a membrane that was excised at ~50 kDa and ~25 kDa. The 50 kDa-25 kDa section was probed with an anti-Myc antibody, which detected Myc-tagged NOK in Tet-exposed cells, with a more intense signal observed in nocodazole-treated cells (Figure 5.5). Alpha tubulin was used as a loading control and the increased level of phosphorylated Histone H3 in nocodazole treated cells

confirmed that cells were enriched in the mitotic phase of the cell cycle, when this Histone mark is maximal (Ota *et al.*, 2002).

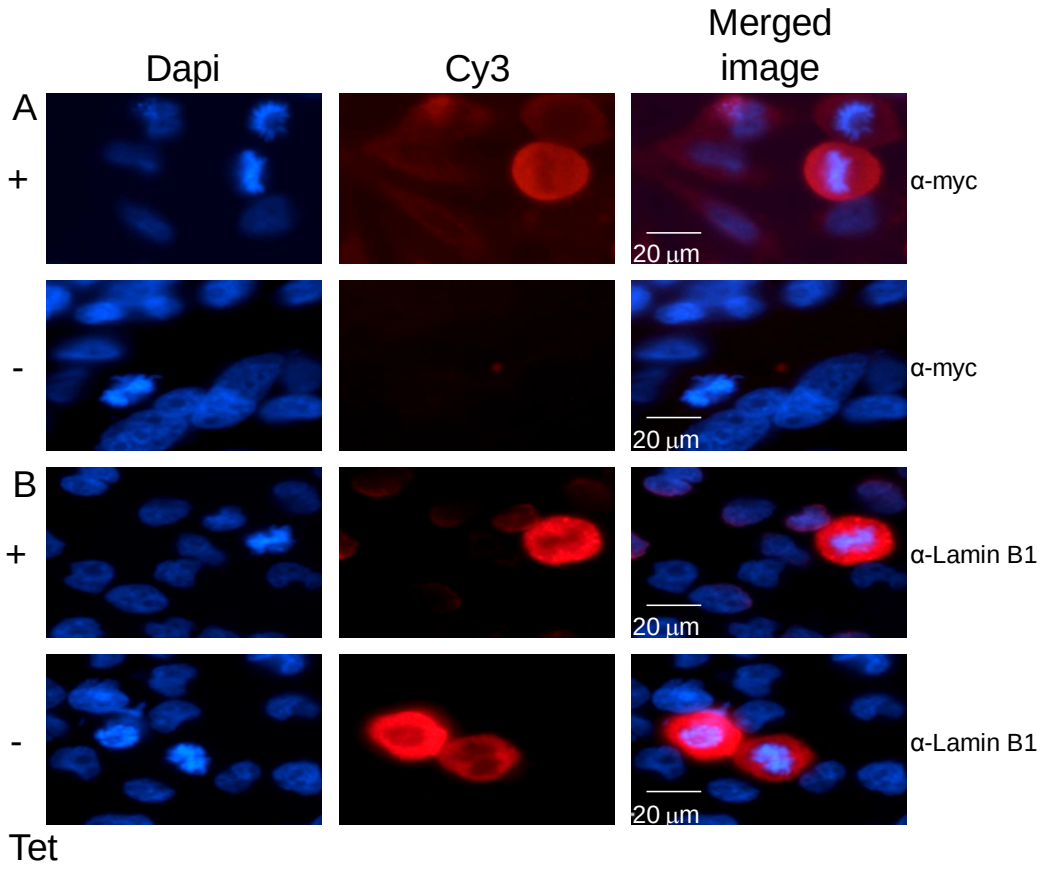

Figure 5.4 Intense NOK staining is observed surrounding mitotic chromatin. HeLa Flp-In T-REx cells were transfected with Myc-tagged full length NOK. The cells in the top panels of both A and B were cultured in media that was supplemented with Tetracycline. Nuclear chromatin was stained with DAPI. Cells were probed with a primary antibody that targeted the A) Myc epitope of Myc tagged NOK, or B) Lamin B1, a resident protein of the inner nuclear envelope. The cells were incubated with a secondary Cy3 fluorophore conjugated antibody that recognised the primary antibodies. The right hand panel is a merged image of the DAPI and Cy3 fluorescence signals.

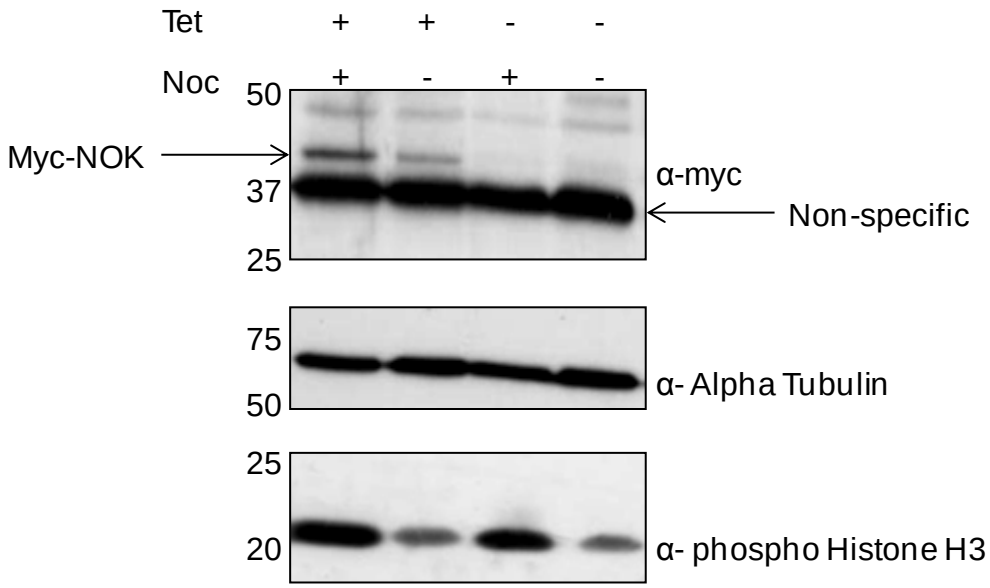

Figure 5.5 Western blot analysis of cells arrested in mitosis. HeLa Flp-In T-REx cells stably transfected with Myc-tagged full length NOK were treated with tetracycline (Tet) and nocodazole (Noc). The lysates were subjected to SDS-PAGE and western blotting. The membranes were probed with either an α-Myc (top panel), α-alpha tubulin (middle panel) or α-phospho Histone H3 (lower panel) antibody. Myc tagged NOK and non-specific bands have been highlighted.

5.5 Epitope-tagged NOK stains the 'nuclear rim' of HeLa cells

In non-mitotic cells that expressed either Myc (Figure 5.6 A) or FLAG-tagged NOK (Figure 5.6 B), the nuclear rim and organelles surrounding the cytosolic side of the nucleus were strongly stained, but notably no fluorescence was detected surrounding the nucleus of Tet-negative cells, which indicated that the detected signal was NOK-specific. Not all cells showed the same intensity of NOK staining, despite all cells being stably transfected in the population. This may indicate that cells expressed different levels of NOK at different stages of the cell cycle, the intense staining observed around mitotic nuclei and in mitotic lysates (Figures 5.4 and 5.5) are further examples of this. The observed fluorescent signals for N-terminal Myc tagged NOK and C-terminal FLAG tagged NOK were similar, which demonstrated that subcellular localization is not affected by the presence of the epitope tag.

Further validation that the observed indirect immunofluorescence was of the epitope tagged NOK and not non-specific background was obtained by a marked decrease in signal in Myc-tagged NOK expressing cells that were treated with a pool of NOK targeting siRNA, when compared to the staining of cells transfected with a non-coding siRNA control pool or cells treated with the transfection reagent alone (Figure 5.7 A). Consistently, siRNA treated Tet-induced cells had a similar level of background staining as the uninduced cells.

In agreement with my immunofluorescence analysis, western blotting also showed that Myc-NOK expression decreased when cells were transfected with a NOK targeting siRNA pool. In the lysates that had been treated with NOK siRNA, no Myc signal was detected at the molecular weight expected for Myc-tagged NOK (Figure 5.7 B). Myc-NOK was still detected in induced lysates treated with the non-coding siRNA control or the transfection reagent lipofectamine. Myc NOK was detected in the Myc tagged NOK control lysate.

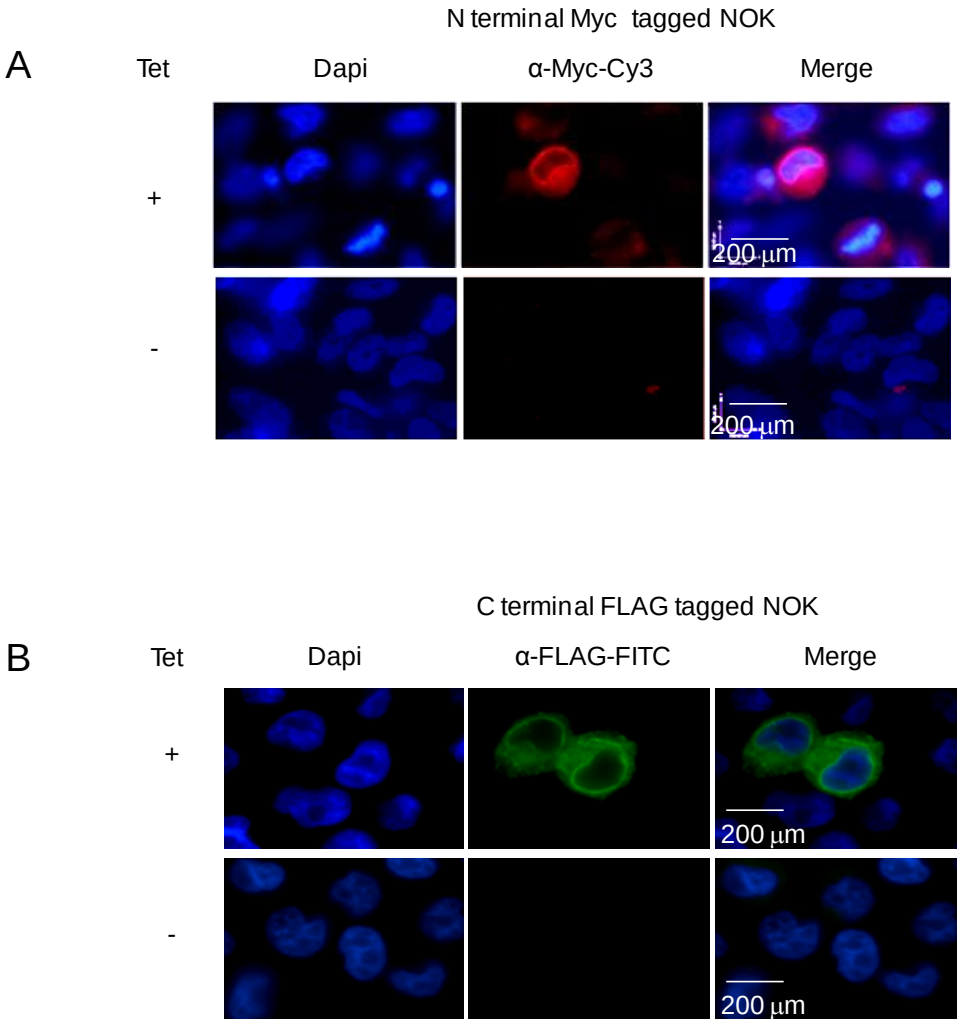

Figure 5.6 Tagged NOK localises to the nuclear membrane. A, B) The localisation of overexpressed NOK was determined by indirect immunofluorescence microscopy. Cells were grown on glass coverslips prior to fixing in 3.7 % paraformaldehyde (PFA). The cells in the upper panels of A and B were treated with Tet A) NOK overexpression in HeLa Flp-In T-REx cells was observed with an α-Myc primary antibody and a Cy-3 conjugated secondary antibody B) FLAG tagged NOK localisation was determined by probing the cells with an α-FLAG primary antibody, which permitted visualisation of the FITC-conjugated secondary antibody.

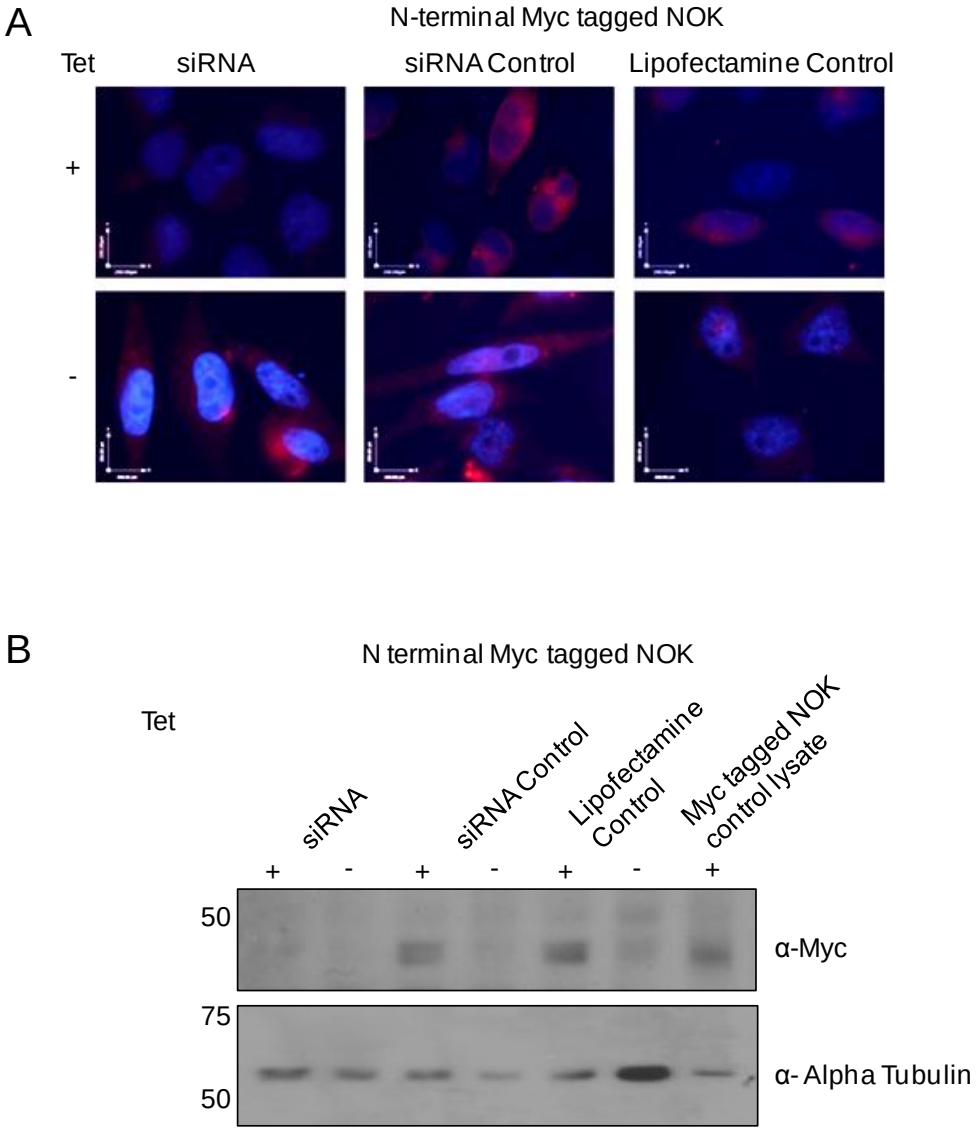

Figure 5.7 Overexpressed NOK protein levels can be decreased by siRNA Two hundred pmoles of an siRNA pool containing equal molar amounts of 4 NOK specific siRNAs, and 200 pmoles of a non-coding siRNA pool were transfected (alongside a lipofectamine control) into Myc tagged NOK expressing HeLa Flp-In T-REx cells that were grown in dishes containing glass coverslips. A) After 64 hours, the cells attached to the glass coverslips were fixed in 3.7 % PFA and stained with DAPI and α-Myc-Cy3 and subjected to immunofluorescence. B) The cells that had adhered to the plastic dishes were harvested in cell lysis buffer containing 1 % Triton X-100. Twenty micrograms of total protein was transferred immunoblotted with an α-Myc antibody, and an α-alpha tubulin antibody to visualise relative protein loading.

5.6 Epitope tagged NOK co-localises with Lamin B1

In Figure 5.6, along with potential endosomal staining, the edge of the nucleus appeared to be highlighted. To determine if NOK localised to the nuclear envelope, the cells expressing Myc-tagged NOK were probed with a Lamin B1 antibody. Lamin B1 is a protein that localizes to the inner nuclear membrane (INM) and is a nuclear membrane marker (Bocock *et al.*, 2010, Dreger *et al.*, 2001). Colocalisation of Myc tagged NOK and Lamin B1 in non-mitotic cells (Figure 5.8) was determined by indirect immunofluorescence, which demonstrated that NOK also localized to the nuclear envelope in addition to the perinuclear region of the cytoplasm, consistent with a previously reported endosomal expression pattern (Ding *et al.*, 2012).

5.7 A sequence that corresponds to the nuclear localization sequence observed in the EGFR family members is also conserved in NOK

To identify any potential nuclear membrane localisation sequences, *MUSCLE* software was used to align NOK with the Nuclear Membrane Localisation Sequence of a well known nuclear membrane protein, Human Cytomegalovirus Glycoprotein B (Meyer and Radsak, 2000). A region of NOK that aligned to the HCMV Glycoprotein B localization sequence was identified, and this included the conservation of two positively charged Arg residues, R377 and R379 in human NOK (Figure 5.9 A). Interestingly, when either of these Arg residues were mutated in Glycoprotein B, its cellular localization was altered dramatically (Meyer and Radsak, 2000). This sequence has also been identified in other known nuclear membrane proteins including the Lamina associated proteins LAP1 and LAP2 and the Lamin B receptor protein (Meyer *et al.*, 2002). Other RPTK proteins that translocate into the nucleus via the nuclear envelope are members of the EGFR family. EGFR translocates through the Nuclear Pore Complexes (NPCs) to the inner nuclear membrane (INM) by the action of importin β, before being released into the nucleus by the INM localised Sec61β (Wang *et al.*, 2010). Incidentally, as well as sharing the tripartite NLS observed in EGFR (Figure 5.9 B), NOK has also recently been shown to co-localise with EGFR in membrane-bound vesicles (Ding *et al.*, 2012). The EGFR NLS sequence is also conserved in the other 3 family members, ErbB2, 3 and 4 (Hsu and Hung, 2007, Chen *et al.*, 2005a). Finally, this signal motif has also been identified in the E3 ligase RNF13, which localizes to endosomes and colocalizes with Lamin B1 in the inner nuclear membrane (Bocock *et al.*, 2010), and published

immunofluorescence staining resembled the immunofluorescence observed for epitope tagged NOK in non-mitotic cells. The RNF13 nuclear membrane localization sequence has been identified in RNF13, and is very similar to the EGFR localization sequence (Bocock *et al.*, 2011) described above. The same NOK Arg residues (R337 and R379) that aligned to the arginine residues critical for Glycoprotein B translocation to the nuclear membrane, also aligned with Arg residues present in the conserved NLS sequences of the EGFR family (Figure 5.9 B) and RNF13 (Figure 5.9 C). In ErbB3 and NOK, the position of this conserved localization sequence is in the C-terminal region of the pseudokinase domain (Figure 5.9 D). In EGFR, ErbB2 and ErbB4 the NLS is located within the juxtamembrane domain (Hsu and Hung, 2007).

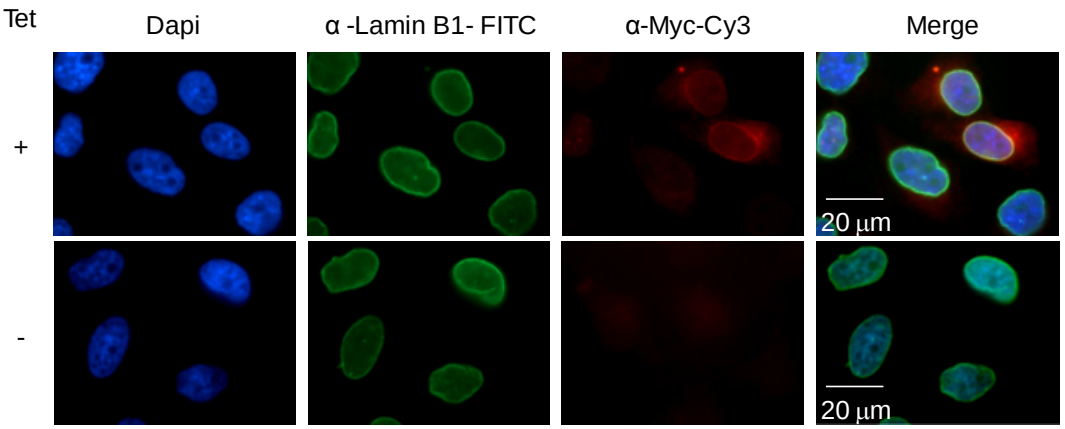

Figure 5.8 NOK colocalised with Lamin B1 at the inner nuclear membrane. Stably transfected Tet-inducible HeLa Flp-In T-Rex cells that expressed Myc tagged NOK were fixed with 3.7% PFA. The cell nuclei were highlighted with DAPI stain, Lamin B1 and a FITC conjugated secondary antibodies were used to highlight the nuclear membrane, and a Myc antibody with a Cy3 fluoprophore secondary was used to analyse the location of Myc-tagged NOK. The individual images were merged using Volocity software (Improvision)

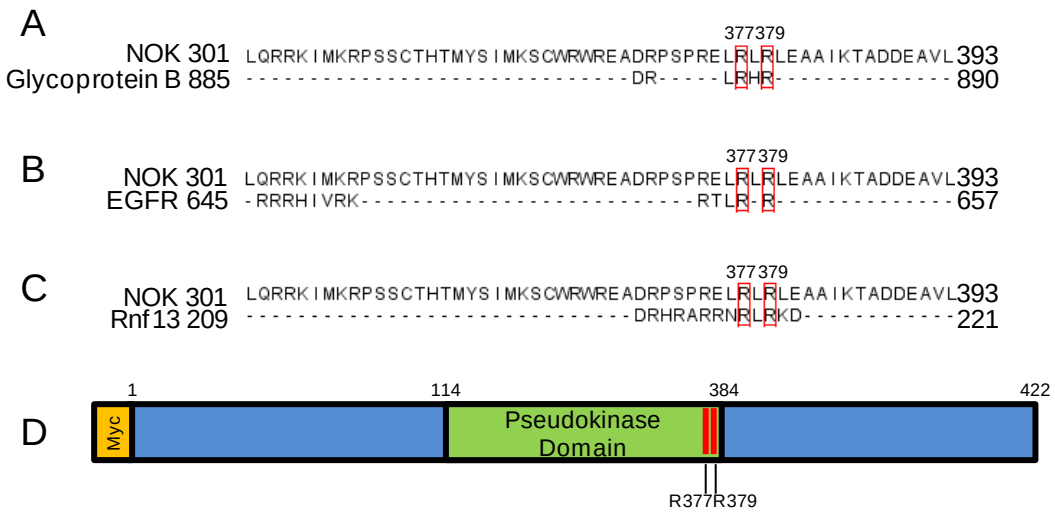

Figure 5.9 NOK R377 and 379 align with Arg residues in published nuclear membrane localisation sequences. The published localisation sequences of A) Glycoprotein B, B) EGFR and C) RNF13 were aligned with NOK using the MUSCLE alignment software and NOK R377 and R379 and the corresponding aligned residues are highlighted in red boxes. D) The position of these two Arg amino acids in relation to the pseudokinase domain of NOK is shown in the cartoon of the full length protein.
The Myc tag is depicted by the yellow box, and the pseudokinase domain in green. For reference the residue numbers corresponding to the domain boundaries are noted above the protein.

5.8 Evaluating putative NOK nuclear localization sequences

The importance of the two conserved Arg residues (R377 and R379) for NOK subcellular localization in the nuclear envelope was determined by immunofluorescence analysis of the point mutants NOK R377A and NOK R379A. The localization of HCMV Glycoprotein B to the inner nuclear membrane was prevented upon mutation of either of the Arg residues corresponding to NOK uncharged Ala residues (Meyer and Radsak, 2000). However, following immunofluorescence analysis of the corresponding NOK single point mutants (Figure 5.10 A and B), no localization change was observed compared to WT (Figure 5.10 C), with the fluorescent signal still detectable around the nuclear envelope and the perinuclear region of the Tet-treated cells. Consistently, there was no signal observed in the Tet-negative cells. To evaluate the effects of mutating both amino acids, doubly-mutated NOK was generated and expressed. As shown in Figure 5.11, this double mutant does display a different localization pattern when compared to NOK WT, NOK R377A and NOK R379A single point mutants and colocalization with the inner nuclear membrane marker Lamin B1 was abolished (Figure 5.11 A). Doubly mutated NOK, on the other hand was not observed in endosome-like structures and did not colocalize with Lamin B1 (Figure 5.11 B). No signal was detected in the cells that were not treated with Tet. The altered localisation indicated that the motif in which these residues occur (and that is also conserved in the EGFR family of tyrosine kinases), is important for the subcellular localisation of NOK.

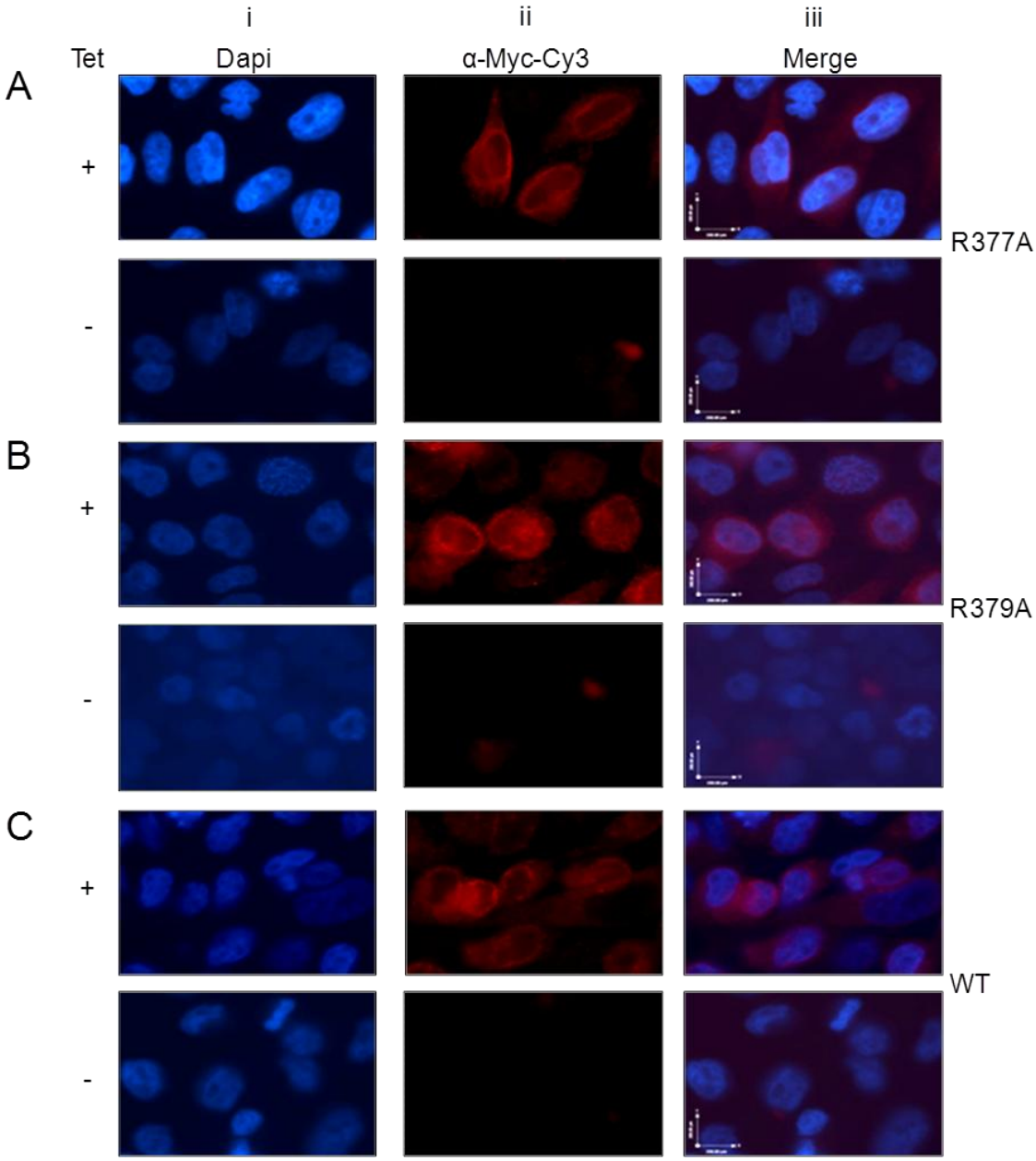

Figure 5.10 Single point mutations to the putative nuclear membrane localisation sequence do not alter NOK localisation HeLa Flp-In T-REx cells overexpressing either A) NOK R377A. B) NOK R379A or C) NOK WT were fixed in 3.7% PFA. A-C i) DAPI stained nuclei. A-C ii) Primary antibody recognises the Myc epitope and the secondary antibody was raised against murine proteins and conjugated to a Cy3 fluorophore. A-C iii) Merged image of i and ii.

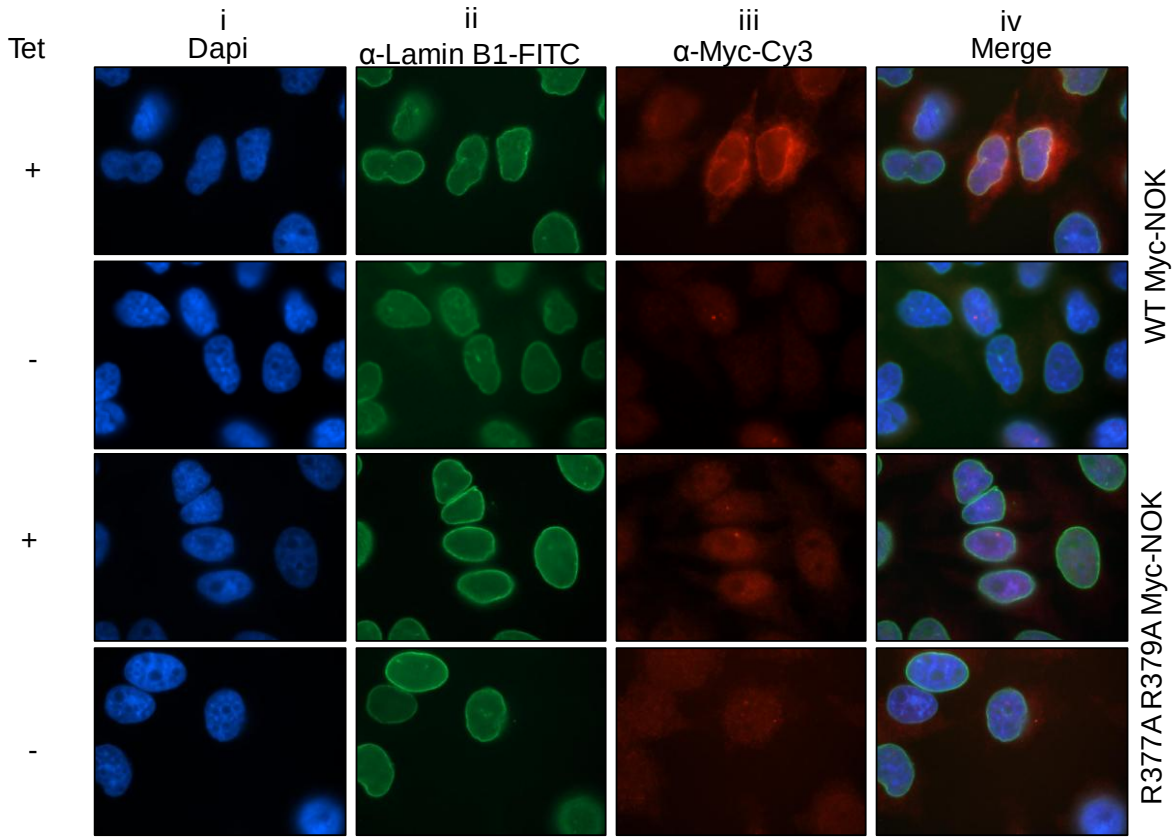

Figure 5.11 The localisation of doubly mutated NOK R377A R379A is altered compared to WT. A and B) HeLa Flp-In T-Rex cells were transfected with WT Myc-NOK whilst C and D) expressed the double mutant Myc-NOK R377A R379A. A-D i) Nuclei were stained with DAPI. A-D ii) The nuclear membrane of the cells was observed by a Lamin B1 antibody and the FITC conjugated secondary. A-D iii) The Myc epitope of Myc-tagged NOK was stained with an anti-Myc antibody and Cy3 fluorophore secondary. A-D iv) Merged image of i, ii and iii. A and C) Cells were treated with Tetracycline

5.9 A point mutation to the conserved β3 lysine of NOK reduces the level of phosphorylated ERK1/2 in cells

It was first reported in 2001 that nuclear localized EGFR was a functional transcription factor that associated with the promoter region of the cyclin D1 gene (Lin *et al.*, 2001). Since then nuclear EGFR has also been shown to bind the promoter regions of several genes including BCRP, Aurora A and iNOS (Brand *et al.*, 2011). To determine the role that NOK plays following its trafficking to the nuclear membrane, it was important to assess whether the pseudokinase domain has the ability to be catalytically active.

To determine whether the catalytic domain of NOK might be functionally important, the levels of phosphoERK1/2 (active ERK1/2) were analysed following overexpression of either NOK, NOK K147M (the 'catalytic' lysine analogous to Trib2 K90 or PKA K72 mutated to an uncharged residue), or NOK G269D L270F (a NOK double mutation termed NOK DFG-in, which reinstates the canonical Mg^{2+} ion binding residue and the Phe residue completing the DFG motif). Previous analysis of ERK 1/2 phosphorylation showed that the levels correlated with the level of overexpression of NOK (Li *et al.*, 2009). However, the level of phosphorylated ERK1/2 detected in lysates overexpressing NOK or NOK DFG-in mutant resembled the levels observed in the uninduced cell lysates. Lysates that contained NOK K147M however, had a reduced level of ERK1/2 phosphorylation, compared to NOK and NOK DFG expressing and uninduced lysates. The levels of total ERK1/2, and alpha-tubulin, which was used as a total protein loading control, were very similar (Figure 5.12), suggesting that NOK might generate an intracellular signal that impinges on ERK activation.

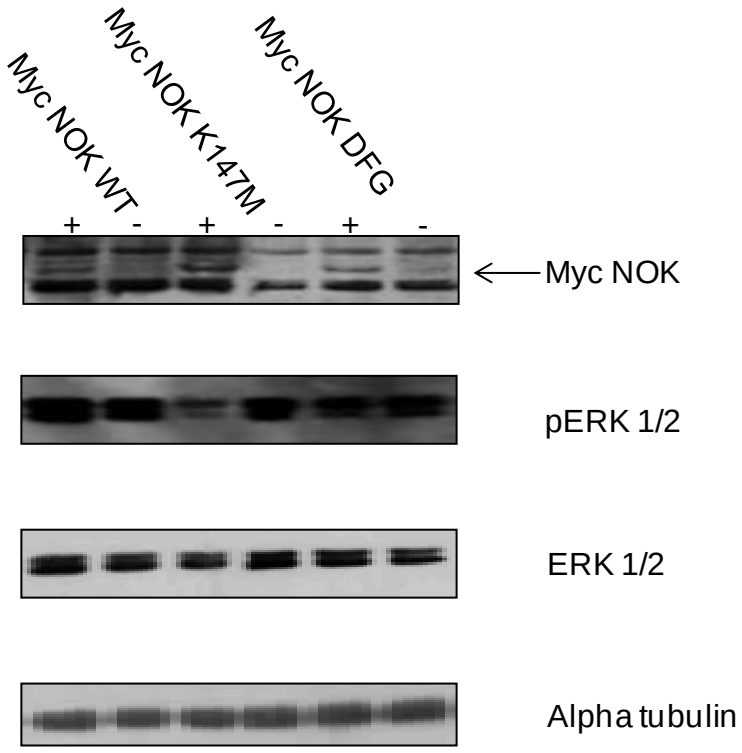

Figure 5.12 The levels of phosphoERK are reduced in cells overexpressing NOK K147M mutant. HeLa Flp-In T-REx cell lysates containing overexpressed NOK WT, K147M and DFG and minus Tet control lysates were resolved by SDS-PAGE. The protein was transferred to membrane by western blot and was probed with an αMyc antibody (top panel) and Myc-NOK is annotated with an arrow, αpERK 1/2 antibody (third panel), α total ERK 1/2 (bottom panel) and α alpha tubulin (bottom panel).

5.10 Lack of evidence for *in vitro* NOK ATP binding or autophosphorylation

In addition to a cellular analysis of NOK, its biochemical functions were also examined *in vitro* using partially-purified recombinant proteins. The potential for NOK to demonstrate some (low) kinase activity is high, especially given recent findings with related tyrosine kinases such as HER3 and the minor deviations from the classical motifs commonly present in active kinases. For example, both Trib2 (see Chapters 3 and 4) and CASK (Mukherjee *et al.*, 2008) are pseudokinases that bind to ATP and autophosphorylate, despite lacking the magnesium coordinating Asp residue in the DFG motif canonically observed in kinases. NOK is an example of another pseudokinase which lacks this motif but it has not yet been determined whether NOK can bind to ATP and if so, whether it is important for its cellular function. To determine whether the NOK pseudokinase domain could hydrolyse ATP *in vitro,* I employed biochemical assays that had previously demonstrated the catalytic functionality of the pseudokinase Trib2. These studies were performed on a NOK Δ transmembrane domain (NOK 98-422) recombinant protein expressed in eukaryotic Sf9 cells, and the WT NOK ΔTM pseudokinase was analysed alongside two mutant NOK proteins designed to prevent ATP binding (K147M) or re-instate activity (DFG-in).

His-tagged NOK 98-422, NOK K147M 98-422 and NOK DFG-in 98-422 were affinity purified from Sf9 cell lysates. NOK K147M is the mutation of a lysine in the β3 sheet of NOK. This Lys side chain in canonical kinases interacts with the phosphates of ATP as it points into the binding pocket (Taylor and Kornev, 2010). Upon overexpression of this mutant in HeLa Flp-In T-REx cells, the level of phosphorylated ERK 1/2 decreased (Figure 5.12), suggesting that ATP binding might be relevant in the cellular environment to NOK signaling. NOK DFG (NOK G269D L270F) is a mutant in which the metal binding motif observed in canonical kinases has been ‘reinstated’ in an effort to induce metal-ion binding and NOK hyperactivation. The residues N-terminal to 98 were not included because the presence of the hydrophobic transmembrane domain was predicted to decrease the protein solubility, potentially preventing analysis of the kinase under standard assay conditions.

Following IMAC purification of NOK and NOK mutants, Coomassie staining revealed that NOK WT and K147M (along with multiple higher MW protein contaminants) had been eluted from the TALON resin, but that NOK DFG-in was undetectable (Figure 5.13 A). The eluted fractions were pooled together (Figure 5.13 B). The yield of soluble NOK was approximately double that of K147M, determined by visual analysis of the Coomassie stained gel, and verified by dye-binding spectrophotometry.

The low amount of NOK obtained following IMAC (both K147M and, especially, DFG-in) prevented further purification of these preparations, because a large amount of each protein was required for comparative biochemical analysis. Non-radioactive kinases assays were therefore performed on ~1 μg (~30 pmoles) of partially purified NOK or NOK K147M in the presence of 1 mM ATP, and either the absence of a divalent cation, or the presence of 10 mM $Mg^{2+,}$ or 10 mM Mn^{2+} ions for 30 minutes. Autophosphorylation was assessed by measuring the levels of phosphotyrosine (a very specific antibody is commercially available) present in NOK by western blot analysis (Figure 5.14 A). Changes to NOK phosphotyrosine levels were analysed as a potential marker for autophosphorylation, since the catalytic motif of NOK is similar to that of other *bona fide* tyrosine kinases and pseudokinases such as HER3, which are known to autophosphorylate *in vitro* and can be readily detected with this antibody (Figure 5.2).

In the assays, the amount of His-tagged NOK or His tagged NOK K147M was comparable, however to obtain 1 μg of NOK K147M, double the amount of partially purified preparation was assayed when compared to WT. The amount of phosphotyrosine present in both WT and K147M NOK is similar under all conditions, even when ATP was absent, which suggests that under these conditions, NOK is unlikely to be catalytically active. At higher apparent molecular weights, when both ATP and magnesium are present, the levels of phosphorylated tyrosine detected was higher for K147M; this was probably due to higher levels of background kinases present in this purified preparation compared to that from WT assays.

Similarly, when NOK was assayed with 1 mM ^{32}P-ATP labeled in the gamma position (~2.2 μCi γ [^{32}P]-ATP per assay) (Figure 5.14 B), only K147M was detectably phosphorylated, with the highest level of phosphorylation observed when

Mg^{2+} ions were added to the reaction mixture. This was also observed for much higher MW proteins present in the preparation, and suggests that NOK K147M phosphorylation was caused by non-specific kinase contaminants, which again would have formed a larger proportion of the reaction mixture for K147M NOK than in the WT assays.

To try to overcome this issue, and eliminate eukaryotic kinase contamination, NOK was next expressed in the same bacterial cell strain used to analyse Trib2 and Trib3 (BL21DE3pLysS, Chapter 3). In order to maximize protein expression, the conditions following induction of protein synthesis by IPTG were partially optimised. The amount of protein following induction of both His tagged NOK (pET-30) and GST-His tagged NOK (pET-41) at either 37°C for 3 hours or 18°C for 18 hours was determined by Coomassie staining (Figure 5.15). The expressed NOK proteins either had the full C terminal domain (98-422), a Δ7 residue (98-415) C terminal domain deletion, which removed an 'autoinhibitory' Y residue (417) that reduced activation of ERK, STAT1 and STAT3 (Li *et al.*, 2007), or was the NOK pseudokinase domain minus the C-terminal tail (NOK 98-400). Whole cell extracts of *E. coli* transformed with NOK were analysed after induction to determine the optimal conditions that expressed the most protein prior to purification. Coomassie staining of SDS-PAGE resolved extracts indicated that the plasmid construct which expressed the greatest amount of NOK was pET-30Ek/LIC (6-His-tagged NOK ~37 kDa) and the optimum incubation conditions post-IPTG induction were 37°C culture for 3 hours. Despite determining the optimum expression conditions of NOK in *E. coli*, it has not been possible to obtain a soluble yield of NOK following lysis and IMAC sufficient for *in vitro* kinase assay analysis, although nanogram amounts of NOK can be purified for analysis by western blotting.

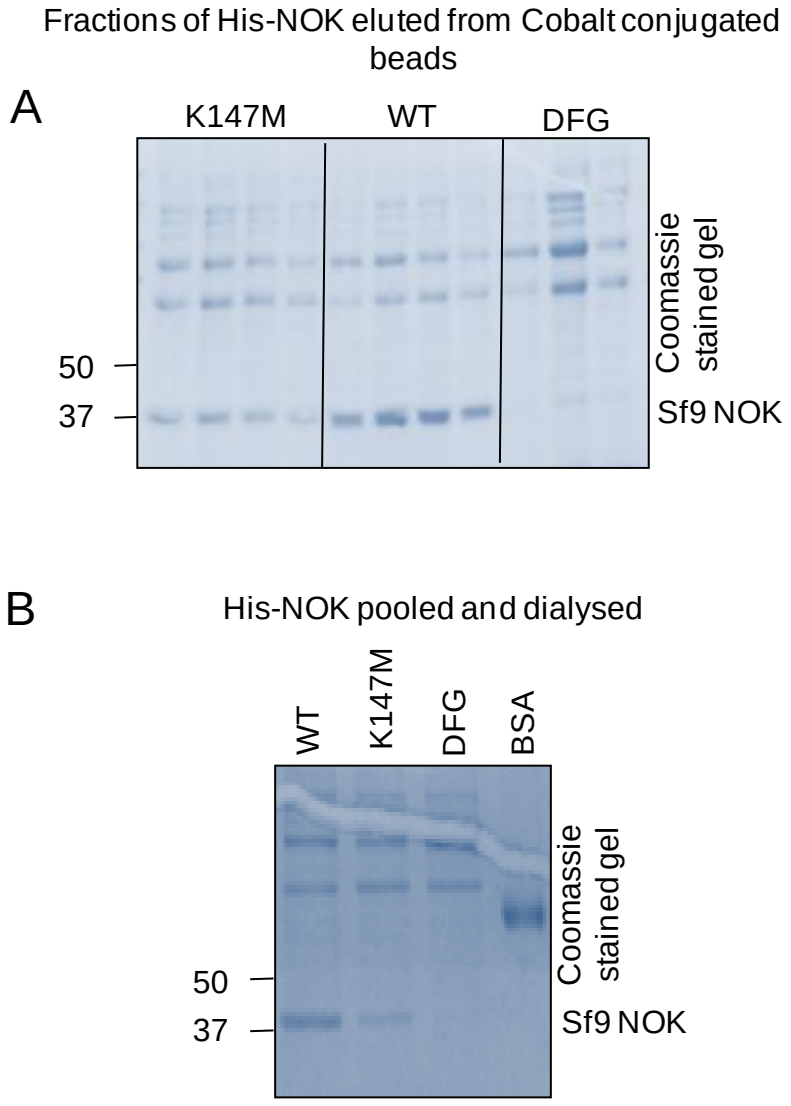

Figure 5.13 Affinity purification of Sf9-expressed human NOK Following the elution of NOK from Sf9 cell lysate A) fractions containing either NOK K147M, WT or DFG were resolved by SDS-PAGE and the proteins visualised by Coomassie staining. B) The fractions were pooled and dialysed and were subjected to gel electrophoresis along with 4 μg BSA. Following coomassie staining, the Sf9 NOK proteins are visible ~ 37 kDa.

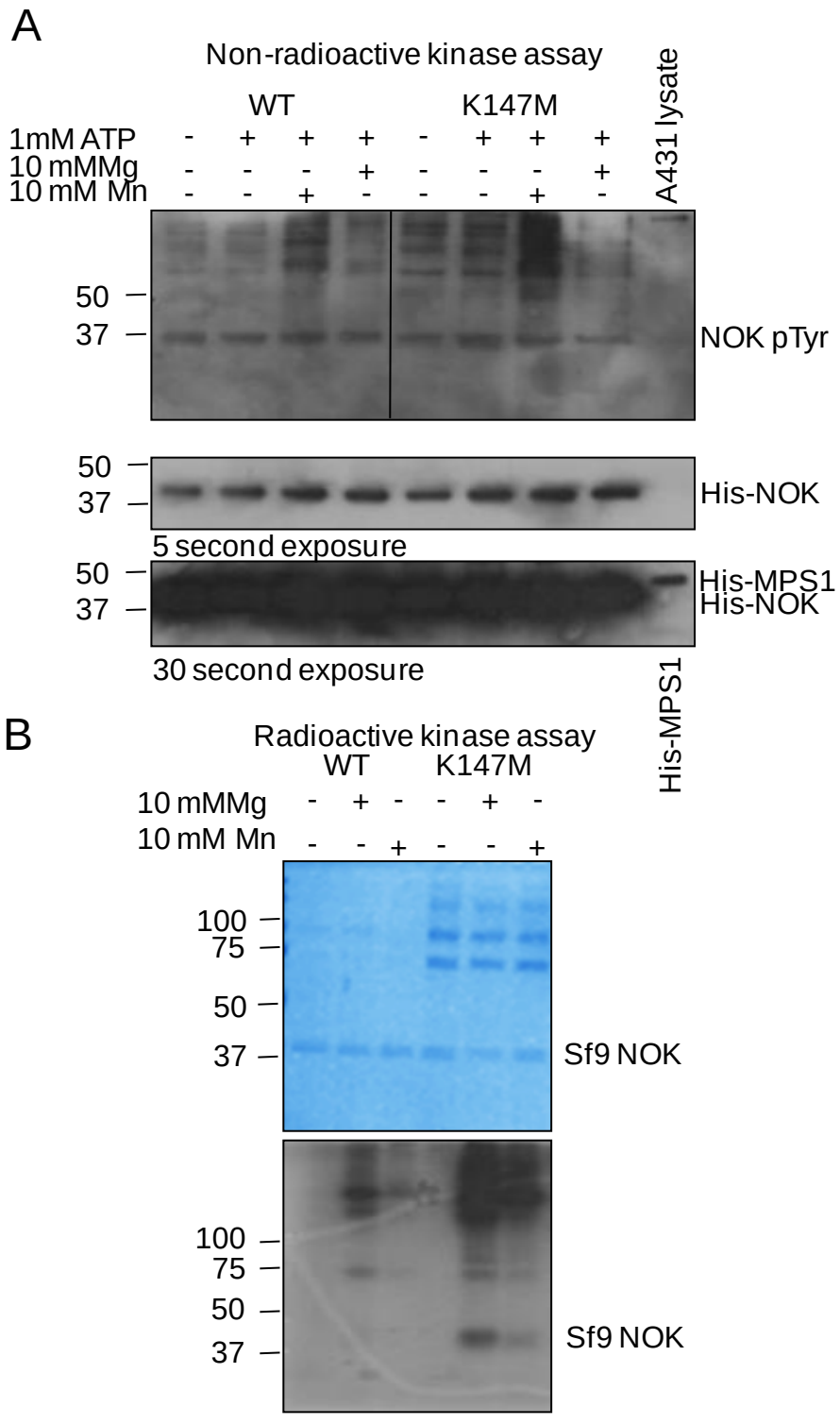

Figure 5.14 Sf9 expressed NOK proteins do not specifically autophosphorylate A) Approximately, 1 µg WT or K147M NOK was assayed in the presence of 1 mM ATP and either in the absence or presence of 10 mM $MgCl_2$ or $MnCl_2$ for 30 minutes at 30 °C. The level of phosphotyrosine determined by anti-phosphotyrosine was used to identify whether NOK was capable of autophosphorylation and A341 lysate was used as an anti-phosphotyrosine control. Protein levels were determined by the detected His-signal and the His-tagged Mps1 loaded to control for the antibody. B) The assay was repeated using radiolabelled 1 mM ATP (~2.2µCi γP^{32} per assay). The protein was stained and subjected to autoradiography.

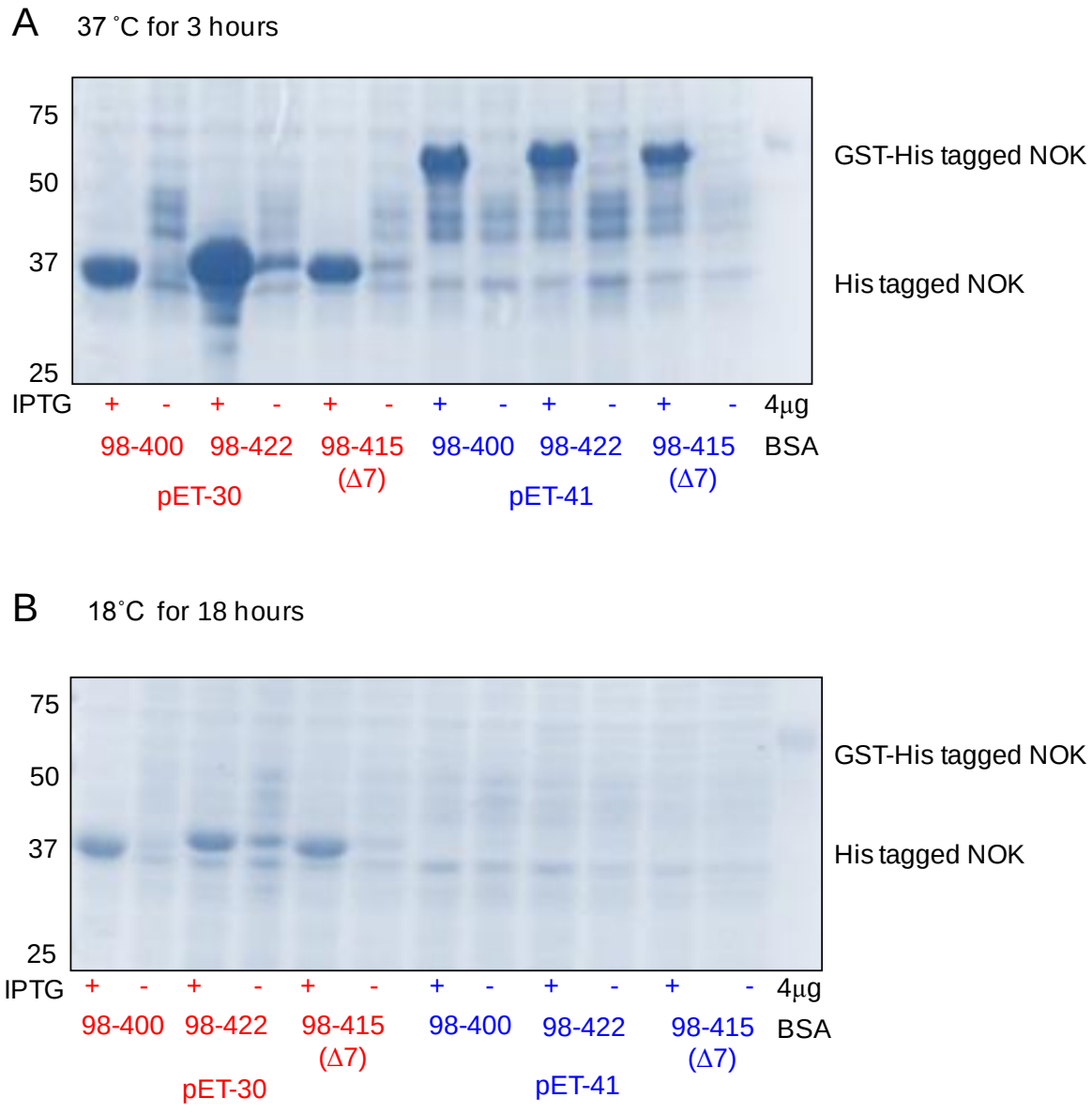

Figure 5.15 Optimising recombinant NOK expression in *E. coli* His tagged NOK 98-400, 98-415 and 98-422 were expressed following the addition of IPTG for either 3 hours at 37 °C (A) or 18 hours at 18 °C (B). Whole cell protein expression levels were compared by coomassie staining the protein following SDS-PAGE analysis of 20 µl of each sample alongside 4 µg BSA.

5.11 Discussion

NOK is a pseudokinase that does not have a conventional DFG motif in any of the vertebrate species in which it has been shown to be expressed at the mRNA level. Despite similar loss of this motif in the Trib2 and CASK pseudokinase domains, both of these proteins have demonstrated the ability to autophosphorylate and bind ATP, although this is independent of metal ions (Chapters 3 and 4). It is currently unproven whether NOK can bind to ATP, or transfer the gamma phosphate to a substrate or itself (*e.g.* autophosphorylate). A published *in vitro* kinase assay that employed immunoprecipitated NOK to demonstrate autophosphorylation, did not experimentally control for the presence of contaminating kinases (Chen *et al.*, 2005b), although as discussed in Chapter 4, the kinases BUBR1, ILK and Titin were previously reported to be catalytically active (based on kinase assay analysis *in vitro*) but it has been subsequently shown, in each of these cases, that they are in fact devoid of catalytic activity, with phosphorylation in an *in vitro* assay being driven by a contaminating kinase(s) (Suijkerbuijk *et al.*, 2012, Wickstrom *et al.*, 2010, Bogomolovas *et al.*, 2014). Data presented in this Chapter confirms that partially purified NOK is contaminated by at least one, but potentially more, tyrosine kinase activities, and it will be interesting to analyze these binding partners more closely, especially if they are active members of the EGFR receptor (see below), whose activities can easily be inhibited using a panel of tyrosine kinase inhibitors.

Other features of the NOK pseudokinase domain include sequences within the catalytic motif (HxDxAARN) that classifies it as a relative of the tyrosine kinase division of protein kinases (Kannan *et al.*, 2007) and a predicted single pass transmembrane domain located towards the N terminus of the polypeptide. This groups NOK within the Receptor Protein Tyrosine Kinase (RPTK) subfamily, and places it as part of a small sub-family of PTK pseudokinases (Lemmon and Schlessinger, 2010). Despite the characterization of NOK as an RPTK, it only has 25 residues N-terminal to the TM domain, which are predicted to be located outside the cell. However, no known ligand binding domain is present amongst these residues, which have little similarity to other extracellular domains when analyzed by bioinformatics BLAST searching. It will be interesting to evaluate the effects of deletion of these residues in a cell-based system. Generally, most RPTKs that

contain ligand binding ectodomains transduce an extracellular signal across the cell membrane into the cytoplasm (Lemmon and Schlessinger, 2010), suggesting that NOK might either aid in this process (similar to HER3 pseudokinase and other EGFR family members), or fulfill a currently unknown role in signaling.

NOK has been implicated in various signaling pathways when overexpressed, including the PI3K and MAPK pathways (Chen *et al.*, 2005b, Liu *et al.*, 2004). Additionally, when NOK was overexpressed in HeLa cells, the level of phosphorylated GSK3β Ser9 was reported to increase, with phosphorylation at this residue inhibiting the tumor suppressive behavior of GSK3β along with increased Thr 308 phosphorylation (the 'PDK1 site') in AKT, which is a physiological upstream GSK3β kinase (Li *et al.*, 2012). A tyrosine residue has also been identified in the C-terminal tail of NOK that inhibited the phosphorylation of ERK, STAT1 and regulated cellular proliferation. When this residue was mutated to a non-phosphorylatable form (Y417F), the levels of phosphorylated ERK, phosphorylated STAT1 and the cellular proliferation of Y417F NOK expressing cells increased (Li *et al.*, 2007).

As its name suggests, high expression of NOK (Novel Oncogene with Kinase domain) has been implicated in a variety of cancers and a multitude of studies have identified increased levels of NOK mRNA expression in samples, and increased NOK mRNA expression could even be detected in early clinical stages of NSCLC (Amachika *et al.*, 2007), suggesting some prognostic power for analyzing NOK. Increased NOK mRNA expression was also discovered in breast tumor samples, where the expression was 6 times higher than in control samples. This study also observed that following transfection of NOK targeting siRNA into the breast cancer cell line T47D, which was the highest NOK mRNA expressing breast cancer cell line tested, growth was inhibited by 50% compared to the controls (Moriai *et al.*, 2006). Cell growth was also attenuated in NOK shRNA expressing prostate cancer cells (Chung *et al.*, 2009) and NOK mRNA was significantly higher in 80% of leukemia patients tested. Following various chemotherapy treatments, the mRNA in all the patient samples reduced and following siRNA treatment of K562 cells, growth was inhibited by 58% (Kondoh *et al.*, 2009). Immunohistochemical stained ovarian tissues showed that the level of NOK expression correlated to the severity of the illness. The cells that were most highly stained, and had the highest NOK expression

were the most malignant, whilst benign tissue stained moderately, and for normal tissue, minimal staining was observed (Jackson *et al.*, 2009). Despite the reported link between NOK expression and the development of cancer, the function of NOK protein in cells remains very poorly understood. The results presented in this Chapter have demonstrated that NOK localizes to the nuclear membrane and shares features of the tripartite NLS signal sequence conserved throughout the EGFR family of RPTKs and the INM-targeted protein RNF13. Mutations to two amino acids in NOK, namely R377 and R379, which align with functionally important Arg residues in the localization sequences of Glycoprotein B, EGFR and RNF13, block the translocation of NOK to the nuclear membrane. The movement of NOK towards the nuclear membrane occurs potentially *via* an endosomal pathway, where NOK has previously been identified to reside along with EGFR (Ding *et al.*, 2012), and staining resembled the endosomal staining observed for RNF13, which is also trafficked to the nuclear membrane via an endosomal pathway (Bocock *et al.*, 2010, Bocock *et al.*, 2011). When NOK co-localized with EGFR in endosomes (Ding *et al.*, 2012), no nuclear membrane localization was reported and the speculated fate of endosomal EGFR was reported as either recycling back towards the cell membrane or trafficking for degradation (Ding *et al.*, 2012). EGFR can also be transported to the nucleus in endosomes. During this transportation it remains membrane associated because of its transmembrane domain (Wang and Hung, 2012). Interestingly, when the transmembrane domain of NOK was removed, the co-localization of NOK with the early endosomal marker (EEA) was abrogated (Ding *et al.*, 2012). Lipid-embedded EGFR interacts with importin β and is integrated into the inner nuclear membrane (INM). Whilst embedded in the INM it interacts with INM-localized Sec61β, which facilitates translocation into the nucleus (Wang *et al.*, 2010). Another example of an RPTK pseudokinase that is translocated to the nucleus is PTK7, which unlike EGFR, has the transmembrane domain sequence cleaved by γ-secretase prior to nuclear entry (Na *et al.*, 2012). A similar mechanism is also observed for the nuclear incorporation of ErbB4, which has a conserved EGFR-like NLS sequence, but a different trafficking mechanism (Williams *et al.*, 2004). If NOK was cleaved like ErbB4, then the N-terminal Myc tagged transmembrane domain would remain embedded in the inner nuclear membrane whilst the released pseudokinase domain entered the nucleus undetected by immunofluorescence microscopy. However, by studying C-terminal FLAG tagged NOK, the staining resembled Myc tagged NOK,

indicating that the protein was unlikely to be cleaved and the peptide remained embedded in the inner nuclear membrane, and was not translocated into the nucleus.

Interestingly the COSMIC database (Catalogue of Somatic Mutations In Cancer version 68) contains a reported cancer-associated NOK mutation at R377Q in a single large intestine carcinoma sample. However a mutant at this position (R377A) stably overexpressed in HeLa cells did not alter the localization of Myc tagged NOK. Instead, a doubly mutated protein, NOK R377A R379A was required to alter the observed localization. The majority of NOK mutations listed in the COSMIC database have only been observed in one tumor sample, and are therefore likely to be very rare, or random mutation events. There are however, four residues that are mutated more than once, and all of these are located towards the C-terminus of the protein: G313E/V, L316F/P, R336C/H, R411K/T. None of these mutations are found in any of the conserved kinase domain motifs that define pseudokinases, although both G313E/V and L316F/P are predicted to be located in the relatively hydrophobic αF helix, which anchors the catalytic and regulatory spines of kinase catalytic domains (Taylor and Kornev, 2011). It is therefore interesting to speculate that these mutations might affect the overall structural conformation of NOK. L316F has been identified in a glioma tumor sample, whilst L316P has been identified in 3 large intestine carcinomas, and it will be interesting to analyse the localization and function of these mutants in cell signaling models.

Nuclear EGFR can act as a co-transcription factor, where it regulates the cyclin D1 promoter (Lin *et al.*, 2001), Aurora A (Hung *et al.*, 2008), c-Myc (Jaganathan *et al.*, 2011), iNOS (Lo *et al.*, 2005), B-Myb (Hanada *et al.*, 2006) and COX2 (Lo *et al.*, 2010, Brand *et al.*, 2013). Nuclear EGFR has demonstrated the ability to increase the stability of PCNA by phosphorylating PCNA Tyr211, therefore increasing cell proliferation. Also, EGFR assists the reparation of DNA-double stand breaks caused by radiation therapy by interacting with DNA-PK and all these function together to enhance oncogenic proliferation and led to an increased patient mortality with implications in cisplatin treatment, treatment with anti-EGFR compounds and radiation resistance (Brand *et al.*, 2013). Interestingly, following treatment of breast cancer cell lines with tamoxifen and raloxifen, NOK mRNA expression increased (Kimbro *et al.*, 2008), which raises the interesting possibility that NOK could be important in drug resistance in cancers.

To determine if small molecule kinase domain targeted therapies could be useful for the treatment of NOK overexpressing cancers, the function of the NOK ATP binding domain needs to be determined. The majority of the literature focusing on NOK mainly reports the NOK mRNA expression levels in different cancers or the influence that the overexpression of NOK has upon signaling pathways. One example of how the presence of NOK affects a cell signaling pathway is observed when NOK binds to AKT, which increases the phosphorylation of AKT Thr308, which in turn increases the level of the Ser9 phosphorylated form of GSK3β, potentially inactivating the tumor suppressing function of this kinase. However, it is unclear whether NOK acts catalytically, or as a protein scaffold, perhaps bringing GSK3β and AKT into closer proximity (Li *et al.*, 2012). One indication that ATP binding by the pseudokinase domain of NOK might be important for its proliferative actions was demonstrated by the transfection of 22Rv1 cells (a prostate cancer cell line) with either a vector that contained NOK or a vector that contained NOK K147R, which like K14M described in this Chapter, represents a subtle mutation to the lysine located in the VAIK motif of the N-lobe β3 sheet designed to block ATP binding. In canonical kinases this lysine interacts with the ATP α- and β- phosphates and often forms part of the catalytic 'triad' stabilizing ATP for hydrolysis. The effects upon proliferation by NOK or NOK K147R overexpression in 22Rv1 cells were determined by MTT analysis 48 hours after transfection. Whilst proliferation of the NOK overexpressing cells was significantly increased compared to the mock transfection control, the cells overexpressing NOK K147R did not demonstrate any cell proliferation enhancement (Chung *et al.*, 2009). In partial agreement with this finding, overexpression of NOK K147M in HeLa Flp-In T-REx cells reduced the levels of phosphorylated ERK 1/2 in cells grown in serum (Figure 5.12) whilst the phosphorylation was not altered in the presence of exogenous WT NOK or DFG NOK when compared alongside controls. Indeed, there was no observed decrease in the levels of phosphorylated ERK 1/2 in the HeLa Flp-In T-REx K147M uninduced lysate, indicating that the reduction observed in K147M expressing lysates could be an effect of a dominant-negative mutation, potentially suggesting that the integrity of the ATP domain is relevant for NOK downstream signalling.

Finally, two potentially interesting tyrosine residues, Y327 and Y356, are located C-terminal to the NOK pseudokinase domain and are conserved in many RPTKs including FGFR, PDGFR, Met, Tie1 and Tek. FGFR1 Y701 (corresponding

to NOK Y327) and FGFR1 Y724 (NOK Y356) are required for the activation of FRS2-mediated ERK pathway amongst others (Chen *et al.*, 2005b), although it has been suggested that FGFR1 Y701 is not a phosphorylation site (Foehr *et al.*, 2001). Stable BaF3 cells expressing an erythropoietin receptor/NOK hybrid protein (EPOR/NOK), or cells that expressed EPOR/NOK Y327F, or EPOR/NOK Y356F were analysed for S-phase progression by assessing ^{3}H Thymidine incorporation in starvation conditions. The replication of BaF3 cells expressing EPOR/NOK doubled after one day of incubation whereas the proliferation of EPOR/NOK Y327F or EPOR/NOK Y356F were reduced and comparable with the proliferation rates of BaF3 untransfected cells, or BaF3 cells transfected with a control plasmid. In a colony formation assay in soft agar supplemented with starved culture medium, the BaF3 cells that expressed EPOR/NOK Y327F or Y356 demonstrated dramatically reduced anchorage independent growth capabilities compared to WT EPOR/NOK. Nude mice transfected with cells expressing EPOR/NOK showed substantial evidence of tumorigenesis and metastasis, with subjects developing enlarged spleens and livers as well as evidence of metastatic growth in the liver, kidneys, lungs, skeletal muscle and intestines of test subjects. All the metastatic growth stained positive for NOK by immunohistochemistry. However, for EPOR/NOK Y327F or EPOR/NOK Y356F expressing mice, there was no evidence of metastasis. Despite using EPOR/NOK constructs, the results were not dependent upon erythropoietin stimulation and the results for EPOR/NOK were consistent with NOK overexpressing cells (Chen *et al.*, 2005b). The results indicated that the two tyrosine residues are essential for NOK mediated tumorigenesis. In the same study, it was reported that EPOR/NOK increased the levels of phosphorylated ERK, phosphorylated AKT and activated STAT5, whilst mutations to the conserved tyrosine residues reduced the levels of all these, but it is unknown how these residues affect the activation of the downstream pathways; whether NOK acts as a scaffold and these tyrosines are docking sites for other signaling proteins or whether they are autophosphorylation substrates has yet to be determined (Chen *et al.*, 2005b).

In this Chapter, I have begun to investigate whether NOK can autophosphorylate *in vitro* after affinity purification from ΔTM Sf9 NOK-expressing cell lysates. Autoradiography demonstrates that, surprisingly, the NOK K147M mutant incorporated radioactive phosphate from ATP during the assay, however contaminating kinases or their substrates was more than likely the cause of this, since

the signals were much more intense for Sf9 K147M, and because these assays probably contained an increased amount of co-purifying kinase activity when compared to WT-NOK. Other groups have published data suggesting that NOK is catalytically active (Chen *et al.*, 2005a, Chung *et al.*, 2009). However, they do not control for the possibility that the detected signals could be caused by other kinases and do not support their data with a NOK mutant that has a reduced ability to autophosphorylate, as might be predicted for K147M NOK based on my experience with Trib2 and Trib3. For example, it was suggested that recombinant NOK phosphorylated a 15 kDa substrate found in 22Rv1 whole cell lysate, although no kinase-dead control or loading control was present, and in the control assay which contained lysate alone (but did not include recombinant NOK), there was a faint band observed at the same MW as the implied 'NOK substrate' (Chung *et al.*, 2009).

Although no signal was observed for Sf9-expressed WT NOK autophosphorylation (Figure 5.14), it is not possible to rule out that it is catalytically inactive. Indeed, HER3 is a distinct, but NOK-related pseudokinase that has an Asn instead of the catalytic Asp in the catalytic motif. It was recently demonstrated that HER3 possesses a weak catalytic activity, abrogated by mutation of K723 (the residue corresponding to NOK K147), equivalent to approximately $1/1000^{th}$ the specific activity of EGFR (Shi *et al.*, 2010). However, this activity was only observed when the intracellular domains of HER3 were artificially clustered onto vesicle surfaces by the attachment of nitrilotriacetate-Ni head groups to the lipids. These interacted with the His-tag at the N-terminus of the intracellular domain of HER3. Without the clustering no autophosphorylation was apparent (Shi *et al.*, 2010), and so this approach might be tested using purified NOK in the future.

It is not known whether NOK can bind to ATP or other ligands. DSF analysis has not yet been performed upon recombinant NOK, and had time permitted it would have been very interesting to identify whether pure preparations of NOK could bind to ATP, thus helping determine whether the ATP binding site of NOK is potentially targetable with small molecules. In Chapter 4, I found that the ATP binding site of Trib2 is potentially druggable. If the ATP binding site of NOK is also accessible by ATP or analogues, then it would be crucial to observe the cellular effects of NOK inhibition by analysis of the downstream signaling pathways such as the MAPK and AKT pathways and also analyze the proliferation and transformation capabilities of

NOK following therapeutic treatment. It would also be interesting to see if this inhibition altered the trafficking of NOK and its cellular localization. Together this would reveal whether NOK, which has already demonstrated potential clinical relevance as a biomarker linked to the severity of ovarian cancers (Jackson *et al.*, 2009), might be a novel drug target in some cancers.

5.12 Conclusion

Preliminary research discussed in this Chapter, alongside a body of published data, has demonstrated that NOK has the properties of an inactive pseudokinase. However, as demonstrated by another RPTK pseudokinase HER3, this does not definitively mean that it cannot autophosphorylate and performing *in vitro* kinase assays upon recombinant NOK clustered in lipid vesicles could highlight any autophosphorylation potential. This work highlights the problems associated with performing *in vitro* kinase assays upon pseudokinases when the correct controls are not in place, and it will be important to obtain HER3 kinase as a positive control in the future. To determine the accessibility of the NOK pseudokinase domain by ATP analogues and therapeutics, it is imperative to employ a ligand binding assay such as DSF, which has already proved to be extremely useful in identifying other pseudokinases that can bind to ATP, such as Trib2, SgK495 (in Chapter 4), HER3 (Littlefield *et al.*, 2014, Davis *et al.*, 2011), the JAK pseudokinase domains (Murphy *et al.*, 2014b) and the very poorly understood pseudokinase SgK071, which binds to ATP but has no known biological function (Murphy *et al.*, 2014b).

The identification of NOK as a nuclear membrane targeted protein is consistent with the presence of a transmembrane domain, and of particular interest considering the oncogenic potential that NOK overexpressing cells demonstrate. It is perhaps suggestive that it may function as a regulatory partner of other nuclear envelope-targeted kinases, perhaps including active kinases such as other members of the EGFR family (Lemmon and Schlessinger, 2010). There have been many examples of nuclear localized RPTKs that are overexpressed in cancers including EGFR (Brand *et al.*, 2011, Brand *et al.*, 2013). It is also important to identify whether after NOK translocation to the inner nuclear membrane, it is transported into the nucleus, possibly by Sec61β, as observed for EGFR (Wang *et al.*, 2010) with which it shares the tripartite NLS, even though my current analysis suggests that NOK remains embedded in the nuclear envelope. Another novel therapeutic

approach for targeting NOK, if the ATP binding site proves not to be suitable for small molecule inhibition, would be to identify whether preventing nuclear membrane localization affects the transforming and metastatic phenotypes displayed by NOK overexpressed cells previously reported (Liu *et al.*, 2004, Chen *et al.*, 2005b, Chung *et al.*, 2009, Li *et al.*, 2007, Moriai *et al.*, 2006).

CHAPTER 6. Future Directions

The work presented in this Thesis proves that Trib2 has maintained sufficient integrity in the pseudokinase domain to facilitate ATP binding and enzymatic incorporation of the γ-phosphate into a protein substrate, Trib2 itself. This behavior can be altered by mutation to key residues located throughout the catalytic domain. Not only can Trib2 bind to ATP, but the ability of Trib2 to bind to ATP and autophosphorylate is severely reduced in the presence of the divalent cations magnesium and manganese. This demonstrates that ATP binding by Trib2 occurs *via* a different mechanism than utilized by canonical kinases, which require magnesium ions to stabilize the negatively charged ATP in the binding pocket (Nagar, 2007). This presents an opportunity that could enable ATP analogues to potentially bind in a way that differs to the binding mode in other kinase domains, which could minimize off-target effects across the >500 member human kinome.

ATP binding by Trib2 has, so far, only been determined for bacterial recombinant Trib2, and to gain further insight into the function of Trib2 ATP binding, the affinity of Trib2 for ATP in a cellular environment needs to be examined. In this thesis, a putative correlation was observed between the ATP binding properties of recombinant Trib2, and the expressed levels of induced Trib2 and Trib2 mutants in human cell lines. The K90M mutant, which had a reduced ability to bind to ATP and autophosphorylate *in vitro* was expressed at a significantly lower level in HeLa Flp-In T-REx cells, potentially indicating that Trib2 stability and/or turnover in cells is regulated by ATP binding, but this suggestion requires further investigation.

In the future, analysis of Trib2 behavior in neurons and brain tissue would be very interesting because compared to other tissues, the level of 'free' (not coordinated to Mg^{2+}) ATP is reported to be relatively high (Taylor *et al.*, 1991). The brain (or any cell type where ATP levels are high) could therefore be a potential biological site that favors Trib2 autophosphorylation (or phosphorylation of a substrate yet to be identified). Intriguingly, analysis of Oncomine data revealed that a variety of brain tissue tumours contained highly overexpressed Trib2 mRNA.

Previous Trib2 analysis has identified that the catalytic domain is important for the oncogenicity of Trib2 overexpressing cells, with the complete catalytic

domain as well as the COP1 binding domain being a requirement for the degradation of the transcription factor C/EBPα (Keeshan *et al.*, 2010). A mutation to K177 in the Trib2 catalytic motif (K177R) reduced C/EBPα degradation and the ability of overexpressing colonies to serially replate in comparison to WT (Keeshan *et al.*, 2010). Recombinant Trib2 K177A, in which the Lys is changed to an uncharged Ala, exhibits a much lower level of autophosphorylation compared to WT, and resembles the activity of K90M Trib2. However, whether this is because the ability of Trib2 to bind to ATP has been reduced by the mutation, or because the mutation impedes the catalytic phospho-transfer remains to be investigated, and DSF would be a very useful tool for this. It would also be very interesting to observe the levels of C/EBPα degradation and the transforming capabilities of cells that overexpress Trib2 K90M, which cannot detectably bind to ATP when analysed by DSF *in vitro*.

In addition, the development of 'knock-in' Trib2 mutant mice, especially those containing alterations to the critical ATP binding residues, could assist in the elucidation of ATP-dependent Trib2 mediated phenotypes in a multicellular organism. In addition, a developing technique is the CRISPR/Cas9 system adapted from bacteria, which permits genomes with engineered gene insertions to be created relatively simply (Wang *et al.*, 2013a) and would allow for the expression of Trib2 mutated genes. This technique operates by generating specific breaks in the DNA using Cas9, which is guided by short RNA sequences that target the region of DNA to be mutated. Following this, the donor template (*e.g*. mutant Trib2 gene flanked by long arms of homologous DNA) is homologously recombined into this specific site (Rong *et al.*, 2014, Ran *et al.*, 2013, Auer *et al.*, 2014, Hsu *et al.*, 2014). Furthermore, this technique also facilitates the deletion of multiple genes simultaneously, which would allow for a combination of Trib2, Trib3 and Trib1 knockout cells or mice to be generated for further analysis of Trib-mediated phenotypes (Wang *et al.*, 2013a).

Further analysis of the ATP binding site in cells could be performed, not by a loss-of-function mutation but by targeting the ATP binding site with a small molecule modulator/inhibitor, and I have demonstrated in this thesis that the Trib2 ATP site is accessible to both ATP and inhibitors. Non-enzymatic assay approaches such as DSF, which was adapted for Trib2 analysis in this study, will be crucial for

this process. A panel of inhibitors could be tested against Trib2 in a 96-well format and binding 'hits' isolated for further study. By treating either a cancer model in which Trib2 expression causes a phenotype, or by using my Trib2-inducible cell lines and intracellular Trib2 ligands, it might be possible to identify phenotypic changes caused specifically by binding to Trib2 rather than other kinases present in the cells.

To negate the problem of off-target inhibitory effects that will probably be observed when the cells are treated with pan-kinase inhibitors, further manipulation of the gatekeeper residue could also be performed with the aim of obtaining an analogue sensitive mutant that retains the level of WT catalytic activity, which is unfortunately lost when the Trib2 gatekeeper residue is mutated to a Gly or Ala. One potential mutation that could be used is F130C, followed by a DSF based screen of electrophilic small molecules.

Structural analysis of Trib2 bound to an inhibitor or ATP would be a very insightful, and essential, next step to determine the mechanism of Mg^{2+} independent ATP binding. X-ray crystallography and NMR spectroscopy would be obvious interesting techniques to use for this. In particular, NMR performed using my ^{15}N-labelled Trib2 preparations (Figure 3.27) would facilitate the analysis of protein dynamics in solution so the individual residues that move in relation to ligand binding could be ascertained and novel inhibitors modeled to the structure, perhaps without crystal artifacts.

Even if the low levels of Trib2 catalytic activity observed *in vitro* are not a requirement for Trib2 mediated degradation of C/EBPα by COP1, binding of an inhibitor could prevent the degradation complex from forming, which relies upon the presence of the catalytic domain and could still be a potential therapeutic targeting site. However, it will be important to carefully analyze whether ligand binding to Trib2 inadvertently *increases* the degradation of C/EBPα by allosterically *stimulating* COP1 activity, which would not be a goal for the development of Trib2 ligands as anti-cancer agents.

Future analysis of NOK should initially clarify whether the pseudokinase domain is catalytically competent to hydrolyze ATP, whether it can solely bind to ATP, or neither of these functions. *In vitro* kinase assays and DSF should be

performed in tandem upon pure preparations of NOK and NOK kinase domain mutants, including NOK K147M, which when overexpressed, reduced the levels of phosphorylated ERK1/2.

The function of NOK translocation to the nuclear membrane also needs to be determined. The stimuli that triggers this trafficking, along with interacting substrates at the INM are still unknown, however, previous co-localization with EGFR in vesicles has been reported (Ding *et al.*, 2012), indicating they could potentially dimerise and NOK could be involved with activation of different HER/EGFR members.

NOK overexpression has been widely reported in the literature, but its function is less clear. Following elucidation of its catalytic capabilities and function at the INM, it will be important to ascertain whether NOK is a suitable therapeutic target. If NOK does bind to ATP then disrupting the binding with an inhibitor and analyzing any changes to cell signaling pathways, including the MAPK and AKT pathways, would help to indicate if NOK mediated activity had been altered. If NOK does not detectably bind to ATP, then another target that could be potentially adapted therapeutically is its localization and it would be interesting to observe any phenotypic changes that occur when NOK localization is altered, for instance the two Arg residues that have been identified in this thesis disrupt the observed nuclear membrane association when mutated, but how this affects overall cell signaling profile has yet to be ascertained.

As discussed above, CRISPR/Cas9 technology could be used to engineer a variety of Trib2 mutant knock in, or gene deletion situations in mice (or human cell lines (Jinek *et al.*, 2013)) and this same procedure could be adapted to NOK quite simply, with the only changes required being to the targeting RNA sequences to make them specific to the genomic NOK location and to the donor gene insert. This could provide information of phenotypes at the level of a multicellular organism caused by mutations to the NOK catalytic domain or by altering the NOK cellular localization.

In this thesis, I have shown that Trib2 is catalytically active *in vitro*, and that NOK localizes to the inner nuclear membrane. However the downstream effects of these activities and targeting events have yet to be determined for either protein and

further analysis will hopefully reveal whether these cancer-implicated pseudokinases could be developed into novel therapeutic targets in the future.

References

ADAMS, J. A. 2001. Kinetic and catalytic mechanisms of protein kinases. *Chemical Reviews,* 101**,** 2271-2290.

ALAIMO, P. J., KNIGHT, Z. A. & SHOKAT, K. M. 2005. Targeting the gatekeeper residue in phosphoinositide 3-kinases. *Bioorganic & Medicinal Chemistry,* 13**,** 2825-2836.

ALIZADEH, A. A., EISEN, M. B., DAVIS, R. E., MA, C., LOSSOS, I. S., ROSENWALD, A., BOLDRICK, J. C., SABET, H., TRAN, T., YU, X., POWELL, J. I., YANG, L., MARTI, G. E., MOORE, T., HUDSON, J., JR., LU, L., LEWIS, D. B., TIBSHIRANI, R., SHERLOCK, G., CHAN, W. C., GREINER, T. C., WEISENBURGER, D. D., ARMITAGE, J. O., WARNKE, R., LEVY, R., WILSON, W., GREVER, M. R., BYRD, J. C., BOTSTEIN, D., BROWN, P. O. & STAUDT, L. M. 2000. Distinct types of diffuse large B-cell lymphoma identified by gene expression profiling. *Nature,* 403**,** 503-11.

AMACHIKA, T., KOBAYASHI, D., MORIAI, R., TSUJI, N. & WATANABE, N. 2007. Diagnostic relevance of overexpressed mRNA of novel oncogene with kinase-domain (NOK) in lung cancers. *Lung Cancer,* 56**,** 337-340.

ASHMAN, L. K. & GRIFFITH, R. 2013. Therapeutic targeting of c-KIT in cancer. *Expert Opinion on Investigational Drugs,* 22**,** 103-115.

ATTWELL, S., MILLS, J., TROUSSARD, A., WU, C. Y. & DEDHAR, S. 2003. Integration of cell attachment, cytoskeletal localization, and signaling by integrin-linked kinase (ILK), CH-ILKBP, and the tumor suppressor PTEN. *Molecular Biology of the Cell,* 14**,** 4813-4825.

AUER, T. O., DUROURE, K., DE CIAN, A., CONCORDET, J. P. & DEL BENE, F. 2014. Highly efficient CRISPR/Cas9-mediated knock-in in zebrafish by homology-independent DNA repair. *Genome Research,* 24**,** 142-153.

BADEA, L., HERLEA, V., DIMA, S. O., DUMITRASCU, T. & POPESCU, I. 2008. Combined gene expression analysis of whole-tissue and microdissected pancreatic ductal adenocarcinoma identifies genes specifically overexpressed in tumor epithelia. *Hepatogastroenterology,* 55**,** 2016-27.

BAIN, J., PLATER, L., ELLIOTT, M., SHPIRO, N., HASTIE, C. J., MCLAUCHLAN, H., KLEVERNIC, I., ARTHUR, J. S. C., ALESSI, D. R. & COHEN, P. 2007. The selectivity of protein kinase inhibitors: a further update. *Biochemical Journal,* 408**,** 297-315.

BANTSCHEFF, M., EBERHARD, D., ABRAHAM, Y., BASTUCK, S., BOESCHE, M., HOBSON, S., MATHIESON, T., PERRIN, J., RAIDA, M., RAU, C., READER, V., SWEETMAN, G., BAUER, A., BOUWMEESTER, T., HOPF, C., KRUSE, U., NEUBAUER, G., RAMSDEN, N., RICK, J., KUSTER, B. & DREWES, G. 2007. Quantitative chemical proteomics reveals mechanisms of action of clinical ABL kinase inhibitors. *Nature Biotechnology,* 25**,** 1035-1044.

BAROUCH-BENTOV, R., CHE, J. W., LEE, C. C., YANG, Y. T., HERMAN, A., JIA, Y., VELENTZA, A., WATSON, J., STERNBERG, L., KIM, S., ZIAEE, N., MILLER, A., JACKSON, C., FUJIMOTO, M., YOUNG, M., BATALOV, S., LIU, Y., WARMUTH, M., WILTSHIRE, T., COOKE, M. P. & SAUER, K. 2009. A Conserved Salt Bridge in the G Loop of Multiple Protein Kinases Is Important for Catalysis and for In Vivo Lyn Function. *Molecular Cell,* 33**,** 43-52.

BARTOVA, I., OTYEPKA, M., KRIZ, Z. & KOCA, J. 2004. Activation and inhibition of cyclin-dependent kinase-2 by phosphorylation; a molecular

dynamics study reveals the functional importance of the glycine-rich loop. *Protein Science,* 13**,** 1449-1457.

BAYLISS, R., FRY, A., HAQ, T. & YEOH, S. 2012. On the molecular mechanisms of mitotic kinase activation. *Open Biol,* 2**,** 120136.

BAYLISS, R., SARDON, T., VERNOS, I. & CONTI, E. 2003. Structural basis of Aurora-A activation by TPX2 at the mitotic spindle. *Molecular Cell,* 12**,** 851-862.

BECHER, I., SAVITSKI, M. M., SAVITSKI, M. F., HOPF, C., BANTSCHEFF, M. & DREWES, G. 2013. Affinity profiling of the cellular kinome for the nucleotide cofactors ATP, ADP, and GTP. *Acs Chemical Biology,* 8**,** 599-607.

BERARDI, R., SANTONI, M., MORGESE, F., BALLATORE, Z., SAVINI, A., ONOFRI, A., MAZZANTI, P., PISTELLI, M., PIERANTONI, C., DE LISA, M., CARAMANTI, M., PAGLIARETTA, S., PELLEI, C. & CASCINU, S. 2013. Novel small molecule EGFR inhibitors as candidate drugs in non-small cell lung cancer. *Oncotargets and Therapy,* 6**,** 563-576.

BILWES, A. M., QUEZADA, C. M., CROAL, L. R., CRANE, B. R. & SIMON, M. I. 2001. Nucleotide binding by the histidine kinase CheA. *Nat Struct Biol,* 8**,** 353-60.

BISHOP, A. C., SHAH, K., LIU, Y., WITUCKI, L., KUNG, C. Y. & SHOKAT, K. M. 1998. Design of allele-specific inhibitors to probe protein kinase signaling. *Current Biology,* 8**,** 257-266.

BLANC, J., GENEY, R. & MENET, C. 2013. Type II Kinase Inhibitors: An Opportunity in Cancer for Rational Design. *Anti-Cancer Agents in Medicinal Chemistry,* 13**,** 731-747.

BOCOCK, J. P., CARMICLE, S., MADAMBA, E. & ERICKSON, A. H. 2010. Nuclear Targeting of an Endosomal E3 Ubiquitin Ligase. *Traffic,* 11**,** 756-766.

BOCOCK, J. P., CARMICLE, S., SIRCAR, M. & ERICKSON, A. H. 2011. Trafficking and proteolytic processing of RNF13, a model PA-TM-RING family endosomal membrane ubiquitin ligase. *Febs Journal,* 278**,** 69-77.

BOGOMOLOVAS, J., GASCH, A., SIMKOVIC, F., RIGDEN, D. J., LABEIT, S. & MAYANS, O. 2014. Titin kinase is an inactive pseudokinase scaffold that supports MuRF1 recruitment to the sarcomeric M-line. *Open Biol,* 4. 10.1098/rsob.140041

BOLANOS-GARCIA, V. M. & DAVIES, O. R. 2006. Structural analysis and classification of native proteins from *E. coli* commonly co-purified by immobilised metal affinity chromatography. *Biochimica et Biophysica Acta (BBA) - General Subjects,* 1760**,** 1304-1313.

BOUDEAU, J., MIRANDA-SAAVEDRA, D., BARTON, G. J. & ALESSI, D. R. 2006. Emerging roles of pseudokinases. *Trends in Cell Biology,* 16**,** 443-452.

BOWERS, A. J., SCULLY, S. & BOYLAN, J. F. 2003. SKIP3, a novel Drosophila tribbles ortholog, is overexpressed in human tumors and is regulated by hypoxia. *Oncogene,* 22**,** 2823-2835.

BRADFORD, M. M. 1976. A rapid and sensitive method for the quantitation of microgram quantities of protein utilizing the principle of protein-dye binding. *Analytical Biochemistry,* 72**,** 248-254.

BRAND, T. M., IIDA, M., LI, C. R. & WHEELER, D. L. 2011. The Nuclear Epidermal Growth Factor Receptor Signaling Network and Its Role in Cancer. *Discovery Medicine,* 66**,** 419-432.

BRAND, T. M., IIDA, M., LUTHAR, N., STARR, M. M., HUPPERT, E. J. & WHEELER, D. L. 2013. Nuclear EGFR as a molecular target in cancer. *Radiotherapy and Oncology,* 108**,** 370-377.

BRENNAN, D. F., DAR, A. C., HERTZ, N. T., CHAO, W. C. H., BURLINGAME, A. L., SHOKAT, K. M. & BARFORD, D. 2011. A Raf-induced allosteric transition of KSR stimulates phosphorylation of MEK. *Nature,* 472**,** 366-36.

BULLOCK, A. N., DEBRECZENI, J. E., FEDOROV, O. Y., NELSON, A., MARSDEN, B. D. & KNAPP, S. 2005. Structural basis of inhibitor specificity of the human protooncogene proviral insertion site in Moloney murine leukemia virus (PIM-1) kinase. *Journal of Medicinal Chemistry,* 48**,** 7604-7614.

BURKE, B. 2001. Lamins and apoptosis: A two-way street? *Journal of Cell Biology,* 153**,** F5-F7.

BURKHARDT, R., TOH, S. A., LAGOR, W. R., BIRKELAND, A., LEVIN, M., LI, X. Y., ROBBLEE, M., FEDOROV, V. D., YAMAMOTO, M., SATOH, T., AKIRA, S., KATHIRESAN, S., BRESLOW, J. L. & RADER, D. J. 2010. Trib1 is a lipid- and myocardial infarction-associated gene that regulates hepatic lipogenesis and VLDL production in mice. *Journal of Clinical Investigation,* 120**,** 4410-4414.

CANTWELL-DORRIS, E. R., O'LEARY, J. J. & SHEILS, O. M. 2011. BRAF(V600E): Implications for Carcinogenesis and Molecular Therapy. *Molecular Cancer Therapeutics,* 10**,** 385-394.

CARRERA, A. C., ALEXANDROV, K. & ROBERTS, T. M. 1993. The conserved lysine of the catalytic domain of protein kinases is actively involved in the phosphotransfer reaction and not required for anchoring ATP *Proceedings of the National Academy of Sciences of the United States of America,* 90**,** 442-446.

CELEJ, M. S., MONTICH, C. G. & FIDELIO, G. D. 2003. Protein stability induced by ligand binding correlates with changes in protein flexibility. *Protein Science,* 12**,** 1496-1506.

CHANDLER, J. M., ALNEMRI, E. S., COHEN, G. M. & MACFARLANE, M. 1997. Activation of CPP32 and Mch3 alpha in wild-type p53-induced apoptosis. *Biochemical Journal,* 322**,** 19-23.

CHEEK, S., GINALSKI, K., ZHANG, H. & GRISHIN, N. V. 2005. A comprehensive update of the sequence and structure classification of kinases. *Bmc Structural Biology,* 5. PMID: 15771780

CHEEK, S., ZHANG, H. & GRISHIN, N. V. 2002. Sequence and structure classification of kinases. *Journal of Molecular Biology,* 320**,** 855-881.

CHEN, Q. Q., CHEN, X. Y., JIANG, Y. Y. & LIU, J. 2005a. Identification of novel nuclear localization signal within the ErbB-2 protein. *Cell Research,* 15**,** 504-510.

CHEN, Y., LI, Y. H., CHEN, X. P., GONG, L. N., ZHANG, S. P., CHANG, Z. J., ZHANG, X. F., FU, X. Y. & LIU, L. 2005b. Point mutation at single tyrosine residue of novel oncogene NOK abrogates tumorigenesis in nude mice. *Cancer Research,* 65**,** 10838-10846.

CHU, M. L. H., CHAVAS, L. M. G., DOUGLAS, K. T., EYERS, P. A. & TABERNERO, L. 2008. Crystal structure of the catalytic domain of the mitotic checkpoint kinase Mps1 in complex with SP600125. *Journal of Biological Chemistry,* 283**,** 21495-21500.

CHUNG, S. Y., TAMURA, K., FURIHATA, M., UEMURA, M., DAIGO, Y., NASU, Y., MIKI, T., SHUIN, T., FUJIOKA, T., NAKAMURA, Y. &

NAKAGAWA, H. 2009. Overexpression of the potential kinase serine/threonine/tyrosine kinase 1 (STYK 1) in castration-resistant prostate cancer. *Cancer Science,* 100**,** 2109-2114.

CILLONI, D. & SAGLIO, G. 2012. Molecular Pathways: BCR-ABL. *Clinical Cancer Research,* 18**,** 930-937.

CITRI, A., SKARIA, K. B. & YARDEN, Y. 2003. The deaf and the dumb: the biology of ErbB-2 and ErbB-3. *Exp Cell Res,* 284**,** 54-65.

CLAUS, J., CAMERON, A. J. & PARKER, P. J. 2013. Pseudokinase drug intervention: a potentially poisoned chalice. *Biochem Soc Trans,* 41**,** 1083-8.

CREEDON, H. & BRUNTON, V. G. 2012. Src Kinase Inhibitors: Promising Cancer Therapeutics? *Critical Reviews in Oncogenesis,* 17**,** 145-159.

CROSS, D. A., ALESSI, D. R., COHEN, P., ANDJELKOVICH, M. & HEMMINGS, B. A. 1995. Inhibition of glycogen synthase kinase-3 by insulin mediated by protein kinase B. *Nature,* 378**,** 785-9.

CVETKOVIC-LOPES, V., BAYER, L., DORSAZ, S., MARET, S., PRADERVAND, S., DAUVILLIERS, Y., LECENDREUX, M., LAMMERS, G. J., DONJACOUR, C. E. H. M., DU PASQUIER, R. A., PFISTER, C., PETIT, B., HOR, H., MUHLETHALER, M. & TAFTI, M. 2010. Elevated Tribbles homolog 2-specific antibody levels in narcolepsy patients. *Journal of Clinical Investigation,* 120**,** 713-719.

D'ABRAMO, M., BESKER, N., CHILLEMI, G. & GROTTESI, A. 2014. Modeling conformational transitions in kinases by molecular dynamics simulations: achievements, difficulties, and open challenges. *Front Genet,* 5**,** 128. DOI: 10.3389/fgene.2014.00128

DAVIS, M. I., HUNT, J. P., HERRGARD, S., CICERI, P., WODICKA, L. M., PALLARES, G., HOCKER, M., TREIBER, D. K. & ZARRINKAR, P. P. 2011. Comprehensive analysis of kinase inhibitor selectivity. *Nature Biotechnology,* 29**,** 1046-1051.

DEDHIA, P. H., KEESHAN, K., ULJON, S., XU, L. W., VEGA, M. E., SHESTOVA, O., ZAKS-ZILBERMAN, M., ROMANY, C., BLACKLOW, S. C. & PEAR, W. S. 2010. Differential ability of Tribbles family members to promote degradation of C/EBP alpha and induce acute myelogenous leukemia. *Blood,* 116**,** 1321-1328.

DETWILLER, K. Y., FERNANDO, N. T., SEGAL, N. H., RYEOM, S. W., D'AMORE, P. A. & YOON, S. S. 2005. Analysis of hypoxia-related gene expression in sarcomas and effect of hypoxia on RNA interference of vascular endothelial cell growth factor A. *Cancer Research,* 65**,** 5881-9.

DING, X., JIANG, Q.-B., LI, R., CHEN, S. & ZHANG, S. 2012. NOK/STYK1 has a strong tendency towards forming aggregates and colocalises with epidermal growth factor receptor in endosomes. *Biochemical and Biophysical Research Communications,* 421**,** 468-473.

DINITTO, J. P., DESHMUKH, G. D., ZHANG, Y., JACQUES, S. L., COLI, R., WORRALL, J. W., DIEHL, W., ENGLISH, J. M. & WU, J. C. 2010. Function of activation loop tyrosine phosphorylation in the mechanism of c-Kit auto-activation and its implication in sunitinib resistance. *Journal of Biochemistry,* 147**,** 601-609.

DODSON, C. A. & BAYLISS, R. 2012. Activation of Aurora-A Kinase by Protein Partner Binding and Phosphorylation Are Independent and Synergistic. *Journal of Biological Chemistry,* 287**,** 1150-1157.

DOUVILLE, E., DUNCAN, P., ABRAHAM, N. & BELL, J. C. 1994. Dual specificity kinases--a new family of signal transducers. *Cancer Metastasis Rev,* 13**,** 1-7.

DREGER, M., BENGTSSON, L., SCHONEBERG, T., OTTO, H. & HUCHO, F. 2001. Nuclear envelope proteomics: Novel integral membrane proteins of the inner nuclear membrane. *Proceedings of the National Academy of Sciences of the United States of America,* 98**,** 11943-11948.

DZEJA, P. P. & TERZIC, A. 2003. Phosphotransfer networks and cellular energetics. *Journal of Experimental Biology,* 206**,** 2039-2047.

EATHIRAJ, S., PALMA, R., HIRSCHI, M., VOLCKOVA, E., NAKUCI, E., CASTRO, J., CHEN, C. R., CHAN, T. C. K., FRANCE, D. S. & ASHWELL, M. A. 2011. A Novel Mode of Protein Kinase Inhibition Exploiting Hydrophobic Motifs of Autoinhibited Kinases Discovery of ATP-independent inhibitors of fibroblast growth factor receptor. *Journal of Biological Chemistry,* 286**,** 20677-20687.

EDER, K., GUAN, H., SUNG, H. Y., WARD, J., ANGYAL, A., JANAS, M., SARMAY, G., DUDA, E., TURNER, M., DOWER, S. K., FRANCIS, S. E., CROSSMAN, D. C. & KISS-TOTH, E. 2008. Tribbles-2 is a novel regulator of inflammatory activation of monocytes. *International Immunology,* 20**,** 1543-1550.

ELPHICK, L. M., LEE, S. E., CHILD, E. S., PRASAD, A., PIGNOCCHI, C., THIBAUDEAU, S., ANDERSON, A. A., BONNAC, L., GOUVERNEUR, V. & MANN, D. J. 2009. A Quantitative Comparison of Wild-Type and Gatekeeper Mutant Cdk2 for Chemical Genetic Studies with ATP Analogues. *Chembiochem,* 10**,** 1519-1526.

EYERS, P. A., ERIKSON, E., CHEN, L. G. & MALLER, J. L. 2003. A novel mechanism for activation of the protein kinase aurora A. *Current Biology,* 13**,** 691-697.

EYERS, P. A. & MURPHY, J. M. 2013. Dawn of the dead: protein pseudokinases signal new adventures in cell biology. *Biochemical Society Transactions,* 41**,** 969-974.

FABBRO, D., COWAN-JACOB, S. W., MOBITZ, H. & MARTINY-BARON, G. 2012. Targeting Cancer with Small-Molecular-Weight Kinase Inhibitors. *Kinase Inhibitors: Methods and Protocols,* 795**,** 1-34.

FERRARI, S., MARIN, O., PAGANO, M. A., MEGGIO, F., HESS, D., EL-SHEMERLY, M., KRYSTYNIAK, A. & PINNA, L. A. 2005. Aurora-A site specificity: a study with synthetic peptide substrates. *Biochemical Journal,* 390**,** 293-302.

FILIPPAKOPOULOS, P., QI, J., PICAUD, S., SHEN, Y., SMITH, W. B., FEDOROV, O., MORSE, E. M., KEATES, T., HICKMAN, T. T., FELLETAR, I., PHILPOTT, M., MUNRO, S., MCKEOWN, M. R., WANG, Y., CHRISTIE, A. L., WEST, N., CAMERON, M. J., SCHWARTZ, B., HEIGHTMAN, T. D., LA THANGUE, N., FRENCH, C. A., WIEST, O., KUNG, A. L., KNAPP, S. & BRADNER, J. E. 2010. Selective inhibition of BET bromodomains. *Nature,* 468**,** 1067-73.

FOEHR, E. D., RAFFIONI, S., MURRAY-RUST, J. & BRADSHAW, R. A. 2001. The role of tyrosine residues in fibroblast growth factor receptor 1 signaling in PC12 cells - Systematic site-directed mutagenesis in the endodomain. *Journal of Biological Chemistry,* 276**,** 37529-37536.

FOSTER, F. M., TRAER, C. J., ABRAHAM, S. M. & FRY, M. J. 2003. The phosphoinositide (PI) 3-kinase family. *Journal of Cell Science,* 116**,** 3037-3040.

FRENCH, P. J., SWAGEMAKERS, S. M., NAGEL, J. H., KOUWENHOVEN, M. C., BROUWER, E., VAN DER SPEK, P., LUIDER, T. M., KROS, J. M., VAN DEN BENT, M. J. & SILLEVIS SMITT, P. A. 2005. Gene expression profiles associated with treatment response in oligodendrogliomas. *Cancer Research,* 65**,** 11335-44.

FRIERSON, H. F., JR., EL-NAGGAR, A. K., WELSH, J. B., SAPINOSO, L. M., SU, A. I., CHENG, J., SAKU, T., MOSKALUK, C. A. & HAMPTON, G. M. 2002. Large scale molecular analysis identifies genes with altered expression in salivary adenoid cystic carcinoma. *Am J Pathol,* 161**,** 1315-23.

FUKUDA, K., GUPTA, S., CHEN, K., WU, C. Y. & QIN, J. 2009. The Pseudoactive Site of ILK Is Essential for Its Binding to alpha-Parvin and Localization to Focal Adhesions. *Molecular Cell,* 36**,** 819-830.

GARSKE, A. L., PETERS, U., CORTESI, A. T., PEREZ, J. L. & SHOKAT, K. M. 2011. Chemical genetic strategy for targeting protein kinases based on covalent complementarity. *Proceedings of the National Academy of Sciences of the United States of America,* 108**,** 15046-15052.

GAUDET, M., REMTULLA, N., JACKSON, S. E., MAIN, E. R. G., BRACEWELL, D. G., AEPPLI, G. & DALBY, P. A. 2010. Protein denaturation and protein:drugs interactions from intrinsic protein fluorescence measurements at the nanolitre scale. *Protein Science,* 19**,** 1544-1554.

GLASS, D. B., MASARACCHIA, R. A., FERAMISCO, J. R. & KEMP, B. E. 1978. Isolation of phosphorylated peptides and proteins on ion-exchange papers. *Analytical Biochemistry,* 87**,** 566-575.

GRANDINETTI, K. B., STEVENS, T. A., HA, S., SALAMONE, R. J., WALKER, J. R., ZHANG, J., AGARWALLA, S., TENEN, D. G., PETERS, E. C. & REDDY, V. A. 2011. Overexpression of TRIB2 in human lung cancers contributes to tumorigenesis through downregulation of C/EBP alpha. *Oncogene,* 30**,** 3328-3335.

GRINER, L. N., MCGRAW, K. L., JOHNSON, J. O., LIST, A. F. & REUTHER, G. W. 2013. JAK2-V617F-mediated signalling is dependent on lipid rafts and statins inhibit JAK2-V617F-dependent cell growth. *Br J Haematol,* 160**,** 177-87.

GROSSHANS, J. & WIESCHAUS, E. 2000. A genetic link between morphogenesis and cell division during formation of the ventral furrow in Drosophila. *Cell,* 101**,** 523-31.

GRUTZMANN, R., PILARSKY, C., AMMERPOHL, O., LUTTGES, J., BOHME, A., SIPOS, B., FOERDER, M., ALLDINGER, I., JAHNKE, B., SCHACKERT, H. K., KALTHOFF, H., KREMER, B., KLOPPEL, G. & SAEGER, H. D. 2004. Gene expression profiling of microdissected pancreatic ductal carcinomas using high-density DNA microarrays. *Neoplasia,* 6**,** 611-22.

GUTMANN, D. H., HEDRICK, N. M., LI, J., NAGARAJAN, R., PERRY, A. & WATSON, M. A. 2002. Comparative gene expression profile analysis of neurofibromatosis 1-associated and sporadic pilocytic astrocytomas. *Cancer Research,* 62**,** 2085-91.

HAN, Y. H., MOON, H. J., YOU, B. R. & PARK, W. H. 2009. The effect of MG132, a proteasome inhibitor on HeLa cells in relation to cell growth, reactive oxygen species and GSH. *Oncology Reports,* 22**,** 215-221.

HANADA, N., LO, H. W., DAY, C. P., PAN, Y., NAKAJIMA, Y. & HUNG, M. C. 2006. Co-regulation of B-Myb expression by E2F1 and EGF receptor. *Molecular Carcinogenesis,* 45**,** 10-17.

HANKS, S. K. & HUNTER, T. 1995. Protein kinases 6. The eukaryotic protein kinase superfamily: kinase (catalytic) domain structure and classification. *Faseb Journal,* 9**,** 576-96.

HANKS, S. K., QUINN, A. M. & HUNTER, T. 1988. The Protein-Kinase Family - Conserved Features and Deduced Phylogeny of the Catalytic Domains. *Science,* 241**,** 42-52.

HANNIGAN, G. E., LEUNGHAGESTEIJN, C., FITZGIBBON, L., COPPOLINO, M. G., RADEVA, G., FILMUS, J., BELL, J. C. & DEDHAR, S. 1996. Regulation of cell adhesion and anchorage-dependent growth by a new beta(1)-integrin-linked protein kinase. *Nature,* 379**,** 91-96.

HANNON, M. M., LOHAN, F., ERBILGIN, Y., SAYITOGLU, M., O'HAGAN, K., MILLS, K., OZBEK, U. & KEESHAN, K. 2012. Elevated TRIB2 with NOTCH1 activation in paediatric/adult T-ALL. *Br J Haematol,* 158**,** 626-34.

HANTSCHEL, O. & SUPERTI-FURGA, G. 2004. Regulation of the c-Abl and Bcr-Abl tyrosine kinases. *Nat Rev Mol Cell Biol,* 5**,** 33-44.

HAO, Y., CHUN, A., CHEUNG, K., RASHIDI, B. & YANG, X. 2008. Tumor suppressor LATS1 is a negative regulator of oncogene YAP. *Journal of Biological Chemistry,* 283**,** 5496-5509.

HAO, Y., TRIADAFILOPOULOS, G., SAHBAIE, P., YOUNG, H. S., OMARY, M. B. & LOWE, A. W. 2006. Gene expression profiling reveals stromal genes expressed in common between Barrett's esophagus and adenocarcinoma. *Gastroenterology,* 131**,** 925-33.

HAQQ, C., NOSRATI, M., SUDILOVSKY, D., CROTHERS, J., KHODABAKHSH, D., PULLIAM, B. L., FEDERMAN, S., MILLER, J. R., 3RD, ALLEN, R. E., SINGER, M. I., LEONG, S. P., LJUNG, B. M., SAGEBIEL, R. W. & KASHANI-SABET, M. 2005. The gene expression signatures of melanoma progression. *Proc Natl Acad Sci U S A,* 102**,** 6092-7.

HATZIVASSILIOU, G., SONG, K., YEN, I., BRANDHUBER, B. J., ANDERSON, D. J., ALVARADO, R., LUDLAM, M. J. C., STOKOE, D., GLOOR, S. L., VIGERS, G., MORALES, T., ALIAGAS, I., LIU, B., SIDERIS, S., HOEFLICH, K. P., JAISWAL, B. S., SESHAGIRI, S., KOEPPEN, H., BELVIN, M., FRIEDMAN, L. S. & MALEK, S. 2010. RAF inhibitors prime wild-type RAF to activate the MAPK pathway and enhance growth. *Nature,* 464**,** 431-435.

HAUN, R. S., SERVENTI, I. M. & MOSS, J. 1992. Rapid, reliable ligation-independent cloning of PCR products using modified plasmid vectors. *Biotechniques,* 13**,** 515-8.

HAYDON, C. E., EYERS, P. A., AVELINE-WOLF, L. D., RESING, K. A., MALLER, J. L. & AHN, N. G. 2003. Identification of novel phosphorylation sites on Xenopus laevis Aurora A and analysis of phosphopeptide enrichment by immobilized metal-affinity chromatography. *Mol Cell Proteomics,* 2**,** 1055-67.

HE, M., BREESE, V., HANG, S., ZHANG, C. X., XIONG, J. J. & JACKSON, C. 2013. BRAF V600E Mutations in Endometrial Adenocarcinoma. *Diagnostic Molecular Pathology,* 22**,** 35-40.

HENGEVELD, R. C. C., HERTZ, N. T., VROMANS, M. J. M., ZHANG, C., BURLINGAME, A. L., SHOKAT, K. M. & LENS, S. M. A. 2012. Development of a Chemical Genetic Approach for Human Aurora B Kinase Identifies Novel Substrates of the Chromosomal Passenger Complex. *Molecular & Cellular Proteomics,* 11**,** 47-59.

HIRATSUKA, T. 2003. Fluorescent and colored trinitrophenylated analogs of ATP and GTP. *Eur J Biochem,* 270**,** 3479-85.

HOVENS, C. M., STACKER, S. A., ANDRES, A. C., HARPUR, A. G., ZIEMIECKI, A. & WILKS, A. F. 1992. Ryk, a Receptor Tyrosine Kinase-Related Molecule with Unusual Kinase Domain Motifs. *Proceedings of the National Academy of Sciences of the United States of America,* 89**,** 11818-11822.

HSU, J.-M., CHEN, C.-T., CHOU, C.-K., KUO, H.-P., LI, L.-Y., LIN, C.-Y., LEE, H.-J., WANG, Y.-N., LIU, M., LIAO, H.-W., SHI, B., LAI, C.-C., BEDFORD, M. T., TSAI, C.-H. & HUNG, M.-C. 2011. Crosstalk between Arg 1175 methylation and Tyr 1173 phosphorylation negatively modulates EGFR-mediated ERK activation. *Nature Cell Biology,* 13**,** 174-181.

HSU, P. D., LANDER, E. S. & ZHANG, F. 2014. Development and Applications of CRISPR-Cas9 for Genome Engineering. *Cell,* 157**,** 1262-1278.

HSU, S. C. & HUNG, M. C. 2007. Characterization of a novel tripartite nuclear localization sequence in the EGFR family. *Journal of Biological Chemistry,* 282**,** 10432-10440.

HU, J. C., YU, H. Y., KORNEV, A. P., ZHAO, J. P., FILBERT, E. L., TAYLOR, S. S. & SHAW, A. S. 2011a. Mutation that blocks ATP binding creates a pseudokinase stabilizing the scaffolding function of kinase suppressor of Ras, CRAF and BRAF. *Proceedings of the National Academy of Sciences of the United States of America,* 108**,** 6067-6072.

HU, W.-J., ZHOU, S.-M., YANG, J. S. & MENG, F.-G. 2011b. Computational simulations to predict creatine kinase-associated factors: protein-protein interaction studies of brain and muscle types of creatine kinases. *Enzyme research,* 2011**,** 328249.

HUANG, D., ZHANG, Y. & CHEN, X. 2003. Analysis of intracellular nucleoside triphosphate levels in normal and tumor cell lines by high-performance liquid chromatography. *J Chromatogr B Analyt Technol Biomed Life Sci,* 784**,** 101-9.

HUANG, D., ZHOU, T., LAFLEUR, K., NEVADO, C. & CAFLISCH, A. 2010. Kinase selectivity potential for inhibitors targeting the ATP binding site: a network analysis. *Bioinformatics,* 26**,** 198-204.

HUBBARD, S. R. 1999. Src autoinhibition: let us count the ways. *Nature Structural Biology,* 6**,** 711-4.

HUNG, L.-Y., TSENG, J. T., LEE, Y.-C., XIA, W., WANG, Y.-N., WU, M.-L., CHUANG, Y.-H., LAI, C.-H. & CHANG, W.-C. 2008. Nuclear epidermal growth factor receptor (EGFR) interacts with signal transducer and activator of transcription 5 (STAT5) in activating Aurora-A gene expression. *Nucleic Acids Research,* 36**,** 4337-4351.

HUSE, M. & KURIYAN, J. 2002. The conformational plasticity of protein kinases. *Cell,* 109**,** 275-82.

IGARASHI, H., KUWAHARA, K., YOSHIDA, M., XING, Y., MAEDA, K., NAKAJIMA, K. & SAKAGUCHI, N. 2009. GANP suppresses the arginine methyltransferase PRMT5 regulating IL-4-mediated STAT6-signaling to IgE production in B cells. *Molecular Immunology,* 46**,** 1031-1041.

IYER, G. H., GARROD, S., WOODS, V. L. & TAYLOR, S. S. 2005a. Catalytic independent functions of a protein kinase as revealed by a kinase-dead mutant: Study of the Lys72His mutant of cAMP-dependent kinase. *Journal of Molecular Biology,* 351**,** 1110-1122.

IYER, G. H., MOORE, M. J. & TAYLOR, S. S. 2005b. Consequences of lysine 72 mutation on the phosphorylation and activation state of cAMP-dependent kinase. *Journal of Biological Chemistry,* 280**,** 8800-8807.

JACKSON, K. A., OPREA, G., HANDY, J. & KIMBRO, K. S. 2009. Aberrant STYK1 expression in ovarian cancer tissues and cell lines. *Journal of Ovarian Research,* 2. DOI: 10.1186/1757-2215-2-15

JAGANATHAN, S., YUE, P., PALADINO, D. C., BOGDANOVIC, J., HUO, Q. & TURKSON, J. 2011. A Functional Nuclear Epidermal Growth Factor Receptor, Src and Stat3 Heteromeric Complex in Pancreatic Cancer Cells. *Plos One,* 6. DOI: 10.1371/journal.pone.0019605

JAISWAL, B. S., KLJAVIN, N. M., STAWISKI, E. W., CHAN, E., PARIKH, C., DURINCK, S., CHAUDHURI, S., PUJARA, K., GUILLORY, J., EDGAR, K. A., JANAKIRAMAN, V., SCHOLZ, R. P., BOWMAN, K. K., LORENZO, M., LI, H., WU, J. S., YUAN, W. L., PETERS, B. A., KAN, Z. Y., STINSON, J., MAK, M., MODRUSAN, Z., EIGENBROT, C., FIRESTEIN, R., STERN, H. M., RAJALINGAM, K., SCHAEFER, G., MERCHANT, M. A., SLIWKOWSKI, M. X., DE SAUVAGE, F. J. & SESHAGIRI, S. 2013. Oncogenic ERBB3 Mutations in Human Cancers. *Cancer Cell,* 23**,** 603-617.

JALEEL, M., SAHA, S., SHENOY, A. R. & VISWESWARIAH, S. S. 2006. The kinase homology domain of receptor guanylyl cyclase C: ATP binding and identification of an adenine nucleotide sensitive site. *Biochemistry,* 45**,** 1888-98.

JIN, G., YAMAZAKI, Y., TAKUWA, M., TAKAHARA, T., KANEKO, K., KUWATA, T., MIYATA, S. & NAKAMURA, T. 2007. Trib1 and Evi1 cooperate with Hoxa and Meis1 in myeloid leukemogenesis. *Blood,* 109**,** 3998-4005.

JINEK, M., EAST, A., CHENG, A., LIN, S., MA, E. & DOUDNA, J. 2013. RNA-programmed genome editing in human cells. *Elife,* 2**,** e00471.

JONES, J., OTU, H., SPENTZOS, D., KOLIA, S., INAN, M., BEECKEN, W. D., FELLBAUM, C., GU, X., JOSEPH, M., PANTUCK, A. J., JONAS, D. & LIBERMANN, T. A. 2005. Gene signatures of progression and metastasis in renal cell cancer. *Clin Cancer Res,* 11**,** 5730-9.

JORDAN, M. A., THROWER, D. & WILSON, L. 1992. EFFECTS OF VINBLASTINE, PODOPHYLLOTOXIN AND NOCODAZOLE ON MITOTIC SPINDLES - IMPLICATIONS FOR THE ROLE OF MICROTUBULE DYNAMICS IN MITOSIS. *Journal of Cell Science,* 102**,** 401-416.

JUNG, J. W., SHIN, W. S., SONG, J. & LEE, S. T. 2004. Cloning and characterization of the full-length mouse Ptk7 cDNA encoding a defective receptor protein tyrosine kinase. *Gene,* 328**,** 75-84.

JURA, N., ENDRES, N. F., ENGEL, K., DEINDL, S., DAS, R., LAMERS, M. H., WEMMER, D. E., ZHANG, X. W. & KURIYAN, J. 2009a. Mechanism for Activation of the EGF Receptor Catalytic Domain by the Juxtamembrane Segment. *Cell,* 137**,** 1293-1307.

JURA, N., SHAN, Y., CAO, X., SHAW, D. E. & KURIYAN, J. 2009b. Structural analysis of the catalytically inactive kinase domain of the human EGF receptor 3. *Proc Natl Acad Sci U S A,* 106**,** 21608-13.

KANNAN, N. & NEUWALD, A. F. 2005. Did protein kinase regulatory mechanisms evolve through elaboration of a simple structural component? *Journal of Molecular Biology,* 351**,** 956-72.

KANNAN, N. & TAYLOR, S. S. 2008. Rethinking pseudokinases. *Cell,* 133**,** 204-205.

KANNAN, N., TAYLOR, S. S., ZHAI, Y., VENTER, J. C. & MANNING, G. 2007. Structural and functional diversity of the microbial kinome. *PLoS Biol,* 5**,** e17. PMCID: PMC1821047

KATO, S., DING, J. X., PISCK, E., JHALA, U. S. & DU, K. Y. 2008. COP1 Functions as a FoxO1 Ubiquitin E3 Ligase to Regulate FoxO1-mediated Gene Expression. *Journal of Biological Chemistry,* 283**,** 35464-35473.

KAWASHIMA, M., LIN, L., TANAKA, S., JENNUM, P., KNUDSEN, S., NEVSIMALOVA, S., PLAZZI, G. & MIGNOT, E. 2010. Anti-Tribbles Homo log 2 (TRIB2) Autoantibodies in Narcolepsy are Associated with Recent Onset of Cataplexy. *Sleep,* 33**,** 869-874.

KEESHAN, K., BAILIS, W., DEDHIA, P. H., VEGA, M. E., SHESTOVA, O., XU, L., TOSCANO, K., ULJON, S. N., BLACKLOW, S. C. & PEAR, W. S. 2010. Transformation by Tribbles homolog 2 (Trib2) requires both the Trib2 kinase domain and COP1 binding. *Blood,* 116**,** 4948-4957.

KEESHAN, K., HE, Y. P., WOUTERS, B. J., SHESTOVA, O., XU, L. W., SAI, H., RODRIGUEZ, C. G., MAILLARD, I., VALK, P., CARROLL, M., ASTER, J. C., DELWEL, R. & PEAR, W. S. 2006. Tribbles homolog 2 (Trib2) inactivates C/EBPalpha and causes acute myelogenous leukemia. *Cancer Cell,*10 (5), 401-411

KEESHAN, K., SHESTOVA, O., USSIN, L. & PEAR, W. S. 2008. Tribbles homolog 2 (Trib2) and HoxA9 cooperate to accelerate acute myelogenous leukemia. *Blood Cells Mol Dis,* 40**,** 119-21.

KELBER, J. A., RENO, T., KAUSHAL, S., METILDI, C., WRIGHT, T., STOLETOV, K., WEEMS, J. M., PARK, F. D., MOSE, E., WANG, Y. C., HOFFMAN, R. M., LOWY, A. M., BOUVET, M. & KLEMKE, R. L. 2012. KRas Induces a Src/PEAK1/ErbB2 Kinase Amplification Loop That Drives Metastatic Growth and Therapy Resistance in Pancreatic Cancer. *Cancer Research,* 72**,** 2554-2564.

KHOKHLATCHEV, A., XU, S. C., ENGLISH, J., WU, P. Q., SCHAEFER, E. & COBB, M. H. 1997. Reconstitution of mitogen-activated protein kinase phosphorylation cascades in bacteria - Efficient synthesis of active protein kinases. *Journal of Biological Chemistry,* 272**,** 11057-11062.

KIMBRO, K. S., DUSCHENE, K., WILLARD, M., MOORE, J.-A. & FREEMAN, S. 2008. A novel gene STYK1/NOK is upregulated in estrogen receptor-alpha negative estrogen receptor-beta positive breast cancer cells following estrogen treatment. *Molecular Biology Reports,* 35**,** 23-27.

KISS-TOTH, E., BAGSTAFF, S. M., SUNG, H. Y., JOZSA, V., DEMPSEY, C., CAUNT, J. C., OXLEY, K. M., WYLLIE, D. H., POLGAR, T., HARTE, M., O'NEILL, L. A. J., QWARNSTROM, E. E. & DOWER, S. K. 2004. Human tribbles, a protein family controlling mitogen-activated protein kinase cascades. *Journal of Biological Chemistry,* 279**,** 42703-42708.

KITAMOTO, A., KITAMOTO, T., NAKAMURA, T., OGAWA, Y., YONEDA, M., HYOGO, H., OCHI, H., MIZUSAWA, S., UENO, T., NAKAO, K.,

SEKINE, A., CHAYAMA, K., NAKAJIMA, A. & HOTTA, K. 2014. Association of polymorphisms in GCKR and TRIB1 with nonalcoholic fatty liver disease and metabolic syndrome traits. *Endocr J*. 61 (7), 683-9

KLAUS, A., ZORMAN, S., BERTHIER, A., POLGE, C., RAMIREZ, S., MICHELLAND, S., SEVE, M., VERTOMMEN, D., RIDER, M., LENTZE, N., AUERBACH, D. & SCHLATTNER, U. 2013. Glutathione S-transferases interact with AMP-activated protein kinase: evidence for S-glutathionylation and activation in vitro. *Plos One,* 8**,** e62497.

KNIGHT, Z. A. & SHOKAT, K. M. 2005. Features of selective kinase inhibitors. *Chemistry & Biology,* 12**,** 621-637.

KONDOH, T., KOBAYASHI, D., TSUJI, N., KURIBAYASHI, K. & WATANABE, N. 2009. Overexpression of serine threonine tyrosine kinase 1/novel oncogene with kinase domain mRNA in patients with acute leukemia. *Experimental Hematology,* 37**,** 824-830.

KORNEV, A. P., HASTE, N. M., TAYLOR, S. S. & TEN EYCK, L. F. 2006. Surface comparison of active and inactive protein kinases identifies a conserved activation mechanism. *Proceedings of the National Academy of Sciences of the United States of America,* 103**,** 17783-17788.

KORNEV, A. P., TAYLOR, S. S. & TEN EYCK, L. F. 2008. A helix scaffold for the assembly of active protein kinases. *Proceedings of the National Academy of Sciences of the United States of America,* 105**,** 14377-14382.

KOST, T. A., CONDREAY, J. P. & JARVIS, D. L. 2005. Baculovirus as versatile vectors for protein expression in insect and mammalian cells. *Nature Biotechnology,* 23**,** 567-75.

KRISHNA, S. N., LUAN, C.-H., MISHRA, R. K., XU, L., SCHEIDT, K. A., ANDERSON, W. F. & BERGAN, R. C. 2013. A Fluorescence-Based Thermal Shift Assay Identifies Inhibitors of Mitogen Activated Protein Kinase Kinase 4. *Plos One,* 8. e81504

KUFAREVA, I. & ABAGYAN, R. 2008. Type-II Kinase Inhibitor Docking, Screening, and Profiling Using Modified Structures of Active Kinase States. *Journal of Medicinal Chemistry,* 51**,** 7921-7932.

KWAN, A. H., MOBLI, M., GOOLEY, P. R., KING, G. F. & MACKAY, J. P. 2011. Macromolecular NMR spectroscopy for the non-spectroscopist. *Febs Journal,* 278**,** 687-703.

LANGE, A., WICKSTROM, S. A., JAKOBSON, M., ZENT, R., SAINIO, K. & FASSLER, R. 2009. Integrin-linked kinase is an adaptor with essential functions during mouse development. *Nature,* 461**,** 1002-1006.

LEMMON, M. A. & SCHLESSINGER, J. 2010. Cell Signaling by Receptor Tyrosine Kinases. *Cell,* 141**,** 1117-1134.

LENERTZ, L. Y., LEE, B. H., MIN, X. S., XU, B. E., WEDIN, K., EARNEST, S., GOLDSMITH, E. J. & COBB, M. H. 2005. Properties of WNK1 and implications for other family members. *Journal of Biological Chemistry,* 280**,** 26653-26658.

LI, J., WU, F., SHENG, F., LI, Y.-J., JIN, D., DING, X. & ZHANG, S. 2012. NOK/STYK1 interacts with GSK-3 beta and mediates Ser9 phosphorylation through activated Akt. *Febs Letters,* 586**,** 3787-3792.

LI, L. J., SUN, L., GAO, F. R., JIANG, J., YANG, Y., LI, C. L., GU, J. J., WEI, Z., YANG, A. C., LU, R., MA, Y., TANG, F., KWON, S. W., ZHAO, Y. M., LI, J. S. & JIN, Y. 2010. Stk40 links the pluripotency factor Oct4 to the Erk/MAPK pathway and controls extraembryonic endoderm differentiation.

Proceedings of the National Academy of Sciences of the United States of America, 107**,** 1402-1407.

LI, Y.-H., ZHONG, S., RONG, Z.-L., REN, Y.-M., LI, Z.-Y., ZHANG, S.-P., CHANG, Z. & LIU, L. 2007. The carboxyl terminal tyrosine 417 residue of NOK has an autoinhibitory effect on NOK-mediated signaling transductions. *Biochemical and Biophysical Research Communications,* 356**,** 444-449.

LI, Y. H., WANG, Y. Y., ZHONG, S., RONG, Z. L., REN, Y. M., LI, Z. Y., ZHANG, S. P., CHANG, Z. J. & LIU, L. 2009. Transmembrane Helix of Novel Oncogene with Kinase-Domain (NOK) Influences Its Oligomerization and Limits the Activation of RAS/MAPK Signaling. *Molecules and Cells,* 27**,** 39-45.

LIANG, K. L., RISHI, L. & KEESHAN, K. 2013. Tribbles in acute leukemia. *Blood,* 121**,** 4265-4270.

LILIENTHAL, E., KOLANOWSKI, K. & BECKER, W. 2010. Development of a sensitive non-radioactive protein kinase assay and its application for detecting DYRK activity in Xenopus laevis oocytes. *BMC Biochem,* 11**,** 20. DOI: 10.1186/1471-2091-11-20

LIM, A. S. P. & SCAMMELL, T. E. 2010. The Trouble with Tribbles: Do Antibodies Against TRIB2 Cause Narcolepsy? *Sleep,* 33**,** 857-858.

LIN, S. Y., MAKINO, K., XIA, W. Y., MATIN, A., WEN, Y., KWONG, K. Y., BOURGUIGNON, L. & HUNG, M. C. 2001. Nuclear localization of EGF receptor and its potential new role as a transcription factor. *Nature Cell Biology,* 3**,** 802-808.

LINDAUER, K., LOERTING, T., LIEDL, K. R. & KROEMER, R. T. 2001. Prediction of the structure of human Janus kinase 2 (JAK2) comprising the two carboxy-terminal domains reveals a mechanism for autoregulation. *Protein Eng,* 14**,** 27-37.

LINDBERG, R. A., QUINN, A. M. & HUNTER, T. 1992. Dual-Specificity Protein-Kinases - Will Any Hydroxyl Do. *Trends in Biochemical Sciences,* 17**,** 114-119.

LITTLEFIELD, P., MOASSER, MARK M. & JURA, N. 2014. An ATP-Competitive Inhibitor Modulates the Allosteric Function of the HER3 Pseudokinase. *Chemistry & Biology,* 21**,** 453-458.

LIU, J. R., WU, X. X., FRANKLIN, J. L., MESSINA, J. L., HILL, H. S., MOELLERING, D. R., WALTON, R. G., MARTIN, M. & GARVEY, W. T. 2010. Mammalian Tribbles homolog 3 impairs insulin action in skeletal muscle: role in glucose-induced insulin resistance. *American Journal of Physiology-Endocrinology and Metabolism,* 298**,** E565-E576.

LIU, L., YU, X. Z., LI, T. S., SONG, L. X., CHEN, P. L., SUO, T. L., LI, Y. H., WANG, S. D., CHEN, Y., REN, Y. M., ZHANG, S. P., CHANG, Z. J. & FU, X. Y. 2004. A novel protein tyrosine kinase NOK that shares homology with platelet-derived growth factor/fibroblast growth factor receptors induces tumorigenesis and metastasis in nude mice. *Cancer Research,* 64**,** 3491-3499.

LIU, Q. S., SABNIS, Y., ZHAO, Z., ZHANG, T. H., BUHRLAGE, S. J., JONES, L. H. & GRAY, N. S. 2013. Developing Irreversible Inhibitors of the Protein Kinase Cysteinome. *Chemistry & Biology,* 20**,** 146-159.

LIU, Y. & GRAY, N. S. 2006. Rational design of inhibitors that bind to inactive kinase conformations. *Nature Chemical Biology,* 2**,** 358-364.

LIU, Y., SHAH, K., YANG, F., WITUCKI, L. & SHOKAT, K. M. 1998. Engineering Src family protein kinases with unnatural nucleotide specificity. *Chemistry & Biology,* 5**,** 91-101.

LIZCANO, J. M., GORANSSON, O., TOTH, R., DEAK, M., MORRICE, N. A., BOUDEAU, J., HAWLEY, S. A., UDD, L., MAKELA, T. P., HARDIE, D. G. & ALESSI, D. R. 2004. LKB1 is a master kinase that activates 13 kinases of the AMPK subfamily, including MARK/PAR-1. *EMBO J,* 23**,** 833-43.

LO, H.-W., CAO, X., ZHU, H. & ALI-OSMAN, F. 2010. Cyclooxygenase-2 Is a Novel Transcriptional Target of the Nuclear EGFR-STAT3 and EGFRvIII-STAT3 Signaling Axes. *Molecular Cancer Research,* 8**,** 232-245.

LO, H. W., HSU, S. C., ALI-SEYED, M., GUNDUZ, M., XIA, W. Y., WEI, Y. K., BARTHOLOMEUSZ, G., SHIH, J. Y. & HUNG, M. C. 2005. Nuclear interaction of EGFR and STAT3 in the activation of the iNOS/NO pathway. *Cancer Cell,* 7**,** 575-589.

LOGSDON, C. D., SIMEONE, D. M., BINKLEY, C., ARUMUGAM, T., GREENSON, J. K., GIORDANO, T. J., MISEK, D. E., KUICK, R. & HANASH, S. 2003. Molecular profiling of pancreatic adenocarcinoma and chronic pancreatitis identifies multiple genes differentially regulated in pancreatic cancer. *Cancer Research,* 63**,** 2649-57.

LOHAN, F. & KEESHAN, K. 2013. The functionally diverse roles of tribbles. *Biochemical Society Transactions,* 41**,** 1096-1100.

LUCET, I. S., BABON, J. J. & MURPHY, J. M. 2013. Techniques to examine nucleotide binding by pseudokinases. *Biochemical Society Transactions,* 41**,** 975-980.

MACEK, B., GNAD, F., SOUFI, B., KUMAR, C., OLSEN, J. V., MIJAKOVIC, I. & MANN, M. 2008. Phosphoproteome analysis of *E. coli* reveals evolutionary conservation of bacterial Ser/Thr/Tyr phosphorylation. *Molecular & Cellular Proteomics,* 7**,** 299-307.

MANNING, G., WHYTE, D. B., MARTINEZ, R., HUNTER, T. & SUDARSANAM, S. 2002. The Protein Kinase Complement of the Human Genome. *Science,* 298**,** 1912-1934.

MASONER, V., DAS, R., PENCE, L., ANAND, G., LAFERRIERE, H., ZARS, T., BOUYAIN, S. & DOBENS, L. L. 2013. The kinase domain of Drosophila Tribbles is required for turnover of fly C/EBP during cell migration. *Developmental Biology,* 375**,** 33-44.

MATA, J., CURADO, S., EPHRUSSI, A. & RORTH, P. 2000. Tribbles coordinates mitosis and morphogenesis in Drosophila by regulating string/CDC25 proteolysis. *Cell,* 101**,** 511-22.

MATSUSHIMA, R., HARADA, N., WEBSTER, N. J. G., TSUTSUMI, Y. M. & NAKAYA, Y. 2006. Effect of TRB3 on insulin and nutrient-stimulated hepatic p70 S6 kinase activity. *Journal of Biological Chemistry,* 281**,** 29719-29729.

MENDROLA, J. M., SHI, F. M., PARK, J. H. & LEMMON, M. A. 2013. Receptor tyrosine kinases with intracellular pseudokinase domains. *Biochemical Society Transactions,* 41**,** 1029-1036.

MEYER, G., GICKLHORN, D., STRIVE, T., RADSAK, K. & EICKMANN, M. 2002. A three-residue signal confers localization of a reporter protein in the inner nuclear membrane. *Biochemical and Biophysical Research Communications,* 291**,** 966-971.

MEYER, G. A. & RADSAK, K. D. 2000. Identification of a novel signal sequence that targets transmembrane proteins to the nuclear envelope inner membrane. *Journal of Biological Chemistry,* 275**,** 3857-3866.

MICHAEL, M., VLAHOVIC, G., KHAMLY, K., PIERCE, K. J., GUO, F. & OLSZANSKI, A. J. 2010. Phase Ib study of CP-868,596, a PDGFR inhibitor,

combined with docetaxel with or without axitinib, a VEGFR inhibitor. *British Journal of Cancer,* 103**,** 1554-1561.

MIYOSHI, N., ISHII, H., MIMORI, K., TAKATSUNO, Y., KIM, H., HIROSE, H., SEKIMOTO, M., DOKI, Y. & MORI, M. 2009. Abnormal expression of TRIB3 in colorectal cancer: a novel marker for prognosis. *British Journal of Cancer,* 101**,** 1664-1670.

MOGHADDAS GHOLAMI, A., HAHNE, H., WU, Z., AUER, F. J., MENG, C., WILHELM, M. & KUSTER, B. 2013. Global proteome analysis of the NCI-60 cell line panel. *Cell Rep,* 4**,** 609-20.

MORIAI, R., KOBAYASHI, D., AMACHIKA, T., TSUJI, N. & WATANABE, N. 2006. Diagnostic relevance of overexpressed NOK mRNA in breast cancer. *Anticancer Research,* 26**,** 4969-4973.

MUKHERJEE, K., SHARMA, M., JAHN, R., WAHL, M. C. & SUDHOF, T. C. 2010. Evolution of CASK into a Mg2+-Sensitive Kinase. *Science Signaling,* 3. DOI: 10.1126/scisignal.2000800

MUKHERJEE, K., SHARMA, M., URLAUB, H., BOURENKOV, G. P., JAHN, R., SUDHOF, T. C. & WAHL, M. C. 2008. CASK functions as a Mg2+-independent neurexin kinase. *Cell,* 133**,** 328-339.

MURPHY, J. M., CZABOTAR, P. E., HILDEBRAND, J. M., LUCET, I. S., ZHANG, J. G., ALVAREZ-DIAZ, S., LEWIS, R., LALAOUI, N., METCALF, D., WEBB, A. I., YOUNG, S. N., VARGHESE, L. N., TANNAHILL, G. M., HATCHELL, E. C., MAJEWSKI, I. J., OKAMOTO, T., DOBSON, R. C. J., HILTON, D. J., BABON, J. J., NICOLA, N. A., STRASSER, A., SILKE, J. & ALEXANDER, W. S. 2013. The Pseudokinase MLKL Mediates Necroptosis via a Molecular Switch Mechanism. *Immunity,* 39**,** 443-453.

MURPHY, J. M., LUCET, I. S., HILDEBRAND, J. M., TANZER, M. C., YOUNG, S. N., SHARMA, P., LESSENE, G., ALEXANDER, W. S., BABON, J. J., SILKE, J. & CZABOTAR, P. E. 2014a. Insights into the evolution of divergent nucleotide-binding mechanisms among pseudokinases revealed by crystal structures of human and mouse MLKL. *Biochemical Journal,* 457**,** 369-377.

MURPHY, J. M., ZHANG, Q., YOUNG, S. N., REESE, M. L., BAILEY, F. P., EYERS, P. A., UNGUREANU, D., HAMMAREN, H., SILVENNOINEN, O., VARGHESE, L. N., CHEN, K., TRIPAYDONIS, A., JURA, N., FUKUDA, K., QIN, J., NIMCHUK, Z., MUDGETT, M. B., ELOWE, S., GEE, C. L., LIU, L., DALY, R. J., MANNING, G., BABON, J. J. & LUCET, I. S. 2014b. A robust methodology to subclassify pseudokinases based on their nucleotide-binding properties. *Biochemical Journal,* 457**,** 323-334.

NA, H. W., SHIN, W. S., LUDWIG, A. & LEE, S. T. 2012. The Cytosolic Domain of Protein-tyrosine Kinase 7 (PTK7), Generated from Sequential Cleavage by a Disintegrin and Metalloprotease 17 (ADAM17) and gamma-Secretase, Enhances Cell Proliferation and Migration in Colon Cancer Cells. *Journal of Biological Chemistry,* 287**,** 25001-25009.

NAGAR, B. 2007. c-Abl tyrosine kinase and inhibition by the cancer drug imatinib (Gleevec/STI-571). *Journal of Nutrition,* 137**,** 1518s-1523s.

NAHTA, R. & ESTEVA, F. J. 2006. HER2 therapy: molecular mechanisms of trastuzumab resistance. *Breast Cancer Res,* 8**,** 215. PMICD: PMC1797036

NAIKI, T., SAIJOU, E., MIYAOKA, Y., SEKINE, K. & MIYAJIMA, A. 2007. TRB2, a mouse tribbles ortholog, suppresses adipocyte differentiation by

inhibiting AKT and C/EBP beta. *Journal of Biological Chemistry,* 282**,** 24075-24082.

NIESEN, F. H., BERGLUND, H. & VEDADI, M. 2007. The use of differential scanning fluorimetry to detect ligand interactions that promote protein stability. *Nature Protocols,* 2**,** 2212-2221.

NINDL, I., DANG, C., FORSCHNER, T., KUBAN, R. J., MEYER, T., STERRY, W. & STOCKFLETH, E. 2006. Identification of differentially expressed genes in cutaneous squamous cell carcinoma by microarray expression profiling. *Mol Cancer,* 5**,** 30. PMCID: PMC1569867

NISHIMURA, T. & TAKEICHI, M. 2008. Shroom3-mediated recruitment of Rho kinases to the apical cell junctions regulates epithelial and neuroepithelial planar remodeling. *Development,* 135**,** 1493-1502.

OH, H., OZKIRIMLI, E., SHAH, K., HARRISON, M. L. & GEAHLEN, R. L. 2007. Generation of an analog-sensitive syk tyrosine kinase for the study of signaling dynamics from the B cell antigen receptor. *Journal of Biological Chemistry,* 282**,** 33760-33768.

OKAMOTO, H., LATRES, E., LIU, R., THABET, K., MURPHY, A., VALENZEULA, D., YANCOPOULOS, G. D., STITT, T. N., GLASS, D. J. & SLEEMAN, M. W. 2007. Genetic deletion of Trb3, the mammalian Drosophila tribbles homolog, displays normal hepatic insulin signaling and glucose homeostasis. *Diabetes,* 56**,** 1350-1356.

OKAMOTO, R., TAKEGAWA, K. & KIMURA, Y. 2014. Regulation of eukaryotic-like protein kinase activity of DspA from Myxococcus xanthus by autophosphorylation. *Journal of Biochemistry,* 155**,** 99-106.

OKAYAMA, H., KOHNO, T., ISHII, Y., SHIMADA, Y., SHIRAISHI, K., IWAKAWA, R., FURUTA, K., TSUTA, K., SHIBATA, T., YAMAMOTO, S., WATANABE, S., SAKAMOTO, H., KUMAMOTO, K., TAKENOSHITA, S., GOTOH, N., MIZUNO, H., SARAI, A., KAWANO, S., YAMAGUCHI, R., MIYANO, S. & YOKOTA, J. 2012. Identification of genes upregulated in ALK-positive and EGFR/KRAS/ALK-negative lung adenocarcinomas. *Cancer Research,* 72**,** 100-11.

OSTERTAG, A., JONES, A., ROSE, A. J., LIEBERT, M., KLEINSORG, S., REIMANN, A., VEGIOPOULOS, A., BERRIEL DIAZ, M., STRZODA, D., YAMAMOTO, M., SATOH, T., AKIRA, S. & HERZIG, S. 2010. Control of adipose tissue inflammation through TRB1. *Diabetes,* 59**,** 1991-2000.

OTA, T., SUTO, S., KATAYAMA, H., HAN, Z. B., SUZUKI, F., MAEDA, M., TANINO, M., TERADA, Y. & TATSUKA, M. 2002. Increased mitotic phosphorylation of histone H3 attributable to AIM-1/Aurora-B overexpression contributes to chromosome number instability. *Cancer Research,* 62**,** 5168-5177.

PAULS, E., NANDA, S. K., SMITH, H., TOTH, R., ARTHUR, J. S. & COHEN, P. 2013. Two phases of inflammatory mediator production defined by the study of IRAK2 and IRAK1 knock-in mice. *J Immunol,* 191**,** 2717-30.

PEARCE, L. R., KOMANDER, D. & ALESSI, D. R. 2010. The nuts and bolts of AGC protein kinases. *Nature Reviews Molecular Cell Biology,* 11**,** 9-22.

PEI, H., LI, L., FRIDLEY, B. L., JENKINS, G. D., KALARI, K. R., LINGLE, W., PETERSEN, G., LOU, Z. & WANG, L. 2009. FKBP51 affects cancer cell response to chemotherapy by negatively regulating Akt. *Cancer Cell,* 16**,** 259-66.

PERSAD, S., ATTWELL, S., GRAY, V., MAWJI, N., DENG, J. T., LEUNG, D., YAN, J., SANGHERA, J., WALSH, M. P. & DEDHAR, S. 2001. Regulation

of protein kinase B/Akt-serine 473 phosphorylation by integrin-linked kinase - Critical roles for kinase activity and amino acids arginine 211 and serine 343. *Journal of Biological Chemistry,* 276**,** 27462-27469.

PETER, A., STEFAN, N., CEGAN, A., WALENTA, M., WAGNER, S., KONIGSRAINER, A., KONIGSRAINER, I., MACHICAO, F., SCHICK, F., HARING, H. U. & SCHLEICHER, E. 2011. Hepatic Glucokinase Expression Is Associated with Lipogenesis and Fatty Liver in Humans. *Journal of Clinical Endocrinology & Metabolism,* 96**,** E1126-E1130.

PIALA, A. T., MOON, T. M., AKELLA, R., HE, H., COBB, M. H. & GOLDSMITH, E. J. 2014. Chloride Sensing by WNK1 Involves Inhibition of Autophosphorylation. *Sci Signal,* 7**,** ra41. DOI: 10.1126/scisignal.2005050

PICCALUGA, P. P., AGOSTINELLI, C., CALIFANO, A., ROSSI, M., BASSO, K., ZUPO, S., WENT, P., KLEIN, U., ZINZANI, P. L., BACCARANI, M., DALLA FAVERA, R. & PILERI, S. A. 2007. Gene expression analysis of peripheral T cell lymphoma, unspecified, reveals distinct profiles and new potential therapeutic targets. *Journal of Clinical Investigation,* 117**,** 823-34.

PLANO, D., AMIN, S. & SHARMA, A. K. 2014. Importance of Sphingosine Kinase (SphK) as a Target in Developing Cancer Therapeutics and Recent Developments in the Synthesis of Novel SphK Inhibitors. *Journal of Medicinal Chemistry*. 57 (13), 5509-24

POLLACK, B. P., KOTENKO, S. V., HE, W., IZOTOVA, L. S., BARNOSKI, B. L. & PESTKA, S. 1999. The human homologue of the yeast proteins Skb1 and Hsl7p interacts with Jak kinases and contains protein methyltransferase activity. *Journal of Biological Chemistry,* 274**,** 31531-31542.

POMEROY, S. L., TAMAYO, P., GAASENBEEK, M., STURLA, L. M., ANGELO, M., MCLAUGHLIN, M. E., KIM, J. Y., GOUMNEROVA, L. C., BLACK, P. M., LAU, C., ALLEN, J. C., ZAGZAG, D., OLSON, J. M., CURRAN, T., WETMORE, C., BIEGEL, J. A., POGGIO, T., MUKHERJEE, S., RIFKIN, R., CALIFANO, A., STOLOVITZKY, G., LOUIS, D. N., MESIROV, J. P., LANDER, E. S. & GOLUB, T. R. 2002. Prediction of central nervous system embryonal tumour outcome based on gene expression. *Nature,* 415**,** 436-42.

PYEON, D., NEWTON, M. A., LAMBERT, P. F., DEN BOON, J. A., SENGUPTA, S., MARSIT, C. J., WOODWORTH, C. D., CONNOR, J. P., HAUGEN, T. H., SMITH, E. M., KELSEY, K. T., TUREK, L. P. & AHLQUIST, P. 2007. Fundamental differences in cell cycle deregulation in human papillomavirus-positive and human papillomavirus-negative head/neck and cervical cancers. *Cancer Research,* 67**,** 4605-19.

QI, L., HEREDIA, J. E., ALTAREJOS, J. Y., SCREATON, R., GOEBEL, N., NIESSEN, S., MACLEOD, I. X., LIEW, C. W., KULKARNI, R. N., BAIN, J., NEWGARD, C., NELSON, M., EVANS, R. M., YATES, J. & MONTMINY, M. 2006. TRB3 links the E3 ubiquitin ligase COP1 to lipid metabolism. *Science,* 312**,** 1763-1766.

QIAO, Y., ZHANG, Y. & WANG, J. 2013. Ubiquitin E3 ligase SCF(beta-TRCP) regulates TRIB2 stability in liver cancer cells. *Biochem Biophys Res Commun,* 441**,** 555-9.

QIN, J., XIE, P., VENTOCILLA, C., ZHOU, G., VULTUR, A., CHEN, Q., LIU, Q., HERLYN, M., WINKLER, J. & MARMORSTEIN, R. 2012. Identification of a Novel Family of BRAF(V600E) Inhibitors. *Journal of Medicinal Chemistry,* 55**,** 5220-5230.

RAN, F. A., HSU, P. D., LIN, C. Y., GOOTENBERG, J. S., KONERMANN, S., TREVINO, A. E., SCOTT, D. A., INOUE, A., MATOBA, S., ZHANG, Y. & ZHANG, F. 2013. Double nicking by RNA-guided CRISPR Cas9 for enhanced genome editing specificity. *Cell,* 154**,** 1380-9.

REESE, M. L. & BOOTHROYD, J. C. 2011. A conserved non-canonical motif in the pseudoactive site of the ROP5 pseudokinase domain mediates its effect on Toxoplasma virulence. *J Biol Chem,* 286**,** 29366-75.

REITERER, V., EYERS, P. A. & FARHAN, H. 2014. Day of the dead: pseudokinases and pseudophosphatases in physiology and disease. *Trends in Cell Biology*. 24(9):489-505.

RIKER, A. I., ENKEMANN, S. A., FODSTAD, O., LIU, S., REN, S., MORRIS, C., XI, Y., HOWELL, P., METGE, B., SAMANT, R. S., SHEVDE, L. A., LI, W., ESCHRICH, S., DAUD, A., JU, J. & MATTA, J. 2008. The gene expression profiles of primary and metastatic melanoma yields a transition point of tumor progression and metastasis. *BMC Med Genomics,* 1**,** 13. DOI: 10.1186/1755-8794-1-13.

RISHI, L., HANNON, M., SALOME, M., HASEMANN, M., FRANK, A. K., CAMPOS, J., TIMONEY, J., O'CONNOR, C., CAHILL, M. R., PORSE, B. & KEESHAN, K. 2014. Regulation of Trib2 by an E2F1-C/EBPalpha feedback loop in AML cell proliferation. *Blood,* 123**,** 2389-400.

RONG, Z., ZHU, S., XU, Y. & FU, X. 2014. Homologous recombination in human embryonic stem cells using CRISPR/Cas9 nickase and a long DNA donor template. *Protein Cell,* 5**,** 258-60.

RORTH, P., SZABO, K. & TEXIDO, G. 2000. The level of C/EBP protein is critical for cell migration during Drosophila oogenesis and is tightly controlled by regulated degradation. *Mol Cell,* 6**,** 23-30.

ROSENWALD, A., ALIZADEH, A. A., WIDHOPF, G., SIMON, R., DAVIS, R. E., YU, X., YANG, L., PICKERAL, O. K., RASSENTI, L. Z., POWELL, J., BOTSTEIN, D., BYRD, J. C., GREVER, M. R., CHESON, B. D., CHIORAZZI, N., WILSON, W. H., KIPPS, T. J., BROWN, P. O. & STAUDT, L. M. 2001. Relation of gene expression phenotype to immunoglobulin mutation genotype in B cell chronic lymphocytic leukemia. *J Exp Med,* 194**,** 1639-47.

ROUSCHOP, K. M. A., VAN DEN BEUCKEN, T., DUBOIS, L., NIESSEN, H., BUSSINK, J., SAVELKOULS, K., KEULERS, T., MUJCIC, H., LANDUYT, W., VONCKEN, J. W., LAMBIN, P., VAN DER KOGEL, A. J., KORITZINSKY, M. & WOUTERS, B. G. 2010. The unfolded protein response protects human tumor cells during hypoxia through regulation of the autophagy genes MAP1LC3B and ATG5. *Journal of Clinical Investigation,* 120**,** 127-141.

SAHARINEN, P., TAKALUOMA, K. & SILVENNOINEN, O. 2000. Regulation of the Jak2 tyrosine kinase by its pseudokinase domain. *Molecular and Cellular Biology,* 20**,** 3387-95.

SALESSE, S. & VERFAILLIE, C. M. 2002. BCR/ABL: from molecular mechanisms of leukemia induction to treatment of chronic myelogenous leukemia. *Oncogene,* 21**,** 8547-8559.

SANCHEZ-CARBAYO, M., SOCCI, N. D., LOZANO, J., SAINT, F. & CORDON-CARDO, C. 2006. Defining molecular profiles of poor outcome in patients with invasive bladder cancer using oligonucleotide microarrays. *J Clin Oncol,* 24**,** 778-89.

SCHEEFF, E. D. & BOURNE, P. E. 2005. Structural evolution of the protein kinase-like superfamily. *Plos Computational Biology,* 1**,** 359-381.

SCHEEFF, E. D., ESWARAN, J., BUNKOCZI, G., KNAPP, S. & MANNING, G. 2009. Structure of the Pseudokinase VRK3 Reveals a Degraded Catalytic Site, a Highly Conserved Kinase Fold, and a Putative Regulatory Binding Site. *Structure,* 17**,** 128-138.

SCOTT, L. M., TONG, W., LEVINE, R. L., SCOTT, M. A., BEER, P. A., STRATTON, M. R., FUTREAL, P. A., ERBER, W. N., MCMULLIN, M. F., HARRISON, C. N., WARREN, A. J., GILLILAND, D. G., LODISH, H. F. & GREEN, A. R. 2007. JAK2 exon 12 mutations in polycythemia vera and idiopathic erythrocytosis. *N Engl J Med,* 356**,** 459-68.

SCUTT, P. J., CHU, M. L. H., SLOANE, D. A., CHERRY, M., BIGNELL, C. R., WILLIAMS, D. H. & EYERS, P. A. 2009. Discovery and Exploitation of Inhibitor-resistant Aurora and Polo Kinase Mutants for the Analysis of Mitotic Networks. *Journal of Biological Chemistry,* 284**,** 15880-15893.

SEGARA, D., BIANKIN, A. V., KENCH, J. G., LANGUSCH, C. C., DAWSON, A. C., SKALICKY, D. A., GOTLEY, D. C., COLEMAN, M. J., SUTHERLAND, R. L. & HENSHALL, S. M. 2005. Expression of HOXB2, a retinoic acid signaling target in pancreatic cancer and pancreatic intraepithelial neoplasia. *Clin Cancer Res,* 11**,** 3587-96.

SEHER, T. C. & LEPTIN, M. 2000. Tribbles, a cell-cycle brake that coordinates proliferation and morphogenesis during Drosophila gastrulation. *Curr Biol,* 10**,** 623-9.

SHAI, R., SHI, T., KREMEN, T. J., HORVATH, S., LIAU, L. M., CLOUGHESY, T. F., MISCHEL, P. S. & NELSON, S. F. 2003. Gene expression profiling identifies molecular subtypes of gliomas. *Oncogene,* 22**,** 4918-23.

SHAW, A. S., KORNEV, A. P., HU, J. C., AHUJA, L. G. & TAYLOR, S. S. 2014. Kinases and Pseudokinases: Lessons from RAF. *Molecular and Cellular Biology,* 34**,** 1538-1546.

SHI, F. M., TELESCO, S. E., LIU, Y. T., RADHAKRISHNAN, R. & LEMMON, M. A. 2010. ErbB3/HER3 intracellular domain is competent to bind ATP and catalyze autophosphorylation. *Proceedings of the National Academy of Sciences of the United States of America,* 107**,** 7692-7697.

SHIN, J., CHAKRABORTY, G., BHARATHAM, N., KANG, C., TOCHIO, N., KOSHIBA, S., KIGAWA, T., KIM, W., KIM, K. T. & YOON, H. S. 2011. NMR solution structure of human vaccinia-related kinase 1 (VRK1) reveals the C-terminal tail essential for its structural stability and autocatalytic activity. *J Biol Chem,* 286**,** 22131-8.

SHOKAT, K. & VELLECA, M. 2002. Novel chemical genetic approaches to the discovery of signal transduction inhibitors. *Drug Discovery Today,* 7**,** 872-879.

SKOTHEIM, R. I., LIND, G. E., MONNI, O., NESLAND, J. M., ABELER, V. M., FOSSA, S. D., DUALE, N., BRUNBORG, G., KALLIONIEMI, O., ANDREWS, P. W. & LOTHE, R. A. 2005. Differentiation of human embryonal carcinomas in vitro and in vivo reveals expression profiles relevant to normal development. *Cancer Research,* 65**,** 5588-98.

SLOANE, D. A., TRIKIC, M. Z., CHU, M. L. H., LAMERS, M. B. A. C., MASON, C. S., MUELLER, I., SAVORY, W. J., WILLIAMS, D. H. & EYERS, P. A. 2010. Drug-Resistant Aurora A Mutants for Cellular Target Validation of the Small Molecule Kinase Inhibitors MLN8054 and MLN8237. *Acs Chemical Biology,* 5**,** 563-576.

STEICHEN, J. M., IYER, G. H., LI, S., SALDANHA, S. A., DEAL, M. S., WOODS, V. L. & TAYLOR, S. S. 2010. Global Consequences of Activation Loop Phosphorylation on Protein Kinase A. *Journal of Biological Chemistry,* 285**,** 3825-3832.

STELLWAGEN, E. 1990. [25] Gel filtration. *In:* MURRAY, P. D. (ed.) *Methods in Enzymology.* Academic Press.

STEWART, R. C., VANBRUGGEN, R., ELLEFSON, D. D. & WOLFE, A. J. 1998. TNP-ATP and TNP-ADP as probes of the nucleotide binding site of CheA, the histidine protein kinase in the chemotaxis signal transduction pathway of Escherichia coli. *Biochemistry,* 37**,** 12269-79.

SU, L. J., CHANG, C. W., WU, Y. C., CHEN, K. C., LIN, C. J., LIANG, S. C., LIN, C. H., WHANG-PENG, J., HSU, S. L., CHEN, C. H. & HUANG, C. Y. 2007. Selection of DDX5 as a novel internal control for Q-RT-PCR from microarray data using a block bootstrap re-sampling scheme. *BMC Genomics,* 8**,** 140. DOI: 10.1186/1471-2164-8-140

SUIJKERBUIJK, S. J. E., VAN DAM, T. J. P., KARAGOZ, G. E., VON CASTELMUR, E., HUBNER, N. C., DUARTE, A. M. S., VLEUGEL, M., PERRAKIS, A., RUDIGER, S. G. D., SNEL, B. & KOPS, G. J. P. L. 2012. The Vertebrate Mitotic Checkpoint Protein BUBR1 Is an Unusual Pseudokinase. *Developmental Cell,* 22**,** 1321-1329.

SUN, L. M., WANG, H. Y., WANG, Z. G., HE, S. D., CHEN, S., LIAO, D. H., WANG, L., YAN, J. C., LIU, W. L., LEI, X. G. & WANG, X. D. 2012. Mixed Lineage Kinase Domain-like Protein Mediates Necrosis Signaling Downstream of RIP3 Kinase. *Cell,* 148**,** 213-227.

TAKASATO, M., KOBAYASHI, C., OKABAYASHI, K., KIYONARI, H., OSHIMA, N., ASASHIMA, M. & NISHINAKAMURA, R. 2008. Trb2, a mouse homolog of tribbles, is dispensable for kidney and mouse development. *Biochemical and Biophysical Research Communications,* 373**,** 648-652.

TALANTOV, D., MAZUMDER, A., YU, J. X., BRIGGS, T., JIANG, Y., BACKUS, J., ATKINS, D. & WANG, Y. 2005. Novel genes associated with malignant melanoma but not benign melanocytic lesions. *Clin Cancer Res,* 11**,** 7234-42.

TAYLOR, J. S., VIGNERON, D. B., MURPHYBOESCH, J., NELSON, S. J., KESSLER, H. B., COIA, L., CURRAN, W. & BROWN, T. R. 1991. Free Magnesium Levels in Normal Human Brain and Brain-Tumors - P-31 Chemical-Shift Imaging Measurements at 1.5-T. *Proceedings of the National Academy of Sciences of the United States of America,* 88**,** 6810-6814.

TAYLOR, S. S., HA, E. & MCKEON, F. 1998. The human homologue of Bub3 is required for kinetochore localization of Bub1 and a Mad3/Bub1-related protein kinase. *Journal of Cell Biology,* 142**,** 1-11.

TAYLOR, S. S. & KORNEV, A. P. 2011. Protein kinases: evolution of dynamic regulatory proteins. *Trends Biochem Sci,* 36**,** 65-77.

TAYLOR, S. S. & RADZIOANDZELM, E. 1994. 3 Protein kinase structures define a common motif. *Structure,* 2**,** 345-355.

TOKARSKI, J. S., NEWITT, J. A., CHANG, C. Y. J., CHENG, J. D., WITTEKIND, M., KIEFER, S. E., KISH, K., LEE, F. Y. F., BORZILLERRI, R., LOMBARDO, L. J., XIE, D. L., ZHANG, Y. Q. & KLEI, H. E. 2006. The structure of dasatinib (BMS-354825) bound to activated ABL kinase domain elucidates its inhibitory activity against imatinib-resistant ABL mutants. *Cancer Research,* 66**,** 5790-5797.

TOMS, A. V., DESHPANDE, A., MCNALLY, R., JEONG, Y., ROGERS, J. M., KIM, C. U., GRUNER, S. M., FICARRO, S. B., MARTO, J. A., SATTLER, M., GRIFFIN, J. D. & ECK, M. J. 2013. Structure of a pseudokinase-domain switch that controls oncogenic activation of Jak kinases. *Nature Structural & Molecular Biology,* 20**,** 1221-3.

TOYODA, H., TANAKA, S., MIYAGAWA, T., HONDA, Y., TOKUNAGA, K. & HONDA, M. 2010. Anti-Tribbles Homolog 2 Autoantibodies in Japanese Patients with Narcolepsy. *Sleep,* 33**,** 875-878.

TRAUT, T. W. 1994. Physiological concentrations of purines and pyrimidines. *Mol Cell Biochem,* 140**,** 1-22.

TREIBER, D. K. & SHAH, N. P. 2013. Ins and Outs of Kinase DFG Motifs. *Chemistry & Biology,* 20**,** 745-746.

TSATSANIS, C. & SPANDIDOS, D. A. 2000. The role of oncogenic kinases in human cancer (review). *International Journal of Molecular Medicine,* 5**,** 583-590.

UNGUREANU, D., WU, J., PEKKALA, T., NIRANJAN, Y., YOUNG, C., JENSEN, O. N., XU, C.-F., NEUBERT, T. A., SKODA, R. C., HUBBARD, S. R. & SILVENNOINEN, O. 2011. The pseudokinase domain of JAK2 is a dual-specificity protein kinase that negatively regulates cytokine signaling. *Nature Structural & Molecular Biology,* 18**,** 971-976.

UNIEWICZ, K. A., ORI, A., RUDD, T. R., GUERRINI, M., WILKINSON, M. C., FERNIG, D. G. & YATES, E. A. 2012. Following Protein-Glycosaminoglycan Polysaccharide Interactions with Differential Scanning Fluorimetry. *In:* REDINI, F. (ed.) *Proteoglycans: Methods and Protocols.*

VEDADI, M., ARROWSMITH, C. H., ALLALI-HASSANI, A., SENISTERRA, G. & WASNEY, G. A. 2010. Biophysical characterization of recombinant proteins: A key to higher structural genomics success. *Journal of Structural Biology,* 172**,** 107-119.

VEDADI, M., NIESEN, F. H., ALLALI-HASSANI, A., FEDOROV, O. Y., FINERTY, P. J., JR., WASNEY, G. A., YEUNG, R., ARROWSMITH, C., BALL, L. J., BERGLUND, H., HUI, R., MARSDEN, B. D., NORDLUND, P., SUNDSTROM, M., WEIGELT, J. & EDWARDS, A. M. 2006. Chemical screening methods to identify ligands that promote protein stability, protein crystallization, and structure determination. *Proceedings of the National Academy of Sciences of the United States of America,* 103**,** 15835-15840.

VERISSIMO, F. & JORDAN, P. 2001. WNK kinases, a novel protein kinase subfamily in multi-cellular organisms. *Oncogene,* 20**,** 5562-5569.

VIGNERI, P. & WANG, J. Y. 2001. Induction of apoptosis in chronic myelogenous leukemia cells through nuclear entrapment of BCR-ABL tyrosine kinase. *Nat Med,* 7**,** 228-34.

VIVOLI, M., AYRES, E., BEAUMONT, E., ISUPOV, M. N. & HARMER, N. J. 2014. Structural insights into WcbI, a novel polysaccharide-biosynthesis enzyme. *IUCrJ,* 1**,** 28-38.

VULPETTI, A. & BOSOTTI, R. 2004. Sequence and structural analysis of kinase ATP pocket residues. *Il Farmaco,* 59**,** 759-765.

WAAS, W. F., RAINEY, M. A., SZAFRANSKA, A. E., COX, K. & DALBY, K. N. 2004. A kinetic approach towards understanding substrate interactions and the catalytic mechanism of the serine/threonine protein kinase ERK2: identifying a potential regulatory role for divalent magnesium. *Biochimica Et Biophysica Acta-Proteins and Proteomics,* 1697**,** 81-87.

WANG, H., YANG, H., SHIVALILA, C. S., DAWLATY, M. M., CHENG, A. W., ZHANG, F. & JAENISCH, R. 2013a. One-step generation of mice carrying mutations in multiple genes by CRISPR/Cas-mediated genome engineering. *Cell,* 153**,** 910-8.

WANG, J., PARK, J.-S., WEI, Y., RAJURKAR, M., COTTON, J. L., FAN, Q., LEWIS, B. C., JI, H. & MAO, J. 2013b. TRIB2 Acts Downstream of Wnt/TCF in Liver Cancer Cells to Regulate YAP and C/EBP alpha Function. *Molecular Cell,* 51**,** 211-225.

WANG, J., ZHANG, Y., WENG, W., QIAO, Y., MA, L., XIAO, W., YU, Y., PAN, Q. & SUN, F. 2013c. Impaired Phosphorylation and Ubiquitination by p70 S6 Kinase (p70S6K) and Smad Ubiquitination Regulatory Factor 1 (Smurf1) Promote Tribbles Homolog 2 (TRIB2) Stability and Carcinogenic Property in Liver Cancer. *Journal of Biological Chemistry,* 288**,** 33667-33681.

WANG, L., SHI, S., GUO, Z., ZHANG, X., HAN, S., YANG, A., WEN, W. & ZHU, Q. 2013d. Overexpression of YAP and TAZ is an independent predictor of prognosis in colorectal cancer and related to the proliferation and metastasis of colon cancer cells. *Plos One,* 8**,** e65539.

WANG, Y. N. & HUNG, M. C. 2012. Nuclear functions and subcellular trafficking mechanisms of the epidermal growth factor receptor family. *Cell and Bioscience,* 2. DOI: 10.1186/2045-3701-2-13

WANG, Y. N., YAMAGUCHI, H., HUO, L. F., DU, Y., LEE, H. J., LEE, H. H., WANG, H. M., HSU, J. M. & HUNG, M. C. 2010. The Translocon Sec61 beta Localized in the Inner Nuclear Membrane Transports Membrane-embedded EGF Receptor to the Nucleus. *Journal of Biological Chemistry,* 285**,** 38720-38729.

WEBER, J. & SENIOR, A. E. 1997. Binding of TNP-ATP and TNP-ADP to the non-catalytic sites of Escherichia coli F1-ATPase. *FEBS Lett,* 412**,** 169-72.

WEI, S.-C., ROSENBERG, I. M., CAO, Z., HUETT, A. S., XAVIER, R. J. & PODOLSKY, D. K. 2012. Tribbles 2 (Trib2) is a novel regulator of toll-like receptor 5 signaling. *Inflammatory Bowel Diseases,* 18**,** 877-888.

WEINER, M. P. & COSTA, G. L. 1994. Rapid PCR site directed mutagenesis. *Pcr-Methods and Applications,* 4**,** S131-S136.

WEISBERG, E., CHOI, H. G., RAY, A., BARRETT, R., ZHANG, J. M., SIM, T., ZHOU, W. J., SEELIGER, M., CAMERON, M., AZAM, M., FLETCHER, J. A., DEBIEC-RYCHTER, M., MAYEDA, M., MORENO, D., KUNG, A. L., JANNE, P. A., KHOSRAVI-FAR, R., MELO, J. V., MANLEY, P. W., ADAMIA, S., WU, C., GRAY, N. & GRIFFIN, J. D. 2010. Discovery of a small-molecule type II inhibitor of wild-type and gatekeeper mutants of BCR-ABL, PDGFR alpha, Kit, and Src kinases: novel type II inhibitor of gatekeeper mutants. *Blood,* 115**,** 4206-4216.

WENNEMERS, M., BUSSINK, J., GREBENCHTCHIKOV, N., SWEEP, F. C. G. J. & SPAN, P. N. 2011a. TRIB3 protein denotes a good prognosis in breast cancer patients and is associated with hypoxia sensitivity. *Radiotherapy and Oncology,* 101**,** 198-202.

WENNEMERS, M., BUSSINK, J., SCHEIJEN, B., NAGTEGAAL, I. D., VAN LAARHOVEN, H. W. M., RALEIGH, J. A., VARIA, M. A., HEUVEL, J. J. T. M., ROUSCHOP, K. M., SWEEP, F. C. G. J. & SPAN, P. N. 2011b. Tribbles homolog 3 denotes a poor prognosis in breast cancer and is involved in hypoxia response. *Breast Cancer Research,* 13. DOI: 10.1186/bcr2934.

WESCHE, H., GAO, X., LI, X. X., KIRSCHNING, C. J., STARK, G. R. & CAO, Z. D. 1999. IRAK-M is a novel member of the pelle/interleukin-1 receptor-

associated kinase (IRAK) family. *Journal of Biological Chemistry,* 274**,** 19403-19410.

WICKSTROM, S. A., LANGE, A., MONTANEZ, E. & FASSLER, R. 2010. The ILK/PINCH/parvin complex: the kinase is dead, long live the pseudokinase! *Embo Journal,* 29**,** 281-291.

WILLIAMS, C. C., ALLISON, J. G., VIDAL, G. A., BUROW, M. E., BECKMAN, B. S., MARRERO, L. & JONES, F. E. 2004. The ERBB4/HER4 receptor tyrosine kinase regulates gene expression by functioning as a STAT5A nuclear chaperone. *Journal of Cell Biology,* 167**,** 469-478.

WOUTERS, B. J., JORDA, M. A., KEESHAN, K., LOUWERS, I., ERPELINCK-VERSCHUEREN, C. A., TIELEMANS, D., LANGERAK, A. W., HE, Y., YASHIRO-OHTANI, Y., ZHANG, P., HETHERINGTON, C. J., VERHAAK, R. G., VALK, P. J., LOWENBERG, B., TENEN, D. G., PEAR, W. S. & DELWEL, R. 2007. Distinct gene expression profiles of acute myeloid/T-lymphoid leukemia with silenced CEBPA and mutations in NOTCH1. *Blood,* 110**,** 3706-14.

WU, C., OROZCO, C., BOYER, J., LEGLISE, M., GOODALE, J., BATALOV, S., HODGE, C. L., HAASE, J., JANES, J., HUSS, J. W., 3RD & SU, A. I. 2009. BioGPS: an extensible and customizable portal for querying and organizing gene annotation resources. *Genome Biol,* 10**,** R130. DOI: 10.1186/gb-2009-10-11-r130

XU, B. E., ENGLISH, J. M., WILSBACHER, J. L., STIPPEC, S., GOLDSMITH, E. J. & COBB, M. H. 2000. WNK1, a novel mammalian serine/threonine protein kinase lacking the catalytic lysine in subdomain II. *Journal of Biological Chemistry,* 275**,** 16795-16801.

XU, M., YU, L., WAN, B., YU, L. & HUANG, Q. 2011. Predicting Inactive Conformations of Protein Kinases Using Active Structures: Conformational Selection of Type-II Inhibitors. *Plos One,* 6. DOI: 10.1371/journal.pone.0022644.

YAMAJI, S., SUZUKI, A., SUGIYAMA, Y., KOIDE, Y., YOSHIDA, M., KANAMORI, H., MOHRI, H., OHNO, S. & ISHIGATSUBO, Y. 2001. A novel integrin-linked kinase-binding protein, affixin, is involved in the early stage of cell-substrate interaction. *Journal of Cell Biology,* 153**,** 1251-1264.

YOKOYAMA, T., KANNO, Y., YAMAZAKI, Y., TAKAHARA, T., MIYATA, S. & NAKAMURA, T. 2010. Trib1 links the MEK1/ERK pathway in myeloid leukemogenesis. *Blood,* 116**,** 2768-2775.

YOKOYAMA, T., TOKI, T., AOKI, Y., KANEZAKI, R., PARK, M. J., KANNO, Y., TAKAHARA, T., YAMAZAKI, Y., ITO, E., HAYASHI, Y. & NAKAMURA, T. 2012. Identification of TRIB1 R107L gain-of-function mutation in human acute megakaryocytic leukemia. *Blood,* 119**,** 2608-11.

YOSHIDA-MORIGUCHI, T., WILLER, T., ANDERSON, M., VENZKE, D., YU, L. P. & CAMPBELL, K. 2013. SGK196 Is a Glycosylation-Specific O-Mannose Kinase Required for Dystroglycan Function. *Glycobiology,* 23**,** 1335-1335.

YOSHIHARA, K., TAJIMA, A., KOMATA, D., YAMAMOTO, T., KODAMA, S., FUJIWARA, H., SUZUKI, M., ONISHI, Y., HATAE, M., SUEYOSHI, K., KUDO, Y., INOUE, I. & TANAKA, K. 2009. Gene expression profiling of advanced-stage serous ovarian cancers distinguishes novel subclasses and implicates ZEB2 in tumor progression and prognosis. *Cancer Sci,* 100**,** 1421-8.

YU, D. H. & HUNG, M. C. 2000. Overexpression of ErbB2 in cancer and ErbB2-targeting strategies. *Oncogene,* 19**,** 6115-6121.

YU, H. Y., HE, K., LI, L. J., SUN, L., TANG, F., LI, R. Z., NING, W. & JIN, Y. 2013. Deletion of STK40 Protein in Mice Causes Respiratory Failure and Death at Birth. *Journal of Biological Chemistry,* 288**,** 5342-5352.

ZANELLA, F., RENNER, O., GARCIA, B., CALLEJAS, S., DOPAZO, A., PEREGRINA, S., CARNERO, A. & LINK, W. 2010. Human TRIB2 is a repressor of FOXO that contributes to the malignant phenotype of melanoma cells. *Oncogene,* 29**,** 2973-82.

ZEQIRAJ, E., FILIPPI, B. M., DEAK, M., ALESSI, D. R. & VAN AALTEN, D. M. F. 2009a. Structure of the LKB1-STRAD-MO25 Complex Reveals an Allosteric Mechanism of Kinase Activation. *Science,* 326**,** 1707-1711.

ZEQIRAJ, E., FILIPPI, B. M., GOLDIE, S., NAVRATILOVA, I., BOUDEAU, J., DEAK, M., ALESSI, D. R. & VAN AALTEN, D. M. F. 2009b. ATP and MO25 alpha Regulate the Conformational State of the STRAD alpha Pseudokinase and Activation of the LKB1 Tumour Suppressor. *Plos Biology,* 7. e1000126

ZEQIRAJ, E. & VAN AALTEN, D. M. 2010. Pseudokinases-remnants of evolution or key allosteric regulators? *Curr Opin Struct Biol,* 20**,** 772-81.

ZHANG, C., CHI, Y. L., WANG, P. Y., WANG, Y. Q., ZHANG, Y. X., DENG, J. T., LV, C. J. & XIE, S. Y. 2012. miR-511 and miR-1297 Inhibit Human Lung Adenocarcinoma Cell Proliferation by Targeting Oncogene TRIB2. *Plos One,* 7. e46090

ZHANG, C., KENSKI, D. M., PAULSON, J. L., BONSHTIEN, A., SESSA, G., CROSS, J. V., TEMPLETON, D. J. & SHOKAT, K. M. 2005a. A second-site suppressor strategy for chemical genetic analysis of diverse protein kinases. *Nature Methods,* 2**,** 435-441.

ZHANG, H., KOO, C. Y., STEBBING, J. & GIAMAS, G. 2013. The dual function of KSR1: a pseudokinase and beyond. *Biochemical Society Transactions,* 41**,** 1078-1082.

ZHANG, J., ADRIAN, F. J., JAHNKE, W., COWAN-JACOB, S. W., LI, A. G., IACOB, R. E., SIM, T., POWERS, J., DIERKS, C., SUN, F., GUO, G. R., DING, Q., OKRAM, B., CHOI, Y., WOJCIECHOWSKI, A., DENG, X., LIU, G., FENDRICH, G., STRAUSS, A., VAJPAI, N., GRZESIEK, S., TUNTLAND, T., LIU, Y., BURSULAYA, B., AZAM, M., MANLEY, P. W., ENGEN, J. R., DALEY, G. Q., WARMUTH, M. & GRAY, N. S. 2010. Targeting Bcr-Abl by combining allosteric with ATP-binding-site inhibitors. *Nature,* 463**,** 501-6.

ZHANG, J. M., YANG, P. L. & GRAY, N. S. 2009. Targeting cancer with small molecule kinase inhibitors. *Nature Reviews Cancer,* 9**,** 28-39.

ZHANG, W., MORRIS, G. Z. & BEEBE, S. J. 2004. Characterization of the cAMP-dependent protein kinase catalytic subunit Cγ expressed and purified from sf9 cells. *Protein Expression and Purification,* 35**,** 156-169.

ZHANG, Y. J., DAVIS, J. L. & LI, W. 2005b. Identification of tribbles homolog 2 as an autoantigen in autoimmune uveitis by phage display. *Molecular Immunology,* 42**,** 1275-1281.

Appendix

Table A

Carcinoma	Total number of samples	Number containing mutant Trib2	Percentage of mutated samples (%)	Amino acid mutation and position
Endometrium	505	8	1.58	F129L R148I R179W E222* V237M R251W R286Q R291W
Large intestine	781	10	1.28	R31K E186K D211N D211N R251W R286*, R290H, V314I, V332I E336D
Stomach	81	1	1.23	S299L
Oesophagus	261	2	0.77	L224V F314L
Skin	334	2	0.60	P69L R142C
Lung	1397	8	0.57	G44V V58L G62E S139F S227I H255R L289V S313C
Urinary tract	366	1	0.27	V249M
Breast	1210	3	0.25	E150K G250E R286Q
Kidney	804	2	0.25	M334I P340R
Pancreas	905	2	0.22	K63R, R286Q
Haematopoietic and Lymphoid	1325	1	0.08	S36N

Table A Analysis of somatic Trib2 mutants identified in the COSMIC database. Missense and nonsense somatic Trib2 mutants are listed in the table along with the cancerous tissue in which they were identified, the number of samples analysed and the percentage of samples that contained a mutated variant of Trib2. The red font highlights the residues discussed in section 1.27.